STRUCTURE, PROPERTIES AND APPLICATIONS OF CONDUCTING GRAPHITE - THERMOPLASTIC COMPOSITES

A THESIS SUBMITTED TO THE
UNIVERSITY OF PUNE FOR THE DEGREE OF
DOCTOR OF PHILOSOPHY
IN PHYSICS

BY

B.T.S. RAMANUJAM

UNDER THE GUIDANCE OF

Dr. S. RADHAKRISHNAN

POLYMER SCIENCE AND ENGINEERING DIVISION
NATIONAL CHEMICAL LABORATORY
PUNE 411008, INDIA

APRIL 2010

Acknowledgements

At the outset, with due devotion, I would like to thank Sri Krishna, the supreme personality of godhead who is the cause of all causes for shedding causeless mercy to complete this work.

I take this opportunity with a deep sense of gratitude to thank my research supervisor Dr. S. Radhakrishnan whose immaculate guidance, thought provoking discussions and constructive criticisms helped me to complete this thesis in a fabulous manner.

I wish to sincerely thank the Director, NCL for permitting me to carry out this research work and providing me excellent facilities.

I also would like to thank Dr. C. S. Gopinath, Dr. P. A. Joy and Dr. K. Krishnamoorthy for helping me to understand various characterization techniques.

My sincere namaskar to Ramashanker Vyasji whose inspiring teachings on Srimad Bhagavatham and Bhagavath Gita made my moral high.

I extend my heartfelt thanks to Mr. Kannan, Mr. Ravikanth Shukla, Mr. Md. Nazrul Islam. Ms. Tuhina Kelkar, Mr. Sivaram Pradhan who made my stay at NCL more pleasant.

I would like to acknowledge my seniors and contemporary colleagues namely Dr. S.D. Deshpande, Dr. Francis, Dr. Santhosh Paul, Dr. Arindam, Dr. Sreejith, Dr. Subramanyam, Dr. S. B. Kar, Dr. Rahul, Ms. Rajashree Mahale, Mrs. Kanchan Nehete, Mr. Narendra Sonawane, Mr. Pradip Sonawane, Mr. Indraneel, Ms. Rucha and Mr. Karan for helping me during the course various measurements.

My special thanks go to Easwar, Mama and Mami whose ceaseless affection made me to feel homely atmosphere.

I would also like to thank GJ Hostel friends starting from Sridhar Reddy, Kishore, Sudhir, Aarif, Ashish, Vilas, Srinivasa Rao, Abhijit Purude, Abhishek Dubey, Mishra, Sarvesh, Abhilash, Srikanth, Sujit, Ganiya, Swaroop, Raju, Patwa, Kamu, Nishant, Mandeep, Bhogesh, Sumantha and others for making my stay at GJ Hostel more memorable.

Being a player of Chennai Super Kings team in GJPL cricket tournaments, I extend my thanks to Venki, Nangaraj, Edwin, Vijay, Suresh, Dharma, Mohan Raj and Palani.

My sincere thanks are also to NCL Tamil members starting from Dr. Mallikarjuna, Vijayanand, Khaja, V. Nagarajan, Selva, Dr. Devaraj, Dr. Selva Kannan, Dr. Prathap Chandran, Dr. Thiru, Dr. Mangal and others for making my stay at NCL memorable and enjoyable.

I extend my thanks to Mr. Sandeep Kothawade, Mr. Prashant Patil and Mr. Hari Krishna who helped me in various regards during my stay at NCL.

My special thanks are to my teachers at various levels namely Dr. R. Natarajan, Mr. S. N. Sridharan, Mr. J. Srinivasan of A. M. Jain College, Chennai, Retired Prof. Dr. B. Gnanaprakasam of Presidency College, Chennai, Prof. K. Shahi of IIT-Kanpur, Prof. B. Krishnan of D.G. Vaishnav College, Chennai. Their inspiring teachings and constant encouragement made me to choose research career.

I would like to thank my Parents, Brothers, Sisters, Relatives and Friends for their support, constant encouragement, affection and understanding.

Date:

National Chemical Laboratory B.T.S. Ramanujam

Pune

CERTIFICATE

This is to certify that the work incorporated in this thesis entitled **"Structure, Properties and Applications of Conducting Graphite - Thermoplastic Composites"** submitted by Mr. B.T.S. Ramanujam was carried out by him under my supervision at the National Chemical Laboratory, Pune. Such material as has been obtained from other sources has been duly acknowledged in this thesis.

Date:

National Chemical Laboratory
Pune-411008

Dr. S. Radhakrishnan
(Research Guide)

DECLARATION

I hereby declare that the work incorporated in the thesis entitled **"Structure, Properties and Applications of Conducting Graphite – Thermoplastic Composites"** submitted for the degree of Doctor of Philosophy to the University of Pune, has been carried out by me at Polymer Science and Engineering Division, National Chemical Laboratory, Pune under the supervision of Dr. S. Radhakrishnan. The work is original and has not been submitted in part or full by me for any other degree of diploma to this or any other university.

Date:

National Chemical Laboratory (B.T.S. Ramanujam)

Pune-411008 Research Student

Contents

ABSTRACT

The present dissertation deals with structure, properties and applications of conducting graphite-thermoplastic composites. Electrical and thermal properties of composites were studied.

Conducting Polymer Composite (CPC) is a class of conducting polymers being focused for wide range of applications such as fuel cells, EMI shielding devices etc. The conductivity of the composites depends on volume fraction, particle size, orientation, dispersion of fillers along with the processing routes. The reduction of percolation threshold and cost of the materials are the key factors. In this regard use of more concentrations of nanofillers like CNT, graphene will not be economical. Hence hybrid composites serve better purpose in the reduction of percolation threshold and the total filler loading to achieve maximum conductivity. Hence a systematic study of electrical and thermal properties of binary and hybrid composites was carried out. Accordingly three polymer matrices such as Polyether sulfone (PES), Polyphenylene sulfide (PPS) and Polypropylene (PP) were chosen. The fillers used were graphite, carbon black (CB), expanded graphite (ExGr) and carbon nanofiber (CNF). This thesis is organized in six chapters as described below.

Chapter-1 describes a brief literature survey on conducting polymer binary and hybrid composites to emphasize the motivation for the selection of the topic. Theory of electrical conduction in conducting polymer composites, charge transport, impedance spectroscopy, thermal conductivity and various electrode processes have been outlined.

Chapter-2 presents various synthesis procedures of composites and the characterization techniques employed in the study of conducting composites.

Chapter-3 comprises of preparation, dc, and ac electrical conductivity studies of PES-7 wt% graphite-filler (filler- CB, CNF, ExGr) systems. The composite, PES-7 wt% graphite-CB was prepared by solution blending and powder mixing routes to understand the role of preparation routes. The electrical conductivity variation of PES-graphite, PES-CB, PES-ExGr and PES-CNF composites was also studied. The effect of heat treatment on the conductivity of binary composites was investigated. Thermal conductivities of few composites were measured.

Chapter-4 deals with preparation and electrical characterization of PPS-graphite, PPS-ExGr, PPS-CNF, PPS-7 wt% graphite-filler (filler = CB, ExGr and CNF). Thermal analysis of binary composites was carried out. In-situ polymerization of PPS-ExGr composites and their characterization were done. Thermal conductivity of few PPS based composites was measured. Effect of preparation route like melt crystallization on the electrical percolation was studied.

Chapter-5 constitutes investigations of preparation routes such as powder mixing and melt crystallization on the electrical conductivity variation of both PP based binary and hybrid composites. The dc conductivity studies on PP-graphite, PP-CB, PP-Exgr, PP-CNF and PP-7 wt% graphite-filler (filler=CB, ExGr and CNF) were carried out. Aspect ratio of fillers was correlated with electrical percolation threshold.

Chapter-6 describes summary and salient conclusions of the above investigations reported in this thesis.

List of Abbreviations

CMC	Ceramic-Matrix Composites
CPC	Conducting polymer composite
CNT	Carbon nanotube
CNF	Carbon nanofiber
CF	Carbon fiber
CB	Carbon black
CPE	Constant phase element
δ	Lattice mismatch factor
DCM	Dichloromethane
DPS	Diphenyl sulfone
DSC	Differential scanning calorimetry
EVA	Ethyl vinyl acetate
ExGr	Expanded graphite
EPDM	Ethylene-Propylene-Diene monomer
ESCA	Electron spectroscopy for chemical analysis
FT-IR	Fourier transform infra-red
GO	Graphite oxide
GEM	Generalized effective medium theory
HDPE	High density polyethylene
ICP	Intrinsically conducting polymer
MWCNT	Multi walled carbon nanotube
MMC	Metal matrix composites
NMP	N-methy-2-pyrollidone

PP	Polypropylene
PTC	Positive temperature coefficient
PPS	Poly (p-phenylene sulfide)
PANI	Polyaniline
PA	Polyacetylene
PA6	Polyamide-6
PPy	Polypyrolle
PTH	Polythiophene
PPP	Poly (p-phenylene)
PPV	Poly (p-phenylene vinylene)
PS	Polystyrene
PMMA	Polymethyl methacrylate
PU	Polyurethane
PMC	Polymer-Matrix composites
PET	Polyethylene terephthalate
SEM	Scanning electron microscopy
SWCNT	Single walled carbon nanotube
TGA	Thermo-gravimetric analysis
TEM	Transmission electron microscopy
XPS	X-ray photoelectron spectroscopy
XRD	X-ray diffraction
FWHM	Full Width at Half Maximum
PP-g-MA	Maleic anhydride grafted Polypropylene

Chapter-1

Introduction

1.1. Introduction

The impact of materials on the society can be gauged from the advent of new materials for various applications including household articles. Various properties i.e. mechanical, electrical and thermal of materials developed for different applications should meet the standard. For example bipolar plate material which is conducting polymer composite based for fuel cell applications should exhibit very high electrical (~ 10 S/cm) and thermal conductivities (10 W/m-K) as set by US department of energy. Moreover depending on the operating conditions better mechanical properties of those plates with light weight and compactness also become indispensable criteria. In many cases single material will not possess all required properties. Hence a combination of different materials with desired properties has to be made. Thus the term composite is used when two or more discreet materials are mixed to provide proper balance between physical and mechanical properties which the constituents alone could not offer. Even nature has capitalized on this effect as the cortical bone is made of a ceramic (calcium phosphate crystallite) and organic fibers (collagen fibers). The preparation and processing routes of composites have a great impact on the properties. The introduction of performance and process apart from structure-property correlation which is the main focus of solid state physicists and metallurgists changed the course of composite research. High performance is the driving force of advanced composites research. In automobile industries materials are labeled after the fabrication processes and not by composition. Thus the field of composites has generated a new way of thinking.

1.2. Classification of Composites

Many composites are composed of just two phases i.e., matrix and the dispersed phase. The properties of composites are a function of the properties of the constituent phases, their relative amounts and the geometry of the dispersed phase including particle size, shape, distribution and orientation. The composites can be classified according to the nature of the dispersed phase and the matrix. The matrix can be metal, ceramic or polymer.

1.2. 1. Classification on the Basis of Dispersed Phase

1.2.1.a. Particle Reinforced Composites

In this type, the dispersed phase is equiaxed i.e., particles dimensions are approximately the same in all directions. The matrix can be ceramic, metal or polymer. This can be further classified in to two types as follows

(i) Large particle composites: Filler size in this case is in microns. Particle-matrix interaction in this case can't be treated on the atomic or molecular level.

(ii) Dispersion strengthened composites: In this case the particle size of fillers lie between 10 nm to100 nm. Atomic or molecular level interaction exists. The matrix bears the major portion of the applied load and the small dispersed particles hinder the motion of dislocations resulting in improvements in yield strength, hardness and tensile strength. For example, addition of 3 vol% thoria finely dispersed increases high temperature strength of nickel alloys which is an example of this class of composites.

1.2.1.b. Fiber Reinforced Composites

In this case, the dispersed phase has the geometry of a fiber i.e. a large length-to-diameter ratio. Design goals of fiber reinforced composites include high strength and stiffness. Depending on the fiber length it can be further classified in to (i) continuous (aligned) fiber reinforced composites and (ii) short fiber reinforced composites.

1.2.1.c. Structural Composites

They are normally composed of homogeneous and composite materials. Properties of such composites not only depend on the properties of the constituent materials but also on the geometrical design of various structural elements. They are further classified in to,

(i) Laminar composites: These types of composites are composed of two dimensional sheets or panels that have a preferred high strength direction as found in wood and continuous aligned fiber reinforced plastics.

(ii) Sandwich panels: They are a class of structural composites consisting of two strong outer sheets or faces separated by a layer of dense material or core which has lower strength and stiffness. They are found in various applications such as roofs, floors and walls of buildings.

1.2. 2. Classification on the Basis of Matrix

1.2.2.a. Metal-Matrix Composites (MMCs)

In these types of composites, the matrix will be a ductile metal. The reinforcement may improve specific stiffness, abrasion resistance, creep resistance, thermal conductivity etc. They may be utilized at higher service temperature. Advantages of this class of composites include greater resistance to degradation by organic fluids and non flammability. They are more expensive than polymer matrix composites. The reinforcement can be in the form of particulates, fibers and whiskers.

1.2.2.b. Ceramic-Matrix Composites (CMCs)

Ceramic materials are resilient to oxidation and deterioration at elevated temperatures. The fracture toughness value of ceramic materials is low typically between 1 and 5 $MPa\sqrt{m}$ where as for metals it is greater by 5 to 100 times that of a ceramic material. The fracture toughness of ceramic materials can be significantly improved by embedding particulates, fibers or whiskers of one ceramic material that have been embedded in to a matrix of another ceramic. Crack propagation is restricted and arrested due to the presence of fillers.

1.2.2.c. Polymer- Matrix Composites (PMCs)

Polymer matrix composites are composed of a matrix from thermoset (unsaturated polyester, epoxy etc.) or thermoplastic (polycarbonate, nylon etc.) and embedded glass, carbon, steel or kelvar fibers. PMCs are characterized by the following properties,

- High tensile strength
- High stiffness
- High fracture toughness
- Good corrosion resistance
- Low cost

The properties of PMCs depend on additives as well as the matrix. One of the disadvantages of PMCs is their high coefficient of thermal expansion.

1.2. 3. Hybrid Composites

In general, this class of composites is prepared by adding two or more kinds of fibers/fillers in a single matrix. Hybrids have a better combination of properties than

composites containing only a single fiber. Carbon fiber-glass fiber loaded in to a polymeric matrix can be an example of this type. When the composites are stressed in tension, failure is normally non-catastropic. The carbon fibers are first to fail at that time the load is transferred to the glass fiber. Similarly the hybrid composites have been used for enhancing electrical conductivity[1] by adding two conducting fillers in a polymer matrix.

1.3. Fillers Properties

Fillers selection is primarily determined by the particle size distribution, the particle shape, aspect ratio, surface area and the packing of them in a matrix. From spherical filler to cubic, block, flake to fiber the surface area increases along with aspect ratio as shown in Figure 1.1. Further with high surface area and aspect ratio only low loading of fillers will be required to achieve desired property level. The particle size distribution should be broad which makes sure minimum voids as the small particle can occupy void spaces between large particles.

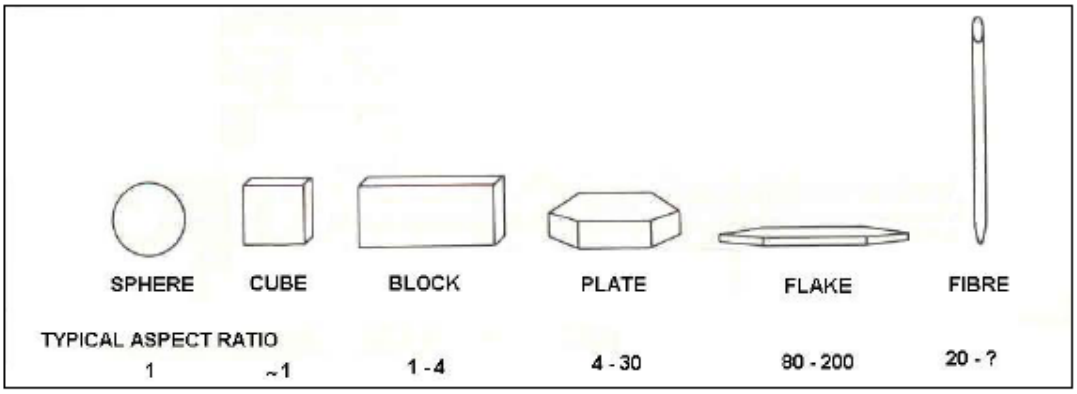

Figure.1.1. Aspect ratio variation with filler shape

Tensile strength of composites is dependent on filler packing characteristics, sizes and interfacial bonding. The packing fraction P_f reflects the size distribution and shape of the particles. Poorly packed particles with low P_f will have larger, less uniform zones of matrix between particles so that when a stress is applied, the weakest links, consisting of smaller matrix zones bear the strain and break readily. More uniformly packed systems with high P_f can uniformly distribute the strain providing higher strengths. Hall and Petch have derived the following equation 1 for the yield stress σ_y of a polycrystalline materials[2].

$$\sigma_y = \sigma_i + Kd'^{-1/2} \quad (1)$$

where σ_i is the yield stress for a crystal of the same material in which there are no grain boundaries. K is a constant and d' is the grain diameter. Thus the yield strength increases with decrease in the grain diameter.

Similarly hardness of plastics is a function of relative filler volume and filler modulus. It is further dependent on degree of dispersion, interfacial bonding etc. In general, hardness increases with moduli of fillers.

The flow properties of polymer composites depend on the concentration and dispersion of fillers. Thus depending on the end applications, the choice of fillers should be made. Out of all types of composites, PMCs are of great interest because they are easily processible and economical. As this thesis aims at developing conducting polymer composites, further discussions will be limited to only polymer composites.

1.4. Nanocomposites-Size does Matter!

When the size of the filler added to a polymer matrix lies in nanometer range (1 nm-100 nm), the composites are known to be nanocomposites. Nanocomposites show better property enhancement compared to microcomposites listed below due to increase in surface to volume ratio.

- Increase in mechanical properties i.e., strength, modulus and dimensional stability
- Decrease in permeability to water, gases and hydrocarbons
- Better thermal stability and higher heat distorsion temperature
- Chemical resistance
- Higher electrical conductivity

Nanofiller addition reduces the filler concentration to obtain any property enhancement compared to microcomposites.

1.5. Synthesis of Nanocomposites

The addition of nanofiller in polymer matrices leads to enhancement in various properties. The synthesis of many nanofillers results in increase in the production cost where as micron sized fillers do not show property enhancement at low loading. High loading of micron sized fillers leads to processing difficulties. So it will be better to

get cheap fillers which may be further processed to obtain their nanostructures. In this regard clays and graphite have been focused for improving mechanical and electrical properties of polymer nanocomposites. Both fillers have agglomerated layered structure and easily available. Nylon-6-clay composites synthesized by Toyota central research and development laboratory in 1986 revealed the possibility of achieving remarkable improvement in thermal and mechanical properties[3]. Clays are nothing but layered silicates and the gap between the layers is known as gallery or interlayer. The inorganic cation in the interlayer can be substituted by other cations. The exchange of metal ions by cationic surfactant like bulky alkyl ammonium ions increases the gallery space depending on the polymer matrix. Thus the modified filler is known as organo clays which form polymer layered silicate nano composites. Mainly three types of routes are employed in the polymer layered silicate composites.

1.5.1. In-situ Intercalative Polymerization

In this route first the clay particles are allowed to swell in the liquid monomer. Subsequently, liquid monomer occupies the gallery of clays. Polymerization can be initiated either by heat or radiation, diffusion of a suitable initiator, or by an organic initiator, or catalyst fixed through cationic exchange inside the interlayer before swelling by the monomer. Examples:

In-situ polymerization of nylon-6, nylon-12, polypropylene (PP), polyethylene terephthalate (PET) etc., with organo modified clay (MMT)[4-6]. Similarly polystyrene-MMT[7], polyethylene-clay[8] nanocomposites have been synthesized by in-situ polymerization route.

1.5.2. Intercalation by Solvent Methods

In this method first the clay particles are swelled in non polar solvents like toluene and then the polymer is dissolved in the solvent and intercalates between the clay layers. Finally the solvent is evaporated under vacuum. The major advantage of this method is that intercalated nanocomposites can be synthesized with polymers with zero polarity also.

Examples:

Solution intercalation of PP, polystyrene (PS), polymethyl methacrylate (PMMA) etc., with organo modified MMT[4-6].

1.5.3. Melt Intercalation

The layered silicate is mixed with the polymer matrix in the molten state. If the layer surfaces are sufficiently compatible with the chosen polymer, the polymer can crawl into the interlayer space and form intercalated, and/or exfoliated nanocomposite. In this technique, no solvent is required.

Examples:

PS, polyurethane (PU)[7-8], nylon[9], PET[10], PP[11]etc., with organo modified MMT.

Similarly graphite-polymer nanocomposites have also been synthesized by in-situ polymerization, melt blending, solution mixing routes etc. Graphite has layer structure which up on exfoliation leads to graphene formation which is a two dimensional graphite monolayer. Because of the high aspect ratio of graphene, the electrical conductivity is enhanced to a great extent when mixed with polymers. Since graphite has no functional groups it is chemically treated to form graphite oxide (GO)[12] which can be dispersed well in polymer matrices. The advantage of oxygen containing functional group on GO sheets makes them compatible with many polymers. Polystyrene/graphite nanocomposites by chemical reduction of exfoliated and dispersed isocyanate-treated GO sheets in a solution have been synthesized[12]. This method is suitable for polymers soluble in organic solvents. Du *et al*.[13] have reported poly(arylene sulfide)/graphite nanocomposites by melt mixing method. It has been done in two steps. First GO undergoes redox reaction with polysulfide ions and the resultant sulfur nano particles are dispersed on the surface of graphenes. This composite is melt mixed with the polymer to get nanocomposites. The resultant composite exhibits a conductivity of 69 S/cm. George *et al*.[14] have prepared ethyl vinyl acetate (EVA)-expanded graphite (ExGr) nanocomposites by solution blending route. Addition of for 4 wt% expanded graphite in EVA resulted in enhancement of tensile strength by 35% along with enormous increase in thermal conductivity.

Thus the preparation route affects greatly the properties of nanocomposites. So far all discussions were pertained to insulating filler and matrix but a special emphasis need to be given to a new class of polymers known as “Conducting Polymers” as the present thesis is focused on them.

1.6. Conducting Polymers –A New Class of Materials

On the basis of electrical conductivity, materials can be classified in to four types namely 1) Insulators 2) Metals 3) Semiconductors 4) Superconductors. The conductivity of insulator is less than 10^{-9} S/cm and that of metals is greater than 10^{4} S/cm. Semiconductors have conductivity in the range 10^{-4}-10 S/cm. Until the discovery of iodine doped trans-polyacetylene[15] which exhibited conductivity of the order of 10^{3} S/cm, polymers were regarded as insulators. Though organic polymers are insulators, the concept of "doping" which is nothing but oxidation and reduction of polymer backbone, opened up a new class of materials namely "Conducting Polymers" or "Synthetic Metals". The accidental discovery of polyacetylene when the concentration of Ziegler-Natta catalyst was taken one thousand time in excess during acetylene polymerization along with iodine doping fetched Nobel prize to Alan G Mcdiarmid, Hideki Shirakawa and Alan J Heeger in the year 2000. After the discovery of iodine doped trans-polyacetylene, many conducting polymers have been synthesized like Polyaniline, Polypyrolle, Polythiophene etc[16]. π-electrons of the conjugated chains of polymers led to conductivity. Some of the conducting polymers structures are given below in Figure 1.2.

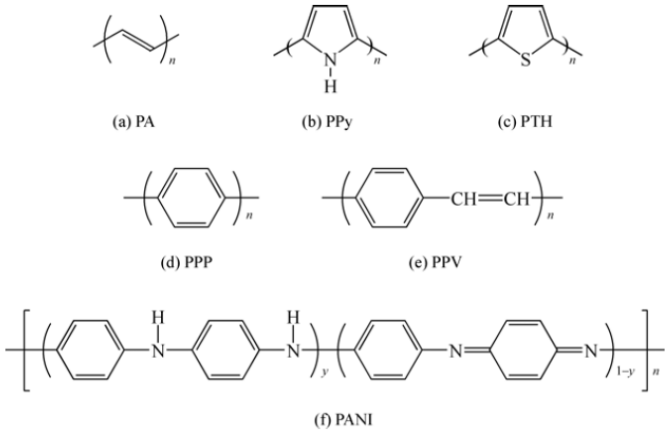

Figure. 1.2. Molecular structure of typical conducting polymers

a) trans-Polyacetylene b) Polypyrrole c) Polythiophenes d) Poly (p-phenylene) e) Poly (p-phenylenevinylene) f) Polyaniline

Conducting polymers can exhibit range of conductivities from insulator to metal depending on the doping degree as shown in Figure 1.3 below.

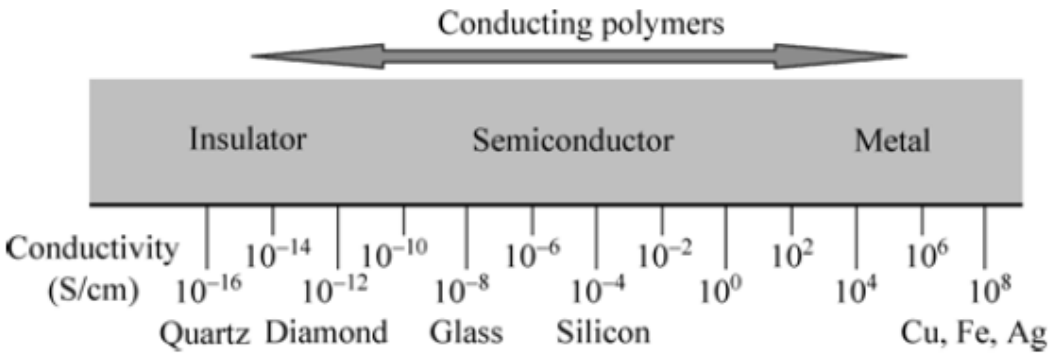

Figure. 1.3. The range of conductivities of conducting polymers including doping

1.7. Classification of Conducting Polymers

Electrically conducting polymers can be classified in to four major types[17]as given below

1. Intrinsically conducting polymers (ICPs) or highly conjugated polymers
2. Polymer charge transfer complexes
3. Organometallic polymeric conductors
4. Conducting polymer composites (CPCs)

1.7.1. Intrinsically Conducting Polymers

This type of conducting polymers has conjugation which is characterized by quasi infinite π system extending over many monomers and they possess a spatially delocalized band like electronic structure. The mechanism of conduction in this type is based on the motion of charged defects within the conjugated framework. Polymers with conjugated backbones have an inherently higher density of conjugated regions with a higher degree of connectivity than polymers with saturated backbones containing only localized moieties. One consequence of this fact is that the former can be rendered metallic and the later are at best semi conductors. Examples of this class are Polyaniline, Polypyrrole, Polythiophene etc.

1.7.2. Polymer Charge Transfer Complexes

Addition of acceptor like molecules to insulating polymers leads to the formation complexes known as polymer charge transfer complexes. The theory of charge transfer complexes has been proposed by Mulliken[18,19]and Dewar[20]. It is likely that donor-acceptor interaction promotes orbital overlap which results in enhanced electron delocalization.

1.7.3. Organometallic Polymeric Conductors

This class is obtained by adding organometallic groups to polymer molecules. The electron delocalization is increased by the overlap of metal d-orbital and π orbital of the organic structure. They find applications in molecular wires, antistatic foils etc. Metallophthalocyanines and poly(ferrocenylene) fall under this category.

1.7.4. Conducting Polymer Composites

Conducting polymer composites can be prepared by dispersion of electrically conducting phase in an insulating polymer matrix. These materials are cost effective and technologically more important as witnessed from the demand of them in various applications such as electromagnetic interference shielding (EMI) devices, electrostatic dissipation (ESD), electronic applications etc. Usually conducting carbon blacks[21-25], metal fillers[26-28], graphite[29-30], expanded graphite[31-35] carbon nanotubes[36-42] (CNTs), carbon nanofiber[43-46] (CNF) etc., are added to make conducting polymer composites.

1.8. Electrical Conductivity in CPCs

The electrical conductivity variation of CPCs is quite different as shown in Figure.1.4. It does not follow rule of mixtures i.e., the conductivity is a linear function of filler concentration V_f, but varies nonlinearly. At a critical concentration (V_c) the electrical conductivity increases to more than 10-12 orders and then remains more or less constant. Below the critical concentration, composites remain as insulators.

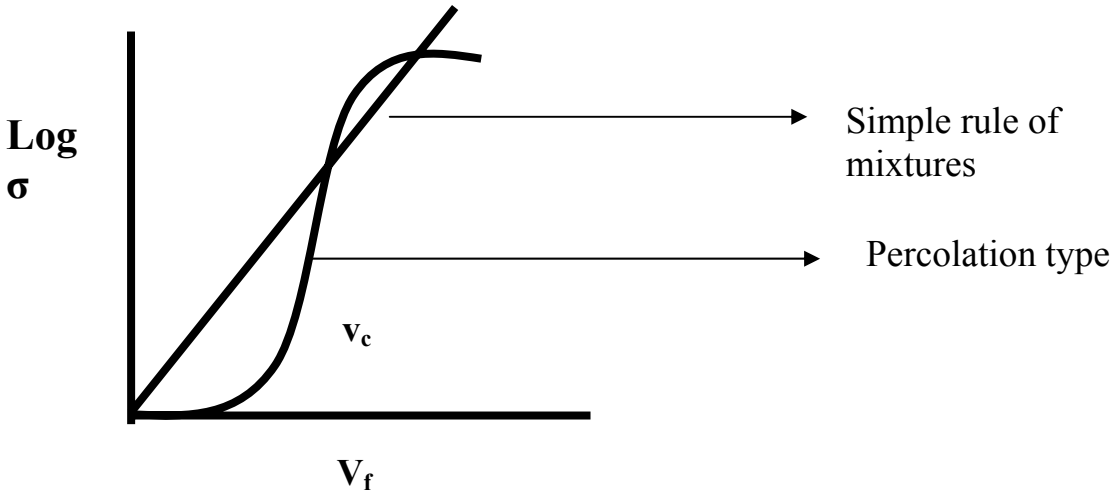

Figure. 1.4. Electrical conductivity variation in CPCs

The nonlinear variation of electrical conductivity of CPCs is an advantage which aids processing as the loading of filler required to cause saturation in electrical conductivity is less. When the filler loading is high, the flow properties of polymers will be affected. So it is very important to reduce the percolation threshold as much as possible retaining other properties. The percolation threshold depends on particle size, shape, concentration, dispersion and orientation of fillers along with processing routes. The electrical conductivity of CPCs is affected by the degree of filling and proximity of conducting particles. There can be three situations,

1. No contact between fillers
2. Close proximity
3. Physical contact

When the conducting particles are isolated, the composite remains as an insulator although its dielectric properties may change significantly. When the conductive particles are in close proximity, current can flow due to electron crossing the gap. Under a given voltage, it increases exponentially with decreasing the gap size. The electron transport across an insulator gap can happen by hopping or tunneling mechanisms. For tunneling conduction, the insulating gap should be less than 50A^{o}[47]. Tunneling is a special case of hopping which does not require energy exchange for electron transport from valence band of ions or molecules to the conduction band of the other side where as hopping requires increase in the energy level of the electrons to cross the gap and hence involves activation energy. When the volume fraction of conducting filler is above the percolation threshold, the composite conducts through particle network by the conduction mechanism of the particles. There can be band type conduction. Hopping and band type conduction can be identified through the frequency dependent conductivity studies. A composite which conducts by hopping mechanism will exhibit higher ac conductivity than dc conductivity. Scarisbrick[48] claims that in highly loaded composites, the filler particles touch each other. This conclusion is arrived from the I-V characteristics of the composite which exhibit a linear variation i.e., ohmic. The network formation need not be a physical contact. This is treated as a percolation process. Percolation model is a statistical

representation which refers to a means of continuous network formation though a lattice, taking in to account the relative concentrations of the two materials.

1.9. Percolation Theory

Percolation theory refers to a class of models that describe properties of materials taking in to consideration the formation of network among its constituents. There are two types of percolation models namely site and bond percolation. In the former case, points are defined on a lattice such that in every lattice site there is probability 'p' for a point to exist. In the later case bonds are defined between neighboring sites on a lattice. The main difference between the two types is that the site percolation lattice, vertices are relevant entity where as in bond percolation, lattice edges are the main.

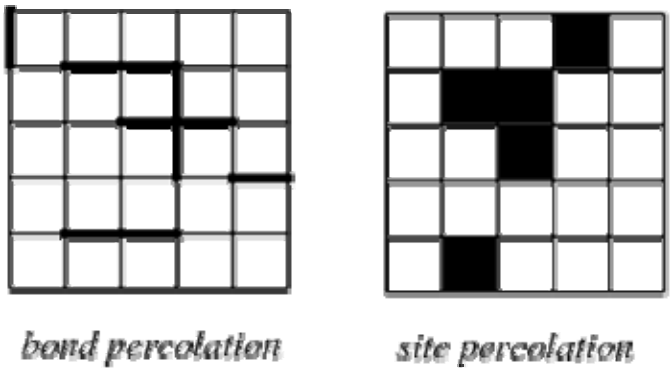

Figure. 1.5. Different types of percolation

In both cases, structures of connected points known as clusters will be formed with increase in the probability 'p'. Eventually, a cluster that has a path that spans the whole system will be formed. If the lattice is infinite in extension, the cluster will be of infinite size. The value of 'p' which creates this cluster is critical probability 'p_c'. The first of such model was used in 1940 to explain polymerization phenomenon that leads to gelation. The term percolation was coined Broadbent and Hammersley in the year 1957. This model is applied to fluids in porous media, to study the effect of dopants in semiconductors etc. In many binary conductive composites, the electrical conductivity variation and the percolation threshold are theoretically predicted by percolation models though this model can't be used for all conducting systems. One of the shortcomings of statistical percolation model is that it requires a specified lattice from which the statistical analysis of 'p_c' is made. In truly random situation lattice can't be specified. Further the percolation theory is applicable to those systems

where the properties of components vary significantly. The phenomenogical nature of percolation equation with fitting parameters that bears no clear correlation to the real features of microstructure. The classical percolation equations are given in equations 2 and 3 respectively below.

$$\sigma_{eff} = \sigma_2 (V_f - V_c/1 - V_c)^{t''} \qquad V_f > V_c \qquad (2)$$

$$\sigma_{eff} = \sigma_1 (V_c - V_f / V_c)^{-s} \qquad V_f < V_c \qquad (3)$$

where σ_{eff} is the effective conductivity of the composite consisting of a conductor with conductivity σ_2 and an insulator with a conductivity σ_1, V_f is the volume fraction of filler, V_c is the percolation threshold. 't''' and 's' are critical exponents characterizing the conductivity in the conducting and the insulating phase, depend on the dimensionality of the network formation. The values of the exponents when three dimensional network formation exists are t''=2 and s=0.87[49] for lattice percolation. For the comment of network formation quite often equation 4 is used.

$$\sigma = \sigma_o (V_f - V_c)^{t''} \qquad V_f > V_c \qquad (4)$$

where σ is the composite conductivity. The percolation exponent is not universal as in many cases the value is greater than two[50-53] for three dimensional network. This is accounted when tunneling conduction is operative in the system[54].

Monte Carlo method is used to model the fillers in polymer matrices to achieve percolation. A grid either in two or three dimension is defined and sites are distributed randomly on the grid by a random number generator. Circles, spheres or line segment with a given length and orientation are placed at a portion of the sites. The system is checked for connectivity between the particles. If two particles contact each other, they are regarded as cluster. If a cluster exists and spans the entire sample, the system is said to percolate otherwise additional particles are added to the grid site and checked for connectivity. This procedure is continued until a cluster is formed which spans the grid. The volume fraction of filler is then reported as the percolation threshold. Pike and Seager[55] obtained threshold data for both circle and squares on a random two dimensional lattice. Balberg and Binenbaum[56] extended the work of Pike and Seager for conducting sticks. Wang and Ogale[57] proposed a more realistic model assuming particles to be hard having impenetrable core surrounded by a soft shell.

With this assumption Monte Carlo simulation was used to find the percolation threshold.

1.10. Various Models Predicting Electrical Conductivity in Binary Composites

1.10.1. Thermodynamic Model

The conductivity variation in CPCs can't be modeled always with statistical percolation taking in to consideration only the network formation. The volume fraction of filler causing variation in the conductivity depends on the type of polymers also and not only on the filler shape and size. Mamunya *et al*.[58] have taken other factors like surface energy of filler, polymer and melt viscosity of the polymer. At all points above percolation threshold, the conductivity variation of the composite is described by equations 5-7.

$$\text{Log } \sigma = \log \sigma_c + (\log \sigma_m - \log \sigma_c)(V_f - V_c/F - V_c)^{k'} \quad (5)$$

and

$$k' = K V_c / (V_f - V_c)^{-0.75} \qquad K = A - B\gamma_{pf} \quad (6)$$

Where σ is the composite conductivity, σ_c- conductivity at the percolation threshold, σ_m – conductivity at F, F- maximum packing fraction, V_f- volume fraction, V_c – percolation threshold, γ_{pf} - interfacial tension, A and B are constants.

$$\gamma_{pf} = \gamma_p + \gamma_f - 2\,\gamma_p\,\gamma_f \quad (7)$$

where γ_p being the surface energy of the polymer and γ_f that of filler. This model is successful in predicting the conductivity variation in carbon black filled composites but not to other fillers[58].

1.10.2. Structure Oriented Model

1.10.2.1. Nielsen Model

This model takes in to account the filler orientation and aspect ratio in the composite. These parameters depend on the processing conditions. For example injection molding of composites leads to alignment of fillers within a polymer due to the flow through the nozzle and the mold. Alignment of fillers can cause anisotropy of electrical conductivity in different direction. Extrusion and injection molding can shorten the fiber length resulting in different aspect ratio of the filler.

One structure oriented model was proposed by Nielsen[59] which relates the conductivity of the composite with the aspect ratio (L/D) and coordination number of

the filler in a binary composite. The equations used in Nielsen's model are given in equations 8-10 below.

$$\sigma_c = \sigma_{poly} [(1 + ABV_f) / (1-B\psi V_f)] \quad (8)$$

$$B = [\sigma_f/\sigma_{poly} - 1] / [\sigma_f/\sigma_{poly} + A] \quad (9)$$

$$\Psi = 1 + [(1-V_m) / (1- V_m^2) V_f] \quad (10)$$

Where V_f is the volume fraction of filler, σ_c- conductivity of the composite, σ_{poly} – polymer conductivity, σ_f – filler conductivity and V_m-maximum packing fraction. In this model A is a function of aspect ratio and B is equal to one for polymer system. Nielsen used these equations to describe electrical, thermal conductivity and the modulus of metal-polymer systems. Bigg[60] showed that those equations describe thermal conductivity of composites but not the electrical conductivity. Weber and kamal[61] proposed two models accounting for the filler concentration, orientation, dimension and aspect ratio. They studied nickel-coated graphite fibers in polypropylene.

1.10.2.2. The Model of McCullough

McCullough took in to consideration transport properties of homogeneous materials. In order to account for the conductivity variation, he introduced chain length factor λ. The values of λ have to be determined by quantitative analysis of the structure of mixtures. The exact procedure of doing this is described in the work of Berger and McCullough[62]**.** The equation developed by them accounts for the anisotropy of the conductivity of the mixtures.

1.10.2.3. Ondracek Model

This model is valid for mixtures having a statistical structure and reaching their equilibrium states. By superposition of conductivities of the individual phases, the conductivity of the mixture is obtained. The model structures involve the conductive phase in the shape of elliptical eggs. The ac conductivity of polyester-aluminium powder mixture is predicted by this model.

1.10.3. Geometrical Percolation Models

In order to explain the percolation phenomenon in dry premixed and sintered mixtures of conductive and insulating powders, this model was proposed. This class of models assumes that during sintering process, the insulating powder particles are

deformed more or less as regular cubic lattices and the conductive powder particles are arranged in more or less in a regular manner.

1.10.3.1. Model of Slupkowski

The diameters of the insulating and the conducting particles are considered as the main influencing parameters as far as electrical conductivity is concerned. Slupkowski ended with following equations 11 and 12.

$$\sigma = 2\,\pi\,\sigma_f \quad d'' \,(\,[x] + P\,) / [D' \ln \{\,1 + ([x] + 1)\,\alpha\,\}] \qquad (11)$$

where σ is the conductivity of the mixture, σ_f the conductivity of the conductive powder. D' is the diameter of the insulating powder particles, d''- diameter of the conducting particle, P the probability for the occurrence of the network, only consisting of conductive particles.

$$[x] = [(1/1\text{-}V_f)^{1/3} - 1]\; D'/2d'' \qquad (12)$$

Where V_f is the volume fraction of the conductive powder.

1.10.3.2. Rajagopal and Satyam Model

This model is valid for wax-graphite system. They used the real material structure in the conductivity derivation. In this model structure, the wax particles consist of cubic grains of edge length D". The graphite particles, being slightly deformed, cover the surfaces of the wax particles and have the diameter d'''. The final equation of the conductivity derived by them is given in equation 13.

$$\sigma = \sigma_f\, 2\, r\, (V_f 3\, D'' - 4\, d''')\, (3\, D'' - 2\, d''') / D''^2\, d''' \qquad (13)$$

where σ is the conductivity of the mixture, σ_f is the conductivity of the conductive particle, V_f is the volume fraction of the conductive powder and r is the radius of the contact area between adjacent conductive particles.

1.11. Effective Media Theories

In this theory a spherical or ellipsoidal grain is considered to be surrounded by a mixture, which has the effective conductivity of the medium. It is mainly applied to composite systems with well separated sub phases for the prediction of large volume average values of electrical and thermal conductivity. This theory is valid for very dilute cases. There are two cases for which effective media theory exists called the symmetric and asymmetric cases. The symmetric case assumes that all space is filled by a random mixture of spherical or ellipsoidal particles of two or more components.

McLachlan[63] proposed a generalized effective medium theory (GEM). The GEM theory has been successfully applied to describe piezoresistive behavior of Fe_2O_3 filled with flexible epoxy.

1.12. Charge Transport in CPCs

Percolation phenomenon and the conduction mechanisms in conducting polymer composites are the two major areas of research as far as electrical properties of CPCs are concerned. The conduction mechanisms in CPCs are not universal. This can be realized from the plethora of mechanisms proposed to describe electrical conductivity variation in binary conducting composites. As far as microscopic conduction processes are concerned Pike and Seager in 1977 commented that "there is an incredible diversity among the models which have been proposed in the published literature". Various conduction mechanisms have been grouped under four categories as proposed by Pike and Seager.

1.12.1. Uniform Model

According to this model, very small conducting particles are dispersed in the insulating polymer matrix. An impurity conduction type mechanism can be expected and is more probable in the low concentration of particles.

1.12.2. Uniform Channel Model

There will be conducting paths due to conducting particles which span the entire sample. The particles can be sintered or randomly boned. In this case tortuosity and density modification of conducting channels causes variations in the conductivity. This model is applicable to the case of high filler concentration.

1.12.3. Non-Tunneling Barrier Model

In this type, the conducting channels are randomly interrupted by semiconducting or weakly insulating barriers. The major mechanisms in this case are Space charge limited conduction, Pool-Frenkel effect and Schottky emission.

1.12.4. Tunneling Barrier Model

In this case the conducting channels formed by the filler particles will be interrupted by thin barriers to allow a tunneling process, either directly between the particles or through one or several intermediate states within the insulator.

Schematically all these models are represented in the following Figure 1.6.

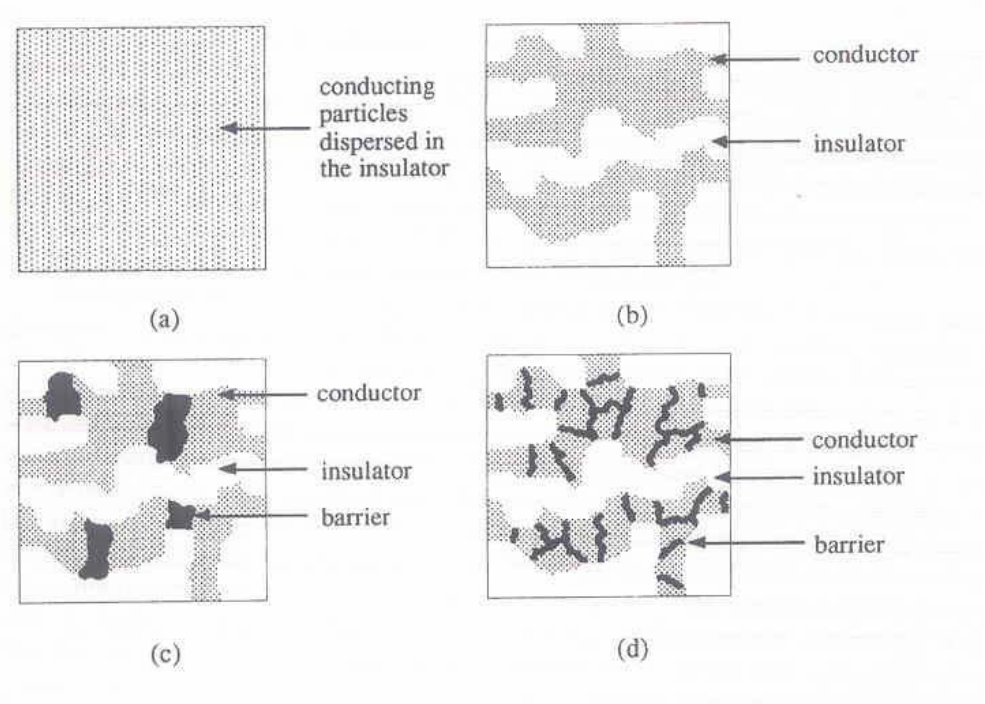

Figure.1.6. a) Uniform model b) Uniform channel model c) Non-tunneling barrier model d) Tunneling barrier model

Since the CPCs have atleast two phases out of which the polymer is an insulator, it is customary to understand the electrical conduction through polymers as polymer film will be surrounding the conducting filler.

1.13. Electrical Conduction in Thin Film Insulator

The conductivity of insulators is very less due to less volume generated charge carriers. The electrical properties of insulators are not only determined by their intrinsic properties but also by the nature of electrode-insulator contact. A suitable contact (Ohmic) is capable of injecting additional charge carriers in to the insulator, far in excess of the bulk generated carriers. Also application of few volt is capable of causing high fields to be generated in a thin film insulator at the cathode-insulator interface. For fields in excess of 10^6 V/cm, field emission injection of relatively large currents from the cathode to the conduction band of the insulator is possible treating majority of charge carriers being electrons. The intrinsic current density carried by an insulator is given by the following equation 14.

$$I = e \mu N_c E \exp (- E_g / 2 K T) \quad (14)$$

Where μ-mobility of the charge (~100 cm^2/V-S), E- the field (10^6 V/cm), E_g is the band gap and N_c is the effective density of states in the insulator. The order of current density obtained by the application of voltage is many order less for the sample. Further, the thermal activation of energy associated with the conductivity of the film is much smaller than what would be expected if the conductivity were intrinsic.

1.14. Metal-Insulator Contact

The insulator between electrodes which are conducting offers barrier for electron injection from the electrode to the sample. The barrier height is very important as the charge carriers have to cross that for conduction. At thermal equilibrium, the work function of metal (ψ_m) and that of the insulator (ψ_i) should be equal. Even when they are not equal when contact between them is made, equilibrium is maintained because of the charge transfer from the electrode to the material and vice-versa. Normally at reasonable fields, the charge carriers available to enter the insulator will be sufficient to account for the carrier replenish. Under this condition, I-V characteristics of the sample will be "bulk limited". At high fields or if the contact is blocking, the current capable of being supplied by the cathode to the insulator will be less than that capable of being carried in the bulk of the insulator. Under these conditions the I-V characteristics of the sample will be controlled primarily by conditions existing at the cathode-insulator interface. This conduction process is referred to as "emission or contact limited". There can be three types of contact that can exist at the metal-insulator interface as given below,

1) Ohmic contact
2) Neutral contact
3) Blocking contact

1.14.1. Ohmic Contact

This type of contact exists when the work function of the electrode (ψ_m) is less than that of the insulator (ψ_i) which means that the electron can be readily supplied from the electrode. Under this condition electrons are injected from the electrode to the conduction band of the insulator, thus giving space charge region in the insulator. The space charge region is shown in the following Figure 1.7.

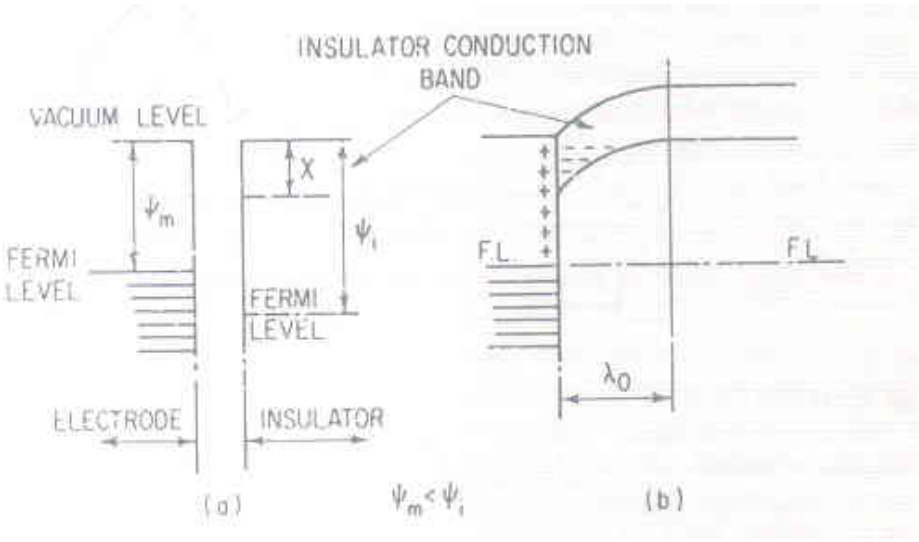

Figure. 1.7. Band diagram for Ohmic contact

In order to satisfy charge-neutrality requirements an equal amount of positive charge, Q_c accumulates on the electrode surface. The electrostatic interaction between the positive and negative charges induces a local field within the surface of the insulator, the strength of which falls of with distance from the interface and zero at the edge of the space charge region. This field causes the bottom of the conduction band to rise with distance of penetration until it reaches the equilibrium value $\psi_i - \chi$ where χ is the insulator affinity. The field E within the accumulation region is related to the space charge density $\rho(x)$ within the accumulation region by Poisson's equation given in equation 15.

$$dE / dx = \rho(x) / \varepsilon\varepsilon_o \qquad (15)$$

where ε is the dielectric constant and ε_o is the permittivity of free space.

1.14.2. Neutral Contact

This happens when the work function of the electrode is equal to that of the insulator i.e., $\psi_i = \psi_m$. The total amount of charge injected in to the insulator is zero which means the conduction band is flat up to the interface and no band bending exists.

1.14.3. Blocking Contact- Schottky Barrier

This kind of contact exists when the work function of the electrode is greater than that of the insulator i.e., $\psi_m > \psi_i$. A space charge region of positive charge, the depletion region is thus created in the insulator and equal negative charge resides on the electrode. As a result of electrostatic interaction, the bottom of the conduction band

bends until the Fermi level within the bulk of the insulator lies ψ_i below the vacuum. The insulator is assumed to have large density of donors.

1.15. Barrier Limited Conduction

1.15.1. Tunneling Conduction

When the energy of the electron is less than the interfacial potential barrier in a metal-insulator-metal junction up on which it is incident, classical physics predicts that the electron cannot penetrate the barrier. The quantum mechanical wave function $\psi(x)$ of the electron has finite value within the barrier. The wave function decays rapidly with the depth of penetration of the barrier from the electrode-insulator interface and for barrier of macroscopic thickness, is essentially zero. However if the barrier is thin (< $100A^o$), the wave function has a non zero value at the opposite interface which means that it can pass from one electrode to the other. When this happens, one can say that electrons have tunneled the barrier. These phenomena are shown in Figure 1.8.a and b respectively.

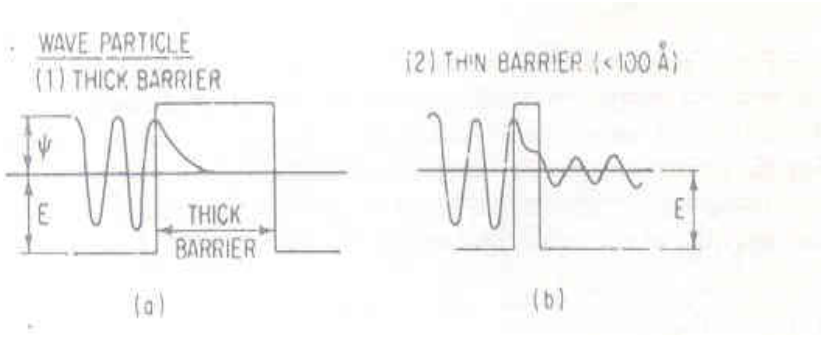

Figure. 1.8. Tunneling conduction a) thick barrier b) thin barrier

At very high voltages, Fowler-Nordheim tunneling occurs. The current-voltage characteristic is given by the following equation 16.

$$J = 3.38 \times 10^{10} (E^2/ \varphi') \exp (- 0.69 \varphi'^{3/2} / E) \quad (16)$$

Where J is the current density, E is the filed in the insulator and φ' is the barrier.

1.15.2. Schottky Conduction

Image force effects play an important role in the conduction process when the contact is electrode limited. The potential at the electrode-insulator interface changes smoothly due to image forces. This arises as a result of the metal surface becoming polarized (positively charged) by an escaping electron, which in turn exerts an

attractive force. The potential energy of an electron due to image force is given in equation 17 as given below.

$$\varphi'_{im} = - e^2 / 16 \pi \varepsilon_o \varepsilon^* x \quad (17)$$

Where x is the distance of the electron from the electrode surface, ε^*- high frequency dielectric constant. The potential step with respect to Fermi level at a neutral barrier with image potential as a function of the distance x is given in equation 18.

$$\varphi'(x) = \varphi'_o + \varphi'_{im} = \varphi_o - e^2 / 16 \pi \varepsilon_o \varepsilon^* x \quad (18)$$

Where φ'_o is the distance between the Fermi level of electrode and the bottom of the insulator conduction band.

When an electric field exists at a metal-insulator interface, it interacts with the image force and lowers the potential barrier. The potential energy of the barrier under the influence of the field with respect to the Fermi level of the electrode is given in equation 19.

$$\varphi'(x) = \varphi'_o - e^2 / 16 \pi \varepsilon_o \varepsilon^* x - e E x \quad (19)$$

The above equation has maximum at $x_m = (e / 16 \pi \varepsilon^* \varepsilon_o E)^{1/2}$

The change $\Delta\varphi' = [\varphi'_o - \varphi' (x_m)]$ in the barrier height due to interaction of the applied field with the image potential is given in equation 20.

$$\Delta\varphi'_s = (e^3 / 4\pi \varepsilon_o \varepsilon^*)^{1/2} E^{1/2} = \beta E^{1/2} \quad (20)$$

Because of image force lowering of the barrier, the electrode-limited current does not saturate according to Richardson law $J = A T^2 \exp (- \varphi'_o/K_BT)$ but rather obeys Richardson-Schottky law as given in equation 21.

$$J = A T^2 \exp (- \varphi'_o / K_BT) \exp (\beta E^{1/2} / K_BT) \quad (21)$$

Where $A = 4\pi em (kT)^2 / h^2$. The above equation was first applied to metal-vacuum interfaces. This is illustrated in the following Figure 1.9.

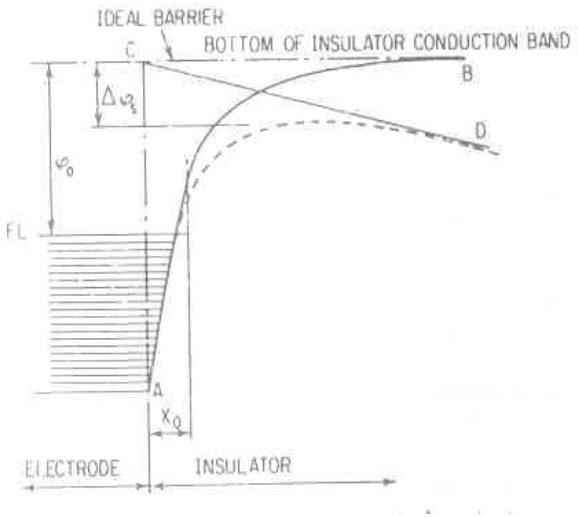

Figure. 1.9. Schottky effect at a neutral contact

1.16. Bulk Limited Conduction

Two major types of conduction falls under this category as given below.

1. Space charge limited conduction if ohmic contact exists (SCLC)

2. Pool-Frenkel conduction i.e., the field assisted thermal release of carriers from traps in the insulator.

1.16.1. Space Charge Limited Conduction

This type of conduction is important because the injection current is independent of the mechanism of charge generation and only depends on the transport and trapping of the carriers within the crystals. I-V relationship of an organic semi conductor is linear at low voltages but becomes nonlinear at high field. The nonlinearity can happen due to two reasons.

1. At high field, there will be a large concentration of charge carriers present between the electrodes which constitute space charges.

2. The existence of traps in samples also can cause nonlinearity in I-V characteristics of organic semiconductors. They may be due to wide range of crystal defects like dislocation, stacking faults, impurities etc. The traps may be deep or shallow. When the distance from the bottom of the trap and the bottom of the conduction band is large compared to K_BT, one can speak of deep traps.

The main effect of shallow traps is to reduce the mobility of the carriers, since the thermal energy suffices to re-dissociate a carrier from the trap. The liberation of carriers from deep trap is a rare event. Filled traps don't contribute to space charge.

Assuming that the number of charge carriers to be n', and local electric field 'E' are functions of locations in the sample (x) and the steady state current density is given in equation 22 below.

$$J = e\, n'(x)\, \mu\, E(x) \tag{22}$$

The relation between the field gradient and the number of charge carriers is defined by Poisson's equation as given in equation 23.

$$dE(x) / dx = en'(x) / \varepsilon \tag{23}$$

where ε is the dielectric constant.

The integral of the local field across the sample is the applied potential V as given in equation 24.

$$\int_0^x E(x)dx = V \tag{24}$$

When ohmic contact exists, immediately adjacent to electrodes, the electric field is zero and there is an infinite supply of charge carriers. i.e., $n'(0) = \infty$; $E(0) = 0$.

Substituting n(x) from Poisson's equation in to the equation of current, the current density obtained is described by equations 25-27.

$$J = \varepsilon\, \mu\, E(x)\, [\, dE(x)/dx] \tag{25}$$

Integrating $Jx = \varepsilon\, \mu\, E^2(x) /2$ and

$$V = \int_0^d (2J / \varepsilon\, \mu)^{1/2}\, x^{1/2}\, dx \tag{26}$$

Which yields

$$J = 8\, \varepsilon\, \mu\, V^2 / 9\, d^3 \tag{27}$$

Where d is the distance between the electrodes.

The above equation is known as child's law for trap free insulator. Without traps the above equation shows that the SCLC is independent of temperature which is contrary to the observation. When traps are present the space charge current will be decreased by several orders of magnitude. In presence of traps, the current density due to SCLC is given in equation 28 below.

$$J = 8 \varepsilon \mu \Theta V^2 / 9 d^3 \quad (28)$$

Where Θ is the trap limiting parameter which is defined as given in equation 29 below.

$$\Theta = \rho_f / \rho_t = N_c / N_t \exp(-E_t / KT) \quad (29)$$

E_t – energy level of the trap, N_c – number of free carriers without traps, N_t – Number of shallow traps. Figure 1.10 shows I-V Characteristics due to SCLC mechanism.

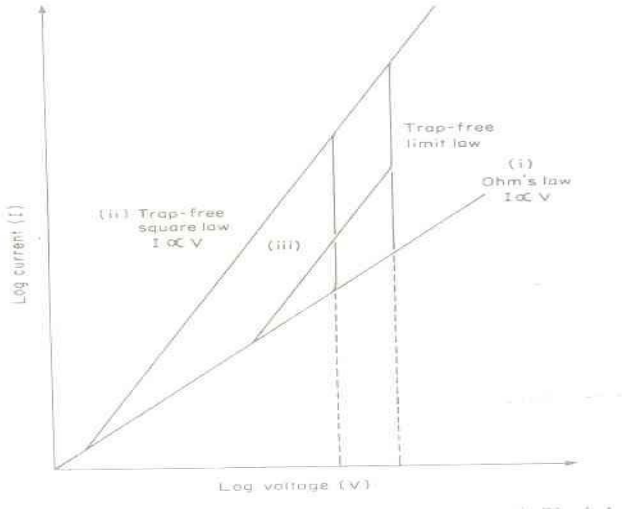

Figure. 1.10. I-V Characteristics of a solid with space charge conduction

1.16.2. Pool-Frenkel Mechanism

Field assisted thermal ionization is known as Pool-Frenkel effect. The nature of forces binding electron to the centre in a donor is columbic and therefore of relatively long range where as in traps it is noncoloumbic and short range. The process is a bulk analog of Schottky effect at an interfacial barrier. Since the potential energy of an electron in a coulombic field is four times that due to image force effects, the Pool-Frenkel attenuation of a coulombic barrier in a uniform electric field is twice that due to Schottky effect at a neutral barrier as given in equation 30.

$$\Delta\varphi_{PF} = (e^2 / \pi \varepsilon_0 \varepsilon^*)^{1/2} E^{1/2} = \beta_{PF} E^{1/2} = 2 \Delta\varphi_{Schottky} \quad (30)$$

This result has been applied to host atoms in bulk semi conductors and insulators. In general for Pool-Frenkel conduction the I-V behaviour is as given in equation 31.

$$\text{Log } I \alpha E^{1/2} \quad (31)$$

The following Table1 summarizes various conduction mechanisms and the corresponding

J-V relations.

Table 1

J-V characteristics various conduction processes

Conduction Mechanism	J-V Relation
1. Schottky Emission	$J = A T^2 \exp(-\varphi' / kT) \exp(\beta_{Schottky} E^{1/2} / k T)$
2. Pool-Frenkel Effect	Same as above $\beta_{PF} = 2 \beta_{Schottky}$
3. Space Charge Limited Conduction (SCLC)	$J = (8/9) \mu \Theta \varepsilon V^2 / d^3$
4. Fowler-Nordheim Tunneling	$J = (3.38 \times 10^{10} E^2 / \varphi') \exp(-0.69 \varphi'^{3/2} / E)$

Where J is the current density, A is Richardson-Schottky constant (120 A/cm^2), T is the temperature, φ'- the barrier height, $\beta_{Schottky}$- Richardson-Schottky exponent, V is the voltage, d- the thickness of the layer, μ- the mobility of the charge carriers, Θ- the trap parameter, ε is the dielectric constant of the medium and E is the field across the barrier.

1.17. Electrical Contact Between Filler Particles

The composite resistivity is largely dependent on the contact between the filler particles. Two effects contribute to contact resistance. One is constriction resistance and the other being tunneling resistance between the particles. Thus the contact spots are the regions of largest resistance and thus of highest electrical losses.

The mechanical properties of fillers need to be known for the description of contact resistance and area of the contact spot. The radius 'a' of the contact spot can be calculated from the elastic properties of the filler particles if the force between them and the particle radius are known. It is assumed that the contact arises between a protrusion or sharp edge of one particle and a flat surface of a neighbor particle. If the protrusion has a radius 'r'' at the contact spot, the elastic force between the grains for small deformation is given in equation 32[64] below.

$$F = (2/3) (Y'/1-\nu'^2) (a^3 / r') \quad (32)$$

Where Y' is the Youngs modulus and ν' is Poisson's ratio. The constriction resistance is described by equation 33 given below.

$$R_c = (1/2)\ \rho_b\ [2\ E/3\ (1-\nu'^2)]^{1/2}\ F^{-1/3}\ r'^{-1/3} \qquad (33)$$

where ρ_b is the bulk resistivity of filler particles. Thus easier the particle can be deformed under applied force, the larger the protrusion radius becomes. Hence soft materials can be expected to yield smaller constriction resistance compared to hard materials.

1.18. Are Polymers Dummy Candidates???

The mechanical and thermal properties of polymers have significant influence on the electrical properties of conducting composites. Various polymers such as epoxy, elastomers etc. have different mechanical properties. The constriction resistance between filler particles depends on the contact forces between the grains. Higher contact forces may improve the conductivity. Hence, internal stresses in the polymer matrix caused by shrinkage, external mechanical actuation or thermal expansion play an important role on the electrical conductivity of conducting composites.

1.18.1. Internal Elastic Properties

Shrinkage of polymers during processing can induce internal stress. This not only reduces interparticulate distance of fillers but also causes cracks. The origin of internal stress differs for duromers, elastomers and thermoplastic materials. In elastomers and duromers, cross-linking can cause shrinkage where as in thermoplastics thermal shrinkage is the main factor. Miller[65] studied the resistivity of silver (Ag) filler in epoxy resin during curing. While the epoxy hardened, the resistivity of the composite decreased by two to five orders of magnitude.

Larger change in resistance for TiB_2 in epoxy resin is obtained than silver in epoxy during curing. Thus these studies show that the thermal contraction of a composite can have a huge influence on the resistivity. Even this contraction is observed for high loading of fillers i.e., loading corresponding to above percolation threshold, which can't be explained by percolation theory. When the hardness of the filler is increased, the particles do not stick together and makes the resistivity of the composite sensitive to a small micromechanical changes. TiB_2 has higher hardness compared to Ag.

1.18.2. Thermal Properties

Polymers show three different reversible transitions i.e., crystallization and melting for semicrystalline polymers and glass transition for amorphous polymers. All these transitions are related to large volume change or pronounced change in the thermal expansion. For particulate composites when heated nearer to the melting temperature, the interparticulate distance can be increased resulting in increased resistivity. A strong positive temperature coefficient of resistance (PTC) in conducting polymers close to the melting temperature was first discovered by Pearsen at Bells lab in 1939. Kohler observed a significant change in resistivity for PTC materials. After his work, industrial focus on the PTC materials increased. The transition from low resistivity to higher values can be used for current limiting applications.

Band theory is used to delineate between materials such as conductors, semi conductors and insulators. When the interaction between atoms increases, the width of the allowed energy band decreases implying increase in the effective mass (the parameter relating to the response of the charge carrier to an applied field) of the charge carrier and hence mobility decreases. Polymers are either semicrystalline or amorphous in nature. In semicrystalline polymers, the phase boundary can act as a trap and hence the crystallinity of polymer affects electrical properties. Further many polymers have polar groups and each dipole can act as electron/hole trap. So polymer structure also affects electrical conductivity. Thus the role of polymers though insulating in nature is commendable. Hence polymers are “not dummy candidates”.

1.19. DC and AC Behavior of Conducting Polymer Composites (CPCs)

In the case of semiconductors and insulators, the temperature dependent conductivity can be expressed as given in equation 34 below.

$$\sigma = \sigma_o \exp (- E_a / K_B T) \quad (34)$$

Where E_a is the activation energy, σ_o is the conductivity at infinite temperature. In the case of conducting particles dispersed in an insulating phase, when contacts are not formed, activation energy is required which makes the charges to migrate from one site to the other. The absence of extensive physical contacts of the inclusions or any conducting path, through which the current can percolate the whole system, prompts to investigate conductivity in the field of another charge transport mechanism. When

the concentration of conducting phase falls below the percolation threshold two models have been employed. One is variable range hopping (VRH) and the other being random free energy barrier model proposed by Dyre. The term hopping refers to sudden displacement of a charge carrier from one position to another neighboring position. It includes jump over a barrier and quantum mechanical tunneling.

1.19.1. Variable Range Hopping Model (VRH Model)

The temperature dependence of dc conductivity and the inherent charge transport mechanism in amorphous and disordered materials can be described by means of VRH model. The mechanism originally proposed by Mott is a phonon assisted charge transport process[66-67]. The charge carriers move (hop) from a localized state to a nearby localized state of different energy or to a localized state of similar energy with spatial separation from the initial state. If i and j denote the initial and the final state, the transition rate Γ_{ij} according to Mott is given in equation 35 below.

$$\Gamma_{ij} = \nu_o \exp (- 2 \alpha R_{ij}) \exp (- \Delta E_{ij} / K_b T) \quad (35)$$

Where α^{-1} is the decay length of the localized wave function, R_{ij} – hopping distance, ΔE_{ij}- energy difference between the two states and ν_o being a constant dependent on the strength of the charge carrier-phonon interaction which can be considered to represent the number of hop attempts per unit time.

Most of the hops have to be upward in energy. At high temperature many phonons are available which can assist in upward hopping. As these phonons freeze, the charge carrier has to look further and further to find an energetically accessible state. Consequently, the average hopping distance decreases with lowering the temperature and hence the name variable range hopping. The conductivity in VRH model decreases smoothly than in semiconductors. The VRH description is applicable to electrons, holes, polarons, bipolarons etc. If the interaction between charge carriers is neglected, the dependence on temperature of dc conductivity is given in equation 36.

$$\sigma (T) = \sigma_o \exp [- (T_o/T)^{\gamma}] \quad (36)$$

Where the parameter σ_o is the limiting value of conductivity at infinite temperature. T_o being the characteristic temperature that determines the thermally activated hopping among localized states at different energies and considered as a measure of

disorder[68-69]. γ is related to the dimensionality 'l'' of the transport process via equation 37.

$$\gamma = 1/1+l' \text{ where } l'=1,2,3. \quad (37)$$

In the conventional VRH model the parameters σ_o and T_o are functions of localization depth and density of states and described by equations 38-39.

$$\sigma_o = [\, 9\, N(E_F) / (\, 8\, \alpha\, K_B\, T\,)\,]^{\frac{1}{2}}\, e^2\, \nu_o \quad (38)$$

$$T = \lambda'\, \alpha^3 / [K_B\, N(E_F)] \quad (39)$$

Where $N(E_F)$ is the number of density of states at Fermi energy. ν_o is the hopping frequency which can be considered as an optical phonon frequency and λ' being dimensionless constant depending on the considered phonon process i.e., multiple or few phonon process. The applicability of VRH model is examined by plotting the experimental results in the form of $\log \sigma\, T^{1/2} = f(T^{-\gamma})$. The VRH model can be applied to conducting polymers[70].

1.19.2. Random Free-Energy Barrier Model

This model is known as symmetric hopping model, proposed by Dyre[71]. It describes frequency dependent conductivity over a wide range of frequencies in disordered solids at constant temperature. This model is based on the ascertainment that dc conductivity is thermally activated process where as ac conductivity is less temperature dependent. Thus the activation energy (E_a) of ac conductivity is lesser than that of dc measurements. In this model he assumed non-interacting charge carriers remain at sites with minimum energy. By employing a continuous time random walk approximation, Dyre arrived at the following equation 40 for ac conductivity in disordered solids.

$$\sigma_{ac}^{*} = \sigma_{dc}\, [j\omega\tau / \ln (\, 1 + j\omega\tau\,)] \quad (40)$$

Where σ_{dc} is the dc conductivity, ω the angular frequency and τ the relaxation time.

1.19.3. Hopping Conduction

In general, at constant temperature, ac conductivity can be expressed as given in equation 41 below.

$$\sigma_{ac}\,(\omega) = \sigma_{dc} + A\, \omega^n \quad (41)$$

Where σ_{dc} is the limit of $\omega \rightarrow 0$ limiting value of σ_{ac}. A and n are parameters and they depend on temperature and filler content. The above equation is called "the ac universality law". When the exponent 'n' lies between zero to one i.e. $0 < n \leq 1$, the conduction is by hopping. The critical frequency from where the conductivity increases has been found to depend on temperature and the conductive filler. The universal law is found to satisfactorily describe the ac behavior of ion-conducting solids[72-73], polymer composites[74-75] etc. The main differences between hopping and band transport are described below.

1) Phonon resists electron motion in band conduction where as it initiates electron hops in hopping conduction.

2) Absorption decreases with frequency of an applied field because of less collision in the case of band transport and the reverse is true for hopping type of transport.

3) Extended states σ (T=0) = σ_o for band conduction, where as for hopping conduction it is zero.

In the previous sections, the ac and dc conductivity studies of conducting polymer composites have been dealt very briefly. One more efficient characterization of solids not only CPCs but also electrochemical cells, solid state batteries etc, which gives wealth of informations about the electrical properties of the systems is the "Impedance Spectroscopy".

1.20. Impedance Spectroscopy (IS)

In an electrode-electrolyte system, where the electrolyte may be solid or liquid, the interfacial effect plays a dominant role in affecting the electrical conductivity. At an interface, physical properties, crystallographic, mechanical, compositional and electrical change precipitously and heterogeneous charge distribution affects the over all electrical conductivity. The more the number of interfaces, the polarization effects will be different as the solid electrolytes are polycrystalline materials having more grain boundaries, when the potential is applied. The rate at which the polarized region will change when the applied voltage is reversed is characteristic of the interface. Thus impedance spectroscopy is a very powerful tool to characterize any kind of solid or liquid material, ionic, semi conducting, mixed electronic-ionic and even insulators. Any intrinsic property that influences the conductivity of an electrode material system

or an external stimulus can be studied by IS. The parameters derived from an IS spectrum fall generally in to two types.

1. Those pertinent only to the material itself, such as conductivity, dielectric constant, mobilities of charges etc.

2. Those pertinent to an electrode-material interface region and diffusion coefficient of neutral species in the electrode itself.

The concept of electrical impedance was first introduced by Oliver Heaviside in 1880 and was soon after developed in terms of vector diagrams and complex representations by A.E. Kennelly and especially by C.P. Steinmetz. Impedance is a more general concept which takes phase in to consideration. An impedance Z(ω) is a complex quantity which

has real and imaginary part as shown in Figure 1.11 and is decribed by equations 42-44.

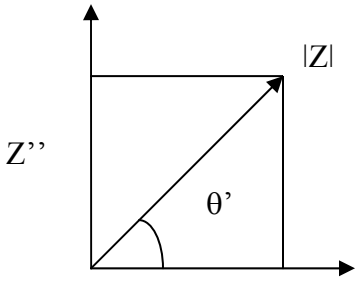

Figure. 1.11. Impedance resolved in to real and imaginary parts

. $$Z(\omega) = Z' + j\,Z'' \text{ where } j = \sqrt{-1} \quad (42)$$

$$\text{Re}\,(Z) = Z' = |Z| \cos\theta', \text{ Im}\,(Z) = Z'' = |Z| \sin\theta' \quad (43)$$

With phase angle

$$\theta' = \text{Tan}^{-1}\,(Z''/Z') \text{ and } |Z| = [(Z')^2 + (Z'')^2\,]^{1/2} \quad (44)$$

The impedance is time-invariant provided the system itself is time-invariant. This is due to the fact that impedance measurement deals with applying a monochromatic

signal $V(t) = V_m \sin(\omega t)$ involving the single frequency $\nu = \omega/2\pi$ which is applied to a cell and the resultant steady state current $I(t) = I_m \sin(\omega t + \theta')$ measured. In the impedance equation, the original time variation of the applied voltage and the resulting current has disappeared. Conventional IS consists of measurement of Z as a function of ω or ν over a wide frequency range. It is from the resulting structure of $Z(\omega)$ vs ω response that one derives information about the electronic properties of the full electrode-material system. The real electrode-materials system exhibits nonlinear behavior. For such systems IS measurement is meaningful in general only for signals of magnitude such that the over all electrode-material response is electrically linear. This can be made sure that the applied potential difference amplitude V_m is less than the thermal voltage $V_T = K_B T/e$ which is about 25 mV at 25°C. Under this condition the response of the system becomes linear.

1.20.1. Impedance Related Functions

Impedance by definition, a complex quantity and there are several measured and derived quantities. All of them may be generally called Immittances. First is the admittance $Y = Z^{-1} = Y' + jY''$; $I = Y\ V$ where Y is the admittance, I and V are the current and voltage respectively. Interms of resistance and capacitance components if $Z = R_s(\omega) - jX_s(\omega)$ and $Y = G_p(\omega) + jB_p(\omega)$, where reactance $X_s = [\omega\ Cs(\omega)]^{-1}$ and the susceptance $B_p = \omega C_p(\omega)$. Subscripts s and p stands for series and parallel. The other two quantities are the modulus function $M = j\omega C_c Z = M' + jM''$ and the complex dielectric constant or dielectric permittivity $\varepsilon = M^{-1} = Y/(j\omega C_c) = \varepsilon' - j\varepsilon''$. In these expressions $C_c = \varepsilon_o A_c/d$ is the capacitance of the empty measuring cell of electrode area A_c and electrode separation length is d. Four immittance functions related to each other.

1.20.2. Physical Models for Equivalent Circuit Elements

Experimental impedance data is approximated by the impedance of an equivalent circuit made up of ideal resistors, capacitors, inductors and probably various distributed elements. In such a circuit, a resistance represents a conductive path and a given resistor in the circuit might account for the bulk conductivity of the material. Similarly capacitances and inductances are generally associated with space charge polarization. In the impedance theory, the passive components are assumed to be

ideal. In the real system they are distributed in space. There are two types of distributions. The first is associated directly with nonlocal processes such as diffusion, which can occur even in completely homogeneous materials, one whose physical properties such as charge mobility are the same everywhere. The other type, exemplified by the constant phase element (CPE), arises because of microscopic properties themselves are distributed.

1.20.3. Some Simple Equivalent Circuits

Model 1

Resistance and capacitor in series

$$Z_{RC} = R_s - j / \omega C$$

when $\omega \rightarrow \infty$ or for very large C, $Z_{RC} \rightarrow R_s$. The complex plane or Nyquist diagram is given below.

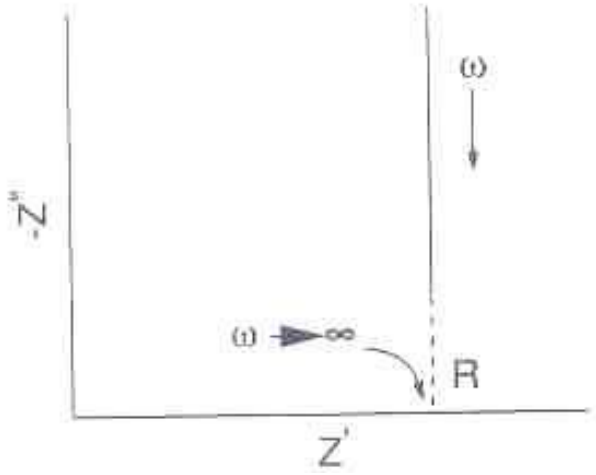

This model can be used to model a metal with undamaged high impedance coatings.

Model 2

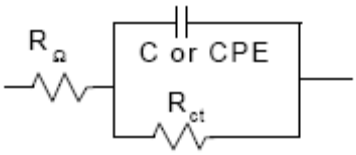

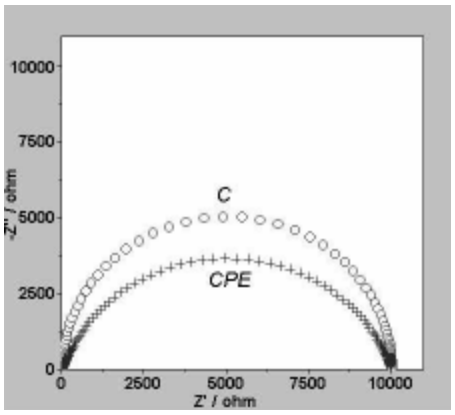

This equivalent circuit is known as Randle's circuit. It is being used to model a electrochemical cell. It includes solution resistance (R_Ω), double layer capacitance (C) and charge transfer resistance (R_{ct}). It is used to model corrosion processes and it is the starting point for other more complex models.

Model 3

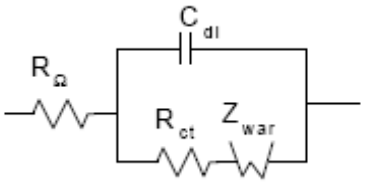

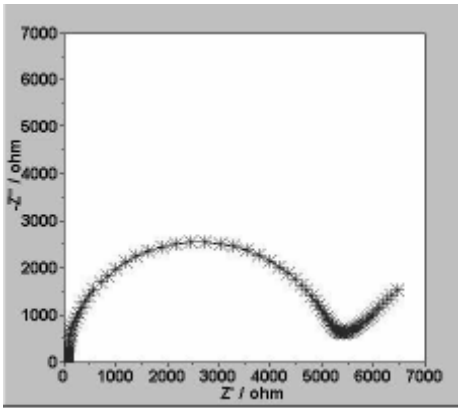

This model is used to describe electrode processes when both kinetics and diffusion are important. Z_{war} is the Warburg impedance which measures the difficulty of mass transport of the electroactive species. For kinetically favored reactions $R_{ct} \rightarrow 0$ and Z_{war} predominates. For difficult reactions $R_{ct} \rightarrow \infty$ and R_{ct} predominates.

1.20.4. Impedance Theory Applied to Conducting Polymer Composites

Conducting polymer composites can be modeled as parallel combination of resistor and capacitor with a resistor connected in series as shown in Figure 1.12.

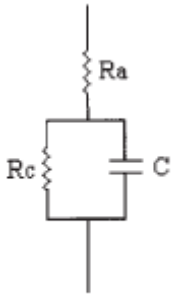

Figure. 1.12. Equivalent circuit of CPCs

Where R_a is the aggregate resistance, R_c is the bulk resistance of the material and C is the capacitance of a parallel plate capacitor with C =ε A/d. where ε is the dielectric constant of the polymer, A- area of the plate and d- distance between the plates. This model is applied to many two phase CPCs especially CB-polymer composites. The impedance of the above equivalent circuit is given in equations 45-47.

$$Z = R_a + 1/ (1/R_c + j\omega C) \quad (45)$$

$$= R_a + Rc/(1+\omega^2C^2R_c^2) - j\ (\omega R_c^2C)/(\ 1+\omega^2C^2R_c^2) \quad (46)$$

$$= Z_1 + j\ Z_2 \quad (47)$$

where Z_1 and Z_2 are real and imaginary parts. The relation between them can be written as given in equation 48 given below.

$$\{Z_1 - (2R_a + R_c)/2\}^2 + Z_2^2 = (R_c/2)^2 \quad (48)$$

Thus plotting Z_1 and Z_2 in Argand plane will describe a circle in the upper quadrant with center at $(2R_a + R_c)/2, 0)$ and a radius of $R_c/2$. At $\omega = \omega_p$, the real and imaginary parts can be equaled and the capacitance is obtained by the following equation 49.

$$R_c = 1/\ \omega_p C \quad (49)$$

Thus impedance measurements become very handy to evaluate the capacitance. In CPCs, conductive filler-polymer-filler configuration can be thought of as parallel plate capacitor and hence the interjunction capacitance can be obtained from impedance measurements.

1.20.5. Applications of Impedance Spectroscopy

1.20.5.1.Fuel Cells

The typical spectra of oxygen reduction reaction (ORR) at Pt/Nafion interface under different potential are shown in Figure 1.13. There are two pronounced arcs

accounting for the charge transfer at high frequencies and mass transport at low frequencies. The charge transfer arc decreases with increasing polarization due to the increased rapidity of the electrochemical kinetics and impedance arc due to mass transfer is progressively dominant.

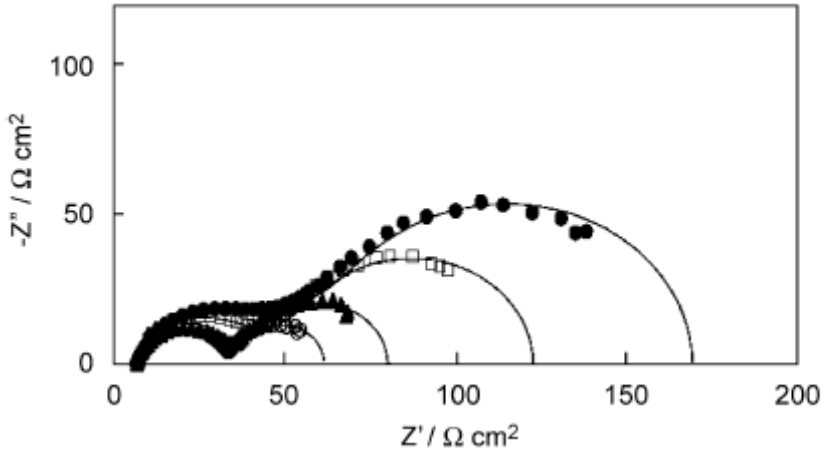

Figure 1.13. Impedance plot of oxygen reduction reaction at Pt/Nafion interface

The representative equivalent circuit, a modified Randles cell is given in Figure 1.14.

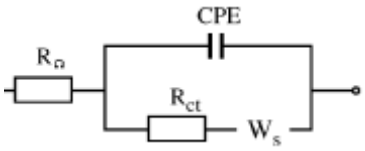

Figure. 1.14. Equivalent circuit diagram for ORR in fuel cell

In the Figure 1.14, R_Ω, R_{ct} and W_s represent ohmic resistance, charge transfer resistance and infinite length Warburg resistance. The conventional double layer capacitance is replaced by constant phase element (CPE) because the capacitance caused by the double layer charging is distributed along the length of the pores in the porous electrode. In addition in the Nyquist diagram, one may observe the infinite diffusion as a straight line with slope equal to one instead of finite diffusion as a semicircle at low frequency range. Wagner *et al*.[76] have summarized that

1. Without diffusion limitation only one arc appears.
2. With finite diffusion, two arcs appear with the low frequency arc corresponding to Nearnst-impedance
3. With infinite diffusion, a 45^o straight line, corresponding to Warburg impedance, is observed at low frequencies.

1.20.5.2. In Corrosion

Corrosion is defined as the spontaneous degradation of a reactive material by an aggressive environment. This phenomenon is electrochemical in nature. Impedance spectroscopy (IS) has been applied extensively in the analysis of the mechanism of corrosion of iron and other metals in aqueous solution. Keddam distinguished between various mechanisms that had been proposed for the electro dissolution of iron in acidified sodium sulfate solution. Since this particular study provides an excellent review of how impedance spectroscopy is used to discern reaction mechanisms. He calculated through his model, the interfacial impedance, which matches perfectly with the experimental results.

1.20.6. Limitations of Impedance Spectroscopy

1. In equivalent circuit analysis, the circuit elements are assumed to be ideal. The microscopic properties of the electrolytic cells are distributed in space. Under this condition ideal circuit elements may be inadequate to describe the electrical response. It has been observed that the use of distributed impedance elements like constant phase elements (CPE) in the equivalent circuit greatly aids the process of fitting observed impedance data for a cell with distributed properties.

2. An equivalent circuit involving three or more circuit elements can often be arranged in various ways and still yield exactly the same impedance.

1.21. Applications of Conducting Polymer Composites

1.21.1. Bipolar plates

A fuel cell is an electrochemical energy conversion device and not storage devices like batteries. It has continuous supply of fuel such as hydrogen, methanol etc and oxidant like oxygen, air etc. So long as fuel and oxidants are supplied one can derive power out of a fuel cell. Thus a fuel cell is a magic box which converts energy i.e. chemical energy to electrical energy. There are six major types of fuel cells such as alkaline fuel cells, polymer electrolyte membrane fuel cells (PEMFCs), direct methanol fuel cells, phosphoric acid fuel cells, solid oxide fuel cells and molten carbonate fuel cells. Out of these six types PEMFCs are focused for transport applications. Typical electrochemical reaction occurring at electrodes in a PEMFC is given below.

Anode : $H_2 \rightarrow 2H^+ + 2e^-$

Cathode : $1/2O_2 + 2H^+ + 2e^- \rightarrow H_2O$

Overall : $H_2 + 1/2O_2 \rightarrow H_2O$ + Electrical Energy + Heat Energy

Theoretical open circuit potential of PEMFC is 1.229V and the free energy is ΔG = -235.76 KJ/mol.

It can be seen from the above chemical reaction that the bye product is only water and thus fuel cell results in a clean energy. A typical fuel cell is shown in Figure 1.15.

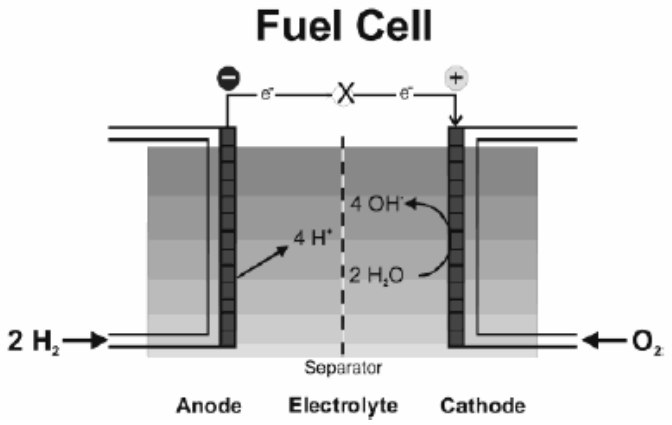

Figure. 1.15. Typical Fuel cell operation

Major layers of fuel cell are given below.

1. Membrane Electrode Assembly (MEA) which contains anode, cathode and the polymer membrane.
2. Catalyst (Platinum based).
3. Hardware (Backing layer, Current collector-Bipolar plates, End plates).

The electron stripped from the hydrogen molecule at the catalyst layer travels through external circuit to cause oxygen reduction at the cathode. The medium is a polymer membrane which allows protons to go through and forms a barrier for the flow of electrons. Normally, Nafion is used as a polymer membrane which is nothing but perflourinated membrane. The catalyst particle size is quite important and when it is in nanoscale, more hydrogen molecule will be stripped of their electrons. Gas diffusion layer allows gas molecules to reach the catalyst layer and also it exhibits conductivity for the electron transfer. It is usually made of porous carbon material.

Out of different components, bipolar plates are very important and further discussions will be focused on them only.

Bipolar plates are essential to distribute the fuel and oxidant, carry electrons to the external circuit, connect individual fuel cells in a stack etc. They should satisfy the following requirements to be commercialized.

1. Exhibit very high electrical and thermal conductivities.
2. Chemically inert and should remain inert for extended period of time.
3. Light weight, easily manufacturable by mass production techniques.
4. Non permeability of reactant gases.
5. Good mechanical properties and thermal stability.

Further the fuel cell stack should be light weight. Major weight of a fuel cell assembly corresponds to that of bipolar plates.

Commonly used bipolar plate material is graphite[77,78]. The major drawback of graphite based bipolar plates is that the flow filed should be machined which increases the cost as graphite is more brittle. So, several attempts have been made to look for alternate materials for bipolar plate applications. In this regard, stainless steel bipolar plates have been made with flow field patterns which are cheaper than the graphite plates. The density is more which can be compensated by making very thin bipolar plates made out of them. The main problem with these plates is the corrosion stability. When fuel cell is operated with humidity the stainless steel plate slowly corrodes which limits the cycle life of the fuel cell. Davies *et al*.[79] evaluated the short term and long term performance of different stainless steel plates. Surface oxide formation limits the out put of the fuel cell. In order to avoid that gold coating has been made on to the plates which increases the cost of the plate. A less expensive and light weight alternative is conducting polymer composites based bipolar plates. The polymer could be thermoplastic or thermosets. Usually thermoplastics are used since it can be recycled. Since the polymer composites based bipolar plates can be easily injection or compression molded which reduces the cost to a great extent. The flow properties of polymer will be affected due to increase in the filler loading as the viscosity of the polymer increases. In order to have high electrical conductivity and better flow properties, the filler concentration has to be kept minimum i.e., the

percolation threshold should be minimum. In this regard very high aspect ratio conducting fillers could be focused. Besmann *et al*.[80] fabricated a plate with carbon fiber and phenolic resin. Kuan *et al*.[81] have made vinly ester-graphite based bipolar plates by bulk molding process. About 60 wt% of graphite is loaded in the resin to have high conductivity. Thus the conducting polymer composites as fuel cell bipolar plate material have thrown lot of challenges as regard to electrical conductivity and minimization of filler concentration.

1.21.2. Thermal Interface Materials

Thermal interface pastes are needed for improving contacts, which are critical to the cooling of microelectronics. A thermal paste consists of an organic vehicle and a solid component that is thermally conductive. The solid component is in the form of particles and are dispersed and suspended in the vehicle. Thermal conductivity of the suspended phase is not the only parameter which should be taken in to account for its use as an interface materials. Other factors are the conformability and spreadability. Even if the interface material may be an excellent thermal conductor, poor conformability would make it ineffective as thermal interface materials. Carbon black paste acts as a thermal interface material when the surfaces of the plates used for heat transfer is smooth. For smooth surfaces CB paste is more effective than the silver paste though the thermal conductivity of silver is higher than that of CB. This is due to poor conformability of silver. The conformability of thermal interface material depends on both filler and the matrix. A stiff matrix will not allow the composite material to conform. Yu *et al*.[82] have reported that graphite nano platelets in epoxy act as a thermal interface material. The thermal conductivity of nanoplatelets will be poor in the perpendicular direction than the parallel as these nanoplatelets have a tendency to arrange parallel to the surface. The same is true for carbon nanotubes based thermal interface materials unless CNTs are vertically aligned. In short the requirements of a material to be used as thermal interface materials are given below.

1. High thermal conductivity
2. Low thermal contact resistance
3. Ability to wet out a surface
4. Mechanical compliance

Conventional approach is to fill the polymer (Grease, Silicone, Rubber etc) with conductive filler. The high degree of loading of filler affects the mechanical compliance. Zhang *et al*.[83] have made aligned CNT for thermal interface material application. Thus the application of conducting polymer composites in the development of thermal interface material can be realized.

1.22. Mechanical Properties of Conducting Polymer Composites

Intrinsic properties of polymers combined with the advantages of fillers led to the creation of many new materials. These materials have one or a combination of excellent mechanical, thermal and chemical properties. The mechanical properties of binary filled systems not only depend on the material properties of the individual phases and percentage of filler but also the size, shape, orientation and state of adhesion between the filler and the matrix is critical. The general effect of filler on mechanical properties can be predicted easily. However, ultimate stress and strain in composites not only depend on the matrix and filler properties but also on the fabrication processes. Flaws, voids and temperature profile affect the fracture properties. One effect of filler in the polymer is to increase the modulus. There are various models which are described to fit the mechanical behavior especially tensile modulus such as series model, series-parallel model, Cox equation, the Halpin-Tsai equations etc[84]**.** Another parameter which has not received that much attention as the modulus of the composites is ultimate tensile strength (UTS). This is primarily due to the complexity of fracture mechanisms. The prediction of UTS requires knowledge of the ultimate properties of the filler and the matrix, perfection of alignment and spatial distribution of filler particles, particle size and shape etc. with the applications mentioned in the above section, the mechanical properties of bipolar plate is crucial for its commercialization. Zheng *et al*.[85] have reported 16.8% enhancement in tensile modulus at 3 wt% loading of expanded graphite in HDPE and the composites were prepared by melt blending route. Zheng *et al*.[86] have reported 13% increment in tensile modulus for solution blended PMMA-5 wt% graphite composite. Chodak *et al*.[87] have measured the mechanical properties of PP-CB composites prepared by injection and compression molding. Young's modulus increases with the loading of CB up to 40 wt%. Yeh *et al*.[88] compared the experimental data of elastic modulus and

strength of MWCNT/phenolic resin and short carbon fiber/phenolic composites at the same filler contents up to 4 wt% of fillers. The nanotube reinforced systems showed better performance, although the improvements were not remarkable. Tai *et al*.[89] have examined the mechanical properties of SWCNT/phenolic composites. Loading over 1 wt% SWCNT leads to decrease in the Young's modulus. This has been accounted for the insufficient impregnation of the resin at higher loading. Thostenson and Chou[90] examined the processing-structure-property relationship in CNT/epoxy composites. Grimmer and Dharan[91] have shown that the addition of 1 wt% CNT to the polymer matrix can improve fatigue life of woven glass fiber/epoxy composites by 60%. Kalaitzidou *et al*.[92] have studied the effect of addition of exfoliated nanoplatelets in PP matrix on the flexural strength, impact strength and modulus. At lower loading of exfoliated nanoplatelets, better improvement in the mechanical properties is observed.

1.23. Thermal Conductivity Studies

Thermal conduction is a phenomenon by which heat is transported from high to low temperature regions of a substance. The property that characterizes the ability of a material to transfer heat is the thermal conductivity. It is best defined in terms of the expression given in equation 50 below.

$$q = -k\, dT/dx \qquad (50)$$

Where q denotes the heat flux or heat flow, per unit time per unit area, k is the thermal conductivity and dT/dx is the temperature gradient through the conducting medium.

Heat is conducted in solids by both phonons and electrons. The thermal conductivity is due to the sum of these two mechanisms. Usually one predominates the other. In high purity metals the electronic contribution is more than the phonon as the electrons are not easily scattered as phonons and have high velocities. The thermal conductivity of common metals ranges from 20-400 W/m-K. Since free electrons are contributing to electrical and thermal conductivity in metals, theoretical treatments suggest that the two conductivities should be related to Wiedemann-Franz law as given below in equation 51.

$$L = k / \sigma T \qquad (51)$$

Where L is a constant independent of temperature, other symbols have the usual meaning.

Since the ceramic materials lack large number of free electrons, phonons are responsible for thermal conduction. Further these phonons are not as efficient as free electrons for the transport of energy as they are easily scattered by the lattice imperfections. The scattering of lattice vibration is more pronounced with the increase of temperature and hence the thermal conductivity diminishes with the increase in the temperature. Porosity has inverse effect on thermal conductivity. More pores lead to decrease in the thermal conductivity.

For polymers, energy transfer is accomplished by the vibration and rotation of the chain molecules. The magnitude of thermal conductivity depends on the crystallinity of the polymer which increases with the increase in crystallinity. This is due to the more effective coordinated vibration of the molecular chains for the crystalline state. Thermal conductivity of many binary composites such as polyethylene-graphite[93], nylon-6,6-CF[94], HDPE-Al[95] etc. has been reported.

1.24. Aim and Scope

The above literature on the binary conducting composites clearly emphasizes the importance of conducting polymer composites to be applied for various applications such as fuel cells, thermal interface materials etc. where it is customary to reduce the filler loading retaining high electrical and thermal conductivities i.e. the electrical percolation threshold should be reduced as minimum as possible. To achieve low percolation threshold, high aspect ratio fillers like CNT, CNF, graphene etc. are added to various polymer matrices. This leads to increase in the cost of the final product made out of them. This particular aspect prompts us to think of hybrid composites where two conducting fillers are used out of which one will be cheaper. The second conducting filler when used in small amounts act as connectors and hence the electrical conductivity will be increased which otherwise is obtained at a very high loading of the filler in binary composites. This approach helps us to use the costly high aspect ratio fillers in small amount and thus the over all cost of the composite can be reduced. Further high loading of fillers in binary composite will hinder the flow properties of the polymer and hence processing becomes difficult.

The idea of improving electrical conductivity by the addition of second conducting filler in a thermoset matrix was first done by Radhakrishnan[96]. Following this Lin *et al*.[97] have used tin-lead alloy as the second component along with short carbon fiber filled PES. Towards the development of bipolar plates, highly conducting composites based on Polyphenylene sulfide (PPS)-graphite with carbon nanofiber and carbon black as second components have been made after compounding and injection molding[98,99]. Similarly electrical conductivity of Polypropylene (PP)-synthetic graphite binary and hybrid composites with CB and short carbon fiber have been reported[100]. Further the percolation threshold for PP-synthetic graphite has been reported to be at 25-30 wt% after injection molding[101]**.** In many injection molded PP-graphite based hybrid composites, electrical conductivity is studied with high loading of the second conducting component grater than 15 wt%[102]. Thus there is a great need to use second conducting fillers in small quantity retaining higher electrical conductivity of hybrid composites in order to process them easily and to be used for various applications mentioned above. The objective of the present thesis can be classified in to four parts.

1. Effect of aspect ratio of fillers on the dc, ac electrical behavior, charge transport in polymer-graphite based hybrid and binary composites and evaluation of a model through impedance spectroscopy studies.
2. Effect of processing routes on the electrical percolation threshold of hybrid composites.
3. Role of polymer matrix on the electrical conductivity of hybrid composites.
4. Thermal conductivity studies of few conducting composites as part of application.
5. Structure development in the polymer matrix due to processing and thermal analysis where ever required.

In order to bring the electrical percolation threshold down, three polymer matrices such as amorphous Polyether sulfone (PES), semicrystalline Polypropylene (PP) and Polyphenylene sulfide (PPS) were selected. In addition, fillers like graphite, carbon black (CB), expanded graphite (Exgr) and Carbon nanofiber (CNF) were chosen. All hybrid composites prepared were polymer-graphite based. PES is a high temperature thermoplastic polymer and no reports are found in the literature related to hybrid

composites, dc and ac behavior nearer to the percolation threshold. The same is true for PP and PPS based hybrid composites. Apart from that PP is easily processible and PPS is thermally stable exhibiting excellent mechanical properties. The choice of fillers is due to cost and easy availability. Graphite and CB are cheap and expanded graphite can be prepared from graphite. CNF is bit costlier but not to that extent of CNTs and available in large quantities.

1.25. References

1. Radhakrishnan S, Ramanujam BTS, Adhikari A, Sivaram S. J Power Sources 2007;163(2):702.

2. Raghavan V. Materials Science and Engineering. New Delhi: Prentice Hall of India;1998.

3. Kawasumi M. Journal of Polymer Science, Part A: Polymer Chemistry 2004, *42*, 819.

4. Zheng QH, Yu AB, Lu GQ, Paul DR. J Nanoscience and Nanotechnology 2005;5:1574.

5. Ray SS, Okamoto M. Progress in Polymer science 2003; *28*:1539.

6. Alexandre M, Dubois P. Materials Science and Engineering: R 2000; *28* (1–2):1.

7. Okamoto M, Morita S, Kokata T. Polymers 2001;42:2685.

8. Gopakumar T. Polymers 2002;43:5483.

9. Fornes T, Yoon P, Keskkula H, Paul D. Polymers 2001;42:9929.

10. Davis C, Mathias L, Gilman D, Schiraldi J, Shields P, Trulove T, Delong H. J Polym Sci Polym Phys 2002;40:2661.

11. Usuki A, Kato M, Okada A, Kurauchi T. J Poly Sci 1997;63:137.

12. Stankovich S, Dikin DA, Dommett GHB, Kohlhaas K, M Zimney EJ, Stach EA, Piner RD, Nguyen ST, Ruoff RS. *Nature* 2006;442: 282.

13. Du X, Xiao M, Meng Y, Allan SH. Polymer Int 2004;53(6):789.

14. George JJ, Bhowmick A. J Mater Sci 2008:43(2):702.

15. H. Shirakawa, E. J. Louis, A. G. MacDiarmid, C. K. Chiang, A. J. Heeger. J Chem Soc Chem Commun 1977:578

16. Encyclopedia of Nanoscience and Nanotechnology (Ed. H. S. Nalwa). 2004;2:153.

17. Hermann AM. Appl Phys Commun 1983;3(1&2):59.

18. Mulliken RS. J Am Chem Soc 1950;72:600.

19. Mulliken RS. J Chem Phys 1951;19:514.

20. Dewar MJS, Rogers H. J Am Chem Soc 1962; 84:395.

21. Bayer RK, Ezquerra, TA, Zachmann HG, Balta Calleja,FJ, Martizen Salazar J, Meins W, Diekow RE, Wiegel P.J Mater Sci 1988;23: 475.

22. Ezquerra TA, Bayer RK, Zachmann HG, Balta Calleja FJ. J Mater Sci 1988;23:4121.

23. Martizen Salazar J, Bayer RK, Ezquerra TA, Balta Calleja FJ. Colloid Polym Sci 1989; 267: 409.

24. Pinto G, Cipriano LG, Ana JM. Polym Composites 1999;20: 804.

25. Yacubowicz J, Narkis M, Benguigui L. Poly Eng Sci 1990;30:459.

26. Baker ZQ, Abdelazeez MK, Zihlif AM. J Mater Sci 1988;23: 2995.

27. Chiang WY, Chiang YS. J Appl Polym Sci 1992;46:673.

28. Huang CY, Chiou TW. Eur Polym J 1998;34:37.

29. Tchmutin IA, Ponomarenko AT, Krinichnaya EP, Kozub GI, Efimov ON. Carbon 2003;41:1391.

30. Saini P, Choudhari V, Sood KN, Dhawan SK. J Appl Polym Sci 2009;113:3146.

32. Zheng G, Wu J, Wang W, Pan C. *Carbon* 2004;42**:**2839

33. Usuki A, Kojima Y, Kawasumi M, Okada A, Fukushima Y, Kurauchi T, Kamigaito OJ. Mater Res 1993;8:1179.

34. Chen G-H, Wu C-L, Wang W-G, Wu D-J, Yan W-L. Polymer 2003;44:1781.

35. Ezquerra YA, Kulescza M, Alta-Calleja FJ. Synth Met 1991;41: 915.

36. Winey KI, Kasiwagi T, Mu M. MRS Bull 2007;32(4):348.

37. Bryning MB, Islam MF, Kikkawa JM, Yodh AG. Adv Mater 2005;17(9):1186.

38. Martin CA, Sandler JKW, Shaffer MSP, Schwarz MK, Bauhofer W, Schulte K, Windle AH. Compos Sci Technol 2004;64(15):1236.

39. Du FM, Fischer JE, Winey KI. Phys Rev B 2005;72(12):121404. 1.

40. Du FM, Scogna RC, Zhou W, Brand S, Fischer JE, Winey KI. Macromolecules 2004;37(24):9048.

41. Yuen SM, Ma CCM, Wu HH, Kuan HC, Chen WJ, Liao SH, Hsu CW, Wu HL. J Appl Polym Sci 2007;103(2):1272.

42. Allaoui A, Bai S, Cheng HM, Bai JB. Compos Sci Technol 2002;62(15):1993.

43. Chatterjee A, Alam K, Klein P. Mater Manuf Process 2007;22(1):62.

44. Cortes P, Lozano K, Barrera EV, Bonilla-Rios J. J Appl Polym Sci 2003;89(9):2527.

45. Higgins BA, Brittain WJ. Eur Polym J 2005;41(5):889.

46. Yang YL, Gupta MC, Dudley KL, Lawrence RW. J Nanosci Nanotechnol 2005;5(6):927.

47. Blythe T, Bloor D. Electrical Properties of Polymers. Newyork: Cambridge University Press;2005.

48. Scrisbrick RM. J Phys D: Appl Phys 1973;6:2098.

49. Nan CW. Prog Mater Sci 2002;37(1):1

50. Ezquerra TA, Mohammadi M, Kremer F, Vilgis T, Werner G.

51. Ezquerra TA, Kulescza M, Santa cruz C, Balta-colleja FJ. Adv Mater 1990;2:597.

52. Wu J, McLachlan DS. Phys Rev B 1997;56:1236.

53. Quivy A, Deltour R, Jansen AGM, Wyder P. Phys Rev B 1989;39:1026.

54. Balberg I. Phys Rev Lett 1987;59:1305.

55. Pike GE, Seager CH. Phys Rev B: Solid state 1974;10:1421.

56. Weber M, Kamal MR. Polym Compos 1997;18(6):711.

57. Wang SF, Ogale AA. Compos Sci Technol 1996;46:93.

58. Mamunya ET, Davidenko VV, Lebedev EV. Compos Interf 1997;4:169.

59. Clingermann ML, King JA, Schulz KH, Meyers JD. J Appl Polym Sci 2002;8:1341.

60. Bigg DM. Polym Engg Sci 1977;17:842.

61. Weber ME, Kamal MR. Polym Compos 1997;18:711.

62. Berger MA, McCullough RL. Compos Sci Technol 1985;22:81.

63. McLachlan DS. J Phys 1988;C21:1521.

64. A.W. Bush. Contact Mechanics, in Rough Surfaces edited by T.R. Thomas et al.. London: Longman;1982.

65. B. Miller. J Appl Polym Sci 1966;10:217.

66. Mott NF. Metal-insulator transitions. London: Taylor & Francis;1990.

67. Mott NF. Conduction in non-crystalline materials. Oxford: Clarendon Press;1987.

68. Mandal P, Neumann A, Jansen AGM, Wyder P. Phys Rev B 1997;55:452.

69. Joo J, Long SM, Pouget JP, Oh EJ, Mcdiarmid AG, Epstein AJ. Phys Rev B 1998;57:9567.

70. Mott NF, Davis EA. Electronic conduction in non-crystalline materials. Oxford: Clarendon Press;1979.

71. Dyre JC, Shrøder TB. Rev Modern Phys 2000;72(3):873.

72. Angell CA. Chem Rev 1990;90:523.

73. Roling B. Solid State Ion 1998;105:185.

74. Psarras GC, Manolakaki E, Tsangaris GM. Composites Part A: Appl Sci Manufact 2003;34:1187.

75. Guskos N, Anagnostakis EA, Likodimos V, Bodziony T, Typek J, Maryniak M. J Appl Phys 2005;97:024304.

76. Wagner N. J Appl Electrochem 2002;32(8):859.

77. Larminie J, Dicks A , Fuel Cell Systems Explained. Wiley; 2003.

78. Makkus RC, Janssen AHH, de Bruijn FA, Mallant RKAM. Fuel Cells Bull 2000;3(17):5.

79. Davies DP, Adcock PL, Turpin M, Rowen SJ. J Appl Electrochem 2000;30:101.

80. Besmann TM, Klett JW, Henry Jr. JJ, Lara-Curzio E. J. Electrochem. Soc 2000; 147:4083.

81. Kuan H-C, Ma C-CM, Chen KH, Chen SM. Journal of Power Sources 2004;134:7.

82. Yu A, Ramesh P, Itkis ME, Bekyarova E, Haddon RC. J Phys Chem C 2007;111(21):7565.

83. Zhang K, Chai Y, Yuen MMF, Xiao DGW, Chan PCH. Nanotechnology 2008;19: 215706.

84. Chow TS, Penwell RC. Mechanical and Thermal Properties in Metal-Filled Polymers Properties and applications edited by Bhattacharya SK. Newyork: Marcel Dekker;1986.

85. Zheng W, Lu X, Wong S. J Appl Polym Sci 2004;91:2781.

86. Zheng W, Wong S. Compos Sci Technol 2003;63:225.

87. Chodak I, Omastova M, Pionteck J. J Appl Polym Sci 2001;82:1903.

88. Yeh MK, Tai N-H, Lin Y-J. Compos Part A 2008;39(4):677.

89. Tai N-H, Yeh M-K, Peng T-H. Compos Part B 2008;39(6):926.

90. Thostenson ET, Chou T-W. Carbon 2006;44(14):3022.

91. Grimmer CS, Dharan CKH. J Mater Sci 2008;43(13):4487.

92. Kalaitzidou K, Fukushima H, Drzal LT. Composites Part A: Applied Science and Manufacturing 2007;38(7):1675.

93. Agari Y, Uno T. J Appl Polym Sci 1986;32:5705.

94. Heiser JA, King JA. Polym Compos 2004;25(2):186.

95. Tavman LH. J Appl Polym Sci 1996;62:2161.

96. Radhakrishnan S. J Mater Sci Lett 1985;4:1445.

97. Li L, Yih P, Chung DDL. J Electron. Mater 1995;24(1):47.

98. Huang J, Baird DG, Mcgrath JE. J Power Sources 2005;150:110.

99. Mighri F, Huneault MA, Champagne MF. Polym. Engg. Sci 2004;44(9):1755.

100. Yeetsorn R, Fowler M, Tzoganakis C, Yuhuva W, Taylor M. Macromol Symp 2008;264:34.

101. King JA, Johnson BA, Via MD, Ciarkowski CJ. J Appl Polym Sci 2009;112:425.

102. Dweiri R, Sahari J. J Power Sources 2007;171:424.

Chapter-2

Experimental and Characterization Techniques

2.1. Introduction

This chapter deals with details of experimental procedures employed for the synthesis of composites and the corresponding characterization techniques. As mentioned in the chapter 1, three thermoplastic polymer matrices were chosen for making conducting composites such as Polyether sulfone (PES), Polyphenylene sulfide (PPS) and Polypropylene (PP). Fillers used were graphite, carbon black (CB), expanded graphite (ExGr) and carbon nanofiber (CNF). Hybrid composites were polymer-graphite based. The dc, ac conductivity behaviors of various conducting composites was investigated. The structure, properties and morphology of different composites were characterized by various physico-chemical characterization techniques as described in this chapter.

2.2. Materials

The chemicals and materials used along with their grade and make are given in the following Table 2.1.

Table 2.1

Materials used

Chemical / Material	Grade	Make
Acetone	LR grade	Merck
Methanol	LR grade	Merck
Xylene	LR grade	Merck
Dichloromethane	LR grade	Merck
NMP	LR grade	Merck
Sodium sulfide	LR grade	Merck
PES	3600P	Gharda chemicals, India
PP	SM85N	IPCL, India
PPS	Ryton P-4 powder	Chevron Philips, Singapore
Natural graphite	Better than 200 mesh	Carbon enterprises, India
Carbon black	Degussa	Carbon enterprises, India
Expanded graphite	-	ARCI, Hyderabad, India
Carbon nanofiber	PR-24-XT- HHT	Pyrograph products, USA

2.3. Synthesis of PES-graphite Binary and Hybrid Composites

PES-graphite binary and hybrid composites were prepared by two routes as described below.

1. Solution blending
2. Powder mixing

In the former route, a known amount of polymer was dissolved in 100 ml dichloromethane keeping the composite weight to be 5 gm. To this, required amount of graphite was added and the stirring continued for 20 hr. CB, CNF and expanded graphite were first sonicated in 70 ml of DCM for 5 hr and then added to the dissolved polymer after which the stirring was continued for 20 more hr. For making hybrid composites, filler in small amount was first ultrasonicated for 5 hr in 70 ml DCM and then added to the dissolved polymer. The resultant mixture was stirred for 5 hr. To this mixture, graphite was added and stirred for another 15-18 hr. The resultant mixture was dried and then crushed to make powder. The dried powder was sieved (100mesh) and pellets were made for electrical and thermal studies.

PES was first sieved (100 mesh) and then used for making powder mixed composites. For binary composites, required amount of graphite and CB corresponding to 5 gm of the composite was added and then mixed for 15 min. For hybrid composites, to PES required amount of CB was added first and mixed for 10 min. Then graphite was added and the mixing was continued in an agate mortar for another 15 min. Pellets were made for various studies.

2.4. Synthesis of PPS-graphite Binary and Hybrid composites

PPS based composites were made by following routes mentioned below.

1. Powder mixing
2. Melt crystallization
3. In-situ polymerization for PPS-ExGr composites

2.4.1. Powder Mixing

Binary composites such as PPS-graphite, PPS-CB, PPS-ExGr, and PPS-CNF were prepared by mixing graphite and PPS in a mortar for 15 min. Other binary composites were prepared by mixing the required amount of filler after sonication in 50 ml acetone for 4 hours and then mixed with PPS. The resultant mixture was sonicated for

another half an hour and dried in a Petri dish. The chunks were crushed and pellets were made by applying 3 ton pressure for 3 min.

Hybrid composites with CB, CNF and ExGr as second conducting fillers were made by first sonicating required amount those fillers (keeping composite weight to be 3 gm) in 50 ml of acetone for five hours and added to required amount of PPS. Sonication was carried out for one more hour. To this mixture graphite was added and sonication was continued for half an hour. The resultant mixture was poured in a Petri dish and dried before the chunks were crushed and sieved. Pellets were made out of sieved mixture.

2.4.2. Melt Crystallized PPS Based Composites

In melt crystallization, the composites, both binary and hybrid, kept in between Teflon sheets were heated to 300^{o}C for 3 min. Due to melting and spreading of the polymer, sheets were formed. The outer layer was scrapped by polish paper and the electrical measurements were done.

2.4.3. Lab Synthesized PPS-Exgr Composites

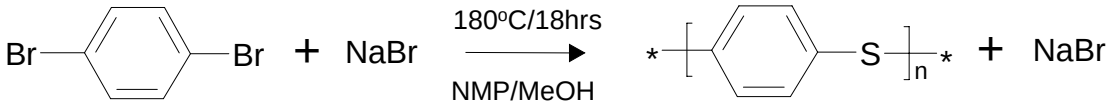

Figure. 2.1. PPS Synthesis

PPS was synthesized by making 1,4-dibromobenzene in NMP to react with sodium sulfide dissolved in methanol with 1:1.1 molar ratio as shown in Figure 2.1. The excess methanol was distilled out and the reaction was carried out at 180^{o}C for 18 hr. The resultant powder was washed with excess methanol and vacuum dried. PPS thus synthesized was mixed in different proportion with ExGr and binary composites were made. In another set of experiment, ExGr was first soaked in NMP and then in-situ polymerization of PPS was carried out.

2.5. Synthesis of PP-graphite Binary and Hybrid composites

Two processing routes were employed for the preparation of both types of composites. Since PP exists in granular form, it can't be ground by ordinary means due to low T_g[1]. Hence it is necessary to make PP powder for making composites.

2.5.1. Preparation of PP Powder

PP granules were dissolved in xylene at 140^{o}C and then cooled till gel formation was completed. The gel was precipitated in excess acetone with vigorous stirring which led to the formation of PP powder. The powder was vacuum dried at 60^{o}C for 10 hr and used for various studies.

2.5.2. Preparation of PP Based Binary and Hybrid Composites by Powder Blending

PP-Graphite composites were prepared by mixing appropriate amount of PP powder with graphite keeping the composite weight to be 3 gm. The mixture was mixed for 15 min thoroughly in an agate mortar and pellets were made for various studies. Other binary composites such as PP-CB, PP-CNF, and PP-ExGr were prepared by sonicating required amount of filler in 50 ml acetone for four hours and the added to PP powder in 50 ml acetone. The mixture was further sonicated for half an hour and the solvent was evaporated. The resulting mixture was ground and used for various characterizations.

Similarly hybrid composites were prepared by sonicating the second conducting filler in 50 ml acetone for 4 hr and then mixed with PP powder in 50 ml acetone. The resulting mixture was sonicated for about half an hour. To this mixture, required amount of graphite was added and sonicated further for another half an hour. The mixture after solvent evaporation was mixed well in a mortar and then pellets were made.

2.5.3. Melt Crystallization of PP Based Binary and Hybrid Composites

The pellets of powder mixed composites were kept in between two glass slides and heated to 180^{o}C for few minutes so that the polymer was molten and spread to form sheets after which they were transferred in to a beaker containing water. The sheets were scrapped by a polish paper to remove the polymer and used for various characterizations.

2.6. Preparation of Samples for Electrical Conductivity Studies

Pellets were prepared by taking 0.3 gm of composites in a die by applying 3 ton pressure for 3 min. The pellets prepared were used for electrical conductivity and melt crystallization studies.

2.7. Characterization Techniques

2.7.1. Electrical Measurements

The room temperature electrical resistance (R) of composites was measured in a specially constructed cell by applying a constant load 8 Kg/cm^2 to eliminate contact resistance with Keithley 6514 electrometer. From the measured value of thickness (l) of samples and cross section (A), the conductivity was calculated from the following equation 1.

$$\sigma = R\ A/l \qquad (1)$$

Where σ is the dc conductivity.

AC conductivity studies were carried out by loading the sample in the specially constructed cell and connecting that with Solartron impedance analyzer (Model SI 1255) with dielectric interface (Model 1296) in parallel plate configuration. Few experiments were also done on Alpha A-Novacontrol, instrument. The impedance software was used to obtain impedance plots which were fitted with ZVIEW software to extract model parameters.

2.7.2. X-ray Diffraction

X-ray diffraction[2] is a great tool to study the structural changes happening due to processing etc. The binary composites were characterized by wide angle X-ray diffraction. Xpert pro powder x-ray diffractometer was used (Cu K_α radiation with λ_i = 1.541 A^o) to obtain the xrd pattern of samples. The useful range of scan was limited to 10-30^o. The crystallite sizes of fillers were calculated from Scherer's formula given in equation 2.

$$t' = [B\ \lambda_i / \Delta\theta'\ \cos\theta'] \qquad (2)$$

Where B = 0.9

λ_i = wave length of X-ray (1.541 A^o)

$\Delta\theta'$ = Breadth of the peak in radian

θ' = Diffraction angle

t' = Crystallite size

2.7.3. Differential Scanning Calorimetry (DSC)

The glass transition temperature of PES based composites, melting and crystallization temperature of PP and PPS based composites were obtained from the DSC analysis

where a temperature scan of 50-250^{o}C was employed for PES and PPS based composites and 50-200^{o}C for PP based composites The interaction between the filler and the matrix is clearly brought out by shift in the T_g of the polymer. The effect of fillers if they act as nucleators was revealed through a shift in the crystallization temperature to higher values. All scan were recorded in Nitrogen atmosphere with a heating and cooling rate of 10^{o}C/min. The sample amount used can vary between 3-8 mg. The first heating run was not taken for data analysis as it was used to destroy the prehistory of the sample. Second cooling and third heating runs were considered for data analysis. DSC Q-10 model from TA instruments, USA was used for carrying out scans.

2.7.4. Thermo Gravimetric Analysis (TGA)

The thermal stability of polymers and composites can be found out through TGA[3] analysis. The entrapment of low molecular weight compound like Diphenyl sulfone within the layers of graphite was found out through TGA where the weight loss was plotted against the temperature. The sample was heated from room temperature to 500^{o}C in nitrogen atmosphere with a heating rate of 10^{o}C/min. Perkin and Elmer TGA machine was used for TGA analysis.

2.7.5. Scanning Electron Microscopy (SEM)

SEM[4] is very important for micro structural investigation when it is related to properties, processing and behavior of materials. The SEM provides informations related to topological features, morphology, phase distribution, compositional differences etc. The SEM is also capable of determining elemental composition of micro volumes with the addition of an x-ray or electron spectrometer. The strength of SEM lies in its inherent versatility due to the multiple signal generated, simple image formation process, wide magnification range and excellent depth of filed. The cross sections of PES based samples were seen in SEM after etching the sample in DCM vapor for about an hour. The samples were mounted vertically and analyzed. Similarly cross sections of PP based composites were seen after etching the sample in hot xylene for one hour. PPS based composites cross section was observed after etching in toluene vapor for one hour. Through SEM analysis, in many samples, thickness of graphite and length of the fibers like CNF were measured which was

coupled with transmission electron microscopy results to comment on the aspect ratio. All samples were coated with thin layer of gold in plasma coating unit to prevent charging on the specimen. The SEM Leica-440 unit was used to grab the images.

2.7.6. Transmission Electron Microscopy

Transmission electron microscopy[5] is the premier tool for understanding the internal microstructure of materials at the nanometer level. Further the resolution can be few tenths to few nanometers, depending up on the imaging conditions and simultaneously obtain electron diffraction pattern from specific regions in the images as small as 1 nm. PES based selected samples were drop casted on copper grids after dissolving PES in DCM and TEM pictures were taken. Pristine carbon nanofiber and expanded graphite after sonication were drop casted on to copper grids and analyzed. TEM Joel model 1200 was employed to take TEM pictures.

2.7.7. Infra-red Spectroscopy (IR)

IR spectrum was recorded to confirm the formation of PPS which was prepared by the reaction outlined in section 2.4.3. The powder specimen was mixed with KBr and then loaded in Shimadzu FT-IR 8300 spectrometer and analyzed in the range of 400-4000 cm^{-1}.

2.7.8. Thermal Conductivity Measurement

Thermal conductivity of various samples was measured in Quickline-10 instrument, provided by Anter Corporation, USA, by the ASTM E1530 guarded heat flow meter method. In this method, sample to be tested is held under a reproducible compressive load between polished metal surfaces, each controlled at a different temperature. The lower contact surface is part of calibrated heat flux transducer. As heat flows from the upper surface through the sample to the lower surface, an axial temperature gradient is established in the stack. By measuring the temperature difference across the sample along with the output from the heat flux transducer, thermal conductivity of the sample can be determined when the thickness is known. Test section schematic is given in Figure 2.2.

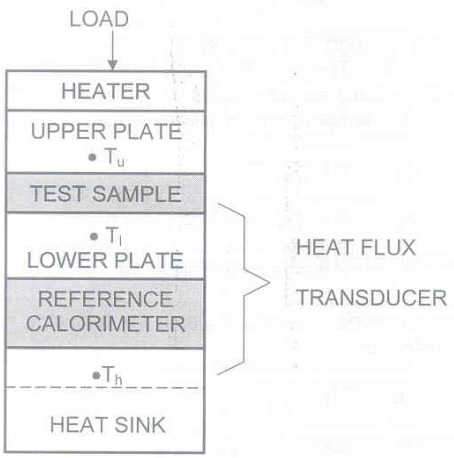

Figure. 2.2. Thermal conductivity test meter schematic

At thermal equilibrium, the Fourier heat flow equation applied to the test sample becomes

$$R_s = [(T_u - T_l) / Q] - R_{int} \quad (3)$$

Where R_s - thermal resistance of the sample

T_u - upper plate surface temperature

T_l - lower plate temperature

Q - heat flux through the test sample

R_{int} – total internal resistance between sample and surface plates

The thermal resistance of the sample is defined as

$$R_s = l / k \quad (4)$$

Where l– sample thickness

k - thermal conductivity

The thermal resistance is included in equation 3 as the instrument measures only the temperature difference. The heat flux through the sample is measured with a transducer located just below the sample. The heat flux transducer consists of a reference calorimeter with high conductivity surface plates on either side. Sample thermal resistance is given by

$$R_s = F (\Delta T_s / \Delta T_r) - R_{int} \quad (5)$$

Where F – proportionality constant

ΔT_s – temperature difference across the sample

ΔT_r – temperature difference across the reference calorimeter

To determine F and R_{int}, the instrument must be calibrated. Equation 5 shows that there is a linear relationship between R_s and (ΔT_s / ΔT_r). By measuring the temperatures to determine the ΔT ratio for several samples of known thermal resistance and plotting the results on graph, a straight line can be drawn through all the data points. The slope of the line is F and the y-intercept is R_{int}. The thermal resistance of the sample should fall within the range of samples used for calibration. The accuracy with this instrument is ± 3% to ± 8% depending on the thermal resistance of the sample. The lowest practical value of R_s that can be measured is 0.0002 m^2K/W.

2.7.9. Hardness Measurement

The hardness of plastics is normally measured by the shore durometer test. In this method, the resistance of plastics toward indentation is measured and provides an empirical hardness value that does not necessarily correlate well to other properties. Few PES-graphite samples, hardness was measured in shore-D scale commonly used for measuring hardness of hard plastics.

2.7.10. Electron Spectroscopy for Chemical Analysis (ESCA)

X-ray photo electron spectroscopy (XPS)[6] or Electron spectroscopy for chemical analysis (ESCA) uses x-rays of characteristic energy to excite electrons from orbitals in atoms. The photo electrons emitted from the material are collected as a function of their kinetic energy, and the number of photoelectrons collected in a defined time interval is plotted versus kinetic energy. Peaks appear in the spectrum at discrete energies are due to emission of electrons from states of specific binding energies in the materials. The positions of the peaks identify the chemical elements in the material. Peak areas are proportional to the number of orbitals in the analysis volume. The positions and shape of the peaks in the XPS spectrum can also be analyzed in greater detail to determine the chemical state of the constituent elements in the material, including oxidation state, partial charge and hybridization. XPS is used to analyze solid surfaces and gas phase compounds and it is surface sensitive technique. The nominal analysis depth is 1-10 nm. The primary limitation of XPS is the need of ultra high vacuum. Thus low vapor pressure materials can be analyzed. Typically a

photon of frequency ν, has a kinetic energy hν. As this photon passes through a material, it can interact with the electrons in the material. Absorption of the x-ray by an atom can lead to an electronic excitation of the atom. The photon absorption process conserves energy, leaving an electron in the atom to a first approximation with a kinetic energy that is equal to the energy of the incident photon less the initial binding (electronic ground state) energy of the electron. Under proper circumstances, when the electron does not scatter back, it acquires sufficient velocity to escape from the material. These electrons with a specific kinetic energy are focused on to the detector. ESCA of solution blended PES-graphite composites was taken in ESCA 3000 model for finding specific interaction between different groups. Magnesium target (K_α wavelength-1253.6 eV) was used as x-ray source. All spectra were recorded under identical conditions at 50 eV pass energy.

2.8. References

[1] Gowarikar VR, Viswanathan NV, Sreedhar J. Polymer Science; New Age International: New Delhi, 2006.

[2] Cullity BD. Elements of X-ray diffraction, 2nd ed.; Addison-Wesley:Philippines,1978.

[3] Turi EA. Thermal Characterization of Polymeric Materials; Academic Press: London, 1981.

[4] Goldstein JI, Lyman CE, Newbury DE, Lifshin E, Echlin P, Sawyer L, Joy DC, Michael JR. Scanning Electron Microscopy and X-Ray Microanalysis, 3rd ed.; Kluwer Academic: New York, 2003.

[5] Williams DB, Carter CB. Transmission Electron Microscopy: A Textbook for Materials Science; Plenum Press: New York, 1996; Vol. 1.

[6] Briggs D, Seah MP. Practical surface analysis: Auger and X-ray photo electron spectroscopy, 2nd ed.; John Wiley and sons: New York, 1994; Vol. 1.

Chapter-3

Polyether sulfone (PES) Based Composites

3.1.1. Introduction

Polyether sulfone (PES) is a transparent amorphous polymer with very high T_g (213^oC). Its chemical structure is given below.

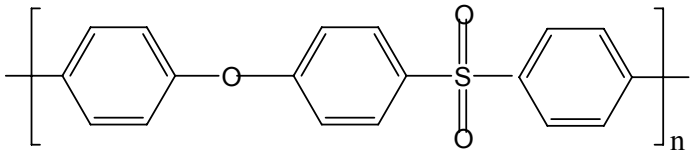

Its dimensional stability at high temperatures (above 200^oC) makes it very attractive to be used in proton exchange membrane fuel cells (PEMFC)[1]. PES, being engineering thermoplastic, can be injection molded. Out of various conducting fillers available, graphite is more attractive as it is a semimetal[2]. This thesis aims at developing both binary and hybrid conducting polymer composites of carbon black (CB), expanded graphite (ExGr) and carbon nanofiber (CNF) along with graphite. Hence a proper introduction to those fillers is necessary. As this section deals with binary and hybrid composites based on graphite and CB, understanding the internal structure of them is very important.

Graphite has a layer structure in which carbon atoms are arranged in a hexagonal pattern within each layer and the layers are stacked in AB sequence. This results in a hexagonal unit cell with cell dimensions c = 6.71 A^o, a = b = 2.46 A^o. There are four atoms per unit cell as labeled by A, A', B and B' in the following Figure 3.1.1. The atoms AB are in one plane and A'B' are in a different layer plane separated by half the crystallographic c-axis. The crystal structure corresponds to a space group $P6_3/mmc$. The adjacent layers are held together by vander Waals force which is very weak and hence foreign molecules can be intercalated between graphite layers. There are two types of graphite namely natural and synthetic graphite. Natural graphite is a mineral consisting of graphitic carbon. It can be further classified into amorphous, flake and crystalline types. Synthetic graphite is produced from coke and pitch. It tends to be of higher purity though not as crystalline as natural graphite and hence the conductivity is less.

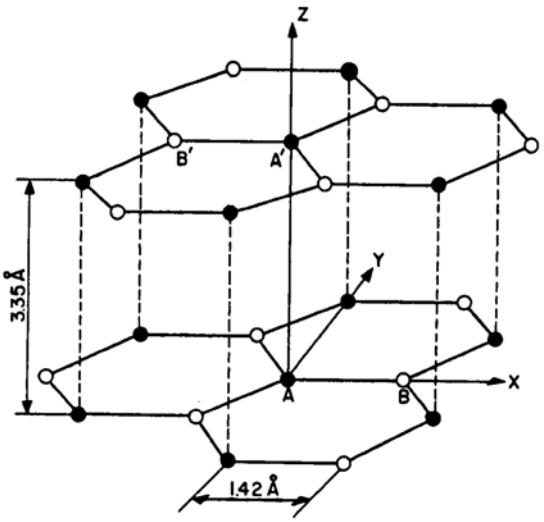

Figure. 3.1.1. Crystal structure of graphite

Carbon blacks (CB) are pure elemental carbon in colloidal form that is produced by incomplete combustion or thermal decomposition of gaseous or liquid hydrocarbons under controlled conditions. They have branched structure and within each aggregate the carbon atoms are arranged in imperfect graphitic form. Depending upon the heat treatment, different types of CB with different particle size can be obtained. Different grades of CB are distinguished chiefly by their surface areas and structures. Furnace blacks, Acetylene black, Vulcan XC-72 etc., are examples of different types.

3.1.2. PES-graphite Binary and Hybrid Composites with CB as Second Filler

In order to understand the effect of second conducting component in a polymer matrix on the electrical conductivity, binary composites need to be studied first to know the percolation threshold, saturation etc. The composites are prepared by two preparation routes namely solution blending and powder mixing. The details of preparation have been discussed in Chapter-2. Figure 3.1.2 represents through plane resistance variation of PES-Graphite and PES-CB solution blended samples. The thickness of the pellet and the area of cross section are kept 5mm and 1 cm^2 respectively. It is clear from the Figure 3.1.2 that the percolation threshold of PES-

graphite composites lies after 5 wt% whereas for the later it is at 10 wt%. The resistance of graphite filled PES is lesser than that of CB filled PES.

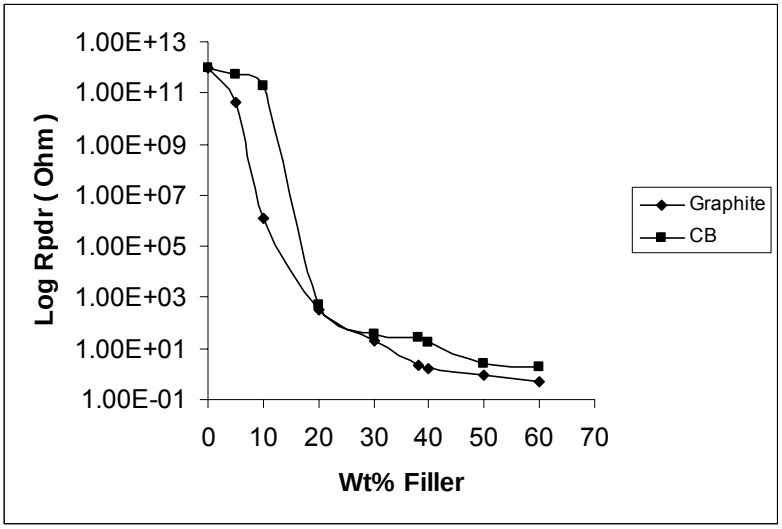

Figure 3.1.2. Through plane resistance variation of PES-Graphite, PES-CB solution blended composites

The percolation threshold signifies network formation. The resistance value saturates at higher loading of fillers i.e., > 50 wt% which indicates the completeness of network formation between filler particles. The higher resistance of CB filled PES composites when compared to graphite filled PES, even though CB particles aggregate size is 80 nm, is due to agglomeration in DCM. In order to understand the effect of addition of CB in PES-graphite system, selected loading of graphite and CB are shown in the following Figure 3.1.3.

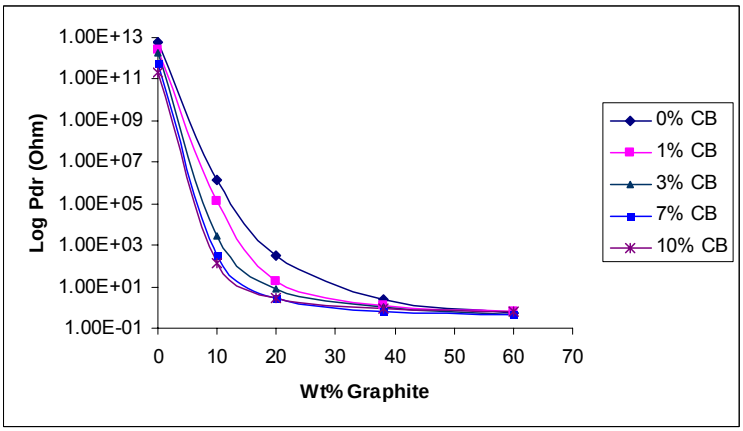

Figure 3.1.3. Through plane resistance of solution blended PES-Graphite-CB composites (sample thickness-5 mm, area of cross section-1 cm^2)

When 1 to 10 wt% CB is added to PES-x wt% graphite (x = 10, 20, 38, 60), the through plane resistance of hybrid composites is decreased. Addition of 7 wt% CB in PES-10 wt% graphite decreases the resistance by more than four orders when compared to 0 wt% CB in the same. The same order of resistance will be obtained with 25-30 wt% graphite added to the polymer in binary composites. Thus hybrid composites are very effective in reducing the filler loading as well as the percolation threshold due to improvement in the contact between filler particles. To understand the effect of preparation routes on the electrical conductivity of PES-graphite-CB hybrid composites, a particular composition namely, PES-7 wt% graphite has been chosen nearer to the percolation threshold. Figure 3.1.4 depicts the effect of addition of CB in PES-7 wt% graphite prepared by both solution blending and powder mixing routes on the dc electrical conductivity. The preparation procedure has been explained in Chapter-2.

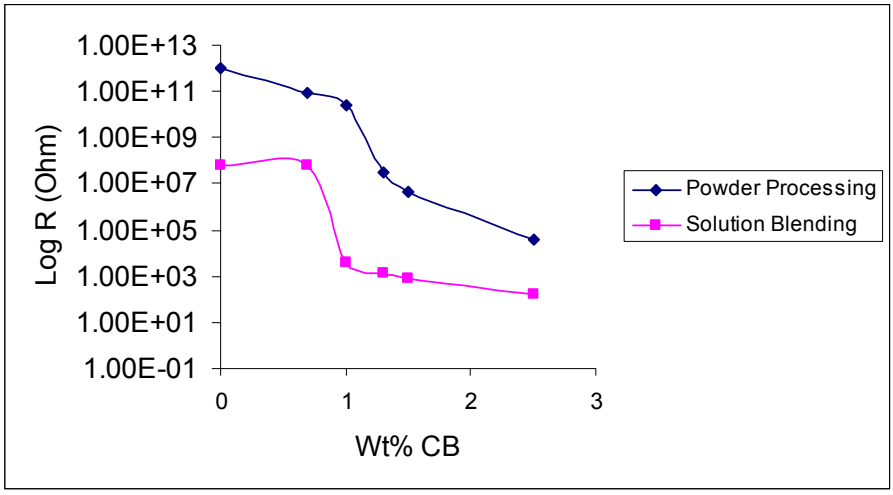

Figure 3.1.4. Effect of preparation routes on the through plane resistance of PES-graphite-CB composites (Thickness 5 mm and area 1 cm^2)

It is clear from the above Figure 3.1.4 that the solution blended PES-7 wt% graphite has two orders lesser through plane resistance than the same prepared by powder mixing route. The reduction in the particle/crystallite size of graphite in solution blending route leads to increase in the surface area and hence establishment of better connectivity between filler particles. The percolation threshold in solution blended hybrid composites is 0.7 wt% whereas for the powder mixed samples it is 1.3 wt%.

Figure 3.1.5 shows the XRD patterns of PES-7 wt% graphite prepared by both routes where PM refers to powder metallurgical route and Sln blend indicates solution blending method. It is clear from the XRD patterns corresponding to 002 reflection of graphite in the polymer that the FWHM of solution blended sample is higher than that of the powder mixed one. This indicates that the crystallite size of graphite is lesser in the solution blended sample than in the powder mixed one. The intensity of 002 reflection of graphite in solution blended sample is less than that of powder mixed sample. Since the diffracted intensity corresponding to a particular plane of a material depends on the number of unit cells which will be less in the solution blended case than that in the powder mixed sample due to crystallite size reduction.

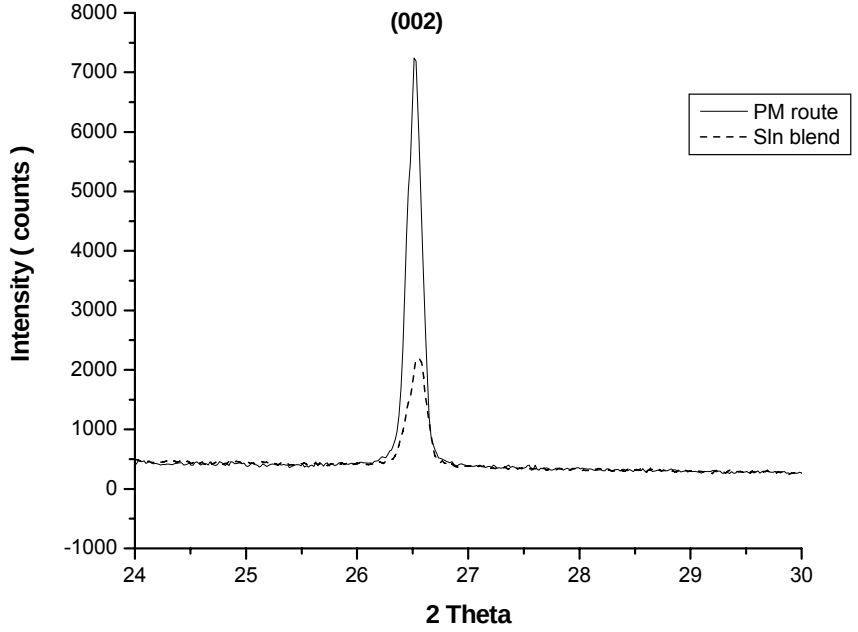

Figure. 3.1.5. XRD pattern of PES-7 wt% Graphite prepared by different routes

3.1.3. Effect of Heat Treatment on Electrical Conductivity of PES-graphite System

The composite bipolar plates are sintered to improve the hardness. Thus it is necessary to understand the effect of sintering on the electrical conductivity of composites. Thus, when PES-graphite composites are sintered above T_g of the polymer (213^oC), crystallite size reduction as well as polymer penetration in the interplanar spacing of graphite could be observed. The crystallite size reduction of

graphite is more in solution blended samples than in powder mixed ones. This is due to better polymer penetration in the gallery of graphite in solution phase. The gallery size of graphite varies from 7-16 A^{o3} as shown in Figure 3.1.6. The polymer penetration in the gallery causes the agglomerated graphite sheets to break and hence the particle size/crystallite size is reduced after sintering. The samples are sintered at 240^{o}C for one hour.

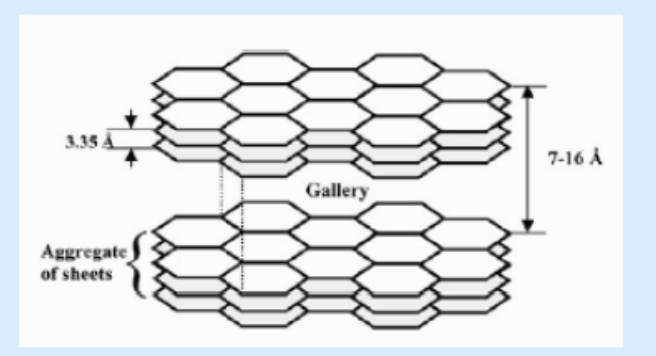

Figure 3.1.6. Gallery space of graphite

Apart from the crystallite size reduction, the intensity of the more prominent peak of graphite i.e., 002 reflection decreases after sintering which is attributed to re-orientation of graphite planes. Above T_g of the polymer, the chain movement becomes easier and causes re-orientation of graphite 002 planes. The XRD patterns corresponding to graphite part of both solution blended and powder mixed PES-7 wt% graphite samples before and after sintering are shown in the following Figure 3.1.7.

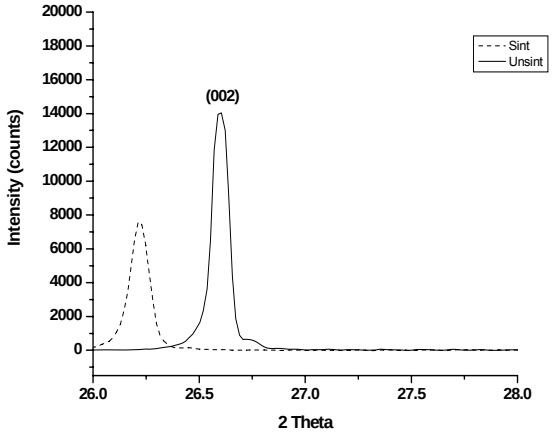

(a)

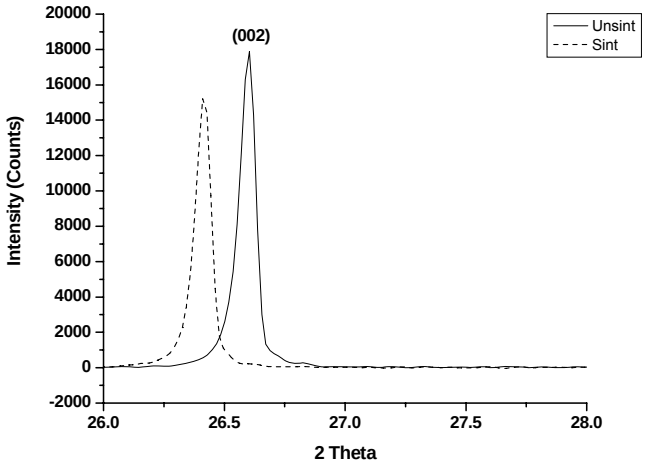

(b)

Figure 3.1.7. XRD patterns of PES-7 wt% graphite a) Solution blended sample
b) Powder mixed sample

In both processing routes, a shift in 2 Theta after sintering towards lower value in the XRD patterns indicates that the interplanar distance of graphite has been increased. This shift is more in the case of solution blended sample than in the powder processed one as shown in Table 1, which summarizes crystallite size calculated from Scherrer's equation[4] and the intensity of 002 reflection of graphite before and after sintering.

Table 1

XRD analysis of PES-7 wt% graphite prepared by different routes

Processing routes	2 Theta		Intensity (Counts)		t' (nm)	
	BS	AS	BS	AS	BS	AS
Solution blending	26.60	26.21	14039	7621	67.03	55.82
Powder mixing	26.60	26.41	17889	10714	83.57	75.18

t' –Crystallite size, BS- Before sintering, AS- After sintering

3.1.4. TEM Analysis

In order to prove the reduction in particle size due to sintering, TEM pictures of solution blended PES-7 wt% graphite before and after sintering are taken and shown in Figure 3.1.8.a and b respectively. It is clear from the pictures that down sizing of particles size indeed occurs after sintering. The average particle size of graphite in unsintered solution blended PES-7 wt% graphite is 68 nm and in sintered sample it is 50 nm. The particle size is averaged over eight values. The scale bar in these pictures is 50 nm.

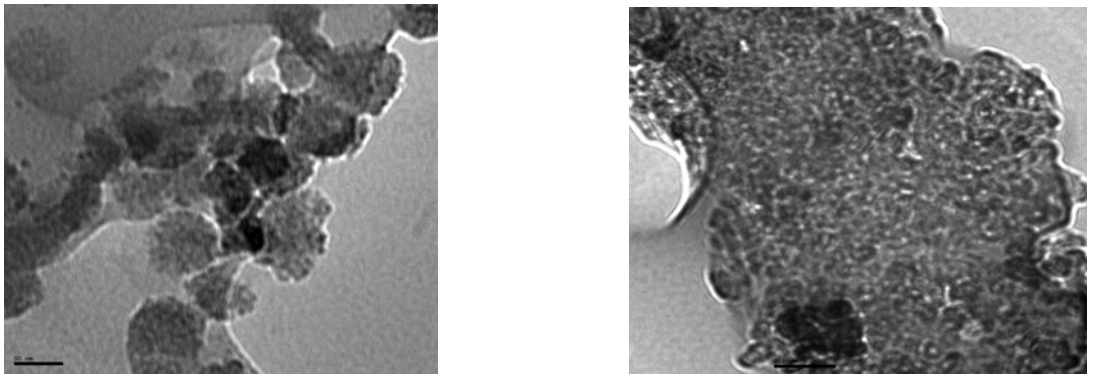

(a) (b)

Figure 3.1.8. TEM pictures of solution blended PES-7 wt% graphite a) unsintered b) sintered samples

The result more or less matches with the values obtained from XRD. The original graphite particles remain as agglomerated structures with particle size in few microns as shown in the following Figure 3.1.9.

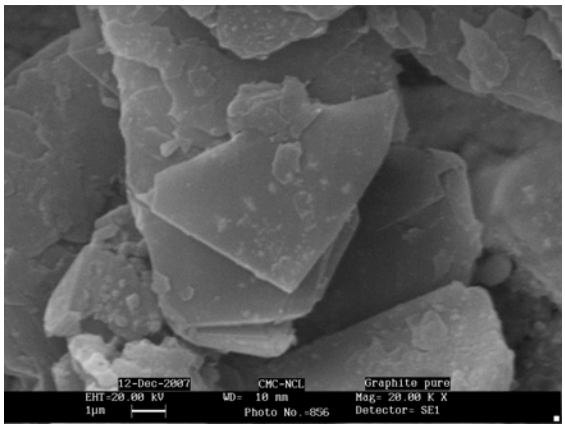

Figure 3.1.9. SEM picture of pure graphite

3.1.5. DC Electrical Conductivity Variation in PES-graphite Composites

Figure 3.1.10 shows dc electrical resistance variation of solution blended PES-graphite composites before and after sintering. Sintering leads to decrease in the through plane resistance due to the reduction in crystallite/particle size of graphite resulting in better contact between the filler particles. At least one order magnitude reduction in through plane resistance (Rpdr) can be observed at lower graphite loadings. Samples with 5 mm thickness and area of cross section 1 cm^2 are used for this analysis. Since the solution blended samples contain more uniformly distributed graphite particles, the anisotropy which is defined as the ratio of through plane to in-plane conductivity will be lesser than powder mixed samples.

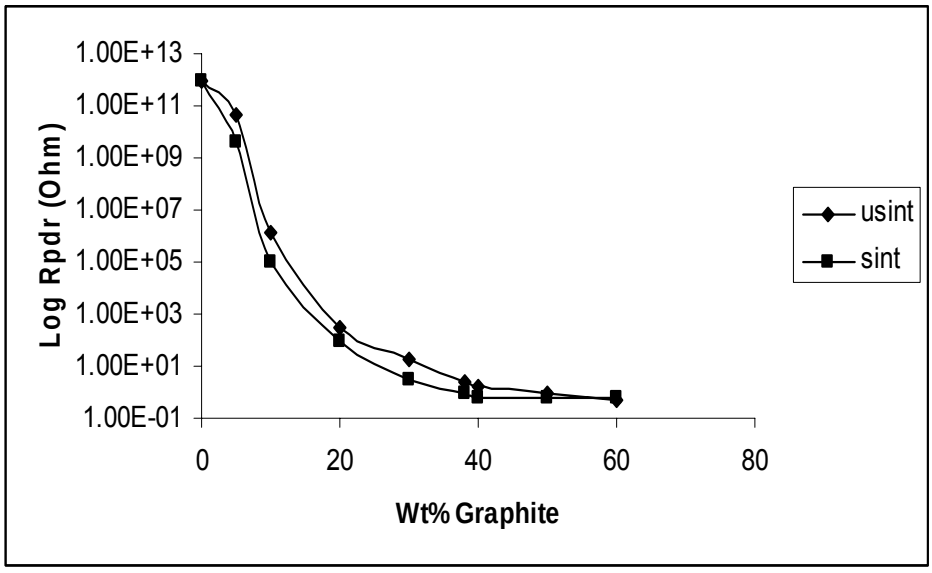

Figure 3.1.10. Through plane resistance of PES-graphite solution blended composites before and after sintering

3.1.6. Hardness Measurement

Hardness is a measure of resistance to plastic deformation. In order to understand the effect of processing routes and sintering, hardness of PES-graphite composites prepared by both solution blending and powder mixing routes have been measured. Also the value of hardness of sintered samples has been compared with that of unsintered samples as shown in Figure 3.1.11.b. It has been observed that the solution blended samples sintered at 240^oC for an hour exhibit higher hardness compared to

the powder processed samples till 50 wt% graphite in PES as shown in Figure 3.1.11.a. The hardness decreases with increasing loading of graphite as it is a soft material tends to agglomerate at higher loading. The lowering of hardness is more pronounced at higher loading (>50 wt%) in composites prepared by both preparation routes. The increase in hardness after sintering can be attributed to the reduction in the particle size leading to uniform distribution of graphite particles in the polymer matrix. Thus in solution blended sintered samples, more reduction in particle size of graphite results in higher hardness than in powder processed samples.

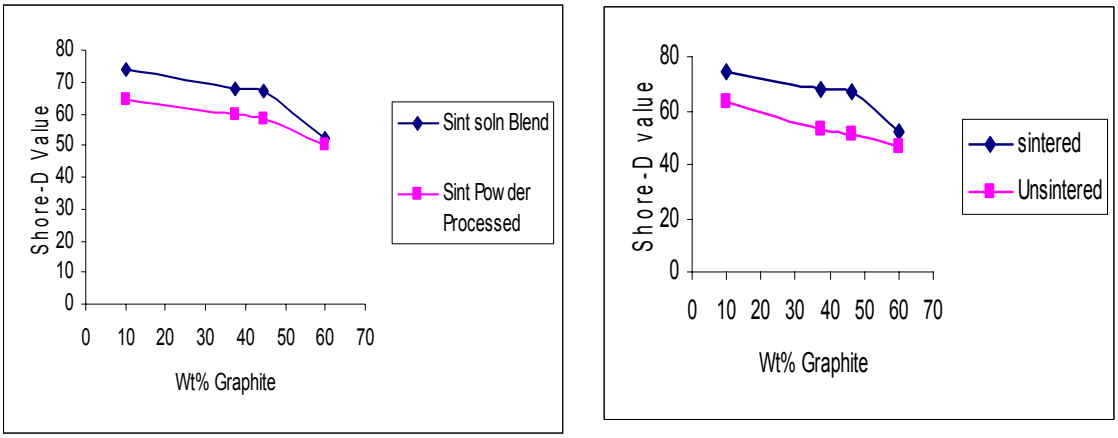

(a) (b)

Figure 3.1.11. Hardness of PES-graphite composites a) Effect of processing routes b) Effect of sintering

3.1.7. Percolation Exponent Determination in Solution Blended PES-graphite Composites

Percolation theory has been applied to find out the dimension of network formation of fillers in an insulating matrix. Above percolation threshold, the conductivity variation predicted by the percolation theory is given by the following equation 1.

$$\sigma = \sigma_o (V_f - V_c)^{t''} \quad \text{for} \quad V_f > V_c \qquad (1)$$

Where σ is the conductivity of the composites, V_f is is the volume fraction of filler above percolation threshold, V_c is the critical volume fraction and 't''' is the percolation exponent signifying dimension of network formation between filler particles. The plot log σ vs log $(V_f - V_c)$ for solution blended PES-graphite composites is shown in Figure 3.1.12 which yields a slope of 2.13. Through plane conductivity of

samples is considered for the extraction of 't'''. For three dimensional network formation t''=2[5]. For solution blended samples the exponent is slightly higher than the universal value signifying tunneling conduction[6-7].

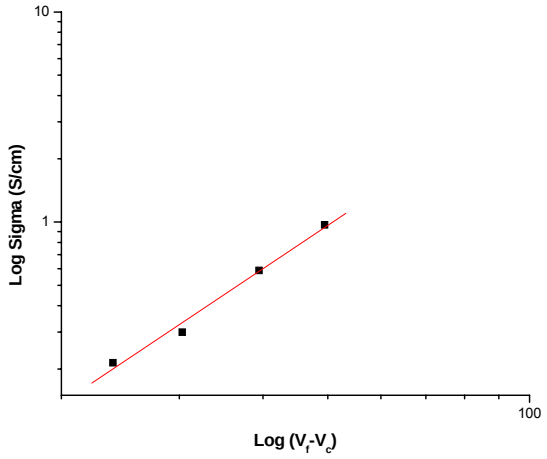

Figure 3.1.12. Log-Log plot of through plane conductivity vs volume fraction of graphite in PES

3.1.8. Polymer-graphite Interaction

In order to understand whether the polymer penetration between graphite layers after sintering is polymer specific or not, a systematic study has been carried out with Polymethyl methacrylate(PMMA)-graphite, Polystyrene(PS)-graphite solution blended samples prepared exactly in the same manner as solution blended PES-graphite samples were prepared. PMMA is an amorphous polymer like PES. Figure 3.1.13 shows the XRD pattern of PMMA-graphite solution blended sample before and after sintering at 130^{o}C since the T_g of PMMA is 105^{o}C. From this Figure 3.1.13, it is evident that no shift in 2 Theta value is observed after sintering. Moreover, the extent of reduction in the intensity corresponding to graphite (002) after sintering is also less.

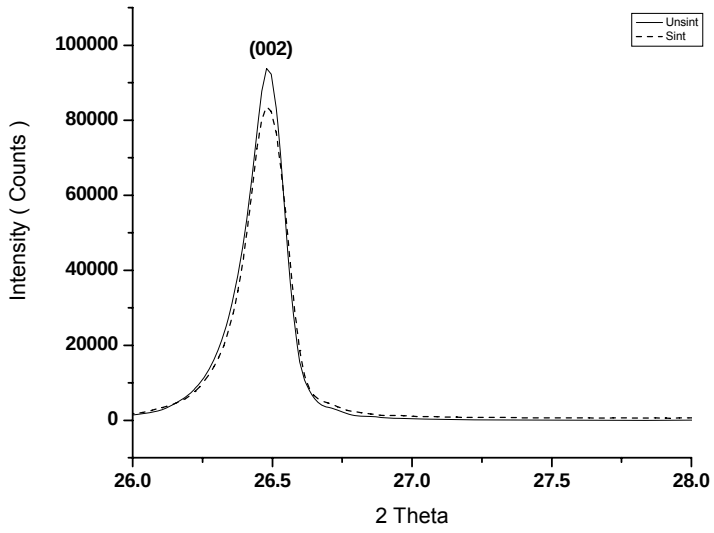

Figure 3.1.13. XRD pattern of graphite part of PMMA-Graphite composites

Thus, it is clear from the above result that the polymer has a major role in forming intercalated structures. More precisely, the interaction between natural graphite and the polymer is more crucial for extensive polymer penetration between graphite layers. The crystallite size reduction and also polymer penetration between graphite layers in PES-graphite system could be due to the interaction between carbon of graphite and sulfur of PES. If the carbon-sulfur interaction is the driving force for penetration of low molecular weight fraction of the polymer in to graphite layers, any sulfone group containing material should exhibit similar trend. Hence a low molecular weight model compound namely Diphenyl Sulfone (DPS) has been blended with graphite in the same manner in DCM, by which PES-graphite composites were made by solution blending technique. The resultant solution blended DPS-38 wt% graphite composite was dried and subsequently TGA analysis of that sample was carried out in nitrogen atmosphere at a heating rate of 10 ^{o}C/min as shown in the following Figure 3.1.14.

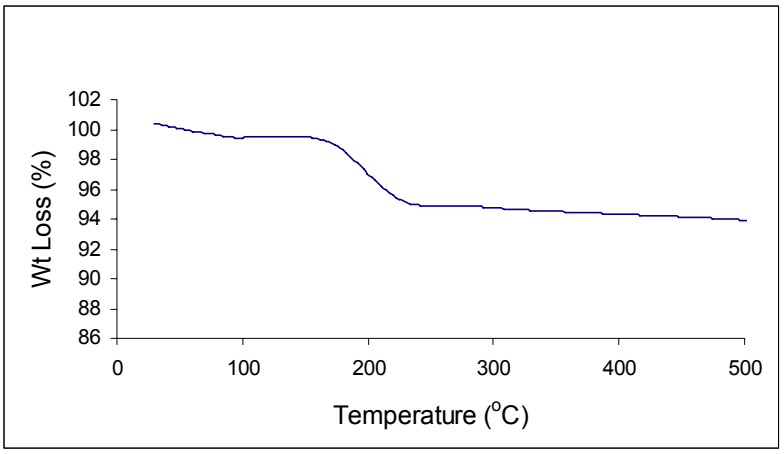

Figure 3.1.14. TGA of DPS-38 wt% graphite

It has been observed from the TGA analysis that there is a weight loss around 160°C corresponding to the sublimation temperature of DPS. Further, It can be ascertained that at least 4% DPS is entrapped between graphite layers till 500°C. Since graphite is a refractory material and the boiling point of the solvent is 40°C, the weight loss in the TGA analysis is none other than DPS. To understand the specific interaction between carbon of graphite and sulfur of PES, XPS analysis has also been carried out and described as follows.

3.1.9 XPS Analysis of PES-graphite Composites

In order to find out the underlying driving force for the extensive polymer penetration between graphite layers, X-ray photoelectron spectroscopy (XPS) studies were carried out on PES, graphite and PES-20 wt% graphite samples. When there is an interaction between different species, there will be an additional peak in the XPS spectrum at different binding energy. As far as PES-graphite system is concerned, the interaction between sulfur of PES and carbon of graphite is clearly revealed in the S 2p spectrum of sulfur of PES than C 1s of carbon of graphite as the number of sulfur atoms are less compared to carbon atoms.

Figure 3.1.15 represents C 1s core level spectra of pure graphite. The peaks at 284.4, 285.6 and 287.0 eV correspond to carbon atoms in graphene planes, etheric and carboxylic carbon[8]. Figure 3.1.16 shows C 1s core level spectrum of graphite mixed with PES.

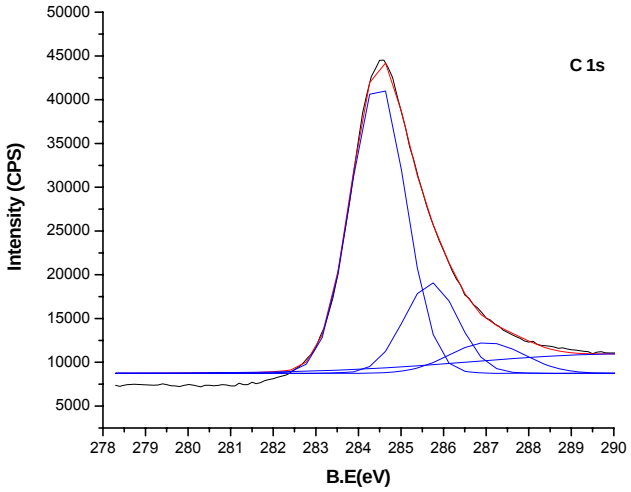

Figure 3.1.15. C1s core level spectrum of pure graphite

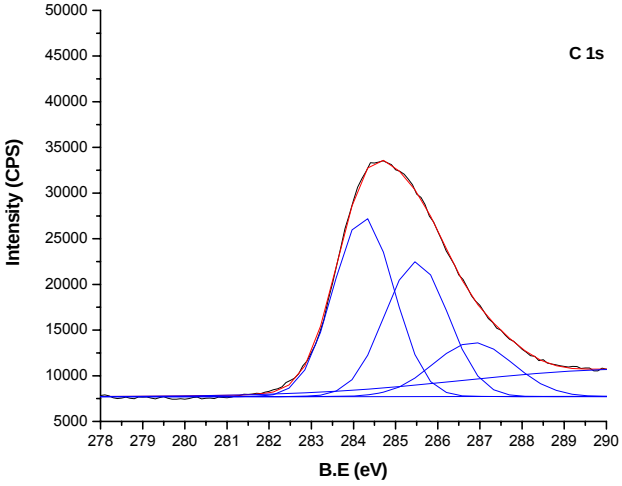

Figure 3.1.16. C 1s core level spectrum of graphite in PES

The reduction in the intensity and increased FWHM can be due to less graphite carbon on the surface. It is to be noted that, though, there is an increase in FWHM of all C 1s peaks, the BE remains the same as that of graphite. Increase in FWHM might be attributed to the matrix effect indicating the distribution of PES in graphite layers and the associated heterogeneity. This factor broadens all the peaks in C 1s regime.

The XPS spectra of S 2p core level corresponding to pure PES and PES-20 wt% graphite have been shown in figure 3.1.17 and 3.1.18 respectively. Two peaks corresponding to S $2p_{3/2}$ at lower binding energy at 167.5 eV and $2p_{1/2}$ at 168.8 eV are

shown. In addition to the above peaks, a new S 2p peak was observed around 171 eV underscoring the interaction between PES and graphite is likely through S atoms. Indeed the interaction between S and graphite layer is expected more than that of O and graphite. This is mainly due to the diffused outer/valence orbitals of S 3p/3s, than the highly electronegative character of oxygen. The above interaction is likely to be reason for extensive polymer penetration inside graphite layers. This has been already demonstrated through systematic XRD studies.

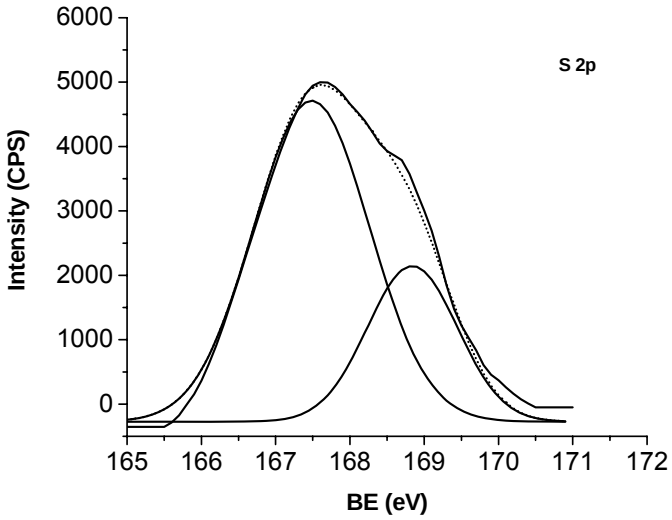

Figure 3.1.17. S 2p Core level spectrum of PES

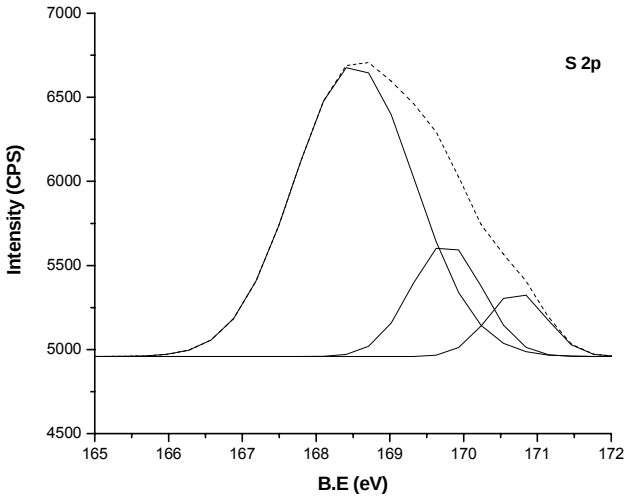

Figure 3.1.18. S 2p core level spectrum of PES mixed with graphite

3.1.10. DSC Analysis

The DSC scans of pure PES, PES-graphite composites during second heating cycle are shown in Figure 3.1.19. The glass transition temperature (T_g) of pure PES is increased by 11°C from 213°C when graphite is mixed with PES by solution blending route. This demonstrates that graphite particles hinder the movement of polymer chains leading to the increase in the T_g. Further more, it has been proved in the literature that increase in the T_g is due to the interaction between the filler and the polymer[9].

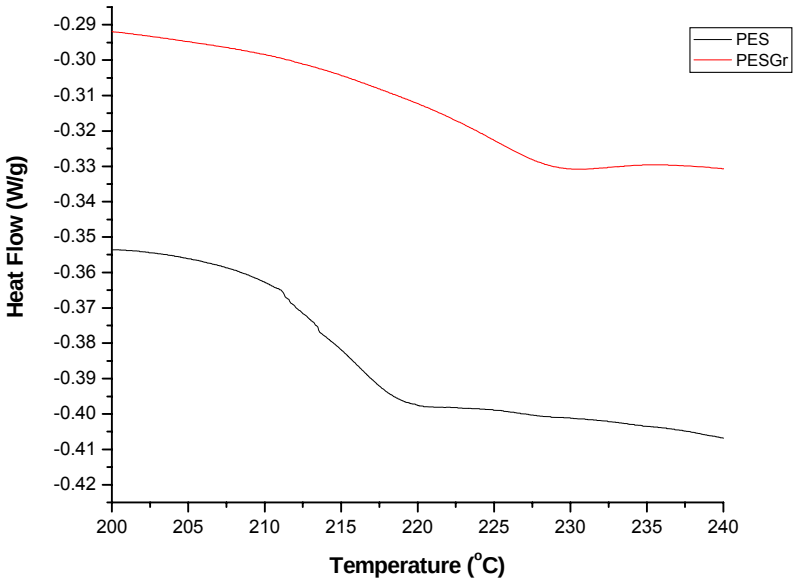

Figure 3.1.19. DSC curves of PES and PES-38 wt% graphite solution blended samples

3.1.11. Frequency Dependent Conductance and Charge Transport in PES-graphite Based Hybrid Composites

The frequency dependent conductance of PES-graphite-CB solution blended hybrid composites is shown in Figure 3.1.20. It is clear that with the addition of CB in PES-7 wt% graphite, conductance increases.

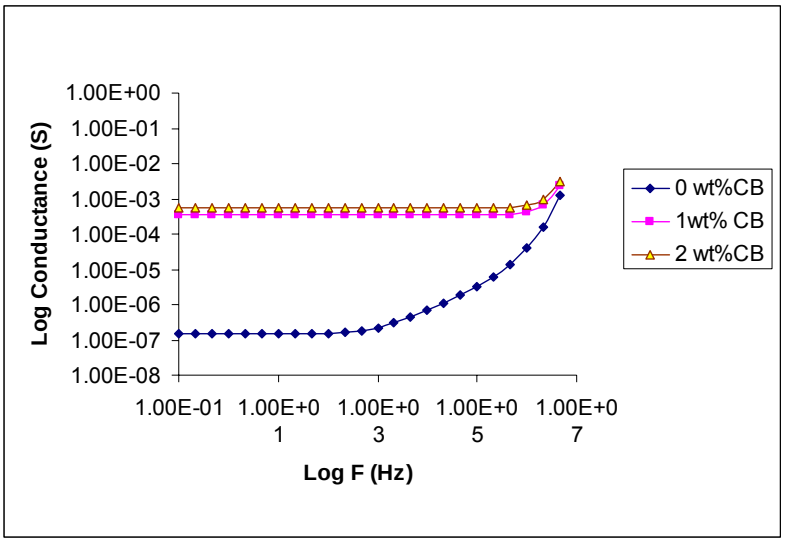

Figure 3.1.20. AC conductance of PES-7 wt% graphite-x wt% CB (x=0,1,2)

With increase in CB loading, the critical frequency at which the conductance starts increasing is shifted to higher values. For 1 wt% CB addition, the conductance is increased by four orders due to network formation as explained in the dc conductivity studies. The plateau region signifies dc conductance which extends further with increasing loading of CB. The charge transport in this system can be found out using the following equation 2.

$$\sigma_{tot} = \sigma_o + A\,\omega^n \qquad (2)$$

Where σ_o is the dc conductivity, A is a constant and 'n' is the exponent signifying the charge transport. When $0<n\leq1$, the charge transport is by hopping. Thus a plot of log σ_{tot} vs log ω should be a straight line with the slope equivalent to exponent 'n'. Figure 3.1.21 clearly depicts the effect of preparation routes on the electrical conductance of PES-7 wt% graphite-2 wt% CB hybrid composite. Solution blended hybrid composite exhibit four order higher conductance when compared to that of powder mixed one.

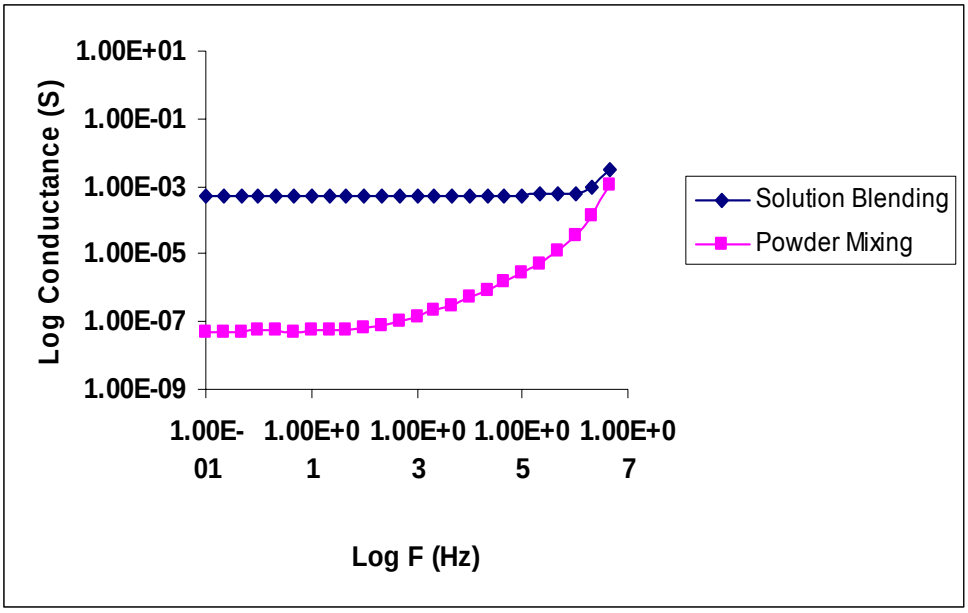

Figure 3.1.21. Effect of preparation route on electrical conductance of PES-7wt% graphite-2 wt% CB

The remarkable increase in conductance of the solution blended sample is due to the reduction in the particle sizes of graphite. The reduction in the CB agglomerates cannot result in this much increase in conductance because without graphite addition, PES-2 wt% CB acts as an insulator as shown in Figure 3.1.2. Table 2 shows the critical exponent for both solution blended and powder mixed samples. For solution blended samples at lower loading of CB corresponding to 2.5 wt% itself hopping conduction begins while for powder mixed samples hopping conduction starts at higher loading i.e. > 2.5 wt% as the exponent becomes less than one. This result also supports the particle size reduction of graphite which is coupled with CB dispersion leading to reduction in the barrier for the charge transport due to the occupation of interspace of graphite by CB particles.

Table 2

Exponent 'n' value for hybrid composites prepared by different routes

Sample	Slope in the high frequency region (n)	
	Solution Blending	Powder Mixing
PES+7wt% Graphite	2.2269	2.4271
PES+7wt% Graphite+1wt%CB	1.1324	2.4267
PES+7wt% Graphite+2.0wt% CB	1.0123	2.2518
PES+7wt%Graphite+ 2.5wt% CB	0.8653	1.9976
PES+7wt% Graphite+3.0wt%CB	-	0.4169

For lower loading of CB in PES-7 wt% graphite, less than 2 and 3 wt% for solution blended samples and powder mixed samples respectively, the exponent value is greater than one signifying capacitive effects coupled charge transport. This kind of result has been published in the literature for different system[10]. For 2.5 wt% CB loading in PES-7 wt% graphite and solution blended, the charge transport is by hopping mechanism as the exponent becomes less than one.

3.1.12. Effective Dielectric Constant Variation in Solution Blended PES-graphite-CB Hybrid Composites

Figure 3.1.22 shows the effective dielectric constant variation of solution blended PES-graphite-CB hybrid composites with respect to frequency. The effective dielectric constant at 0.01 Hz increases from 10^3 for 0 wt% CB in PES-7 wt% graphite to 10^6 for 2 wt% CB addition in the same.

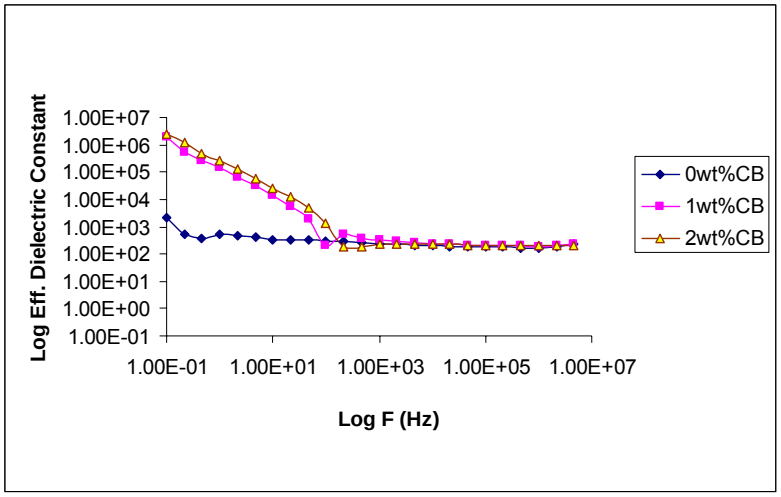

Figure 3.1.22. Effective dielectric constant variation with frequency of hybrid composites

The increase in the effective dielectric constant with the addition of CB is due to the occupation of CB in the intergraphite space. With 2 wt% CB addition in PES without graphite, the composite behaves as an insulator. Loading of 7 wt% graphite in PES without CB results in the effective dielectric constant of 1000. Thus the three order increase in the effective dielectric constant is due to the occupation of CB particles in the space between graphite particles. This is represented by a model shown in Figure 3.1.23.

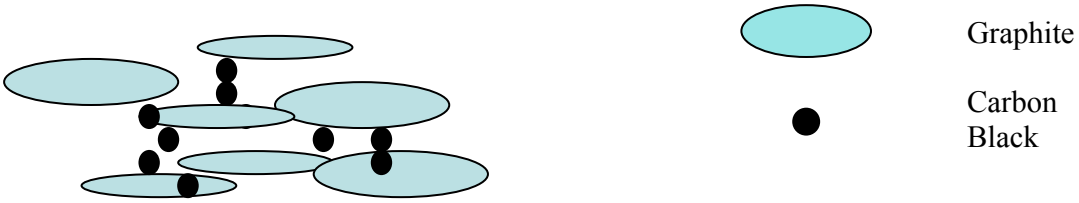

Figure 3.1.23. Model of hybrid composites

If CB particles occupy graphite interspace, the interparticulate distance for the charge transport is decreased. Conducting particles separated by a distance within which polymer of finite thickness remains can be considered as parallel plate capacitors with capacitance given in equation 3 below.

$$C = \varepsilon A / d \quad (3)$$

Where ε is the effective dielectric constant, A is the area of the parallel plate and d is the distance between the parallel plates in a parallel plate capacitor.

If the above model is true, the interjunction capacitance with the addition of CB in PES-7 wt% graphite should increase. The interjunction capacitance of hybrid composites has been evaluated from impedance spectroscopy studies.

3.1.13. Impedance Analysis of PES-graphite-CB Hybrid Composites

Conducting polymer composites can be modeled as a parallel combination of resistor and capacitor with a series resistor as shown in Figure 3.1.24. More precisely, the model resembles Randle's diagram used to model electrode-electrolyte system in electrochemistry. There can be series and parallel arrangement of resistor-capacitors as shown in the Figure 3.1.24 in which R_p and R_c represent the bulk resistance of the sample, R_a is the aggregate resistance of the fillers and C is the interjunction capacitance. Impedance spectroscopy (IS) is more practical in evaluating the individual component in the above model. However it gives lumped values of model parameters. The limitations of IS have been mentioned in chapter 1. Impedance plots often referred to as Cole-Cole plots are useful for extracting interjunction capacitance.

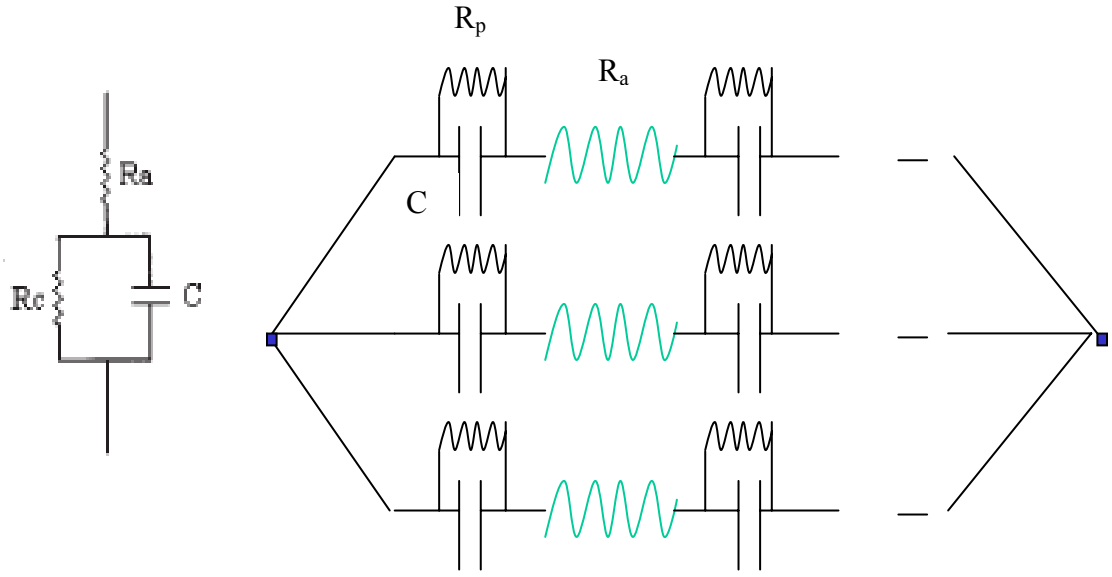

Figure 3.1.24. Model of conducting polymer composites

Impedance analysis of several polymer composites has been done through bode plot[11]. For parallel model, a plot of Z_{real}vs $Z_{imaginary}$ often describes a semicircle in the Argand plane from which the junction capacitance can be calculated using equation 4 given below.

$$R_pC = 1/ \omega_{max} \quad (4)$$

Where R_p is the material resistance, C is the interjunction capacitance and ω_{max} is the frequency at which real and imaginary parts of impedance becomes equal.

Figure 3.1.25.a and 3.1.25.b show the impedance plots of solution blended PES-7 wt% graphite and PES-7 wt% graphite-1 wt% CB hybrid composite respectively.

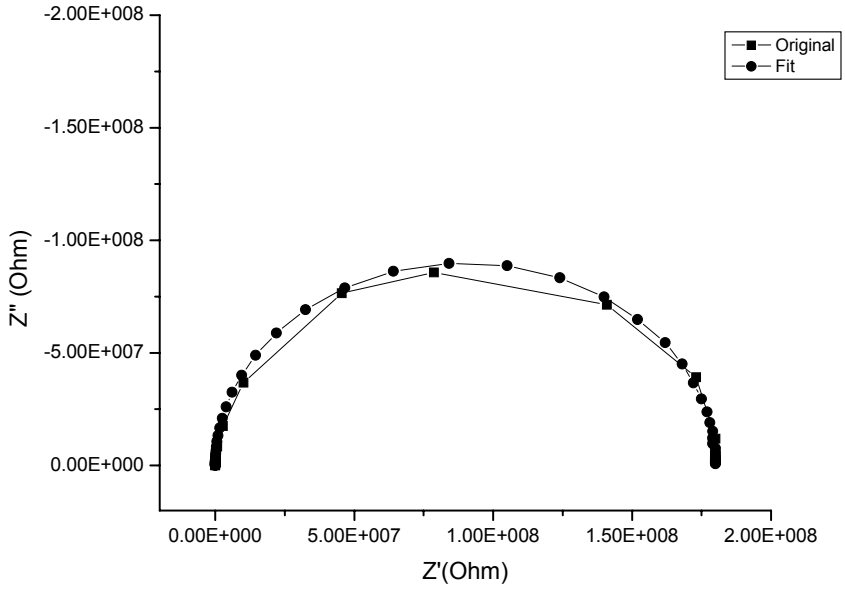

(a)

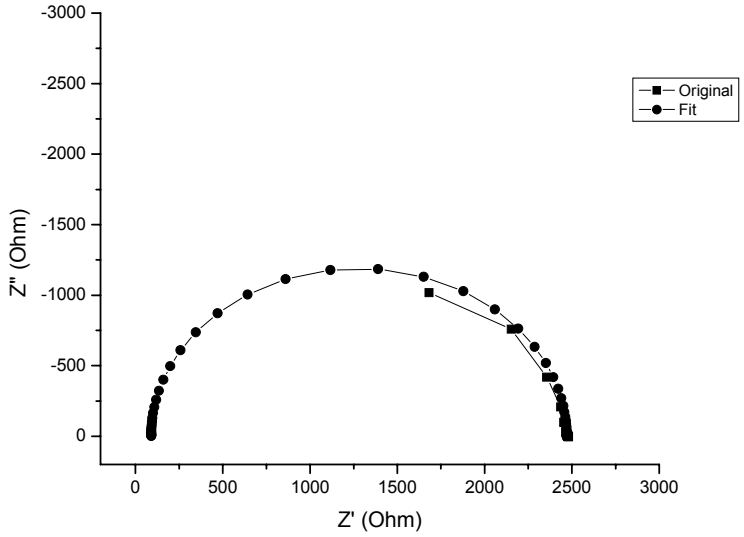

(b)

Figure 3.1.25. Impedance plots of solution blended a) PES-7 wt% graphite b) PES-7 wt% graphite-1 wt% CB

The diameter of the semicircle obtained represents the dc resistance which matches with that of measured value for these composites. It is also clear that with the addition of CB, the diameter of the semicircle decreases which suggest that the samples have become more conducting. When the experimental results are fitted to the parallel model, the various model parameter extracted are presented in Table 3 given below.

Table 3

Parameters derived from Impedance plots of PES-7 wt% graphite-CB solution blended composites

Sample	R_a (Ohm)	R_p (Ohm)	C (pF)
1. PES-7 wt% graphite	370	$1.8x10^8$	38
2. PES-7 wt% graphite-1 wt% CB	90	$2.38x10^3$	61
3. PES-7 wt% graphite-2 wt% CB	05	$9.88x10^2$	96

The above Table 3 depicts that the bulk resistance of the sample decreases with increasing loading of CB. Addition of 2 wt% CB in PES-7 wt% graphite decreases the resistance by eight orders due to the creation of more conducting paths. Further

the interjunction capacitance increases from 38 pF for 0 wt% CB in PES-7 wt% graphite to 96 pF for 2 wt% CB addition in the same. The above results prove the model that CB particles indeed occupy intergraphite space. As already explained in the effective dielectric constant section that graphite without CB or CB without graphite in PES can't increase the effective dielectric constant to that extent. This point supports the existence of graphite-CB-graphite junctions. One striking result is that the aggregate resistance drops down rapidly with CB addition.

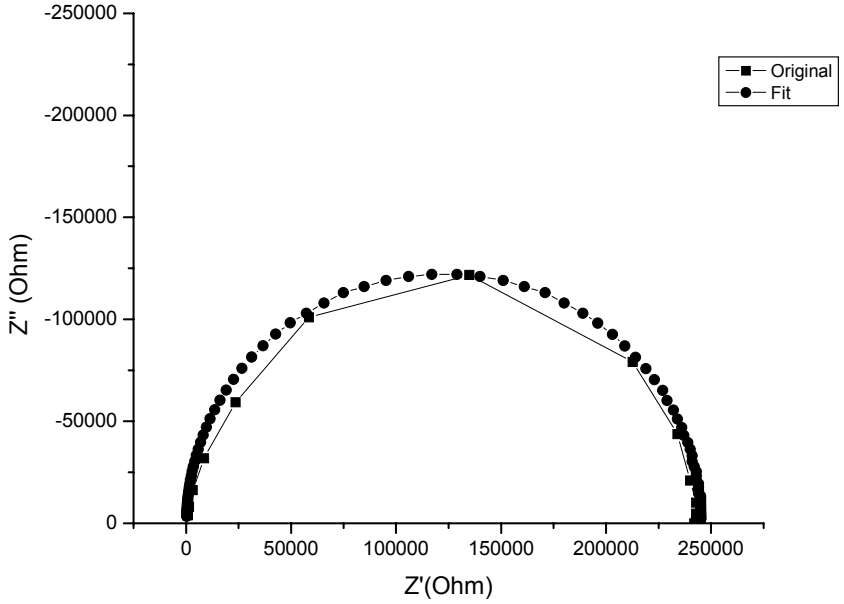

Figure 3.1.26. Impedance plot of PES-7 wt% graphite-2.5 wt% CB powder mixed sample

Similar kind of results has been obtained for powder mixed samples. Figure 3.1.27 shows the impedance plot of powder mixed PES-7 wt% graphite-2 wt% CB. The various model parameters extracted from the impedance plots of powder mixed samples are given in the following Table 4.

Table 4

Model parameters for PES-7 wt% graphite-2.5 wt% CB powder mixed samples

Sample	R_a (Ohm)	R_p (Ohm)	C (pF)
1. PES-7 wt% graphite	250	$5.0x10^{11}$	33
2. PES-7 wt% graphite-2 wt% CB	150	$2.45x10^{5}$	58

In the powder mixed samples also the bulk resistance decreases with the addition of CB in PES-7 wt% graphite but not to that extent by which it decreases for solution blended samples. The increase in the surface area of graphite particles due to particle size reduction in solution blended samples results in rapid reduction in bulk resistance.

Reason for decrease in R_s

The decrease in the aggregate resistance can be understood as follows. The aggregate resistance variation is due to the contact between CB and graphite particles both have different work functions. CB has higher work function than that of graphite.

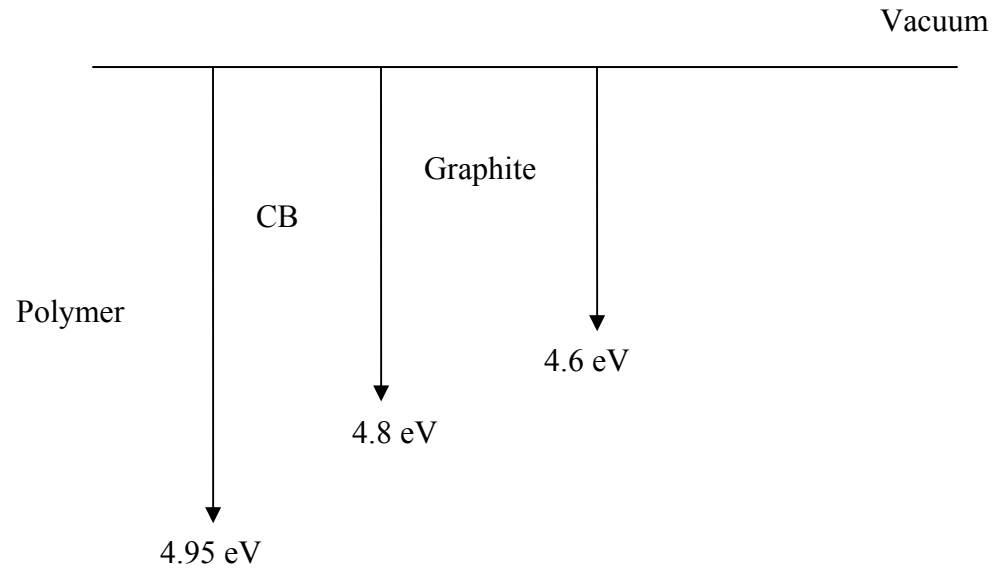

Figure 3.1.27. Work function diagram of fillers

The work function of CB is taken as 4.8 eV which depends up on the grade[12] and that of graphite is 4.6 eV[13]. The polymer work function is taken as 4.95 eV[14]. In order to

understand the charge transport, single polymer-CB-graphite junction is considered which can be assumed to be connected in series. In the absence of CB, for the charge transfer from polymer to graphite, a barrier of 0.35 eV need to be crossed as the barrier is essentially the difference in the work function of materials in contact. In the case of hybrid composites, when CB occupies space between polymer and graphite, the barrier is only 0.15 eV. Thus the charges can be transferred to graphite via CB. When the CB concentration is increased, more CB particles occupy the interspace and hence more charges will be transferred to graphite via CB resulting in decrease in the aggregate resistance. The work function diagram has been shown in Figure 3.1.27.

3.1.14. I-V Characteristics of PES-graphite-PES Junction

I-V characteristic of single PES-graphite-PES junction was measured by sweeping the voltage and measuring the current using Keithley (3600-C) source meter. The film thickness was 40 μm and pure graphite of thickness 3 mm was sandwiched between the films. The plot clearly shows that $I \propto V^{1.9}$ where the exponent is very close to that of space charge limited conduction for which it is two[15]. In binary PES-graphite composites many such junctions exist. Figure 3.1.28 shows the I-V characteristics of single PES-graphite-PES junction

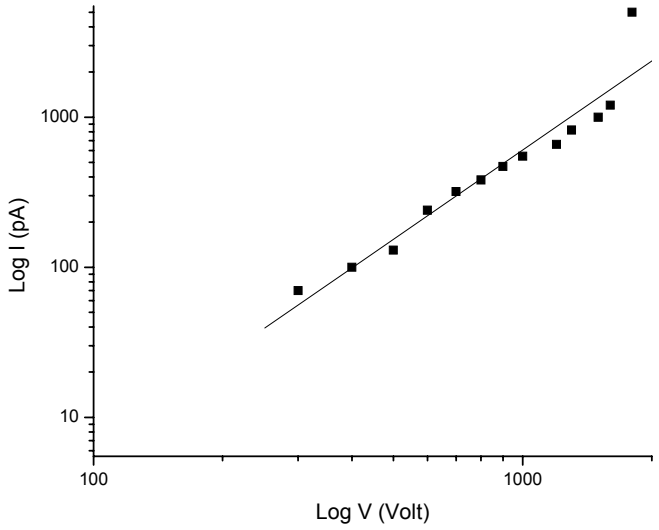

Figure 3.1.28. I-V Characteristics of PES-graphite-PES single junction

3.2. PES-CNF, PES-graphite-CNF Composites

3.2.1. Carbon nanofiber- Introduction

Carbon nanofiber, one of the important conducting fillers is being used for making conducting polymer composites for various applications such as electro magnetic interference shielding devices, anti corrosion coatings etc. It acts as a replacement for the one dimensional carbon nanotubes which are quite expensive though the later has higher electrical and thermal conductivities. Multiwalled carbon nanotubes are three times expensive than vapor grown carbon nanofibers (VGCNFs) where as single walled carbon nanotubes are seven times more expensive that of VGCNF[16].

VGCNFs are produced by catalytic chemical vapor deposition of hydrocarbon such as natural gas, propane, benzene, ethylene etc., or carbon monoxide on the surface of a metal or metal alloy catalyst. The catalyst can be deposited on a substrate or directly fed with the gas phase. The reaction is usually operated at 500^{o}C to 1500^{o}C[17]. VGCNFs are high aspect ratio nanofibers with larger diameter than CNTs. They are hollow core nanofibers comprise of a single or double layer graphite planes stacked parallel or certain angle from the fiber axis. The stacked planes are nested with each other and have different structures including bamboo like, parallel and cup-stacked[18].

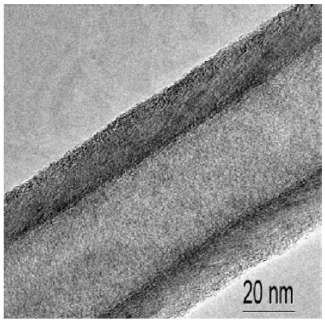

Figure 3.2.1. HRTEM image of VGCNF[19]

VGCNFs have volume resistivity of 6x10^{-5} Ω-cm[20] and thermal conductivity 1950 W/m-K[21] which is lower than that of MWCNT and SWCNT. One of the major drawbacks of VGCNFs is their poor tensile properties as compared to CNTs which depend on their diameter. Though the properties are bit inferior to CNTs, it is being focused for the fact that it is cheaper and ease of preparation process. Hence in the present dissertation, VGCNFs from pyrograph products, USA has been used as nanofiller.

3.2.2. DC Conductivity Variation in PES-CNF Binary Composites

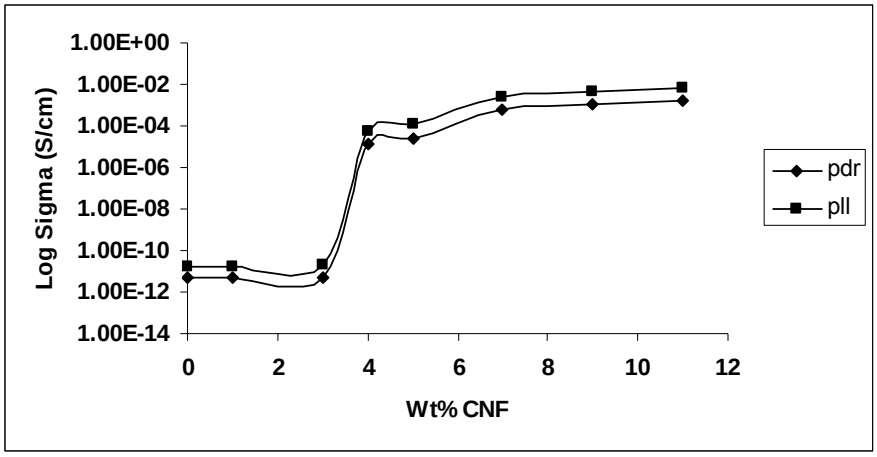

Figure 3.2.2. DC conductivity of PES-CNF composites

The above Figure 3.2.2 depicts the variation of through thickness (pdr) and in-plane (pll) conductivities of PES-CNF composites prepared by solution blending method. As CNFs are bundled, before being added to PES solution, dispersed in DCM for 5 hours by sonication. Further, after mixing, the composites were stirred vigorously for 12 hours and then dried in a Petri dish. The resultant chunks were crushed, sieved and used for making pellets. It can be seen from the above Figure 3.2.2 that the percolation threshold lies at 3 wt%, below which the composites behave as insulators due to lack of network formation between fillers. Above 6 wt% CNF addition, the conductivities saturate due to sufficient network formation. Percolation type of conductivity variation is exhibited by the composites. It should be noted that the in-plane conductivity is higher than that of through plane conductivity due to the alignment of CNF along the surface of the pellet due to high pressure compaction employed while making pellets.

3.2.3. Dimension of Network Formation of Filler in PES-CNF Composites

The slope of log σ vs log (V_f-V_c) according to equation 1 yields a slope which is nothing but the percolation exponent 't'''. The plot of log σ vs log (V_f -V_c) is shown in Figure 3.2.3. The exponent 't''' in this binary system is equal to 2.04 which is more closer to 3D network formation value i.e., 2. The exponent value of 3 has been reported in the literature[22].

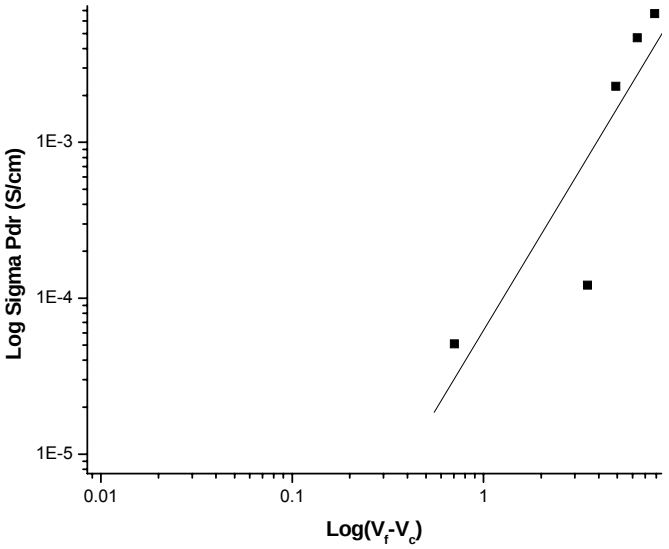

Figure 3.2.3. Log-Log plot of though plane conductivity vs volume fraction of CNF in PES

3.2.4. Effect of Heat Treatment

The effect of sintering above T_g of the polymer i.e., at 240^oC for one hour on the dc conductivity of PES-CNF composites has been studied. Sintering time was varied from 1-5 hrs to find out any variation in electrical conductivity of composites and has been observed that no significant change in resistance with sintering time. So readings corresponding to one hour are reported. It is clear from Figure 3.2.4 that the through plane conductivity of PES-CNF composites after sintering increases.

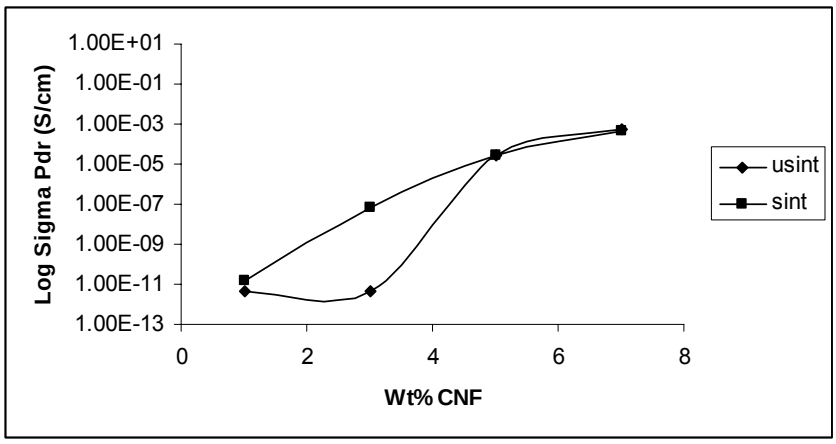

Figure 3.2.4. Through plane conductivity of PES-CNF composites before and after sintering

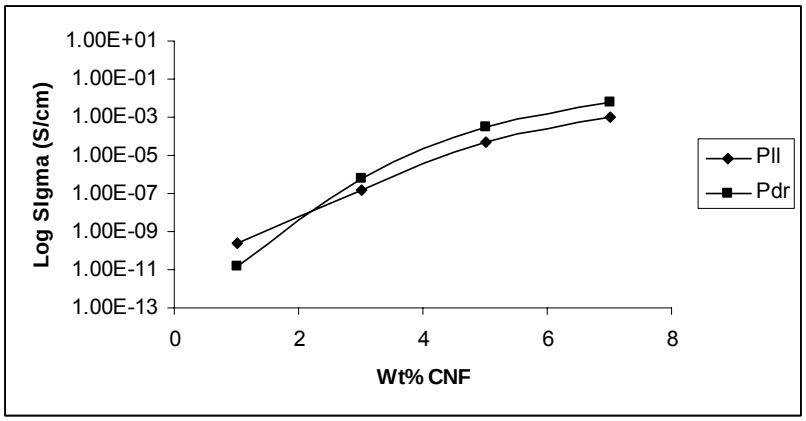

Figure 3.2.5. Conductivity variation of PES-CNF after sintering

The enhancement in the conductivity is more pronounced at 3 wt% which is the percolation threshold of the composites. Figure 3.2.2 shows that the in-plane conductivity of the composites is higher than that of the through plane due to the alignment of the fiber along the surface of the pellet. After sintering, the through plane conductivity increases which can be understood in terms of re-orientation of fibers along the through thickness direction. At 3 wt% filler loading, after sintering, the network formation along the through thickness direction will be completed and hence more than four orders enhancement in the conductivity is observed. It should be remembered that the composite at 3 wt% CNF loading is an insulator before sintering. This kind of re-orientation effect after sintering has already been observed for PES-graphite composites[23]. Further on comparing the through plane and in-plane conductivities of the composites after sintering, below percolation threshold, the later is higher than that of through plane due to lower filler concentration and there may not be enough contacts along the through thickness direction. Above percolation threshold, through plane conductivity is higher than that of in-plane due to re-orientation of fibers along the thickness of the pellet. On the surface of the pellet more polymer will be found due to the movement of polymer chains, resulting in the decreased in-plane conductivity which indeed was observed by us. Cipriano *et al.*.[24] have published that annealing at temperatures above glass transition temperature of polystyrene-CNT and PS-CNF composites prepared by melt blending results in the conductivity enhancement. However the authors have not commented about in-plane conductivity. They have proved that the transition from aligned, unconnected

particles prior to annealing to an interconnected network after annealing through viscoelastic relaxation of the polymer.

3.2.5. Impedance Analysis of PES-CNF Binary Composites

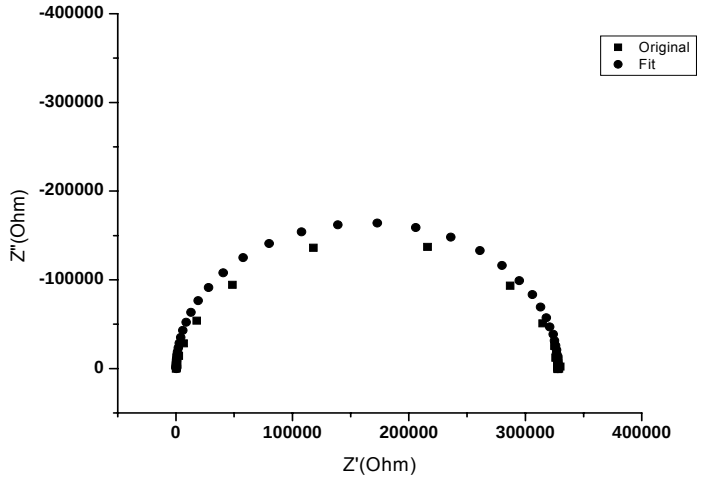

(a)

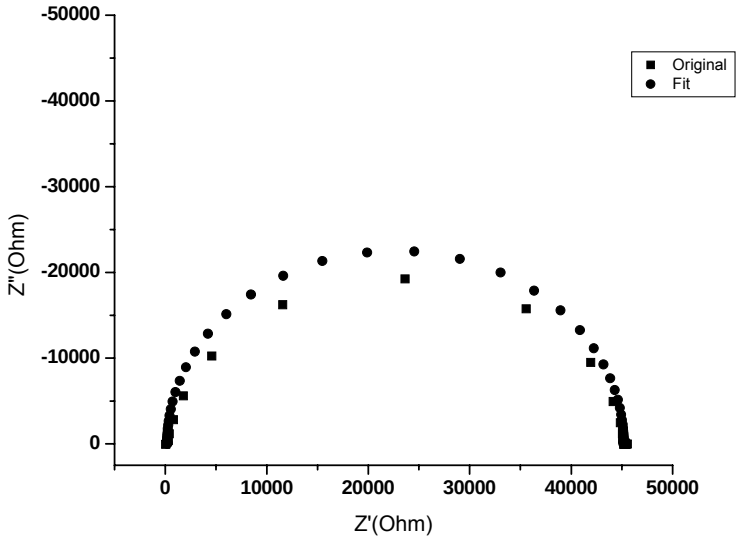

(b)

Figure 3.2.6. Impedance plots of a) PES-3.5 wt% CNF b) PES-3.75 wt% CNF

The above impedance plots shown in Figure 3.2.6 for PES-3.5 wt% CNF and PES-3.75 wt% CNF trace semicircle in Argand plane and hence can be modeled as parallel resistor-capacitor with a series resistor. The different parameters and the model have

been explained in the previous section itself. With increasing loading of CNF, the diameter of the semicircle decreases indicating enhancement in the conductivity of the composites. Different parameters extracted by fitting the experimental curve are shown in Table 5.

Table 5

Parameters extracted from the impedance plot for PES-CNF composites

Sample	R_a (Ohm)	R_p (Ohm)	C (pF)
1. PES-3 wt% CNF	380	6.0×10^{10}	42
2. PES-3.5 wt% CNF	280	3.3×10^{5}	62
3. PES-3.75 wt% CNF	190	45000	68

From the above Table 5, it can bee seen that the interjunction capacitance increases from 42 pF for 3 wt% CNF to 68 pF for 3.75 wt% CNF in PES. Bulk resistance ($R_{p)}$ and aggregate resistance ($R_{a)}$ decrease with CNF loading. The decrease in the aggregate resistance is due to enhanced contact between the filler with increasing filler concentration[25]. Bulk resistance decreases with the addition of CNF due to network formation between fillers.

3.2.6. DSC Analysis of PES-CNF composites

DSC plot of pure PES and PES-5 wt% CNF is shown in Figure 3.2.7. The T_g of the polymer has been increased by 11^oC when CNF is added to the polymer suggesting strong interaction between the polymer and the filler. The CNFs could hinder the movement of polymer chains due to their high aspect ratio resulting in increased T_g of the polymer.

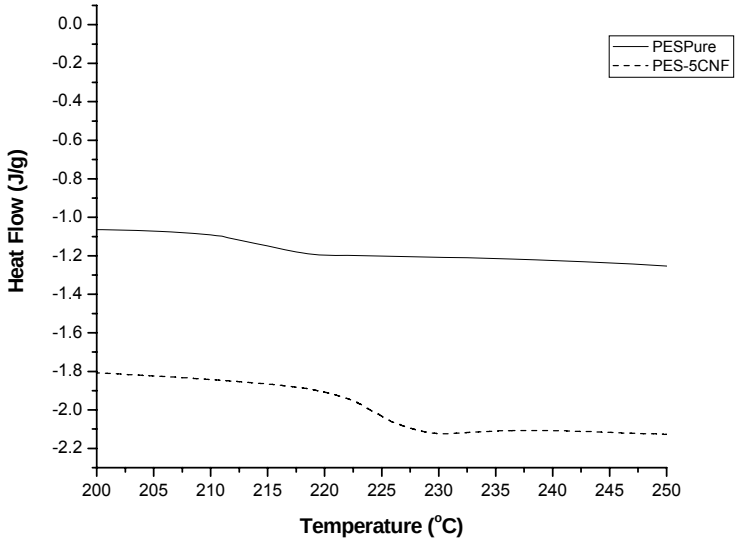

Figure 3.2.7. DSC comparison between pure PES and PES-5 wt% CNF

3.2.7. TEM Analysis of PES-CNF Composites

The TEM pictures of PES-CNF composite after dissolving PES in DCM and sonicating for a minute are shown in Figure 3.2.8.

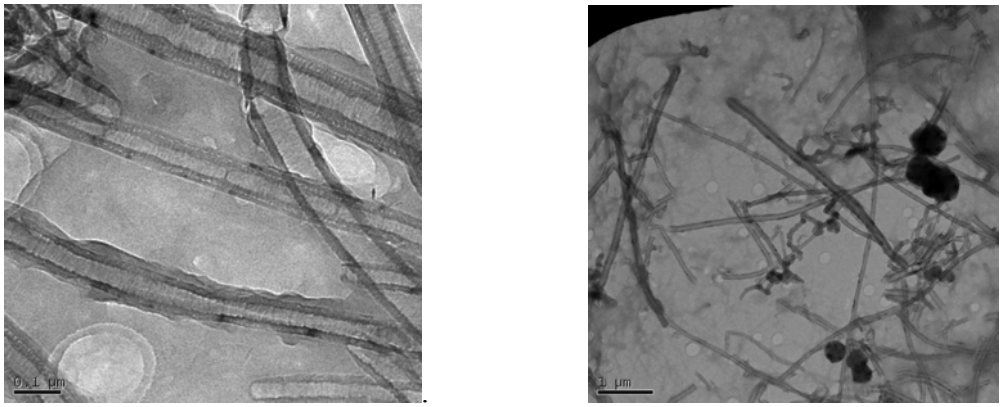

(a) (b)

Figure 3.2.8. TEM pictures of CNF after dissolving PES in DCM

The average length of CNF is taken as 8 μm (taking the average length of 15 tubes) and the tube diameter ~110 nm. The aspect ratio becomes 72.72 which is less compared to the original CNF due to processing.

3.2.8. DC Electrical Conductivity of PES-Graphite-CNF Hybrid Composites

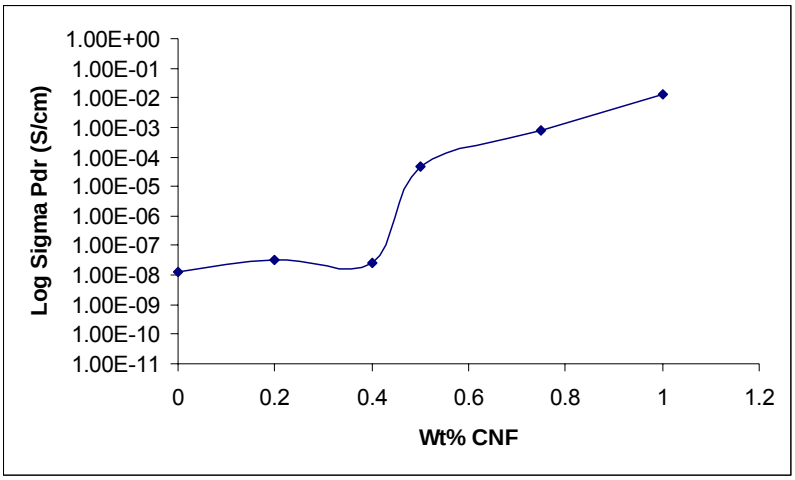

Figure 3.2.9. Through plane conductivity of PES-7 wt% graphite-x wt% CNF

The above Figure 3.2.9 shows the variation of through plane conductivity of solution blended PES-7 wt% graphite-CNF composites. It has been already shown that solution blended PES-7 wt% graphite exhibits a conductivity of the order of 10^{-8} S/cm. With the addition of CNF up to 0.4 wt%, the conductivity increase is not high enough and above 0.4 wt% there exists at least four order increase in the through plane conductivity of the samples. Thus the percolation threshold can be identified at 0.4 wt%. Addition of 1 wt% CNF in PES-7 wt% graphite, the conductivity reaches 0.01 S/cm value. To achieve same value, 40 wt% graphite is required in the absence of CNF. Without graphite at least 10 wt% CNF is required to attain that conductivity value. Thus the importance of hybrid composites can be gauged. The conductivity enhancement is due to the reduction in the barrier between graphite particles for the charge transport along with the establishment of better connectivity between fillers at low loading of high aspect ratio filler like CNFs.

3.2.9. AC Behavior of PES-graphite-CNF Hybrid Composites

With the addition of conducting fillers, insulator-semiconductor transition is realized by the shift of the critical frequency to higher values where the conductance starts to increase. Further the plateau region which is a measure of dc conductivity extends further with increase in the loading of conducting fillers.

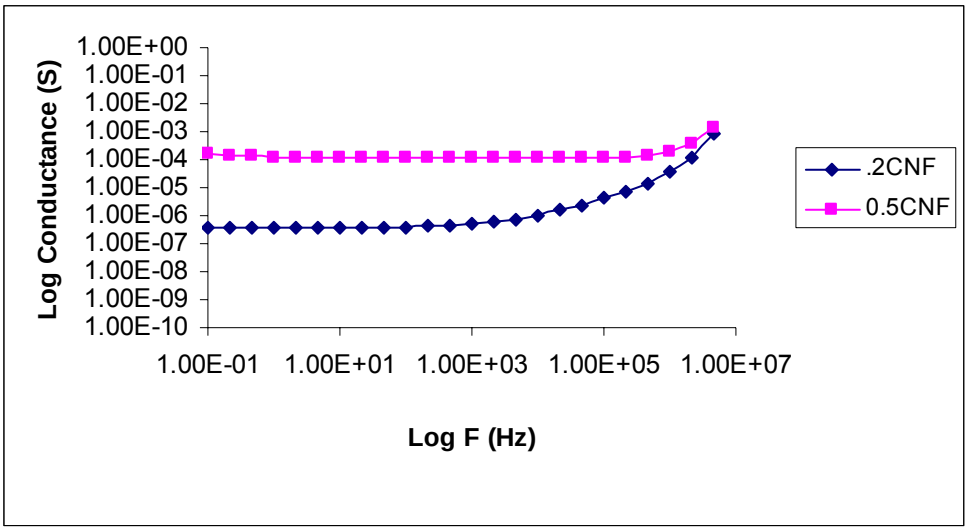

(a)

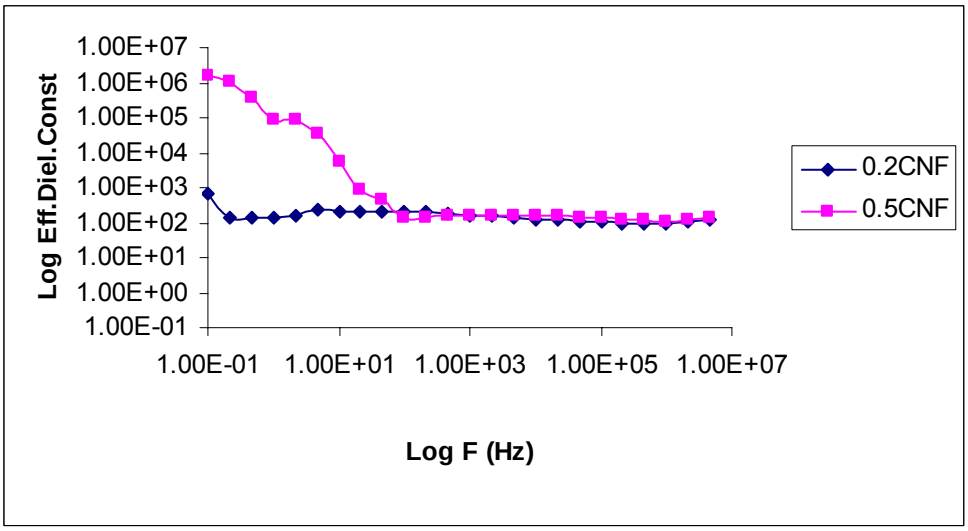

(b)

Figure 3.2.10. a) AC conductance b) Frequency dependent effective dielectric constant of hybrid composites

Figure 3.2.10.a shows two order increase in the conductance for 0.5 wt% CNF addition in PES-7 wt% graphite when compared to 0.2 wt% CNF addition in the same. The barrier between graphite particles is reduced due to the occupancy of CNF in between graphite particles. This is verified by measuring effective dielectric constant as a function of frequency. In Figure 3.2.10.b, the effective dielectric constant

variation with frequency and composition of CNF has been shown. For a fixed CNF loading, the effective dielectric constant decreases up to a certain frequency and then remains more or less constant which is a typical variation observed in disordered systems. The effective dielectric constant at low frequency i.e., at 0.01 Hz increases by three orders for 0.5 wt% CNF in PES-7 wt% graphite when compared to 0.2 wt% CNF addition in the same. Such an increase in the effective dielectric constant cannot be due to CNF dispersion alone. Without graphite PES-0.5 wt% CNF acts as an insulator which can be concluded from the dc conductivity plot of binary composites. Similarly PES-7 wt% graphite solution blended sample exhibits a conductivity of 10^{-8} S/cm which cannot lead to the three orders increase in the effective dielectric constant. Thus the CNFs should occupy predominantly intergraphite space for the loading ranges employed in this study. In order to evaluate the interjunction capacitance, impedance analysis has been carried out as discussed below.

3.2.10. Impedance Analysis of PES-graphite-CNF Hybrid Composites

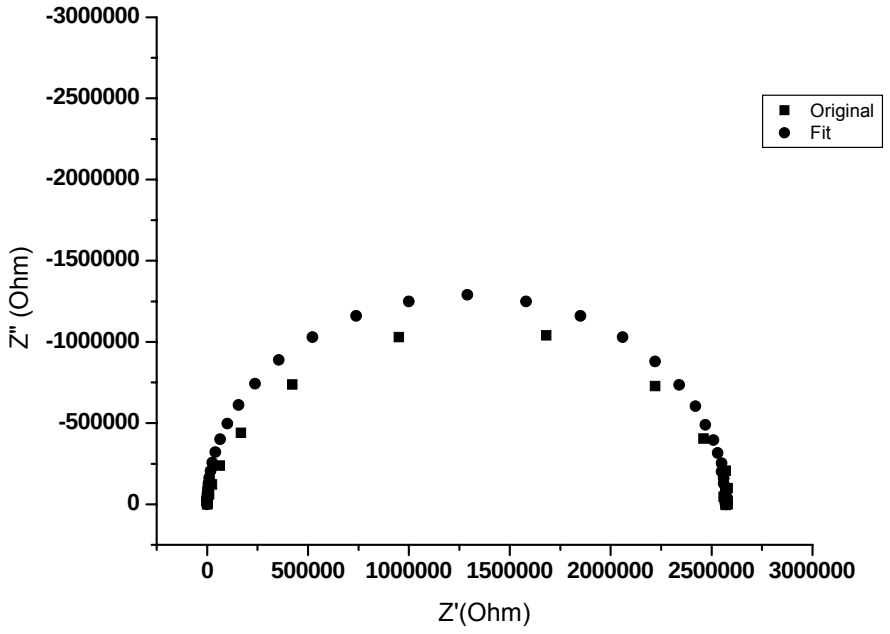

(a)

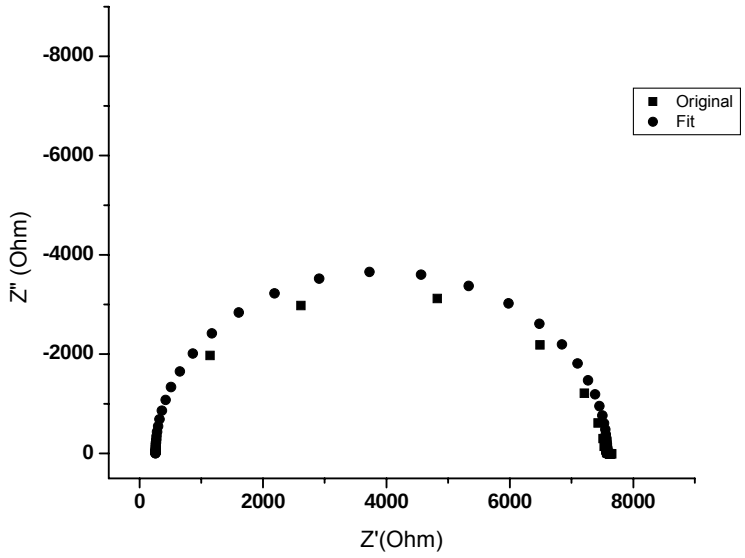

(b)

Figure 3.2.11. Impedance plots of a) PES-7 wt% graphite-0.2 wt% CNF b) PES-7 wt% graphite- 0.5 wt% CNF

The impedance plots of PES-7 wt% graphite-0.2 wt% CNF and PES-7 wt% graphite-0.5 wt% CNF are shown in Figure 3.2.11.a and b respectively. The impedance behavior of PES-graphite-CNF composites is such that they form semicircle in Argand plane suggesting that they can be modeled as a parallel combination of resistor and capacitor with a resistor in series. With the addition of more CNF, the diameter of the semicircle is reduced which implies that the samples have become more conducting. Table 6 lists model parameters obtained after fitting the experimental data to parallel model mentioned above. With the addition of 0.5 wt% CNF in PES-7 wt% graphite, the resistance decreases by five orders due to the network formation of fillers. The interjunction capacitance, with increasing loading of CNF, increases considerably from 38 pF for 0 wt% CNF in PES-7 wt% graphite to 73 pF for 0.5 wt% CNF in PES-7 wt% graphite. This supports the model assumed earlier. Thus the CNF occupies intergraphite space reducing the barrier for the charge transport. It is worth to note is that the aggregate resistance decreases with the addition of CNF in this hybrid composites also.

Table 6

Model parameters for solution blended PES-7 wt% graphite- CNF composites

Sample	R_a (Ohm)	R_p (Ohm)	C (pF)
1. PES-7 wt% graphite	370	1.8×10^8	37.6
2. PES-7wt% Graphite-.2wt% CNF	300	2.57×10^6	61.5
3. PES-7wt% Graphite- .5wt% CNF	260	7320	72.5

The decrease in the aggregate resistance with the addition of CNF can be understood from the work function of individual components. As indicated earlier, polymer work function is 4.96 eV and that of graphite is 4.6 eV. Since the barrier height is nothing but the difference in the work function of materials in contact, for charges to be transported from polymer to graphite a barrier of 0.36 eV need to be crossed. When CNF is added, it reduces the barrier as the work function difference between the polymer and CNF is 0.04 eV. Thus if more CNF is incorporated between polymer and graphite, more charges will be transferred to graphite via CNF resulting in the aggregate resistance decrease. The same arrangement can be thought of as connected in series through out the volume of the sample. Since filed is applied, it makes the charges to flow in one direction. The work function of CNF is taken as 5 eV[26]. In binary composites particle-particle contact increases with enhanced loading of filler particles where as for hybrid composites, the aggregate resistance decrease can be better explained in terms of work function of the individual components as shown in the flowing Figure 3.1.12.

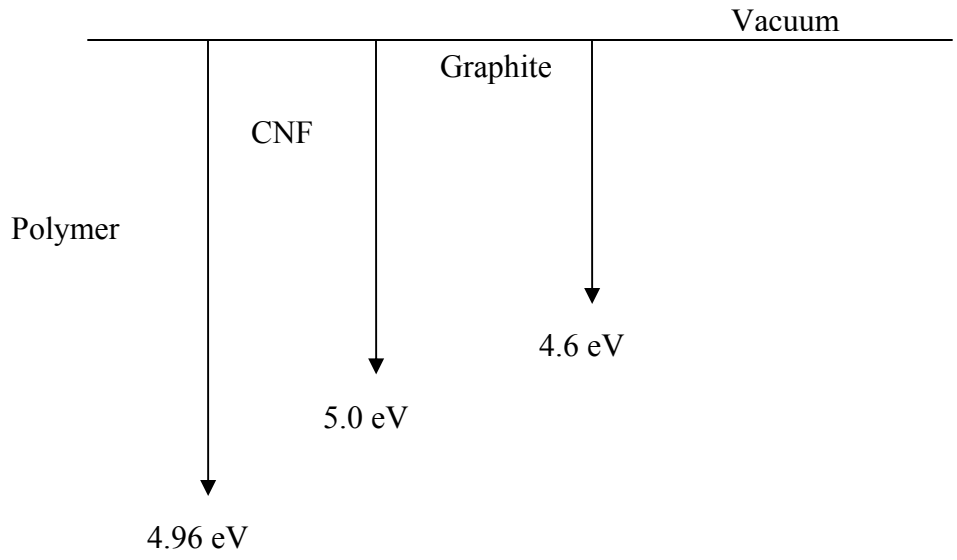

Figure 3.2.12. Work function diagram

3.3. PES-expanded graphite and PES-graphite-expanded graphite Composites

3.3.1. Expanded graphite (ExGr)-Introduction

Expanded graphite is an attractive filler for making conducting polymer composites. It has porous structure with varying pore diameters in the micron range. Though the conductivity of expanded graphite is lesser than that of natural graphite, the percolation threshold can be reduced to a great extent when used as filler. In-situ polymerization leads to the formation of nanosheets resulting in better conductivity[27]. Its morphology is given in the following Figure 3.3.1.

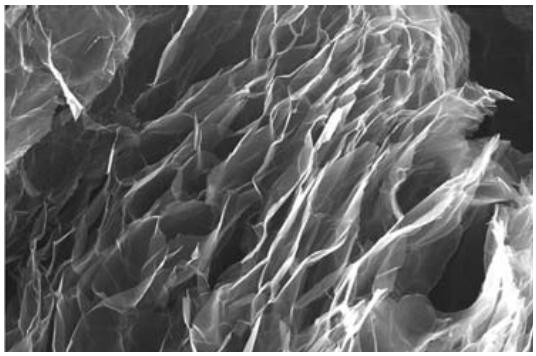

Figure 3.3.1. SEM picture of expanded graphite

Since its density is lower than natural graphite, it is used to make fuel cell bipolar plates. It can be prepared as follows.

A mixture of concentrated sulfuric and nitric acid (4:1 v/v) is mixed with graphite flakes under agitation and the temperature is kept at 80^{o}C. The reaction is continued for 16 hrs. The acid treated natural graphite is washed with distilled water and dried at 100^{o}C to remove water. The dried particle is heat treated at 1050^{o}C for 30 sec to form expanded graphite particles. The c-direction expansion could be few hundred times depending on the intercalation. This method is known as Hummers method being the most frequently used till date and well documented in the literature[28]. Chen *et al.*[29] have prepared expanded graphite by adding natural graphite and $KMNO_4$ into a mixture of acetic anhydride and nitric acid and heat treating the resultant expandable graphite as shown in Figure 3.3.2.

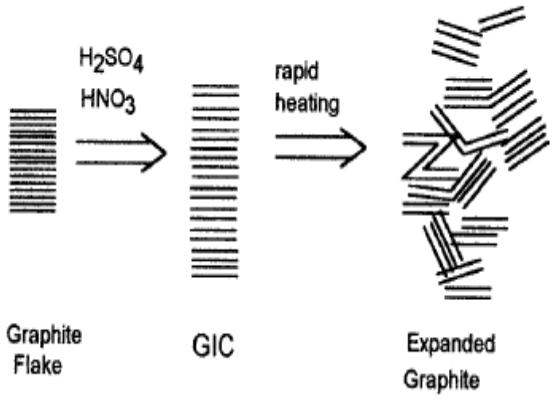

Figure 3.3.2. Expanded graphite synthesis

3.3.2. DC Conductivity Study of PES-ExGr Composites

PES-ExGr composites are prepared by solution blending route after sonicating expanded graphite in 50-70 ml DCM for 5 hrs and then mixed with solution of PES in DCM. The dc conductivity variation of PES-ExGr composites is shown in Figure 3.3.3. It is clear that the percolation threshold lies at 3 wt% ExGr. At low concentrations of Exgr, in-plane conductivity (Pll) is considerably higher than the through plane conductivity (Pdr) due to the alignment of ExGr nanosheets along the pellet surface as high pressure compaction has been employed. The conductivity remains in the insulating range below the percolation threshold due to absence of

network formation between fillers. Above percolation, the conductivity saturates at 0.01 S/cm due to completion of network between fillers.

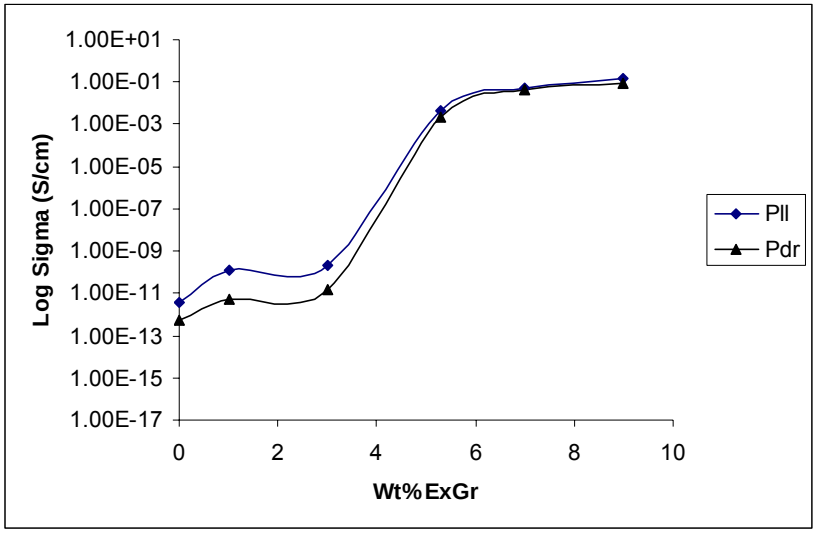

Figure 3.3.3. DC conductivity of PES-expanded graphite composites

Since the expanded graphite particles are ultrasonicated before mixing which led to the formation of nanosheets, low percolation threshold is obtained. The formation of nanosheets has been proved by SEM and TEM analysis to be discussed later.

3.3.3. Dimension of Network Formation between Fillers in PES-ExGr Composites

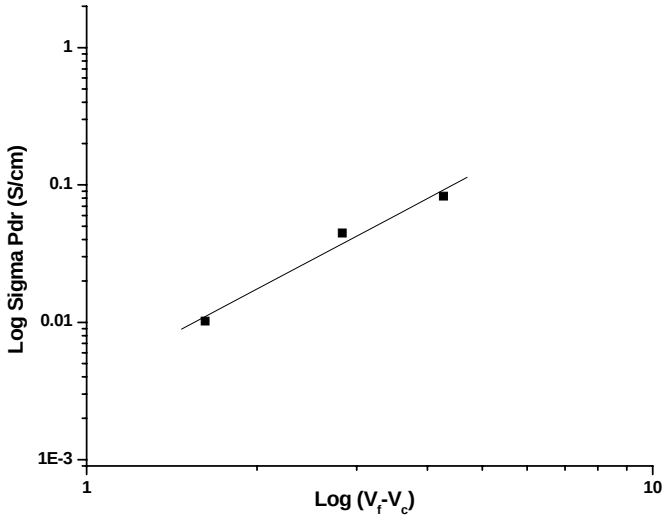

Figure 3.3.4. Plot for extracting percolation exponent of PES-expanded graphite composites

According to equation 1, the slope of the log σ vs log (V_f-V_c) yields percolation exponent which gives information regarding the dimension of network formation. The plot of log σ_{pdr} vs log (V_f -V_c) is shown in Figure 3.3.4. For this system a percolation exponent of 2.18 is obtained. It has been reported in the literature that non universal value of percolation exponent signifies tunneling conduction[7].

3.3.4. Effect of Heat Treatment on Electrical Conductivity of PES-ExGr Composites

The effect of sintering at 240°C for one hour on the electrical conductivity of PES-ExGr composites has been studied and shown in Figure 3.3.5. Enhancement in the through thickness conductivity and reduction in the graphite crystallite size are observed. After sintering, the graphite 002 plane re-orients due to the movement of polymer chains. XRD analysis clearly shows the reduction of crystallite size and intensity of graphite 002 peak as shown in Figure 3.3.6.a and b. Further slight shift in 2 Theta towards lower value indicates polymer penetration as explained for PES-graphite composites.

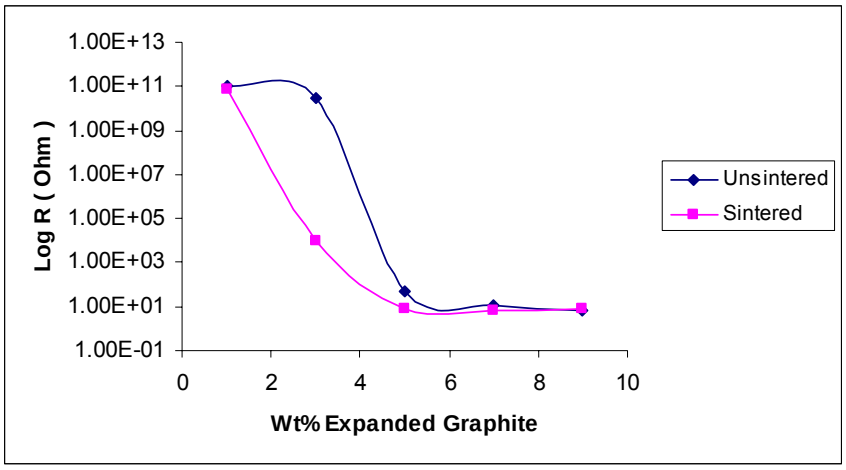

Figure 3.3.5. Through plane resistance of PES-ExGr composites (Sample thickness 5 mm, area 1cm^2)

The above Figure 3.3.5 shows that the through plane resistance decreases with sintering. Particularly six orders reduction is obtained for 3 wt% ExGr addition in PES which is the percolation threshold. Before sintering, PES-3 wt% ExGr remains as an insulator. After sintering, there occurs re-orientation of graphite 002 planes and the contact between them is made along the through thickness direction resulting in

the reduction of resistance. This is possible due to the movement of polymer chains as the sintering is done above T_g of the polymer. Above 3 wt% ExGr the reduction in the through plane resistance is less as before sintering itself the network formation would have been completed. The decrease in the resistance after sintering is due to the crystallite size reduction of expanded graphite leading to uniform distribution of the filler in the polymer matrix. XRD analysis proves this point.

3.3.5. XRD Analysis of PES-ExGr Composites

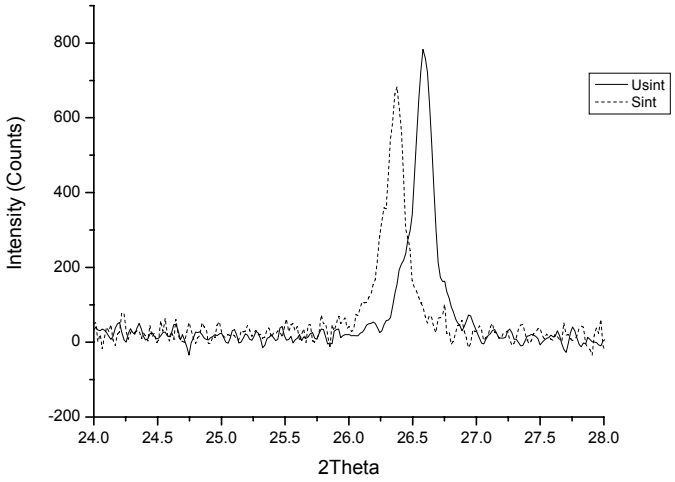

(a)

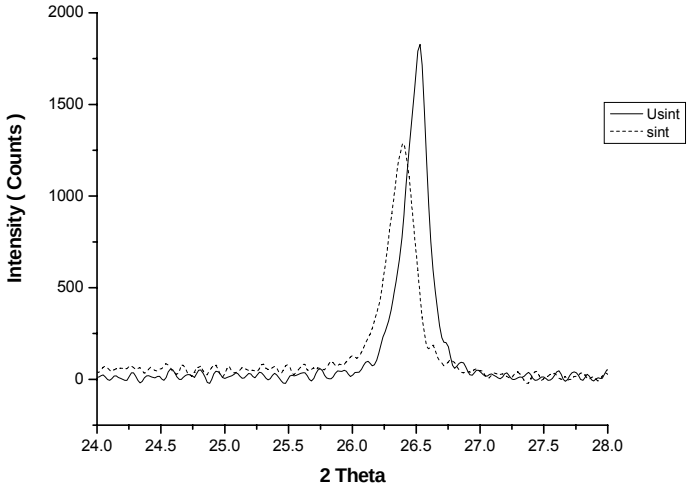

(b)

Figure 3.3.6. XRD patterns of a) PES-3 wt% ExGr b) PES-5 wt% ExGr

The XRD patterns of PES-3 wt% ExGr and PES-5 wt% ExGr are shown in Figure 3.3.6.a and b respectively. One can observe that there is a shift in the 2 Theta towards lower value as well as increase in the FWHM after sintering (shown by the dotted curve in the Figure) which signifies crystallite size reduction. Because of this reduction, the expanded graphite particles are distributed more uniformly resulting in better contact between them and hence the through plane resistance decreases. The shift in 2 Theta value signifies polymer penetration in to the gallery of expanded graphite. Expanded graphite has the structure of graphite with increased interplanar spacing. The following Table 7 summarizes XRD analysis.

Table 7

XRD analysis of PES-ExGr composites

Sample	2 Theta		Intensity (Counts)		Crystallite Size (t') (nm)	
	BS	AS	BS	AS	BS	AS
1. PES-3 wt% ExGr	26.53	26.31	783	683	46.06	42.20
2. PES-5 wt% ExGr	26.53	26.47	1829	1288	39.80	36.60
3. PES-7 wt% ExGr	26.50	26.46	1933	1919	37.50	34.96

BS- Before sintering, AS-After sintering

The above Table 7 clearly shows that after sintering the composites at 240^{o}C for one hour, the crystallite size of graphite is reduced. For all compositions, the intensity of 002 reflection of graphite is decreased after sintering signifying re-orientation of graphite planes. The difference in 2 Theta value before and after sintering obtained for PES-3 wt% ExGr is higher than that obtained for other compositions. It should be remembered that 3 wt% ExGr has been identified as the percolation threshold and hence polymer chain penetrates well in to the graphite sheets. For higher loading of ExGr, the shift is not higher when compared to 3 wt% ExGr suggesting the agglomerated structure of graphite sheets. Like PES-graphite, PES-ExGr also behaves in the similar manner.

3.3.6. SEM Analysis of PES-ExGr Composites

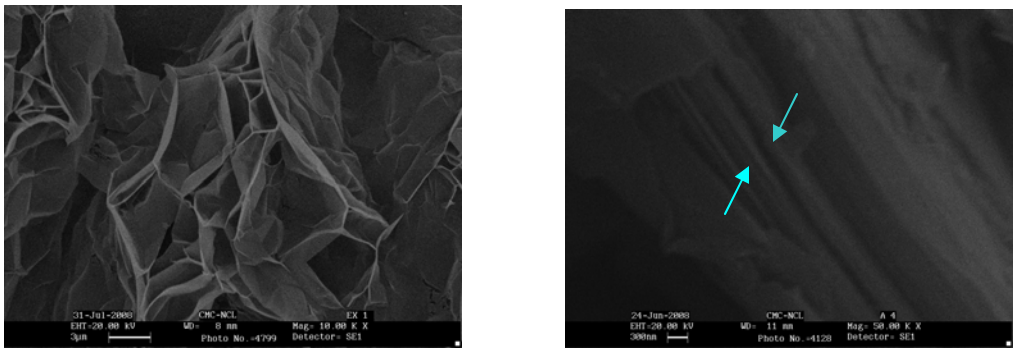

(a) (b)

Figure 3.3.7. SEM pictures of a) pure ExGr b) PES-10 wt% ExGr

The above Figure 3.3.9 clearly shows the porous structure of expanded graphite with size in micron range. Upon sonication and after mixing with the polymer, the cross section of PES-10 wt% ExGr shows several nanosheets (shown by arrows) agglomerated and hence the high aspect ratio of nanosheets leads to better contact between them. Hence the percolation threshold is reduced in this system when compared to graphite filled PES.

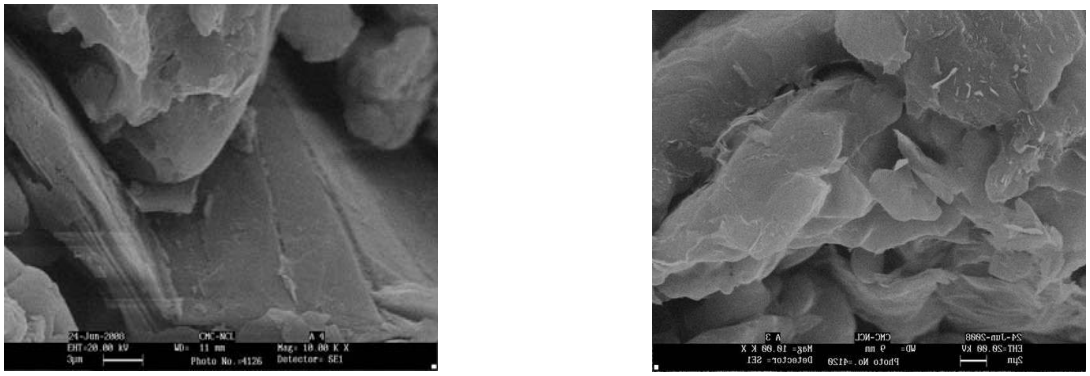

(a) (b)

Figure 3.3.8. SEM pictures of PES-7 wt% ExGr a) unsintered b) sintered sample

The SEM analysis supports the XRD data as agglomerated nanosheets are seen before sintering which became separated after sintering due to polymer penetration leading to improved contact between the fillers as shown in Figure 3.3.8.a and b respectively. This phenomenon results in higher conductivity after sintering.

3.3.7. TEM Analysis of PES-ExGr Composites

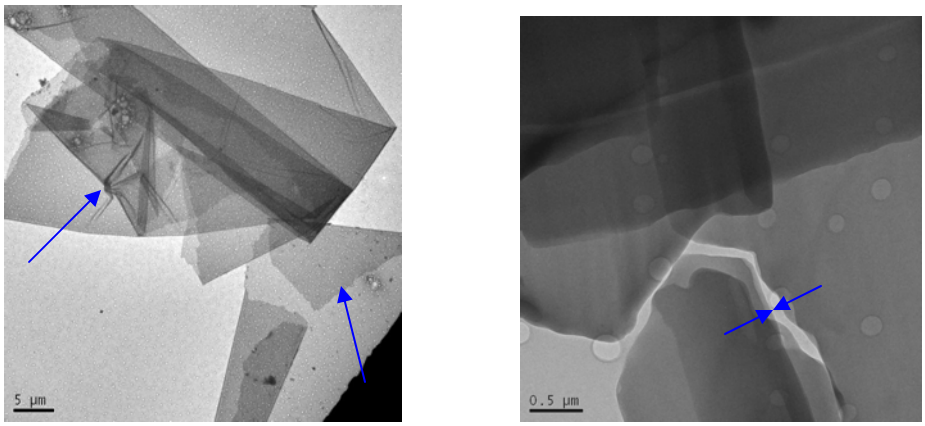

(a) (b)

Figure 3.3.9. TEM pictures of a) sonicated ExGr b) PES-3 wt% ExGr

TEM picture of ultrasonicated expanded graphite shown in Figure 3.3.9.a exhibits vanished pore structure and also nanosheets pile one top of the other as shown by arrows in Figure 3.3.9.b. Nanosheets can be very clearly seen for PES-3 wt% ExGr composites. Since the length of the sheets runs several microns, the aspect ratios of nanosheets are very high which result in low percolation. The aspect ratio of ExGr in PES is 135 as the average length of nanosheets is 8.12 micron and the thickness being 60 nm.

3.3.8. DSC Analysis of PES-ExGr Composites

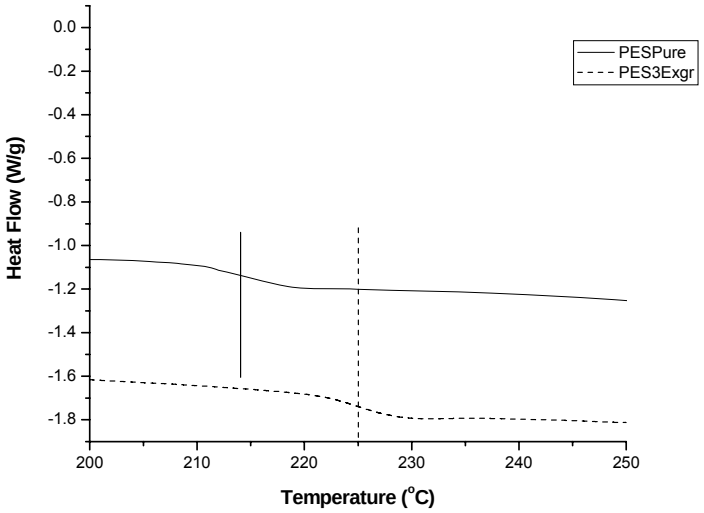

Figure 3.3.10. DSC curves of PES and PES-3 wt% ExGr composite

From the above Figure 3.3.10 it can be seen that the T_g of pure PES (213^oC) has been increased by 12^o due to the addition of 3 wt% ExGr. This shows that the nanosheets hinder the motion of polymer chain and good interaction exists between expanded graphite and PES. This interaction is the driving force for the polymer to penetrate the layers of graphite.

3.3.9. DC Conductivity of PES-graphite-ExGr Hybrid Composites

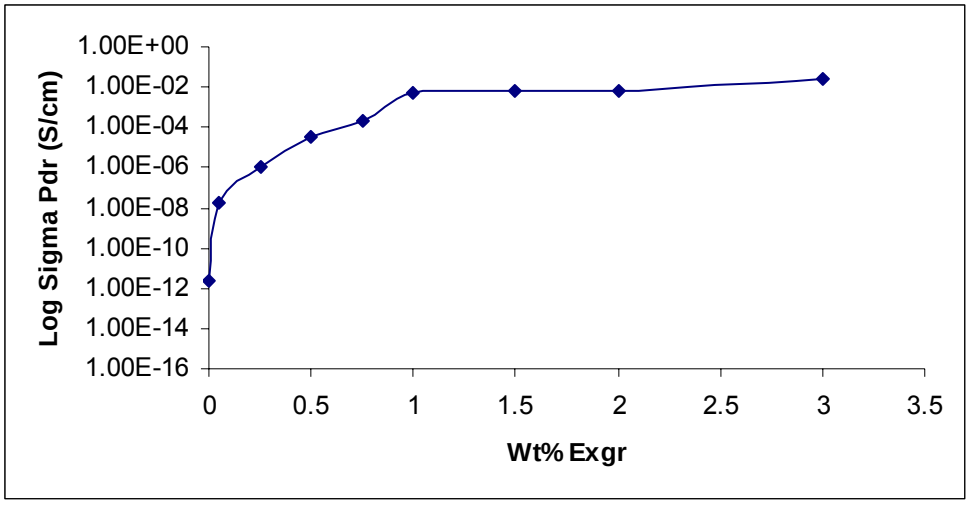

Figure 3.3.11. DC conductivity of PES-7 wt% graphite-x wt% ExGr composites

Since the percolation threshold of PES-graphite solution blended composites lies in between 5-10 wt% graphite, PES-7 wt% graphite has been chosen to study the effect of addition of expanded graphite on the dc electrical conductivity of solution blended PES-ExGr composites. The percolation threshold in these hybrid composites lies at 0.05 wt% ExGr as shown in Figure 3.3.11. Further the saturation in conductivity occurs at 1 wt% ExGr. It should be noted that a conductivity of 0.01 S/cm for hybrid composites will be matched by the conductivity of composites with more than 40 wt% graphite loading without ExGr in PES and more than 8 wt% ExGr without graphite in PES. Thus hybrid composites are so effective in bring down both the percolation threshold and loading of costly fillers. The ExGr nano sheets reduce the barrier for the charge transport by occupying predominantly intergraphite space which will be proved in the following section 3.3.10.

3.3.10. AC Behavior of PES-7 wt% graphite-ExGr Hybrid Composites

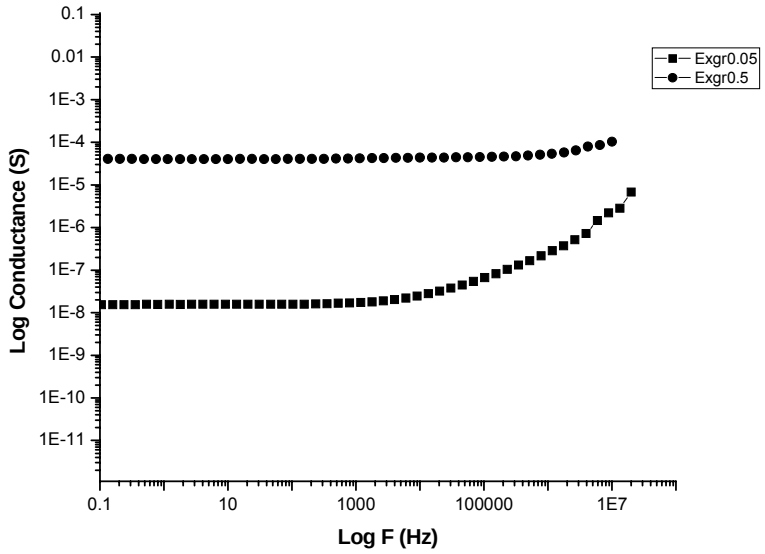

Figure 3.3.12. AC conductance of PES-7 wt% graphite-x wt% ExGr (X=0.05, 0.5)

With the addition of ExGr in PES-7 wt% graphite, the frequency at which the conductance starts increasing is shifted to higher values as shown in Figure 3.3.12. Also the plateau region becomes extended with ExGr loading. The plateau region signifies dc conductance and it increases to more than three orders for 0.5 wt% ExGr addition in PES-7 wt% graphite when compared to 0.05 wt% ExGr loading in the same. The slope of the ac conductance versus frequency plot gives information about the charge transport. For 0.05 wt% ExGr loading in PES-7 wt% graphite, the charge transport is coupled with capacitance effects which can be concluded from the value of the exponent being greater than one. In this case it is 1.21. For 0.5 wt% ExGr in PES-7 wt% graphite, the charge transport occurs by hopping mechanism as the exponent is 0.28 which is less than one. The ExGr nanosheets should predominantly lie in the intergraphite space because without ExGr in PES-7 wt% graphite, the conductivity of the composite obtained is 10^{-8} S/cm. Without graphite, the conductivity of PES-0.5 wt% ExGr lies in the insulating range as evidenced by the dc conductivity plot of these binary composites. The increase in the conductivity is possible only when the above mentioned configuration exists. Considering conducting particle-polymer-conducting particle configuration as a parallel plate

capacitor, if ExGr nanosheets lie in between graphite particles, the interjunction capacitance should increase due to the reduction in the interparticulate distance. This is equivalent to reducing the distance between the parallel plates in the capacitor. Impedance measurement has been carried out to find out interjunction capacitance which increases with ExGr loading.

3.3.11. Impedance Analysis of PES-graphite-ExGr Hybrid Composites

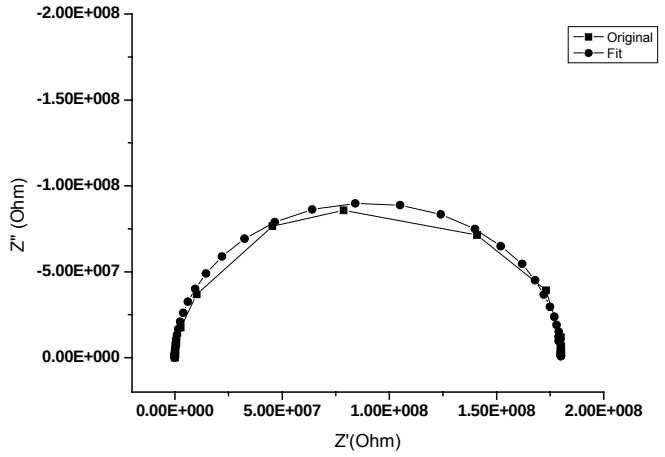

(a)

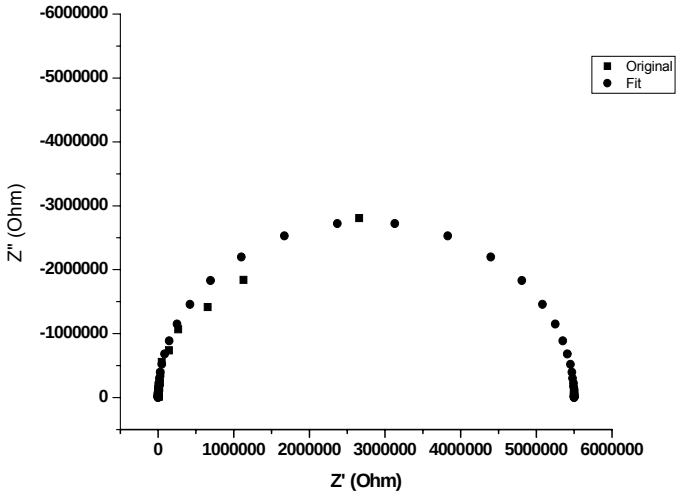

(b)

Figure 3.3.13. Impedance plots of a) PES-7 wt% graphite b) PES-7 wt% graphite-0.05 wt% ExGr solution blended samples

From the impedance plots shown in Figures 3.3.13.a and b, it is vivid that addition of 0.5 wt% ExGr in PES-7 wt% graphite decreases the resistance which is concluded from the reduction in the diameter of semicircle in Argand plane. The experimental results are fitted to parallel capacitor-resistor with a series resistor model and the various parameters extracted are shown in the following Table 8. The notations have the usual meaning as explained in the impedance section of other hybrid composites.

Table 8

Parameters extracted from the model for PES-graphite-ExGr composites

Sample	R_a (Ohm)	R_p (Ohm)	C (pF)
PES-7 wt% graphite	370	1.8×10^8	37.6
PES-7 wt% graphite-0.05 wt% ExGr	250	5.5×10^6	41.2
PES-7 wt% graphite-0.5 wt% ExGr	150	5200	71.0

It is clear from the above Table 8 that the interjunction capacitance increases from 37.6 pF for 0 wt% ExGr in PES-7 wt% graphite to 41.2 pF for 0.05 wt% ExGr and corroborates the assumption that ExGr nanosheets occupy intergraphite space. The interjunction capacitance increases to 71 pF for PES-7 wt% graphite-0.5 wt% ExGr from 37.6 pF for 0 wt% ExGr in PES-7 wt% graphite. The aggregate resistance decrease with increasing loading of ExGr can be explained as follows. Presence of ExGr particles in between graphite particles reduces the barrier for the charge transport. Since expanded work function is presumed to be higher compared to that of graphite as literature bears no reports on the evaluation of work function. Hence the barrier for the charge transfer from the polymer to ExGr becomes lesser and if more ExGr particles are found in between graphite and the polymer, more charges will be transferred to graphite via ExGr resulting in the decrease of aggregate resistance.

3.4. Effect of Aspect Ratio of Second Filler on Electrical Percolation

The aspect ratio of second conducting filler is more important in reducing the percolation threshold as it improves the contact between fillers. The percolation threshold follows inverse relation with the aspect ratio of second conducting fillers. In the systems investigated, ExGr filled hybrid composites exhibit low percolation as the aspect ratio of ExGr is the highest followed by CNF and CB. The following Figure 3.4.1describes the same.

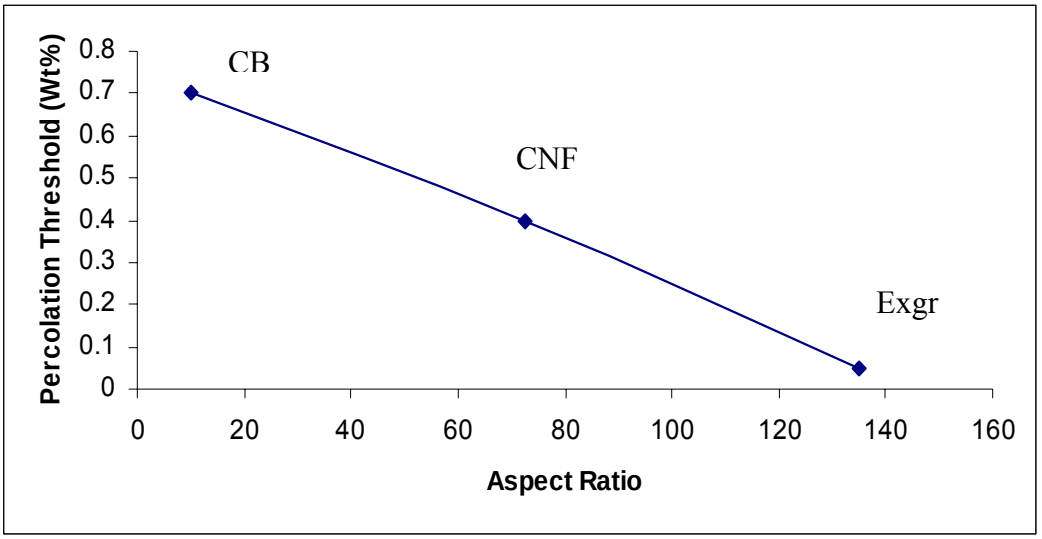

Figure 3.4.1. Effect of aspect ratio of second filler in PES-graphite based composites

3.5. Thermal Conductivity Studies on PES-graphite, PES-graphite-CB Systems

The thermal conductivity measurement details have been mentioned in chapter-2. Compared to electrical conductivity, thermal conductivity is a slowly varying parameter since it is mainly governed by phonons. The electrical conductivity is very sensitive to interparticulate distance where as thermal conductivity is not. The following Figure 3.5.1 shows the variation of thermal conductivity with respect to graphite and CB loading in PES prepared by solution blending route. These systems can find a possible application in heat sinks and fiber spinning spool in order to dissipate heat.

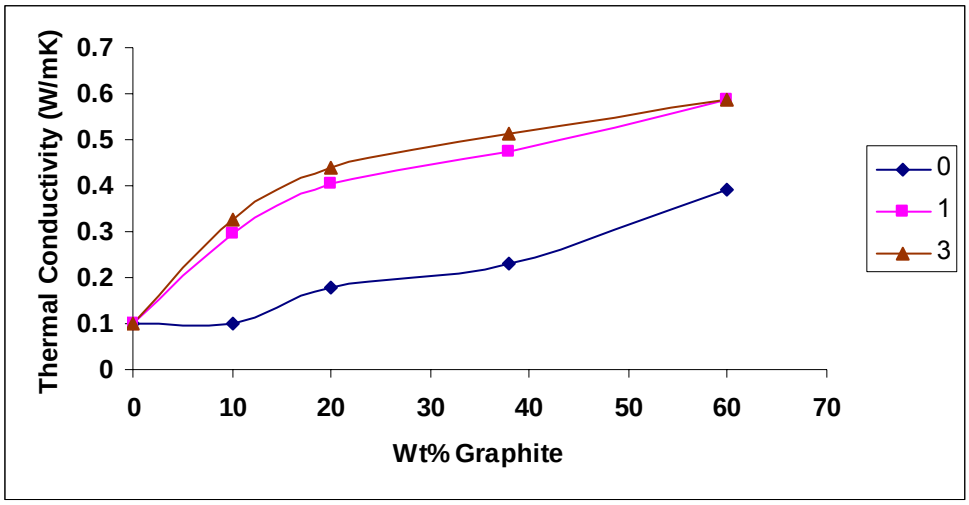

Figure 3.5.1. Thermal conductivity of PES-graphite-CB composites

Similarly addition of ExGr in PES increases the thermal conductivity to a great extent compared to PES-graphite composites as shown in Figure 3.5.2. The thermal conductivity of 0.1 W/m-K for the insulating polymer increases to around 0.42 W/m-K for PES-60 wt% graphite-7 wt% CB.

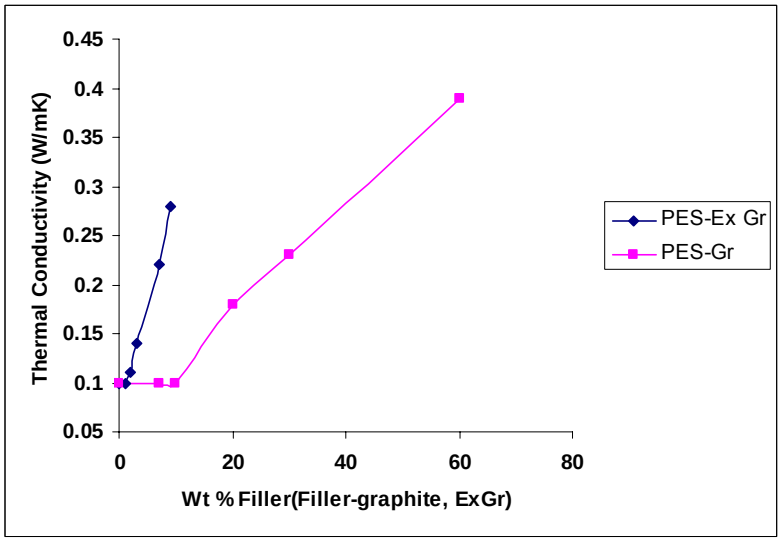

Figure 3.5.2. Thermal conductivity of PES-ExGr and PES-graphite composites

3.6. Conclusions

In order to study the effect of second conducting fillers such as CB, CNF and ExGr on the electrical conductivity of PES-graphite, first dc conductivity variation of PES-graphite composites was studied with varying graphite loading. The hybrid composites were prepared by two methods namely solution blending in DCM and powder mixing routes. The percolation threshold in the solution blended binary composite was found to lie between 5 and 10 wt% graphite. Solution blending route resulted in more reduction of graphite particle size as compared to powder mixing route. Because of high speed stirring, the particle size of graphite was reduced in the former case. Sintering above the T_g of the polymer resulted in re-orientation of graphite 002 planes along with crystallite size reduction. The polymer also penetrated the graphite layer which was understood from the XRD analysis as there was a 2 Theta shift towards lower value. Sintering resulted in enhancement in the through plane conductivity due to downsizing of graphite particles. Hybrid composites were made with PES-7 wt% graphite- x wt% CB with varying loading of CB by solution and powder mixing routes. The solution blending route resulted in enhanced conductivity than that obtained in the powder mixing route for the same composition. The enhancement in the conductivity was due to graphite particle size reduction. Thus the processing routes affected the conductivity of the composites. The hardness measurement showed that the solution blended PES-graphite binary composites exhibited higher value than powder mixed ones due to graphite particle size reduction resulting in better dispersion in the former case. PES-CB solution blended composites exhibited a percolation threshold of 10 wt%. The charge transport in the hybrid composites was by hopping mechanism for higher loading of CB and at lower loading, it was coupled with capacitance effects. The frequency dependent conductance showed insulator-semiconductor transition with the increase in the loading of CB. The increase in effective dielectric constant at low frequency (0.01 Hz) was due to the occupation of CB in the interspace of graphite particles. Through impedance analysis, the interjunction capacitance was evaluated and it was increasing with higher loading of CB proving the assumption. I-V characteristic of single PES-graphite-PES junction

showed that space charge limited conduction was the dominant mechanism in the sandwiched structure.

PES-CNF binary composites prepared by solution blending route, after dispersing CNF in DCM showed a percolation threshold at 3 wt%. The percolation exponent of these binary composites was slightly higher than the universal value for three dimensional network formations. For PES-7 wt% graphite-CNF hybrid composites, the percolation threshold was identified at 0.4 wt% CNF. The ac conductance analysis showed that the insulator-semiconductor transition occurred with the increase in the concentration of CNF. The increase in effective dielectric constant to three orders for 0.5 wt% CNF addition in PES-7 wt% graphite compared to 0.2 wt% CNF in the same suggested that CNF occupied the interspace between graphite particles. The above conclusion was proved by impedance measurements by which interjunction capacitance had been calculated. The interjunction capacitance was found to increase with higher loading of CNF.

PES-ExGr binary composites were prepared by solution blending route after sonicating ExGr in DCM. The percolation threshold was identified at 3 wt%. Sintering of these binary composites above T_g of the polymer led to the increase of through plane conductivity due to re-orientation of graphite sheets. Sintering resulted in crystallite size and intensity reduction due to polymer penetration in the gallery of graphite and re-orientation of graphite 002 planes. Sonication of ExGr led to the formation of nanosheets. The hybrid composites with ExGr as the second conducting filler in PES-7 wt% graphite showed a percolation threshold of 0.05 wt%. In the hybrid composites, the graphite nanosheets occupy predominantly intergraphite space and hence increased the interjunction capacitance obtained through impedance measurement. Finally, the percolation threshold was found to have inverse relation with the aspect ratio of the second conducting filler.

The thermal conductivity of few systems like solution blended PES-graphite-CB and PES-ExGr had been measured and found to increase with the increase in the concentration of conducting fillers. The composites can be used to replace the fiber spinning spool to dissipate heat.

3.7. References

1. http://bdml.stanford.edu/twiki/pub/Haptics/MaterialSelection/Polyethersulfone PES.pdf
2. Chung DDL. J Mater Sci 2002;37:1.
3. Gopakumar TG, Page DJYS. Polym Eng Sci 2004;44:1162.
4. L.E. Alexander, X-ray Diffraction Methods in Polymer Science, J. Wiley, NY, USA, 1969.
5. Nan CW. Prog Mater Sci 2002;37(1):1.
6. Ezquerra TA, Kulescza M, Santa cruz C, Balta-colleja FJ. Adv Mater 1990;2:597.
7. Wu J, McLachlan DS. Phys Rev B 1997;56:1236.
8. Wu YP, Jiang C, Wan C, Holze R. J Power Sources 2002;112:225.
9. Lee KJ, Lee DK, Kim YW, Choe W-S, Kim JH. J Polym Sci:Part B: Polymer Physics 2007;45:2232.
10. Radhakrishnan S, Saini DR. J Mater Sci 1991;26(21):5950.
11. Radhakrishnan S, Sonawane N, Siju CR. Prog Org Coat 2009;64(4):383.
12. Wang YJ, Pan Y, Zhang X, Tai K. J Appl Polym Sci 2005;98(3):1344-1350.
13. Sque SJ, Jones R, Briddon PR. Phys Stat Sol 2007;9:3078.
14. Baun WL. Pure & Appl Chem 1982;54(2):323.
15. Fabish T J, Hair M L. J Colloid Inter Sci 1977;62(1):16-23.
16. Sherman LM. Plast Technol 2007;68:73.
17. Mordkovich VZ. Theor Found Chem Eng 2003;37(5):429.
18. Thostenson ET, Li CY, Chou TW. Compos Sci Technol 2005;65(3–4):491.
19. Tibbetts GG, Lake ML, Strong KL, Rice BP. Compos Sci Technol 2007;67(7–8):1709.
20. Finegan IC, Tibbetts GG. J Mater Res 2001;16(6):1668.
21. Lozano K. JOM-J Miner Met Mater Soc 2000;52(11):A34.
22. Gordeyev SA, Macedo FJ, Ferreira JA, van Hattum FWJ, Bernardo CA. Physica B 2000;279(1–3):33.
23. Radhakrishnan S, Ramanujam BTS, Adhikari A, Sivaram S. J Power Sources 2007;163(2):702.

24. Cipriano BH, Kota AK, Gershon AL, Laskowski AJ, Kashiwagi T, Bruck HA, Raghavan SR. Polymer 2008;49:4846.
25. Wang YJ, Pan Y, Zhang X, Tai K. J Appl Polym Sci 2005;98(3):1344.
26. Shimoi N, Tanaka S-i. J Ceram Process Res 2008;9(5):437.
27. Yu C, Li B. J Compos Mater 2008;42(15):1491.
28. Nakajima t, Matsuo Y. Carbon 1994:32:469.
29. Chen XL, Song KM, Li JH, Liu JP. Carbon 1996:34(12):1599.

Chapter-4

Polyphenylene sulfide (PPS) Based Composites

4.1. Introduction

Poly (phenylene sulfide) is a high temperature, semicrystalline thermoplastic with T_g of ~85^oC and high melting temperature ~280^oC. PPS was first discovered as a bye product of Friedel-Crafts reaction in 1888. PPS has rather unusual thermosetting–thermoplastic characteristics. Edmonds and Hills[1] synthesized PPS by making p-dichloro benzene to react with sodium sulfide after which the need of PPS arose exponentially. Rajan *et al*.[2] reported that the kinetics of the reaction is faster when PPS is synthesized from 1,4-dibromo benzene than from p-dichloro benzene. The crystal structure of PPS was solved by Tabor *et al*.[3] and reported to be orthorhombic unit cell with dimensions a = 8.67 A^o, b = 5.61 A^o, and c = 10.26 A^o, comprising of four monomer unit. It can only be soluble in α-chloronaphthalene at 200^oC. The excellent properties such as good stiffness and rigidity, chemical resistance, dimensional stability and moldability make it to be used in valves, electrical socket, telephone components etc. Although PPS is a successful engineering plastic, its low impact strength and glass transition temperature limits end applications. To improve those parameters, one approach is to blend the semi-crystalline PPS with other polymers[4-5] and the other is to add filler in to PPS matrix such as clay[6], glass fiber[7], expanded graphite[8].

The crystallinity of PPS is an important parameter which affects electrical and mechanical properties to a great extent when filled with various fillers. The effect of crystallinity of PPS on the mechanical properties has been studied by Brady *et al*.[9]. Jog and Nadkarni[10] have studied bulk crystallization of glass fiber reinforced PPS and observed the crystallization rate to be maximum at 170^oC which was understood in terms of heterogeneous nucleation in filled PPS. The molecular weight of PPS also affects the crystallization rate. Increasing molecular weight decreases the crystallization rate. Radhakrishnan *et al.*[11] have studied the effect of surface modification and crystallinity in compression molded PPS. The crystallization kinetics of PPS/LCP blends has been reported by Gabellini *et al*.[12]. Deporter and Baird[13] reported that the changes in crystallinity of PPS cause variations in flexural strength, flexural modulus and transverse tensile strength of PPS-carbon fiber composites. There are many reports on the crystallization aspects related to PPS and

filled PPS. Most of the literature is devoted to the study of mechanical properties variation of filled PPS systems with respect to crystallinity.

As far as electrical conductivity studies in PPS based conducting composites are concerned, few reports are found in the literature[14-16]. Zhao *et al*.[14] have studied electrical, thermal and mechanical properties of PPS-expanded graphite binary composites prepared by melt mixing method. The electrical conductivity and thermal stability of nanocomposites increased with expanded graphite addition in PPS. They further reported that the crystallinity of PPS was increased with the addition of expanded graphite. Towards the development of fuel cell bipolar plate, highly conducting PPS-graphite based both binary and hybrid composites with CNF and CB as second conducting fillers have been reported[15-16]. The binary and hybrid composites were injection molded and studied. In those composites, very high loadings of graphite and second conducting fillers were employed. However there are no systematic studies on electrical conductivity variation of PPS-graphite binary and hybrid composites reported in the literature especially nearer to the percolation threshold. Thus, this chapter deals with the study of electrical conductivity variation in PPS-graphite, PPS-CNF, PPS-ExGr and PPS-graphite-filler (filler-CB, CNF and ExGr) hybrid composites. The electrical conductivity of composites and the percolation threshold depends on processing routes employed. In this study, the composites were prepared by both powder mixing and melt crystallization routes wherever required and reported.

A. Powder Mixing Route

4.2. PPS-graphite, PPS-graphite-CB Composites

4.2.1. DC Conductivity Study of PPS-graphite Powder Mixed Composites

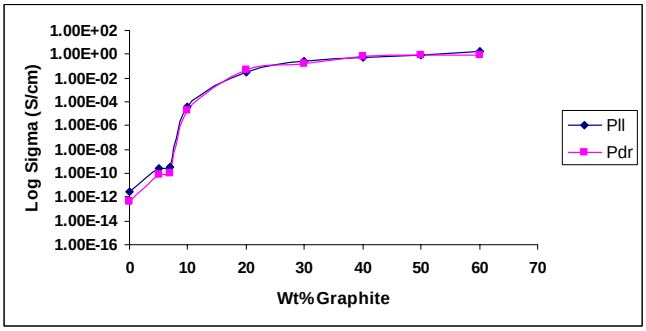

Figure 4.2.1. DC conductivity of PPS-graphite composites

The electrical conductivity variation of PPS-graphite composites made by powder mixing route is shown in the above Figure 4.2.1. Below 7 wt% graphite in PPS, the composites behave as insulators as the amount of graphite is insufficient to form network between them. At 10 wt% graphite, both in-plane (Pll) and through thickness (Pdr) conductivities increase by five orders due to the formation of network between the filler particles. Above 30 wt% graphite, the conductivities saturate indicating completion of conduction networks formed by graphite particles. The percolation threshold is identified at 7 wt% graphite. The in-plane conductivity is slightly higher than through plane conductivity below percolation threshold due to the alignment of graphite particles along the surface of the pellet as high pressure compaction is employed for making pellets. Above percolation threshold, both conductivities match more or less indicating less anisotropy due to the distribution of graphite particles in the polymer matrix.

4.2.2. Percolation Exponent Determination for PPS-graphite composites

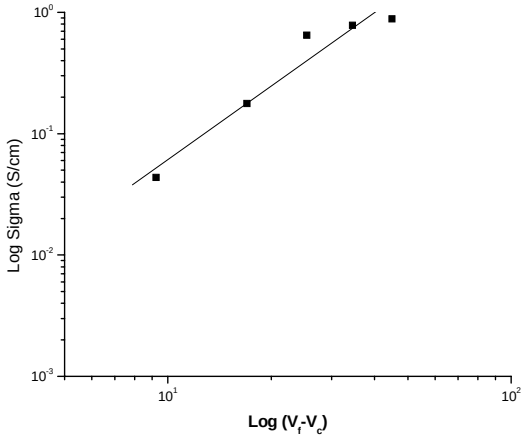

Figure 4.2.2. Plot for determination of percolation exponent in PPS-graphite composites

Since the dc conductivity variation is of percolation type, the dimension of network formation between filler particles can be found out from the percolation theory. The equation 1 mentioned in Chapter-3 describes through plane conductivity variation with the volume fraction of graphite particles. A plot of log σ vs log (V_f-V_c); $V_f > V_c$, where the symbols have the usual meaning as described in Chapter-3, yields

percolation exponent 't'''. For PPS-graphite system the value of 't''' obtained is 2.01 signifying three dimensional network formations between filler particles.

4.2.3. Effect of Heat Treatment on Electrical Conductivity of PPS-graphite Composites

PPS has high melting temperature ~280^{o}C. In order to understand the effect of heat treatment on the dc electrical conductivity, PPS-graphite composites were sintered at 240^{o}C for one hour. Above one hour sintering time, significant change in the conductivity was not observed. The following Figures 4.2.3.a and b show the variation of through plane and in-plane conductivities before and after sintering.

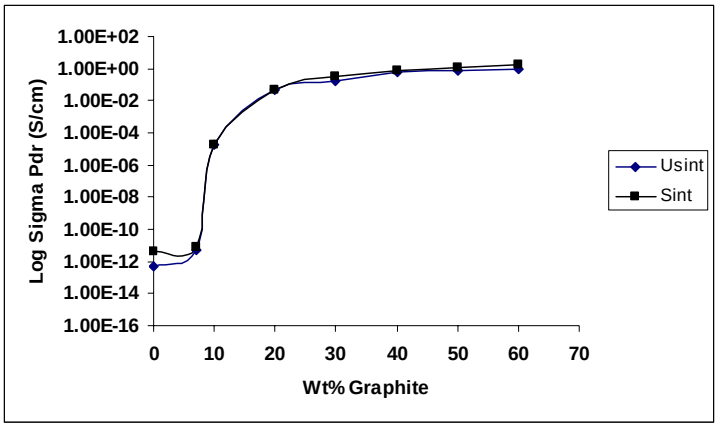

(a)

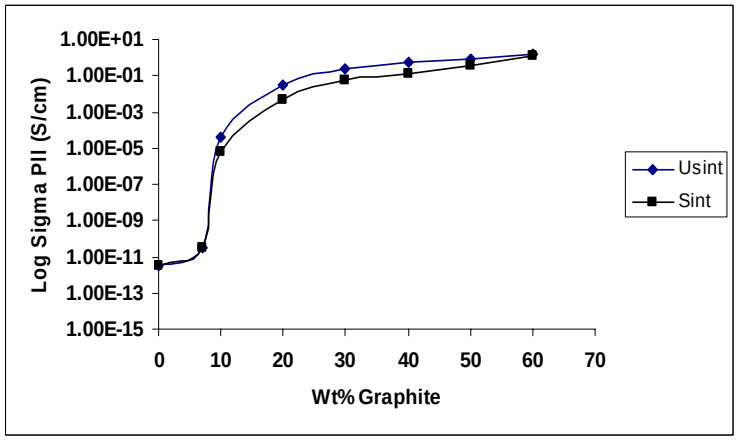

(b)

Figure 4.2.3. a) Through plane b) In-plane electrical conductivity variation of PPS-graphite composites

The conductivities before and after sintering are represented as Usint and Sint respectively in those figures. The through plane conductivity of PPS-graphite composites increases after sintering. The enhancement is more pronounced below the percolation threshold. Above the percolation threshold, the conductivity enhancement is not significant as the network formation would have been completed before sintering itself. Furthermore, there is a reduction of more than one order in in-plane conductivity of composites above the percolation threshold. These results clearly prove that the graphite (002) are re-oriented along through thickness direction due to polymer chain movement as the sintering was done above the T_g of the polymer. XRD analysis can explain the observed changes in electrical conductivity in this system.

4.2.4. XRD Analysis of PPS-Graphite Composites

The XRD patterns of representative samples namely PPS-10 wt% graphite and PPS-40 wt% graphite are shown in Figures 4.2.4.a and b. From these figures, it can be clearly seen that after sintering, the intensity of graphite 002 reflection decreases.

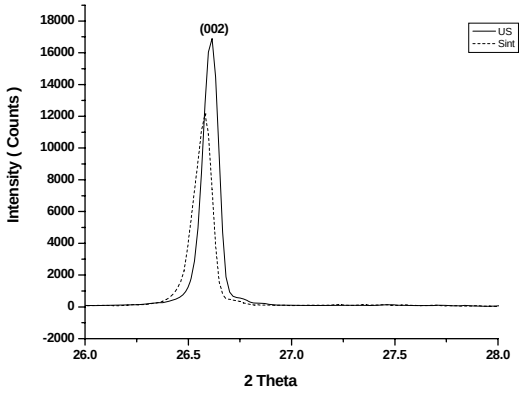

(a)

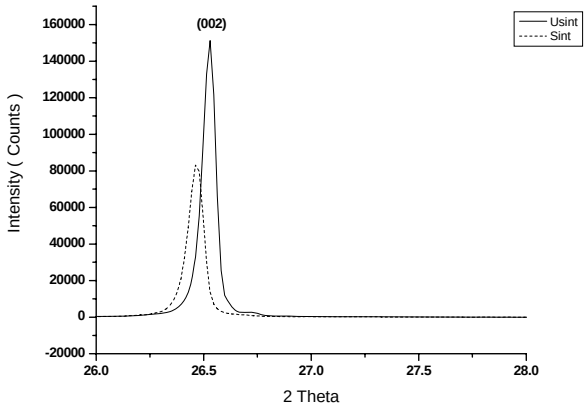

(b)

Figure 4.2.4. XRD patterns of powder mixed a) PPS-10 wt% graphite b) PPS-40 wt% graphite

The XRD patterns of unsintered and sintered samples are represented by Usint and sint respectively. Further the FWHM increases along with a slight shift in 2 Theta towards lower value indicating polymer penetration between graphite planes. The increase in though plane electrical conductivity can be due to the decrease in the graphite crystallite/particle size leading to increase in both the surface area and particle-particle contact. The reduction in the intensity of (002) of graphite signifies re-orientation of those planes along through thickness direction facilitating the contact between fillers in that direction. This is reflected in the enhancement in the conductivity. Table 1 summarizes XRD details as given below. It is clear from Table 1 that for all compositions, crystallite size (t') reduction results after sintering along with 2 Theta shift towards lower value. For crystallite size calculation 002 reflection of graphite is used. The shift in 2 Theta value is similar to that shift observed in PES-graphite systems after sintering. In PES-graphite system a large shift in 2 Theta after sintering was observed. The XRD results prove that polymer can penetrate graphite planes.

Table 1

XRD analysis of powder mixed PPS-Graphite composites

Sample	Before Sintering			After Sintering		
	2θ	Intensity	t'(nm)	2θ	Intensity	t' (nm)
PPS-10wt% Graphite	26.615	16893	68.87	26.581	12157	62.60
PPS-30wt% Graphite	26.581	75671	68.86	26.479	72017	45.90
PPS-40wt% Graphite	26.53	151155	68.85	26.462	83239	62.59
PPS-60wt% Graphite	26.513	233128	68.59	26.36	153650	57.34

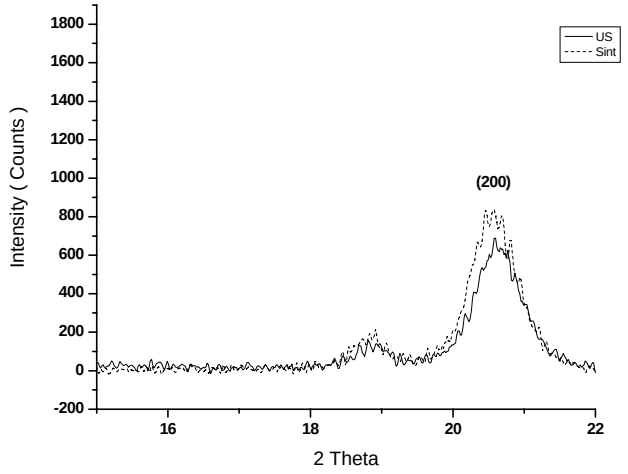

(a)

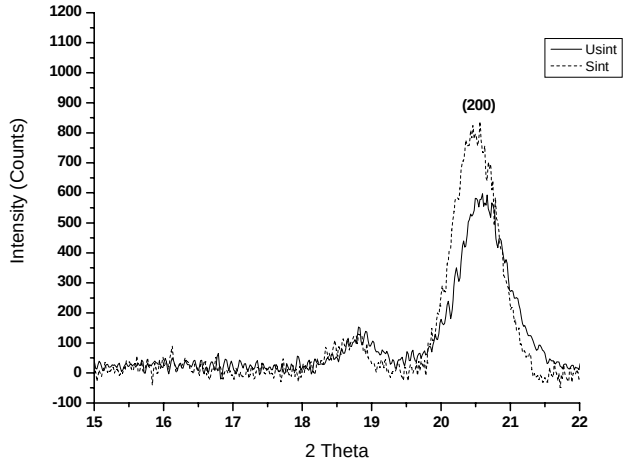

(b)

Figure 4.2.5. XRD patterns of PPS part of a) PPS-10 wt% graphite b) PPS-40 wt% graphite

PPS has orthorhombic crystal structure. It has four major reflections as given below with 2 Theta values.

(110)-18.7, (200)-20.7, (112)-25.6, (211)-27.4. Out of these four reflections, the intensity of 200 reflections is the strongest and hence considered for structural changes analysis. In Figures 4.2.5.a and b, the XRD patterns corresponding to PPS part of PPS-10 wt% graphite and PPS-40 wt% graphite before and after sintering denoted by Usint and Sint respectively are shown. In both cases, the intensity of 200 planes increases after sintering. This suggests that more polymer is found on the surface due to the movement of polymer chains after sintering. Further many planes would have been re-oriented along through thickness direction resulting in the in-plane conductivity decrease after sintering.

4.2.5. SEM Analysis of PPS-graphite composites

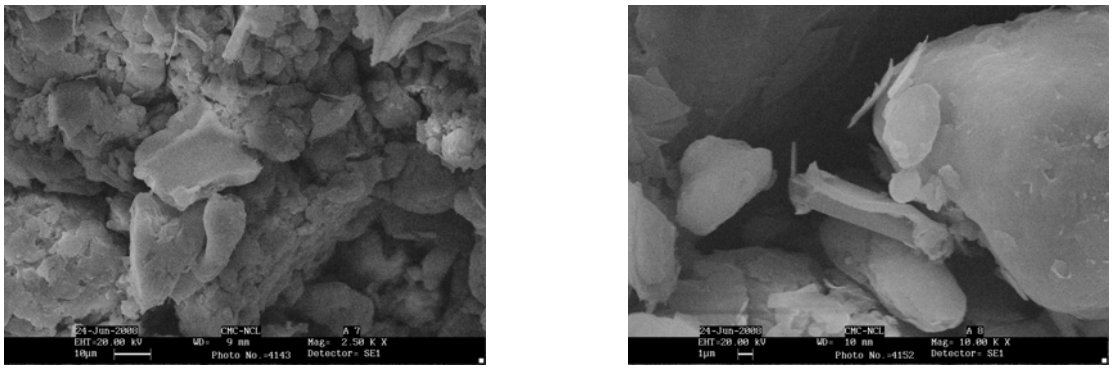

(a) (b)

Figure 4.2.6. SEM pictures of a) unsintered PPS-20 wt% graphite b) sintered PPS- 20 wt% graphite

The surface morphology of PPS-20 wt% graphite composite before and after sintering is shown in Figures 4.2.6.a and b respectively. In the unsintered sample, graphite flakes are buried in the polymer as shown in Figure 4.2.6.a, where as sintering leads to separation of graphite flakes as shown in Figure 4.2.6.b. This is due to the penetration of polymer in to the gallery of graphite resulting in better separation as evidenced by XRD results. Since the agglomerated flakes are separated, the network formation between them is feasible after sintering because of which the conductivity increases.

4.2.6. DSC Analysis of PPS-graphite composites

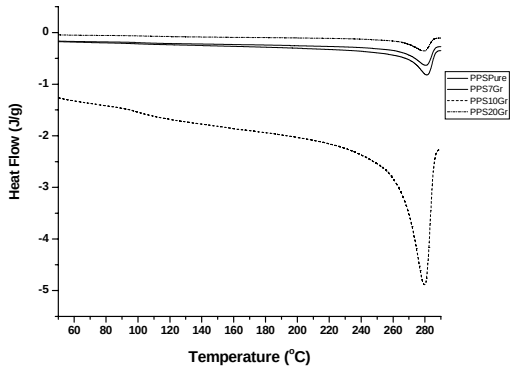

(a)

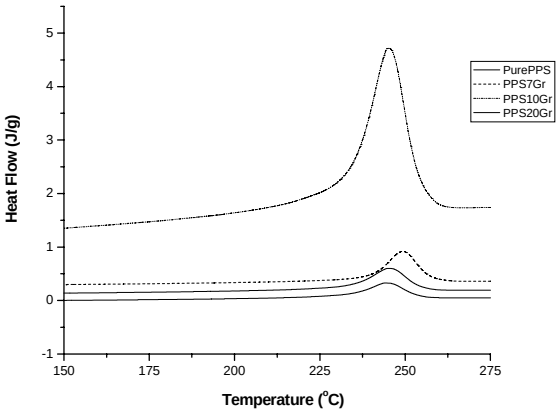

(b)

Figure 4.2.7. DSC curves of PPS-graphite composites a) melting curve b) cooling curve

Table 2

DSC analysis of PPS-graphite composites

Sample	T_m (^oC)	ΔH_m (J/g)	T_c (^oC)	ΔH_c (J/g)
PPS	280.90	60.73	244.84	40.74
PPS-7wt% Graphite	281.06	57.69	249.17	47.67
PPS-10wt% Graphite	279.61	38.97	244.74	35.26
PPS-20wt% Graphite	279.93	29.24	243.96	30.39

The DSC curves of PPS-graphite composites during heating and cooling cycles are shown in Figures 4.2.7.a and b respectively. Second heating cycle is taken for the analysis as the first heating is used to remove the prehistory of the sample. It is clear from Table 2 that the melting and crystallization temperature depend on graphite content. With 7 wt% graphite addition, the crystallization temperature (T_c) increases

by 5°C suggesting the nucleating ability of graphite particles. The increase in the area under the crystallization peak suggests enhanced crystallinity. With increasing loading of graphite particles, the melting temperature (T_m) decreases due to fast heat transfer from the conducting graphite particles to the polymer matrix. T_c and also the area under the crystallization ($\Delta H_{c)}$ curve decrease suggesting agglomeration of graphite particles. Hence, the graphite particles reduce the area of crystallized portion in the polymer. For higher loading of graphite i.e., 10 wt% and 20 wt%, the area under the melting peak ($\Delta H_{m)}$ decreases which is a sign of sharp melting. In short, graphite particles act as nucleator at 7 wt% loading. Decrease in the melting temperature with more conducting particles addition has been reported in the literature[17]. Radhakrishnan[18] reported the crystallinity of this grade PPS to be ~40% through XRD analysis.

4.2.7. DC Conductivity Variation in PPS-Graphite-CB Hybrid Composites

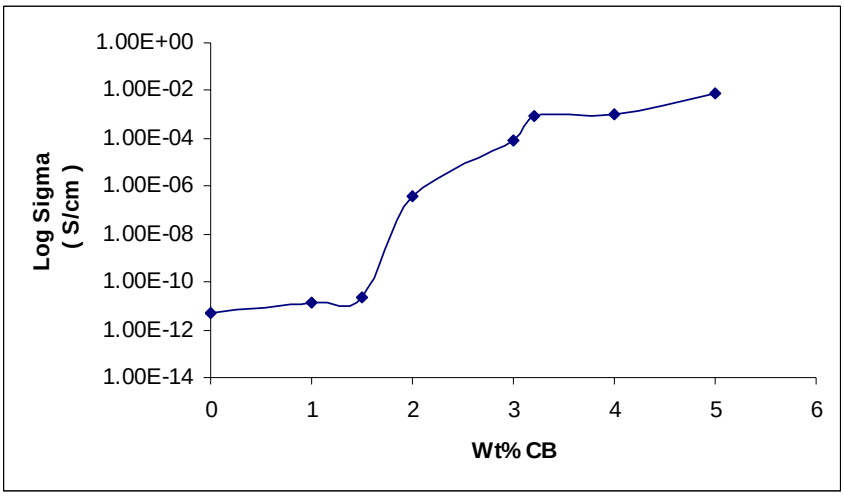

Figure 4.2.8. Through plane conductivity of PPS-7 wt% graphite-x wt% CB

Hybrid composites with CB as the second conducting filler in PPS-7 wt% graphite have been prepared by powder mixing route as described earlier in Chapter-2. From the dc conductivity variation of PPS-graphite, the percolation threshold is identified at 7 wt% graphite. Thus the effect of CB on the electrical conductivity of PPS-7 wt% graphite is shown in Figure 4.2.8. For these hybrid composites, percolation threshold lies at 1.5 wt% CB. Below which the composites behave as insulators. Saturation in electrical conductivity occurs above 3 wt% CB in PPS-7 wt% graphite due to completion in the network formation between fillers. At 2.5 wt% CB, there exists five

order enhancement in the through plane conductivity when compared to the same of 1 wt% CB in PPS-7 wt% graphite. To attain a conductivity of 0.01 S/cm, without CB at least 30 wt% graphite would be required. Thus the hybrid composites are so effective in bringing down not only the percolation threshold but also the quantity of material. In order to understand the effect of CB on the electrical conductivity of hybrid composites, PPS-CB composites have been prepared by powder mixing route after dispersing CB in acetone. The dc conductivity variation is shown in Figure 4.2.9.

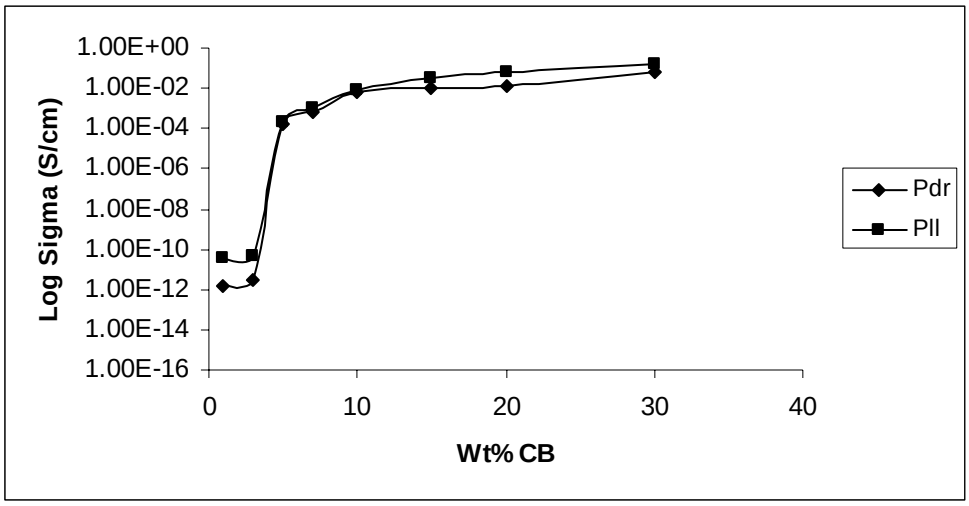

Figure 4.2.9. DC conductivity of powder mixed PPS-CB composites

Since CB particles are very well dispersed in acetone, the percolation threshold of PPS-CB composites lies at 3 wt%. The aggregate size of CB is 80 nm. In this binary composites also, in-plane conductivity (Pll) is observed to be higher than through plane conductivity (Pdr) due to alignment of CB particles along the surface of the pellet. At 20 wt% CB, the conductivity saturates to about 0.01 S/cm due to network completion. Since higher loading of CB leads to rubbing off from the surface of the pellet, small amount of CB can be used as second conducting filler in PPS-graphite composites. The value of conductivity at 20 wt% CB in PPS matches that of PPS-7 wt% graphite-5 wt% CB. Thus the over all content of the filler can be brought down in hybrid composites. The CB particles act as connectors between graphite particles in hybrid composites.

4.2.8. AC Conductance of PPS-graphite-CB Hybrid Composites

Figure 4.2.10.a shows the variation of room temperature electrical conductance of PPS-7 wt% graphite-CB hybrid composites.

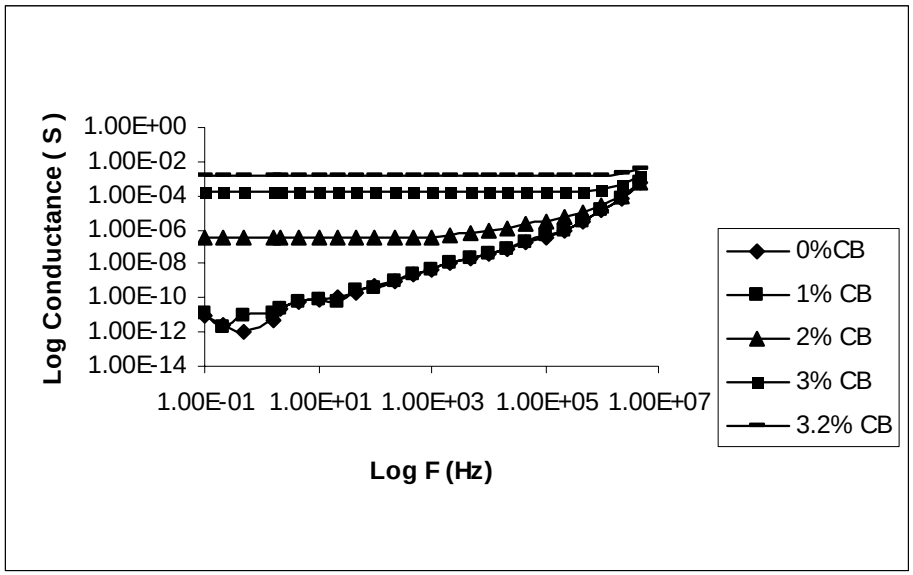

(a)

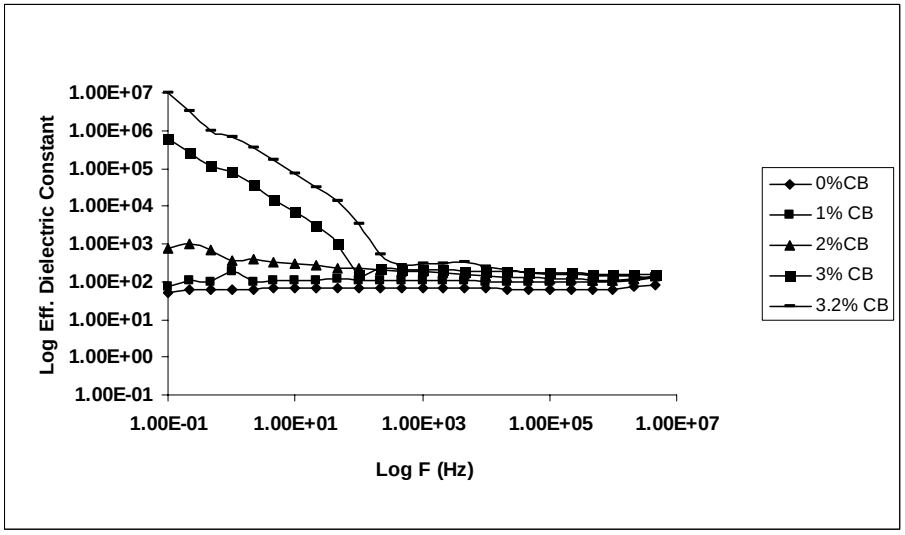

(b)

Figure 4.2.10. a) AC conductance b) Effective dielectric constant vs frequency of PPS- graphite composites

For 0 and 1 wt% CB in PPS-7 wt% graphite, the composites exhibit typical ac response of an insulator i.e., the conductance increases with frequency. The charges accumulated at the grain boundaries will be decreased with increase in the frequency

and hence they are available of conduction. For 2 wt% CB addition, there is four order increase in conductance and the response shows frequency independent and dependent parts. With higher loading of CB, the critical frequency, at which the conductance starts increasing, shifts to higher frequency. This is a reflection of composites switching over to semiconducting state. Increase in the concentration of CB leads to extension of plateau region to higher frequencies signifying enhanced dc conductance. The slope of the ac conductance vs frequency both in log scale yields exponent 'n' which signifies the charge transport in the hybrid composites. When the exponent is less than one, the charge transport is by hopping mechanism. Table 3 summarizes the variation of exponent with composition.

Table 3

Exponent 'n' from ac conductance plot

Composition	n
1.PPS-7 wt% Graphite	2.462
2.PPS-7wt% Graphite-1 wt% CB	2.376
3.PPS-7wt% Graphite-2 wt% CB	2.076
4.PPS-7 wt% Graphite-3 wt% CB	1.186
5.PPS-7 wt% Graphite- 3.2 wt% CB	0.186

It is clear from the above Table 3 that the charge transport at higher loading of CB i.e., greater than 3 wt% is by hopping mechanism as the exponent is less than one. Below that loading, the charge transport is coupled with capacitance effects. The CB particles reduce the barrier between graphite particles by occupying intergraphite space. In order to account for the occupation of CB in hybrid composites, the variation of effective dielectric constant with frequency has been measured and shown in Figure 4.2.10.b. At low frequency i.e., at 0.01 Hz, the effective dielectric

constant increases to almost four orders for 3.0 wt% CB when compared to 0 wt% CB in PPS-7 wt% graphite. Without CB, PPS-7 wt% graphite behaves as an insulator which cannot result in the huge increase in effective dielectric constant. Similarly PPS-3.0 wt% CB is an insulator as evidenced from the dc conductivity plot of PPS-CB composites. Thus the increase in the effective dielectric constant can be attributed to the occupation of CB in between graphite particles. Considering conducting particle-polymer-conducting particle as a parallel plate capacitor, with the occupation of CB in graphite interspace, the distance of parallel plates will be decreased resulting in the increase in effective dielectric constant. If this model is true then increase in interjunction capacitance with higher loading of CB in PPS-7 wt% graphite should be observed. Interjunction capacitance has been evaluated from impedance measurements as discussed below.

4.2.9. Impedance Analysis of PPS-7 wt% graphite- CB Hybrid Composites

Figures 4.2.11.a and b show the impedance plots of PPS-7 wt% graphite-2 wt% CB and PPS-7 wt% graphite-3 wt% CB hybrid composites respectively. With the addition of 2 wt% CB in PPS-7 wt% graphite, the diameter of the semicircle decreases indicating enhanced conductivity of the sample. The conducting polymer composites can be modeled as a parallel resistor-capacitor with a series resistor model as shown in Figure 4.2.12.

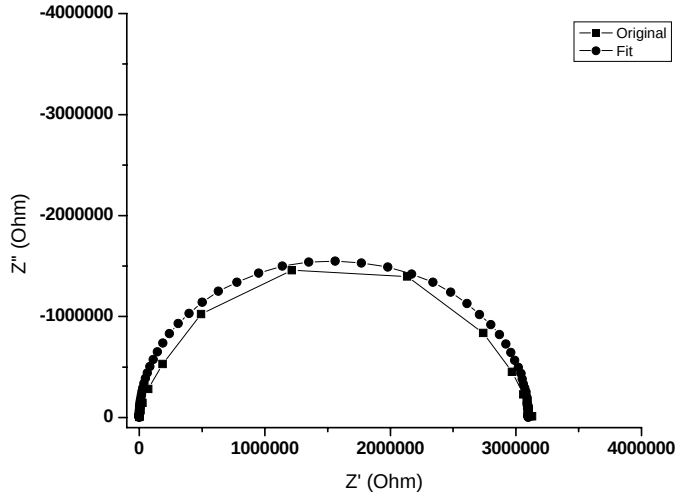

(a)

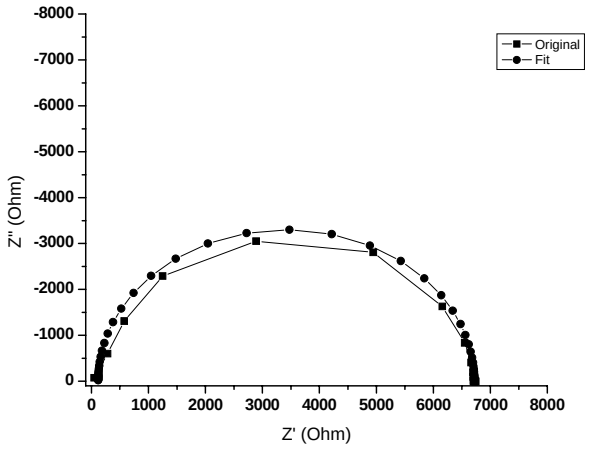

(b)

Figure 4.2.11. Impedance plots of a) PPS-7 wt% graphite-2 wt% CB b) PPS-7 wt% graphite-3 wt% CB powder mixed samples

Various model parameters extracted by fitting the experimental data with a parallel model is given in Table 4, where the symbols have the usual meaning as explained in the impedance section of Chapter-3.

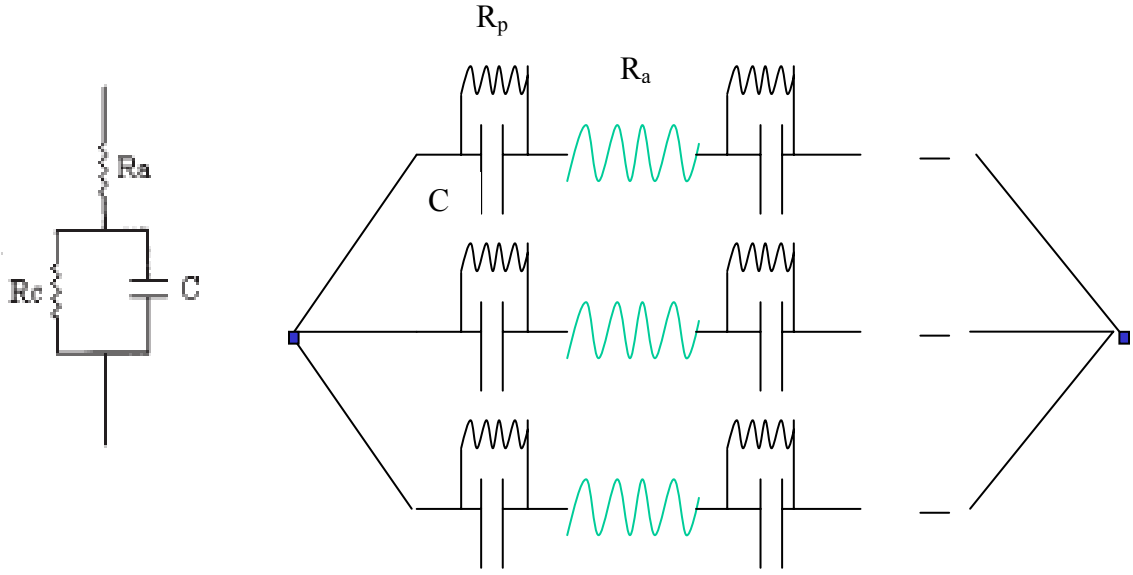

Figure 4.2.12. Model of conducting polymer composites

Table 4

Model parameters extracted from impedance measurements for powder mixed PPS-7wt% Graphite-x wt% CB composites

Sample	R_a (Ohm)	R_p (Ohm)	C (pF)
PPS-7 wt% graphite	330	2.8×10^{10}	44
PPS-7 wt% graphite-2 wt% CB	220	3.1×10^{6}	51
PPS-7 wt% graphite-3 wt% CB	120	6600	75

From Table 4 it can be seen that the interjunction capacitance indeed increases with higher CB loading in PPS-7 wt% graphite. It increases to 75 pF for 3 wt% CB in PPS-7 wt% graphite from 44 pF for 0 wt% CB in the same. Thus the model assumed earlier that the CB particles occupy intergraphite space is true. The bulk resistance decreases with the increasing concentration of CB. It is worth to notice that the aggregate resistance R_a decreases with CB addition. This can be qualitatively understood from the work function of individual components. The polymer work function is taken as 5.2 eV[17]. The work functions of graphite and CB are taken as 4.6 eV and 4.8 eV respectively as mentioned in Chapter-3. Without CB, when polymer is in contact with graphite, a barrier of 0.6 eV needs to be crossed by the charge carriers. However with CB lying in between, the barrier is reduced and it is only 0.4 eV. The barrier is essentially the difference in the work function of individual components. When more CB particles are found in between polymer and graphite more charges will be transferred to graphite via CB and hence the aggregate resistance decreases. This configuration can be thought of as connected in series through out the sample volume to cause conduction. This is pictorially represented in Figure 4.2.13.

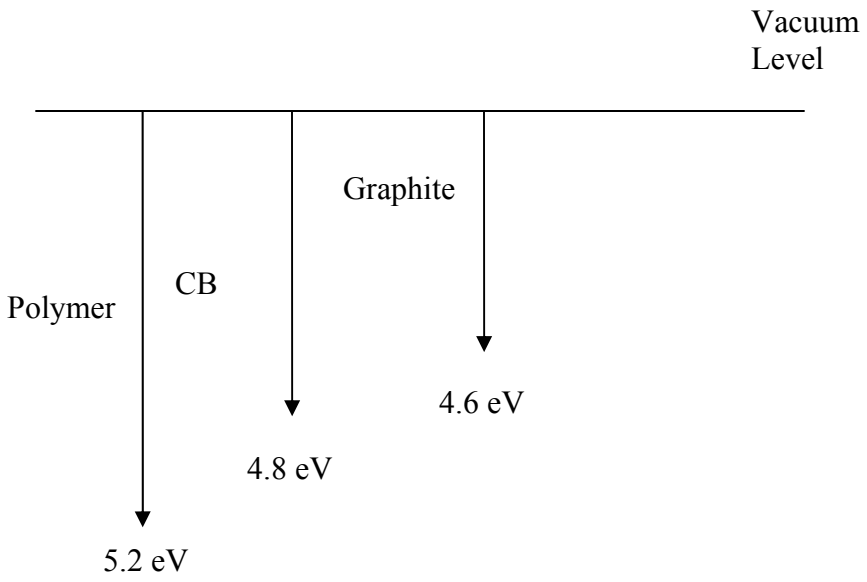

Figure 4.2.13. Work function diagram of fillers

4.3. PPS-ExGr, PPS-graphite-ExGr Composites

4.3.1. DC Conductivity variation in PPS-ExGr Binary Composites

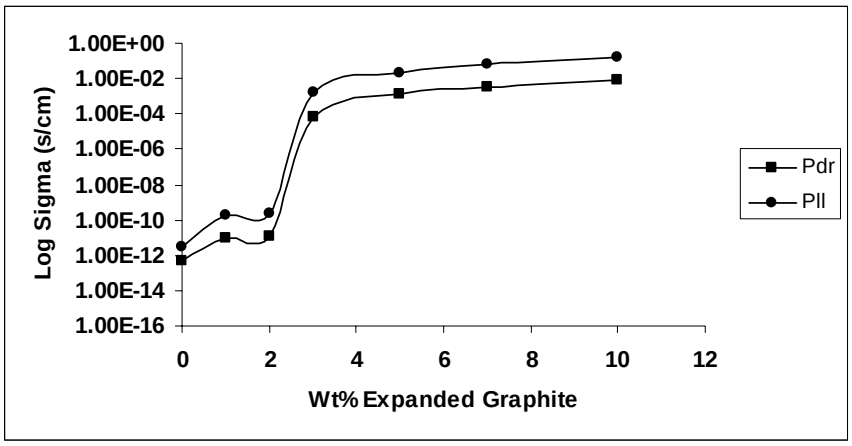

Figure 4.3.1. DC conductivity of PPS-ExGr composites

The dc conductivity variation of PPS-ExGr is shown in Figure 4.3.1. Expanded graphite (ExGr) particles have been sonicated and then mixed with the polymer. Ultrasonication results in the formation of graphite nanosheets which will be proved through SEM and TEM analysis later. The in-plane conductivity (Pll) is higher than that of through plane conductivity (Pdr) due to the alignment of graphite nanosheets along the surface of the pellet. This phenomenon can be attributed to the high pressure compaction technique employed for making pellets. The percolation

threshold is identified at 3 wt%. Such a low value is obtained due to nanosheets formations which have high aspect ratios resulting in better contact between them at low loading itself. The conductivities saturate after 5 wt% due to completion of network formation between filler nanosheets.

4.3.2. Analysis of Network Formation between Fillers in PPS-ExGr Composites

Since percolation type of variation occurs in the dc electrical conductivity of PPS-ExGr composites, percolation theory can be applied to find out the dimension of network formation between filler particles. The density of PPS is taken as 1.35 g/cc and that of expanded graphite 2 g/cc for wt% to vol% conversion. The conductivity variation predicted by percolation theory is given in equation 1 below.

$$\sigma = \sigma_o (V_f - V_c)^{t''} \qquad V_f > V_c \qquad (1)$$

Where σ -the conductivity of the composites, V_f is the volume fraction of filler above percolation threshold and V_c is the critical volume fraction. By plotting log σ vs log (V_f -V_c), the percolation exponent 't''' can be found out. For three dimensional network formation the universal value lies between 1.8 and 2. Figure 4.3.2 shows the plot of log σ (through plane conductivity) vs log (V_f -V_c) from which 't''' value of 1.83 is obtained which reflects three dimensional network structures.

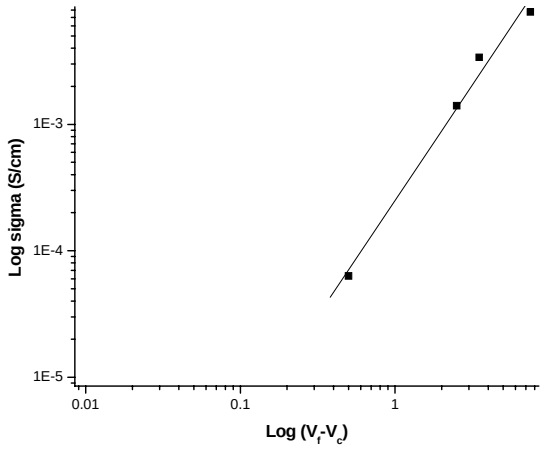

Figure 4.3.2. Plot for obtaining percolation exponent in PPS-ExGr composites

4.3.3. Effect of Heat Treatment on DC Conductivity of PPS-ExGr Powder Mixed Composites

In order to understand the effect of heat treatment on the dc electrical conductivity of PPS-ExGr composites, the composites were sintered at 240^{o}C for an hour. The through plane conductivity increases where as in-plane conductivity decreases after sintering as shown in Figures 4.3.3.a and b respectively.

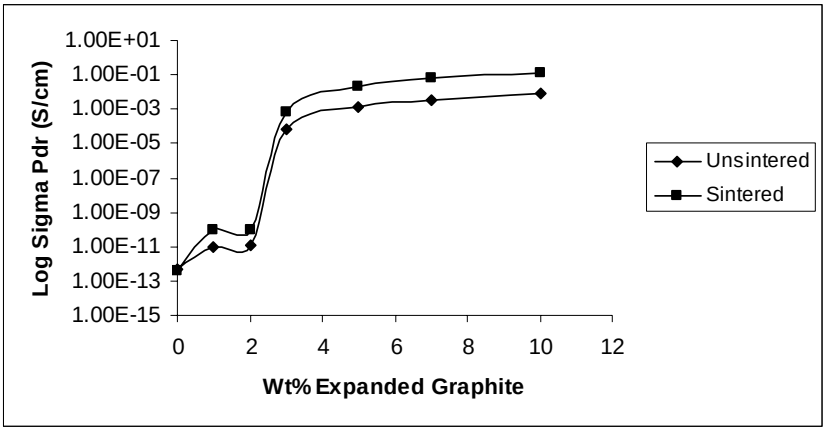

(a)

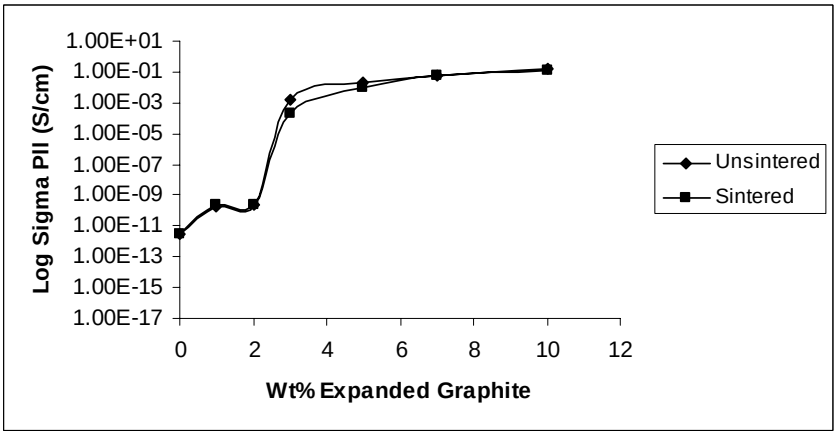

(b)

Figure 4.3.3. a) Through plane b) In-plane conductivities of PPS-ExGr composites before and after sintering

The above figures show the variation of through plane and in-plane conductivities of PPS-ExGr composites before and after sintering. It can be seen that the through plane conductivity increases after sintering for all compositions. In unsintered samples, through plane conductivity obtained is lesser than that of in-plane conductivity due to the alignment of nanosheets along the surface of the pellet. Sintering causes re-

orientation of graphite sheets along through thickness direction as it was carried out above T_g of the polymer, facilitating polymer chains movement in random directions. In fact more polymers are found on the surface of the pellet after sintering. This is reflected in the reduction of in-plane conductivity of the sample after sintering compared to the unsintered sample. At lower compositions, below the percolation threshold, the variation of conductivity is less. Above percolation threshold significant variation can be seen. To support these results, XRD analysis has been done and described below.

4.3.4. XRD Analysis of PPS-ExGr Composites

The XRD patterns of representative samples i.e., PPS-7 wt% ExGr and PPS-10 wt% ExGr before and after sintering are given in Figures 4.3.4.a and b respectively. It can be seen from the diffractograms that the intensity of graphite 002 peak is decreased after sintering. The crystallite size of expanded graphite, calculated from the 002 reflection with increase in FWHM, decreases after sintering. The polymer is able to penetrate well in to the gallery of graphite causing reduction in the crystallite size. The reduction is not much pronounced when compared to solution blended PES-graphite composites. In this case the samples were prepared by powder mixing. The intensity reduction is due to the re-orientation of graphite planes along through thickness direction implying decrease in the number of nanosheets along the surface after sintering. The increase in the through plane conductivity after sintering proves that the graphite planes are re-oriented along that direction.

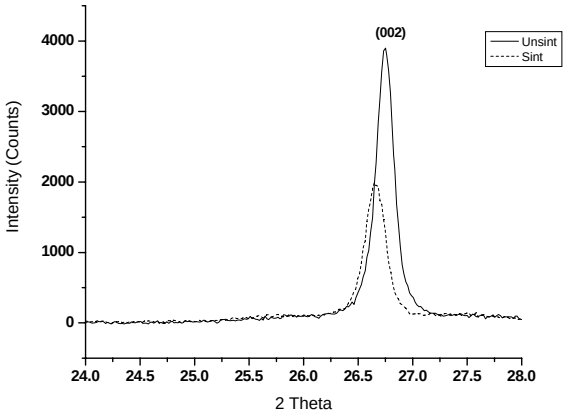

(a)

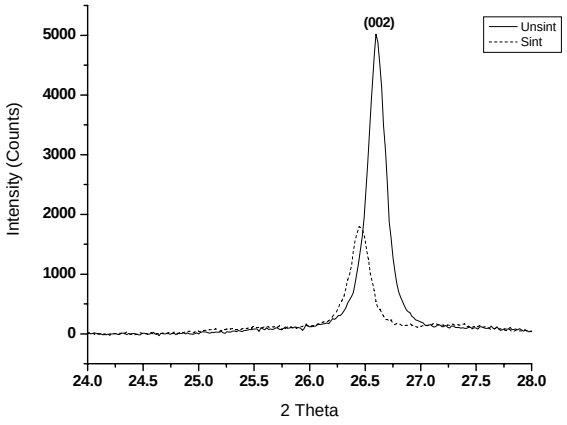

(b)

Figure 4.3.4. Graphite part of XRD pattern of a) PPS-7 wt% ExGr b) PPS-10 wt% ExGr

The above Figures 4.3.4.a and b show clearly intensity reduction as well as crystallize size as discussed before for PPS-7 wt% ExGr and PPS-10 wt% ExGr respectively.

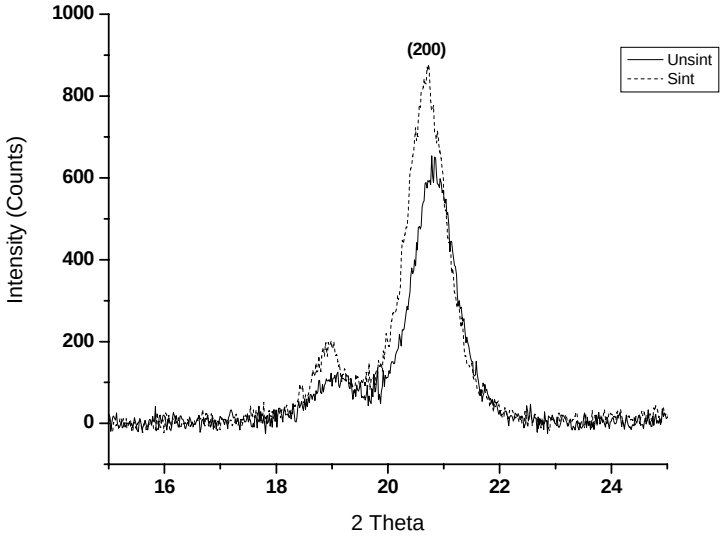

(a)

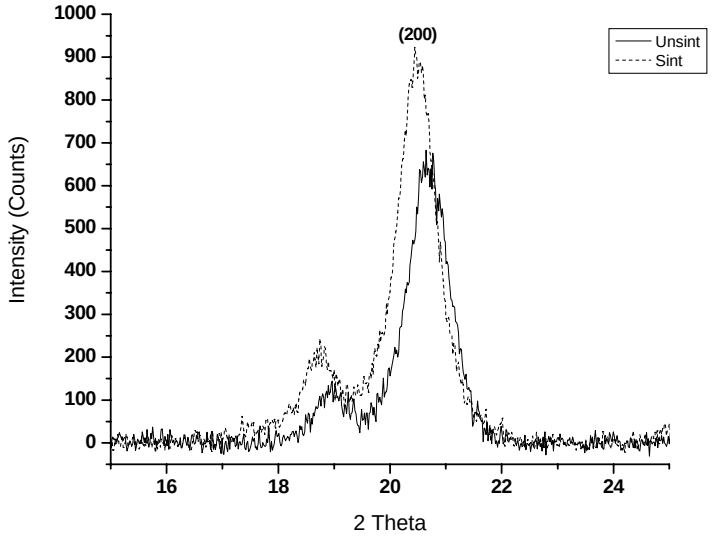

(b)

Figure 4.3.5. PPS part of XRD patterns of a) PPS-7 wt% ExGr b) PPS-10 wt% ExGr

Figures 4.3.5.a and b show the PPS part of XRD patterns of PPS-7 wt% ExGr and PPS-10 wt% ExGr respectively. It is clear from the diffractograms that after sintering the intensity of (200) of PPS increases implying the presence of more polymers on the surface. Hence the in-plane conductivity after sintering decreases. XRD analysis of PPS-ExGr composites is given in Table 5. It is clear from Table 5 that the crystallite size of ExGr decreases after sintering. Before sintering, the crystallite size of ExGr in powder mixed samples remains the same.

Table 5

XRD analysis of PPS-ExGr composites

Sample	2 Theta		Intensity (Counts)		Crystallite Size t' (nm)	
	BS	AS	BS	AS	BS	AS
PPS-5wt% Expanded Graphite	26.76	26.632	1652	1580	31.30	24.59
PPS-7wt% Expanded Graphite	26.751	26.649	3899	1992	31.30	28.7
PPS-10wt% Expanded Graphite	26.598	26.445	5019	1798	31.3	28.7

BS- before sintering, AS- after sintering,

4.3.5. SEM Analysis of Powder Mixed PPS-ExGr Composites

The surface morphology of powder mixed PPS-ExGr composites is shown in Figures 4.3.6.a and b.

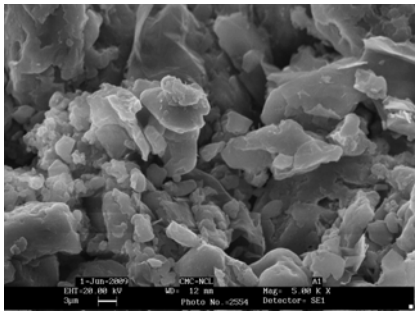

(a)

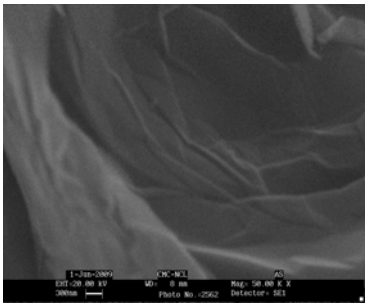

(b)

Figure 4.3.6. SEM pictures of PPS-3 wt% ExGr a) unsintered b) sintered samples

The cross section of PPS-3 wt% ExGr unsintered sample shows that graphite nanosheets formed due to sonication are agglomerated and buried in the polymer matrix. This is shown in Figure 4.3.6.a. Sintered sample shows that the agglomerated nanosheets are teared off due to polymer penetration as evidenced by Figure 4.3.6.b. This result supports XRD analysis of PPS-ExGr composites.

4.3.6. TEM Analysis of Powder Mixed PPS-ExGr Composites

The powder mixed PPS-7 wt% ExGr is compression molded to form a sheet. The sheet was ultra-microtomed, transferred to TEM grids for further analysis. It can be seen from Figure 4.3.7 that the porous structure of ExGr is destroyed and results in nanosheets formation due to sonication. Since the aspect ratios of nanosheets are very high, low percolation results due to better contact between filler particles. The nanosheets formed are indicated by arrows in Figure 4.3.7. Original ExGr has more pores as shown in Chapter-3 in PES-ExGr section which on sonication forms graphite nanosheets

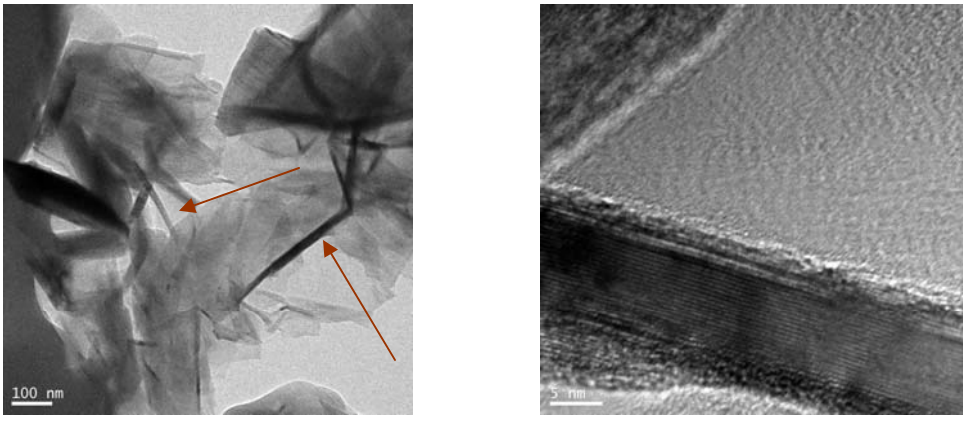

Figure 4.3.7. HRTEM images of ultra-microtomed PPS-7 wt% ExGr

The arrangement of graphene layers in ~15 nm thick nanosheet can be seen in the above HRTEM image.

4.3.7. Electrical Conductivity Variation in PPS-Graphite-ExGr Composites

Hybrid composites are very important to reduce percolation threshold. Since the percolation threshold of PPS-ExGr binary composites lies at 7 wt% ExGr, this particular composition has been chosen to study the effect of ExGr addition as second filler on the through plane electrical conductivity.

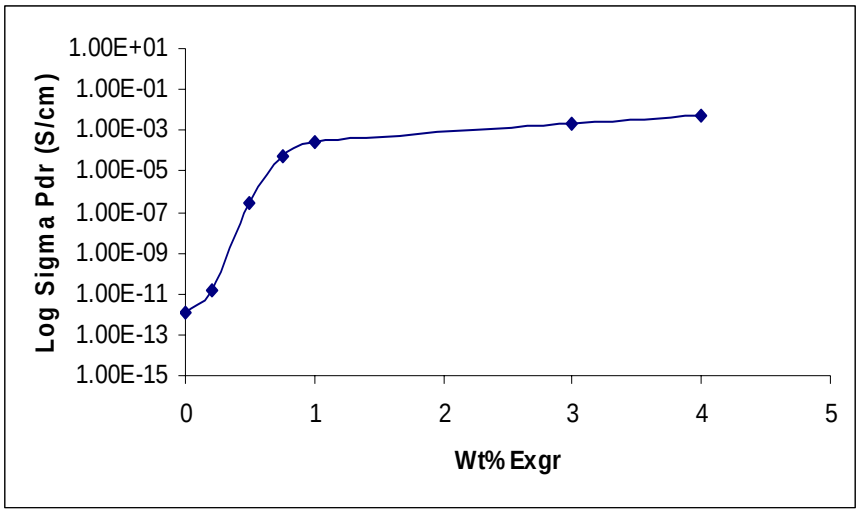

Figure 4.3.8. DC conductivity of PPS-graphite-ExGr hybrid composites

Percolation threshold in hybrid composites lies at 0.25 wt% ExGr. Saturation in electrical conductivity occurs after 1 wt% ExGr in PPS-7 wt% graphite. The ExGr particles form nanosheets after sonication and occupy intergraphite spaces when mixed with PPS-7 wt% graphite. Thus the barrier for the charge transport is reduced resulting in enhanced conductivity. It should be remembered that without ExGr, PPS-7 wt% graphite acts as an insulator. Similarly PPS-0.25 wt% ExGr without graphite also behaves as an insulator. So the possibility remaining for the ExGr nanosheets to occupy intergraphite spaces will be discussed in the following sections.

4.3.8. Frequency Dependent Conductance of PPS-graphite-ExGr Hybrid Composites

Figure 4.3.9.a shows the variation of conductance with frequency. With 0 wt% ExGr addition, PPS-7 wt% graphite exhibits ac conductance variation typical to that of an insulator i.e., conductance increases with frequency. With the addition of 0.5 wt% ExGr, plateau region appears signifying enhanced conductivity of the hybrid composites. In fact insulator-semi conductor transition occurs. With further increase in the loading of ExGr, the plateau region extends more and the frequency dependent conductance starts at higher frequency.

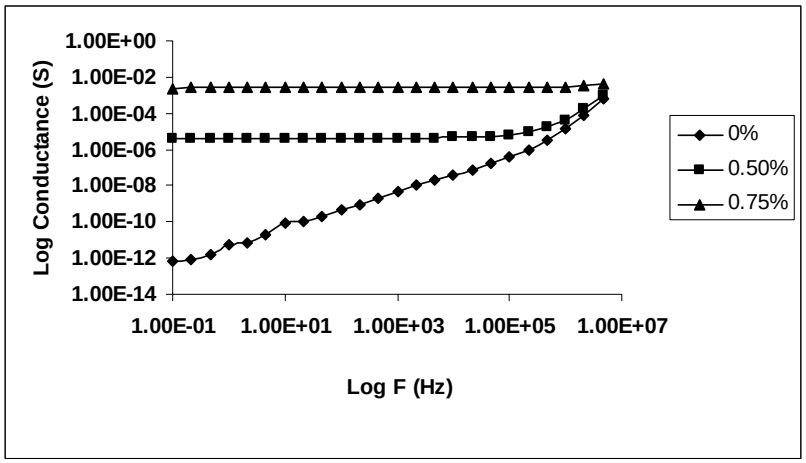

(a)

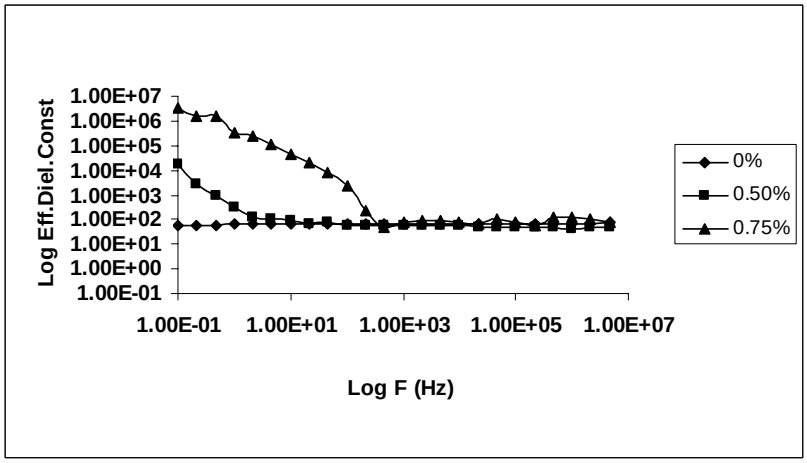

(b)

Figure 4.3.9. a) AC conductance b) Effective dielectric constant vs frequency of PPS-7 wt% graphite-ExGr hybrid composites

The plateau region signifies dc conductance of the samples. For 0.75 wt% ExGr in PPS-7 wt% graphite, the high frequency slope of ac conductance gives a value of 0.28 signifying hopping type of charge transport. Below 0.75 wt% ExGr in PPS-7 wt% graphite, the charge transport is coupled with capacitance effects as obtained for PES-graphite hybrid composites discussed in Chapter-3. The six order enhancement in the dc conductance when 0.5 wt% ExGr is added to PPS-7 wt% graphite is due to the reduction in the barrier for the charge transport because of the occupation of graphite nanosheets in between graphite particles. Considering conducting particle-polymer-

conducting particle as a parallel plate capacitor, if ExGr nanosheets are found in between graphite particles, the distance of the parallel plate capacitor will be decreased resulting in an increase in interjunction capacitance as well as effective dielectric constant. Figure 4.3.9.b supports the above argument as there exists at least four order increase in the effective dielectric constant at low frequency i.e., at 0.01 Hz for 0.75 wt% ExGr in PPS-7 wt% graphite when compared to 0 wt% ExGr addition in the same. In order to evaluate interjunction capacitance, impedance measurement has been carried out on hybrid composites and discussed below.

4.3.9. Impedance Analysis of PPS-graphite-ExGr Composites

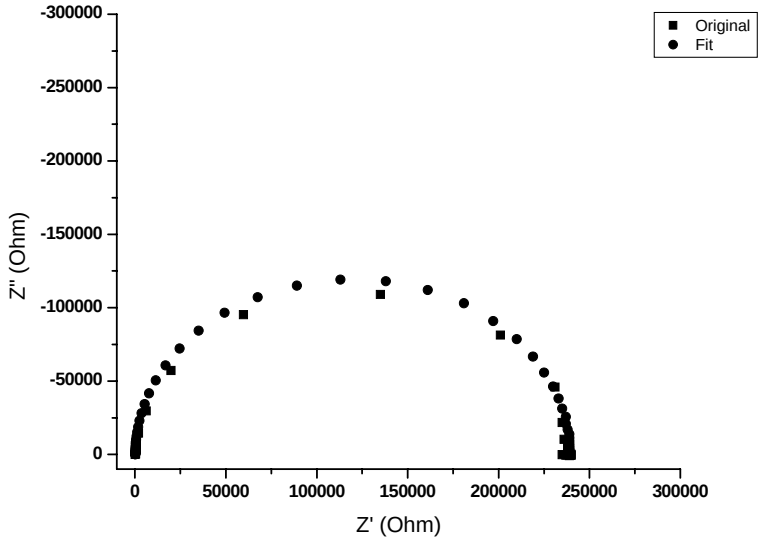

(a)

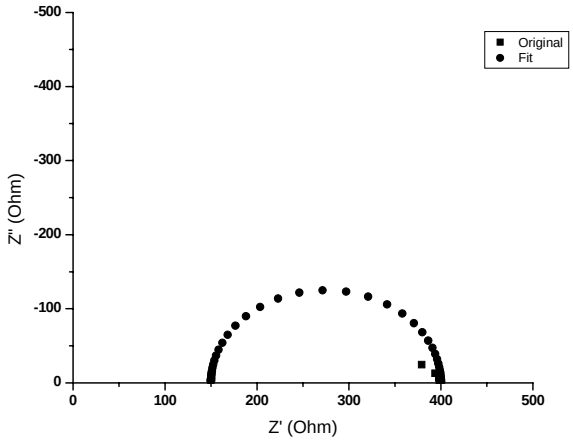

(b)

Figure 4.3.10. Impedance plots of a) PPS-7 wt% graphite-0.5 wt% ExGr b) PPS-7 wt% graphite-0.75 wt% ExGr powder mixed samples

The impedance plots of 0.5 wt% and 0.75 wt% ExGr addition in PPS-7 wt% graphite are shown in Figures 4.3.10.a and b respectively. These hybrid composites exhibit semicircular behavior in Argand plane suggesting that they can be modeled as parallel resistor-capacitor with a series resistor as described in PPS-Graphite-CB hybrid composites section. There can be series and parallel arrangement of above equivalent circuit in the samples. It can be seen that the diameter of the semicircle decreases with the addition of ExGr indicating enhanced sample conductance. The diameter represents dc resistance. Various parameters extracted by fitting the experimental plot to parallel model are described in Table 6 where the symbols have their usual meaning.

Table 6

Parameters extracted from parallel model for PPS-7 wt% graphite-ExGr composites

Sample	R_a (Ohm)	R_p (Ohm)	C (pF)
PPS-7wt% Graphite	350	2.8×10^{10}	44
PPS-7wt% Graphite-0.5wt% ExGr	300	2.39×10^{5}	51
PPS-7wt% Graphite-0.75wt% ExGr	150	250	77

It can be seen from the above Table 6 that with the addition of ExGr, the bulk resistance decreases. Moreover, the interjunction capacitance increases from 44 pF for 0 wt% ExGr addition in PPS-7 wt% graphite to 77 pF for 0.75 wt% ExGr addition in the same. This result strongly supports the occupation of ExGr nanosheets predominantly in intergraphite spaces. Further, the aggregate resistance decreases with increase in the concentration of ExGr. When two particles of different conductivity are mixed with a polymer, the work function of them comes in to picture. It should be noted that no reports are available on ExGr work function determination. PPS work function is taken as 5.2 eV and that of graphite is 4.6 eV. The barrier for the charges to go directly to graphite is 0.6 eV. Since the worfuction of ExGr is not reported in the literature, it is presumed that it will be higher than that of graphite and hence charges will be transported from polymer to graphite via ExGr. If more ExGr particles occupy graphite interspace, more charges will be transferred to graphite via ExGr particles. In this way reduction in the aggregate resistance with the addition of Exgr particles can be better understood.

4.3.10. DSC Analysis of PPS Based Binary and Hybrid Composites

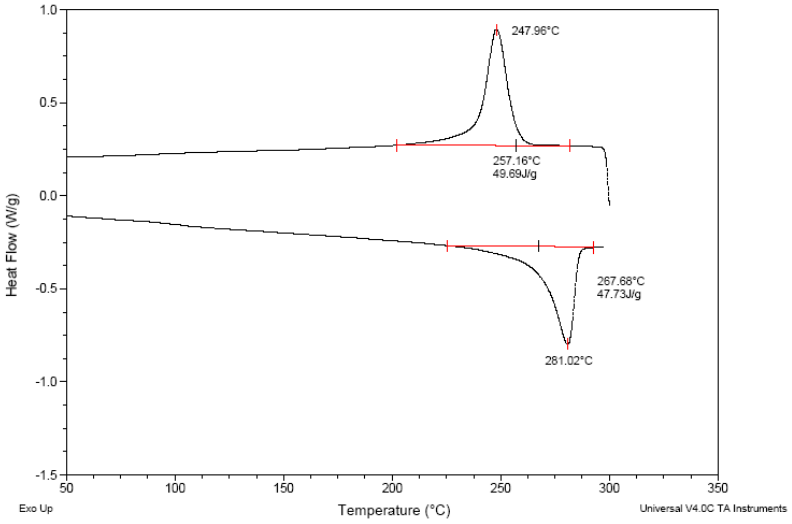

(a)

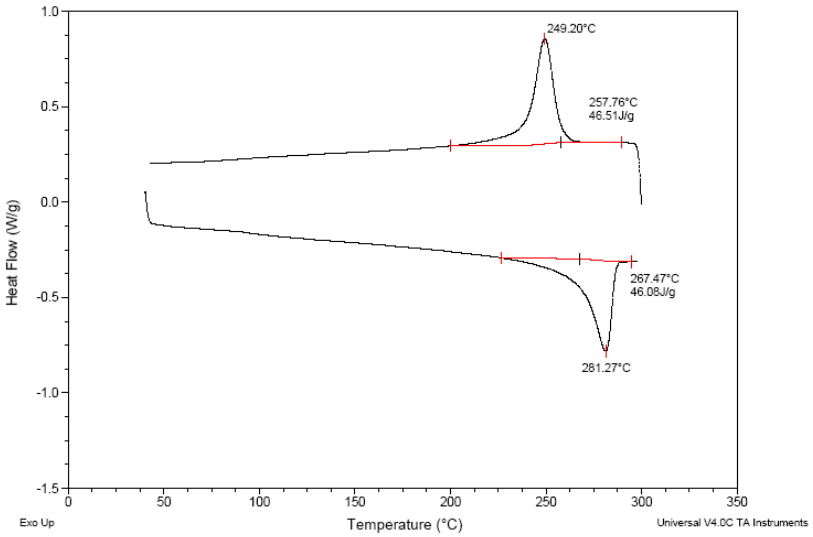

(b)

Figure 4.3.11. DSC plots of a) PPS-3 wt% ExGr b) PPS-7 wt% graphite-0.5 wt% ExGr

The DSC analysis of PPS is given in PPS-Graphite-CB section. Table 7 summarizes various parameters extracted from the DSC plots shown in Figure 4.3.11.a and b.

Table 7

Parameters extracted from DSC thermograms

Sample	T_m (^oC)	T_c (^oC)	ΔH_c (W/g)
PPS Pure	280.90	244.89	40.74
PPS-3wt% expanded graphite	281.02	247.96	49.69
PPS-7wt% Graphite-0.5wt% expanded graphite	281.27	249.20	46.51

With the addition of 3 wt% ExGr in PPS, the crystallization temperature increases by ~ 3^{o}C signifying the nucleating ability of ExGr nanosheets. No significant difference between melting temperature of the polymer is observed with ExGr addition. Since the enthalpy of crystallization (ΔH_c) is higher than that of pure PPS, the crystallinity is increased. For 0.5 wt% ExGr addition in PPS-7 wt% graphite, the crystallization temperature (T_c) increases by ~5^{o}C suggesting that ExGr nanosheets act as nucleators.

The crystallinity is increased in this hybrid composite as revealed through the increase in the area under the crystallization peak. No considerable difference in melting temperature is observed for this composition. The above results evidence better interaction between polymer and the filler.

4.4. PPS-CNF and PPS-graphite-CNF Composites

4.4.1. DC Conductivity of PPS-CNF Binary Composites

CNF is first dispersed in acetone for five hours and then mixed with required amount of PPS. The dc electrical conductivity variation with respect to CNF concentration in PPS is shown in Figure 4.4.1.

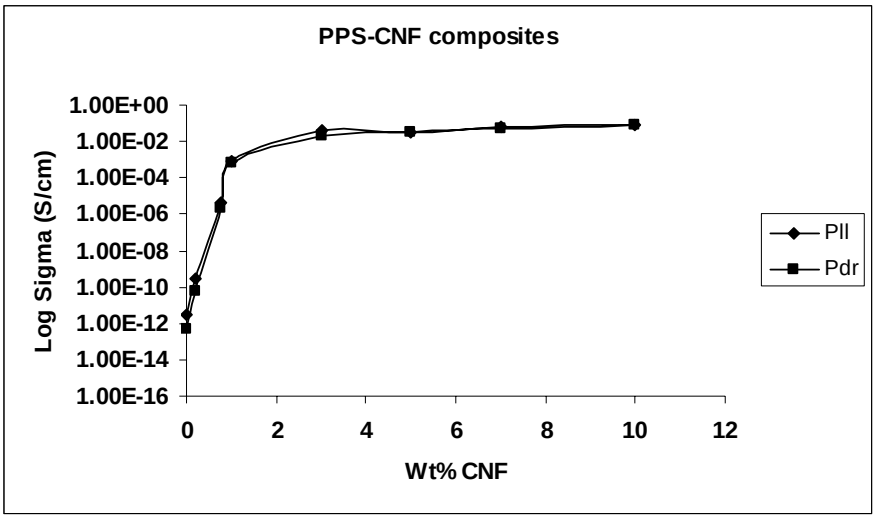

Figure 4.4.1. DC conductivity of powder mixed PPS-CNF composites

After 0.2 wt% CNF in PPS, the dc electrical conductivity shoots up to many orders and regarded as the percolation threshold. Below the threshold, the composites remain as insulators due to insufficient network formation. After 2 wt% CNF in PPS, the conductivity saturates at 0.01 S/cm due to saturation in the network formation between the high aspect ratio fillers. The in-plane (Pll) and through thickness (Pdr) conductivity remains more or less the same indicating very good dispersion of nanofiller in the polymer matrix.

4.4.2. Effect of Sintering on DC Electrical Conductivity of PPS-CNF Composites

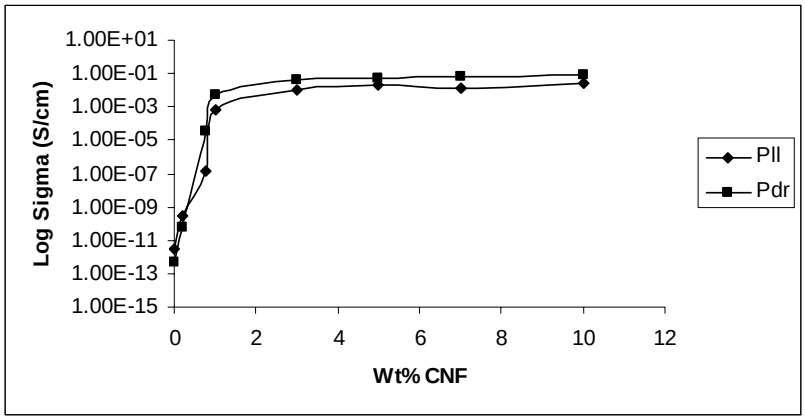

Figure 4.4.2. DC conductivity of PPS-CNF composites after sintering

The composites are sintered at 240°C for one hour. Sintering causes re-orientation of CNF along through thickness direction due to the movement of polymer chains as the sintering temperature is kept above T_g of the polymer. This results in enhancement in the through plane conductivity (Pdr) than in-plane conductivity (Pll) as more polymer will be found on the surface of the sample. The enhancement is considerable at and above the percolation threshold. Below the percolation threshold, no significant change is observed as the composites behave as insulators. The result obtained is similar to that of other PPS based systems.

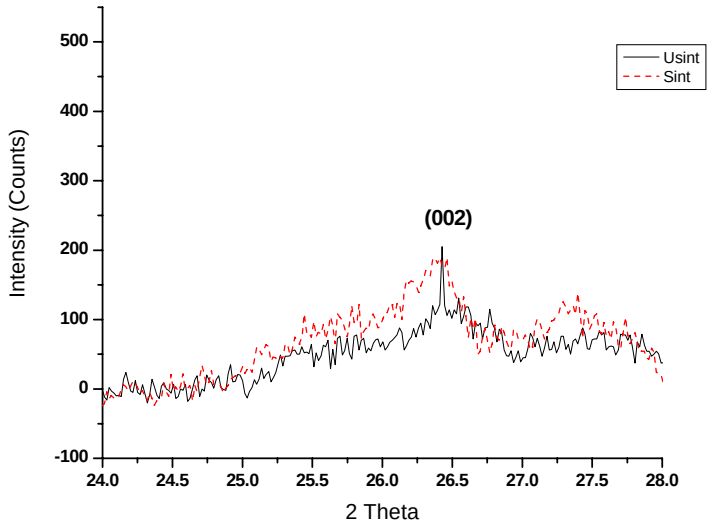

(a)

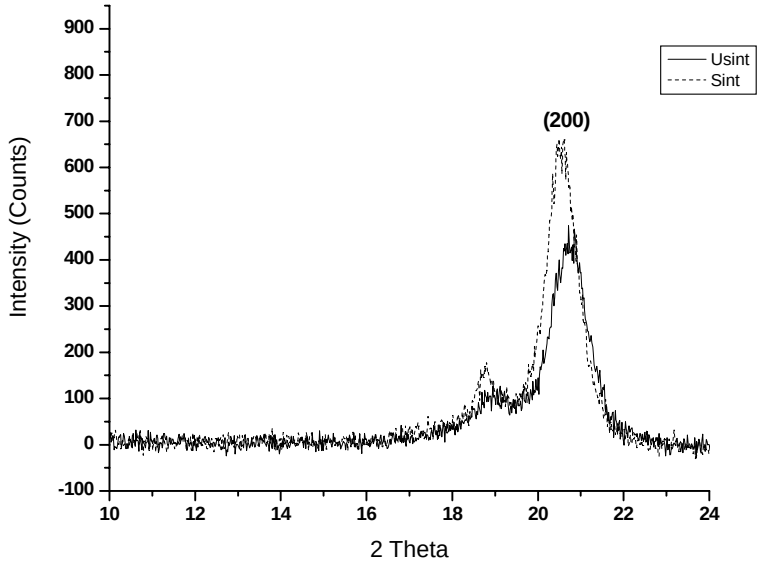

(b)

Figure 4.4.3. XRD Patterns of a) Graphite part b) PPS part of PPS-7 wt% CNF composites

It is clear from the XRD pattern shown in Figure 4.4.3.a that the intensity of 002 reflection of graphite in PPS-7 wt% graphite composite decreases after sintering signifying re-orientation of CNF due to the movement of polymer chains. The XRD pattern of PPS part of PPS-7 wt% graphite shown in Figure 4.4.3.b clearly depicts that the intensity of 200 peak of PPS increases after sintering implying the presence of large amount of polymer on the surface of the pellet. Therefore in-plane conductivity of composites decrease after sintering when compared to that of unsintered samples.

4.4.3. SEM Analysis of PPS-CNF Composites

The surface morphology of pure CNF after sonicating in acetone for five hours and the cross section of PPS-3 wt% CNF composite before and after sintering is shown in Figure 4.4.4.a, b and c respectively. It is clear that there exists a variation in tube diameter as tubes with 200 nm diameter can also be found which could be the agglomerated fibers. Because of high aspect ratio of fibers, low loading is required to register higher conductivity i.e., low percolation threshold results.

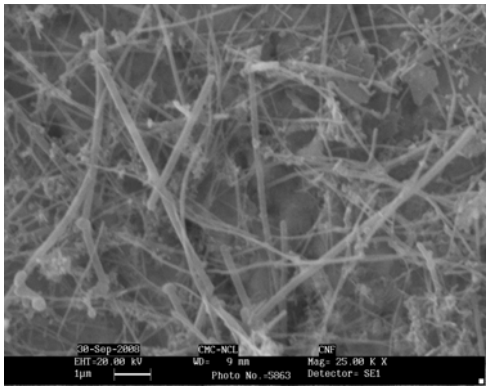

(a)

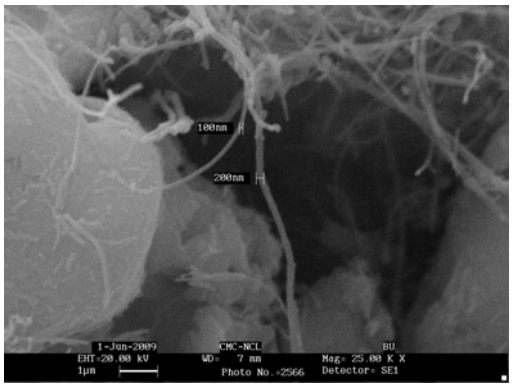

(b)

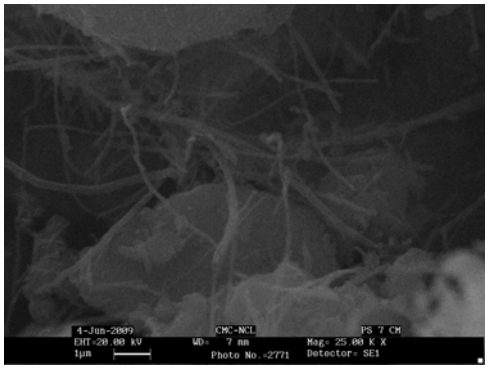

(c)

Figure 4.4.4. SEM pictures of a) Pure CNF b) Unsintered c) Sintered PPS-3 wt% CNF composites

The fibers are well separated after sintering which leads to better contact resulting in the enhancement of through plane conductivity.

4.4.4. TEM Analysis

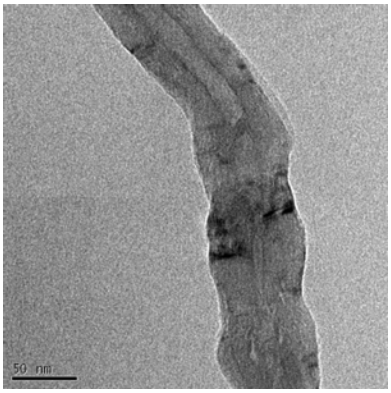

Figure 4.4.5. TEM picture of CNF mixed in PPS

Carbon nanofibers are added to the polymer after sonication in acetone for five hours. After mixing, the composites are sonicated for half an hour more. So it is assumed

that the aspect ratio of CNF will not be changed further due to polymer resistance and the same phenomenon has been observed. Hence for the calculation of aspect ratio of CNF, the sonicated fibers length and diameter have been reported as shown in Figure 4.4.5. Well dispersed CNFs have an average diameter~72 nm and length~8 micron (from SEM) resulting in the aspect ratio of 111 being less as compared to original CNFs.

4.4.5. DSC Analysis of PPS-CNF Composites

The DSC of pure PPS has already been shown in the section of PPS-graphite composites and hence only the DSC of PPS-0.5 wt% CNF is shown in Figure 4.4.6. No significant change in the melting temperature is observed where as almost 4°C enhancement in the crystallization temperature could be observed suggesting the nucleating ability of CNFs. Table 8 describes various parameters obtained from DCS analysis.

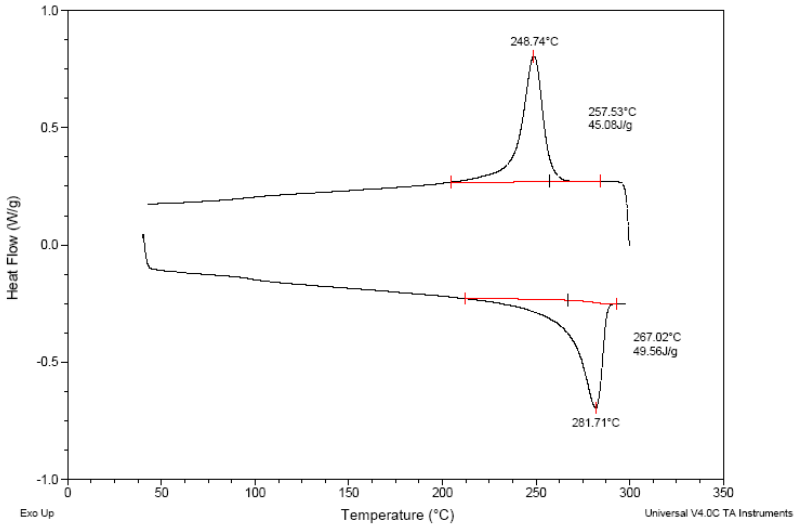

Figure 4.4.6. DSC of PPS-0.5 wt% CNF

Table 8

DSC analysis of PPS-CNF composites

Sample	T_m (°C)	T_c(°C)	ΔH_c (W/g)
PPS pure	280.90	244.89	40.74
PPS-0.5wt% CNF	281.02	248.74	45.08

It is clear from the Table 8 that the area under the crystallization peak increases (ΔH_c) with the addition of CNF indicating increased crystallinity.

4.4.6. PPS-graphite-CNF Hybrid Composites

The dc electrical conductivity variation of PPS-7 wt% graphite-CNF powder mixed composites with the addition of CNF is shown in Figure 4.4.7. The percolation threshold is much lower than 0.2 wt% CNF. In-plane conductivity (Pll) is slightly higher than the through plane (Pdr) one. After 1 wt% CNF in PPS-7 wt% graphite, saturation in conductivity is observed due to complete network formation.

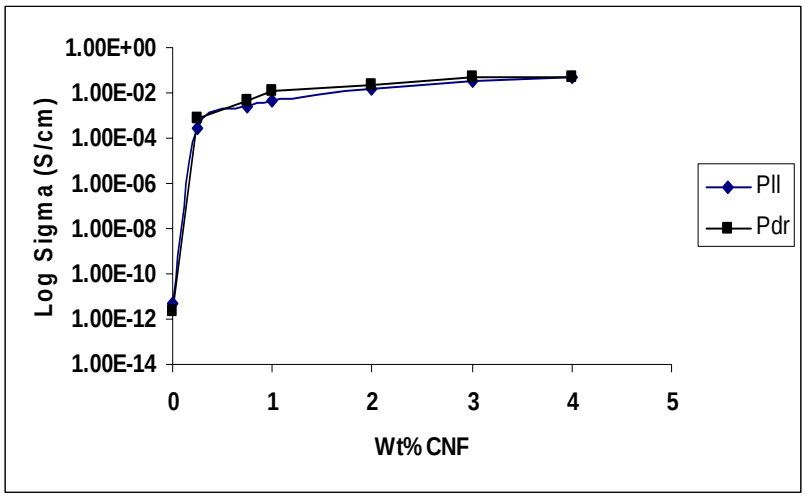

Figure 4.4.7. DC conductivity of PPS-7 wt% graphite- CNF composites

4.4.7. AC Behavior of PPS-graphite-CNF Composites

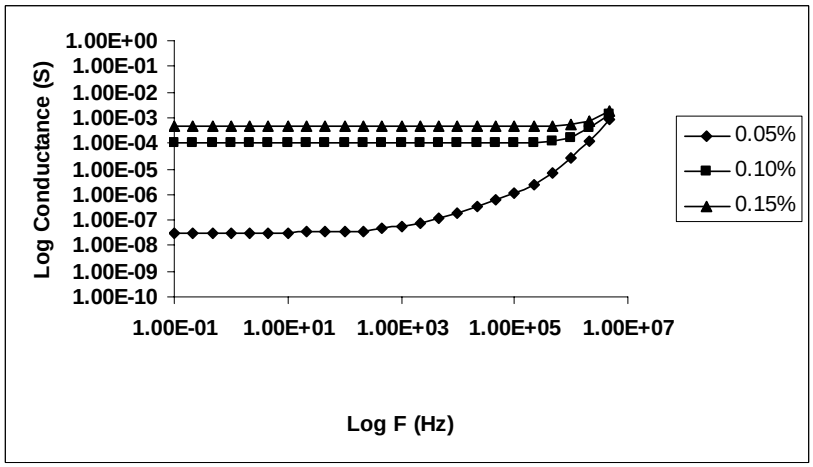

(a)

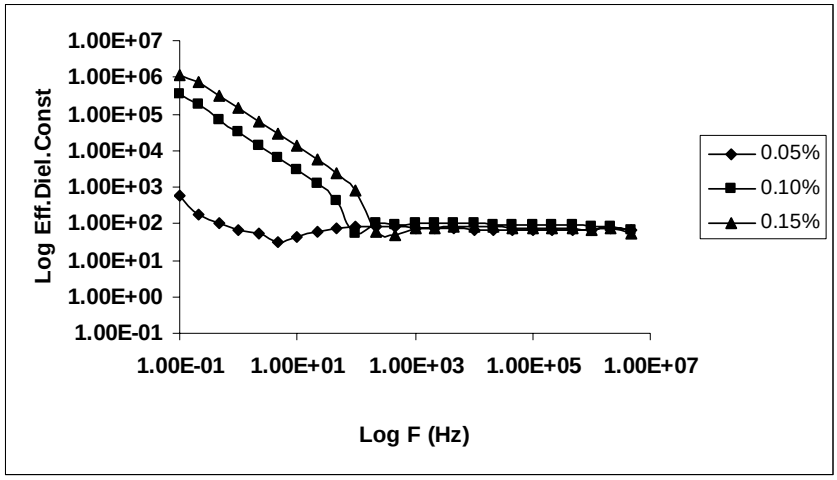

(b)

Figure 4.4.8. a) AC conductance b) Effective dielectric constant variation with frequency of PPS-7 wt% graphite-x wt% CNF (X=0.05,0.1,0.15)

Figure 4.4.8.a shows the variation of conductance of PPS-7 wt% graphite-CNF hybrid composites with frequency. With the addition of 0.05 wt% CNF in PPS-7 wt% graphite, the conductance increases compared to 0 wt% CNF in the same. With increasing loading of CNF, the plateau region extends well and the frequency dependent conductance starts at higher frequency. From this plot it is ascertained that the percolation threshold lies between 0.05-0.1 wt% CNF in PPS-7 wt% graphite. The plateau region signifies dc conductance. The enhancement in the conductivity is due to the occupation of CNFs in between graphite particles, leading to the reduction in barrier for the charge transport. Conducting particle-polymer-conducting particle can be considered as a parallel plate capacitor. If CNF occupies intergraphite space, the distance between parallel plates is decreased which is equivalent to the reduction in interparticulate distance. Based on this hypothesis, the effective dielectric constant and the interjunction capacitance should increase with increase in loading of CNFs. It is to be remembered that without CNF, PPS-7 wt% graphite behaves as an insulator. Similarly without graphite PPS-0.05 wt% CNF exhibits insulating behavior. Thus the enhancement in the conductivity must be due to the occupation of CNF in between graphite particles. Figure 4.4.8.b shows that the effective dielectric constant increases to many fold with CNF addition at low frequency (0.01 Hz) supporting the model.

Effective dielectric constant decreases with increase in the frequency which is a typical variation in disordered systems. After certain frequency, it remains more or less constant. As conducting polymer composites can be modeled as parallel resistor-capacitor with a series resistor, impedance measurement becomes easier to evaluate interjunction capacitance.

4.4.8. Impedance Analysis of PPS-graphite-CNF Composites

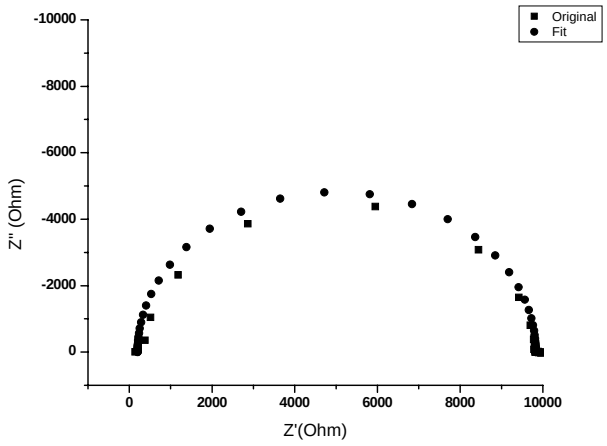

(a)

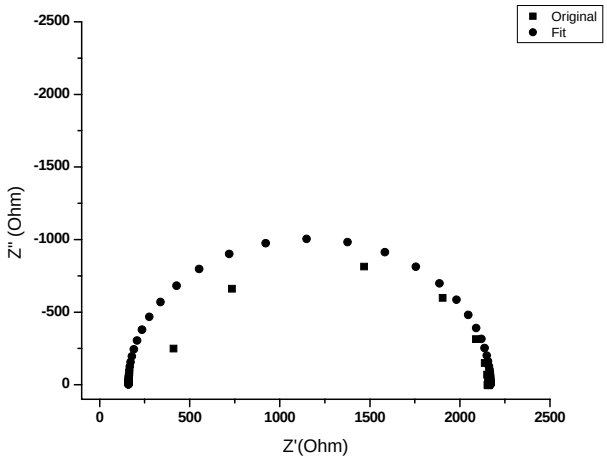

(b)

Figure 4.4.9. Impedance plots of a) PPS-7 wt% graphite-0.1 wt% CNF b) PPS-7 wt% graphite-0.15 wt% CNF

The impedance plots shown in Figure 4.4.9.a and b suggest that with increasing CNF loading in PPS-7 wt% graphite, the diameter of the semicircle decreases. The diameter represents dc resistance. Further the semicircular response of the material suggests that parallel resistor-capacitor model can be used to fit the data. The following Table 9 describes various model parameters extracted from the impedance behavior of hybrid composites.

Table 9

Model parameters for PPS-7 wt% graphite-CNF composites

Sample	R_a (Ohm)	R_p (Ohm)	C (pF)
PPS-7wt% Graphite-0.05wt% CNF	250	$4.9x10^{11}$	49.0
PPS-7wt% Graphite-0.1wt% CNF	200	9630	70
PPS-7wt% Graphit-0.15wt% CNF	160	2010	80.5

From the above Table 9 it can be seen that the interjunction capacitance increases from 49 pF for 0.05 wt% CNF in PPS-7 wt% graphite to 81 pF for 0.15 wt% CNF corroborating that CNFs occupy intergraphite space. The decrease in aggregate resistance can be qualitatively understood from the arrangement and work function of the individual components. As mentioned in the previous Chapter-3 that the work function of CNF is taken as 5 eV and that of polymer 5.2 eV. The work function of graphite is taken as 4.6 eV. Without CNF, for the charge transport from polymer to graphite, a barrier of 0.6 eV needs to be crossed by the charges. When CNFs are found in between polymer and graphite the barrier for the charge transport is reduced being 0.2 eV. So with CNF addition, the interspace between the polymer and graphite is occupied by them and more charges will be transferred to graphite via CNF. Barrier is nothing but the difference in the work function of individual components in contact. The polymer-CNF-Graphite configuration can be assumed to be connected in series throughout the volume of the sample to cause electrical conduction.

4.4.9. Effect of Aspect Ratio on Percolation Threshold of PPS-7 wt% graphite Based Hybrid Composites

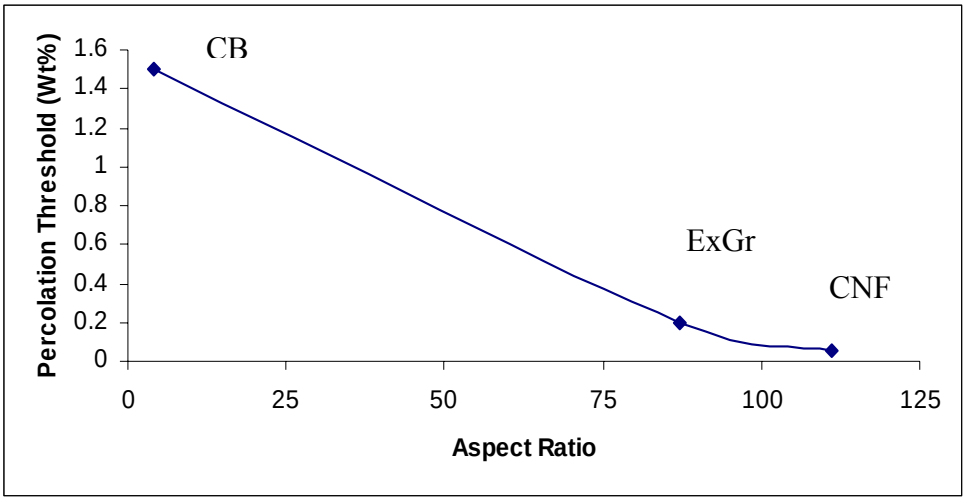

Figure 4.4.10. Effect of aspect ratio of second conducting fillers on electrical percolation threshold

The percolation thresholds of hybrid composites are found to be inversely related to the aspect ratio of the second conducting fillers as shown in the above Figure 4.4.10.

4.4.9.1. CB Aspect Ratio

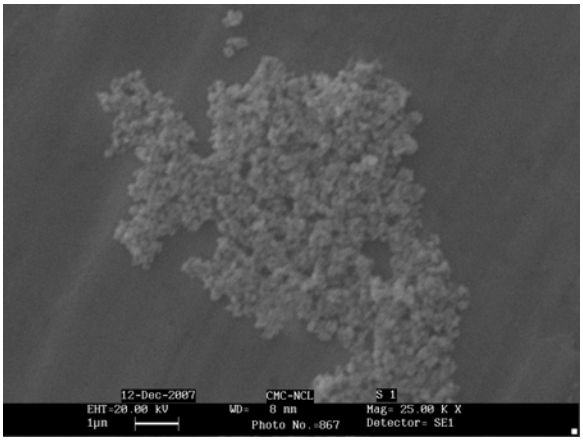

Figure 4.4.11. SEM picture of Carbon Black

CB has more or less spherical shape and agglomerated structure with aggregate size 80 nm. The length of the agglomerates is 300 nm on an average as shown in Figure 4.4.11. So the aspect ratio is rounded of to four.

4.4.9.2. Expanded graphite Aspect Ratio

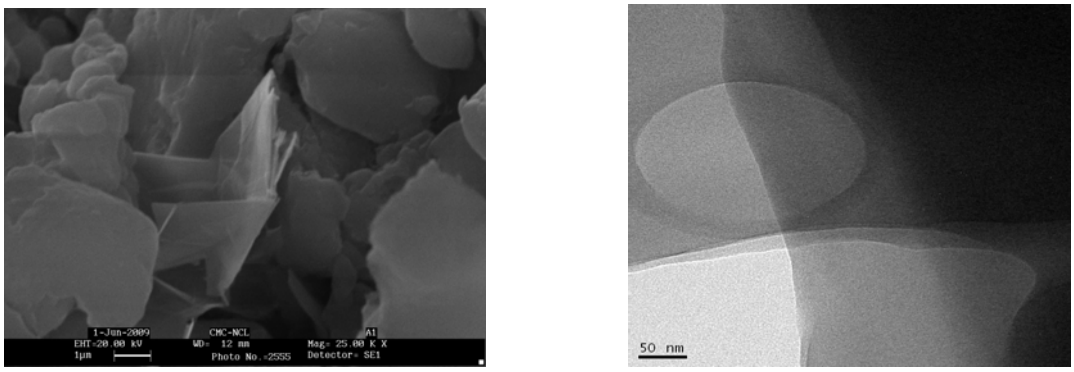

(a) (b)

Figure 4.4.12. a) SEM b) TEM pictures of expanded graphite

The average length of ExGr particles is taken as 2.6 micron as shown in Figure 4.4.12.a and the thickness 30 nm from Figure 4.4.12.b leading to an aspect ratio of 87. CNF aspect ratio has been discussed in section 4.4.4 and its value is 111.

B. Melt crystallization

4.5. Melt Crystallized PPS-graphite Composites

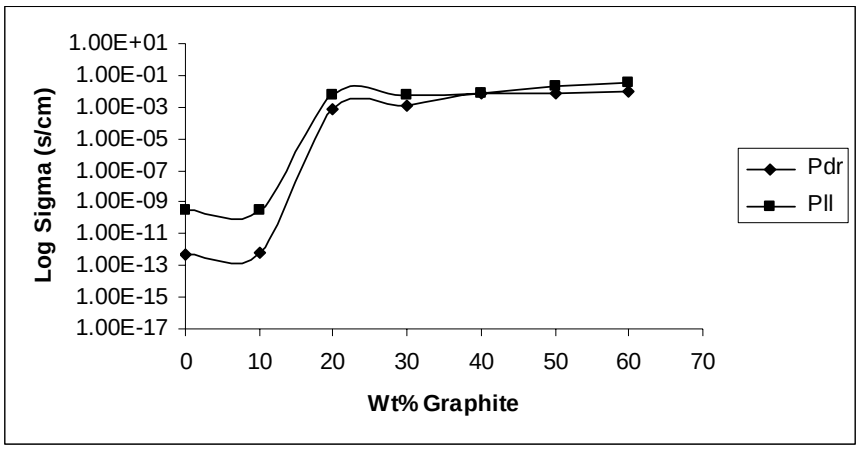

Figure 4.5. DC conductivity of melt crystallized PPS-graphite composites

Melt crystallized samples were prepared by heating the composite to 300^{o}C for two minutes period and immediately transferred to water. The process leads to the formation of sheets which are used for measuring electrical resistance. It is clear from the above Figure 4.5 that for PPS-graphite composites, the percolation threshold lies at 10 wt%. The percolation threshold of the same composites prepared by powder mixing route is 7 wt%. The increase in the percolation threshold is due to the increase in the interparticulate distance in melt crystallized samples as the viscosity decreases

at higher temperature. The in-plane conductivity (Pll) is higher than the through plane (Pdr) one due to the alignment of filler particles along the surface of the sheets.

4.5.1. Melt Crystallized PPS-ExGr Composites

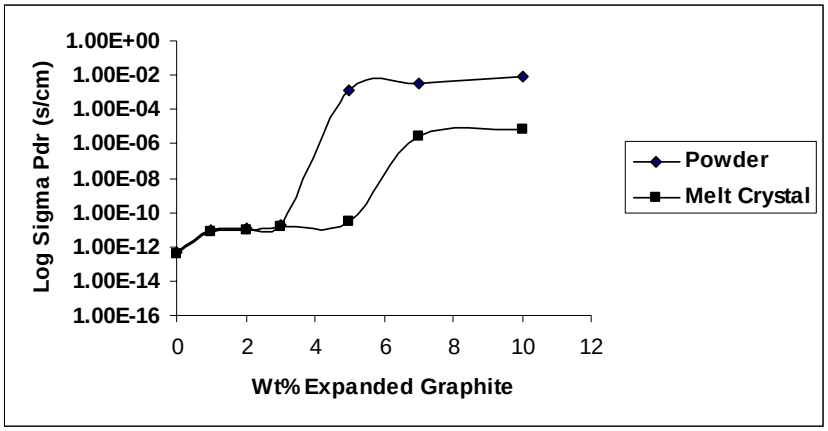

Figure 4.5.1. Effect of preparation routes on the through plane conductivity of melt crystallized PPS-ExGr composites

PPS-ExGr composites were melt crystallized at 300^{o}C and then immediately transferred to water. The sheet formed is used for measurement. The above Figure 4.5.1 clearly shows that the percolation threshold of melt crystallized samples is higher than the powder mixed ones. Through plane conductivity is considered for the analysis. The percolation threshold in melt crystallized PPS-ExGr composites is 5 wt% and for powder mixed samples it is 3 wt%. The difference is due to the increase in interparticulate distance in melt crystallized samples. This phenomenon could be attributed to decrease in the polymer viscosity at 300^{o}C. Further the saturation in through plane conductivity occurs at higher loading in melt crystallized samples than the powder mixed ones. The value of conductivity in the saturated region of melt crystallized sample is lesser than that of powder mixed one because of polymer wrapping.

4.5.2. XRD Analysis of Melt Crystallized PPS-graphite Sample

The XRD pattern of melt crystallized PPS-7 wt% graphite does not show any new structural features when compared with powder mixed one. The PPS reflections are reduced in intensity due to quenching as enough time is not given for the crystals to grow in this process. The intensity of graphite 002 peak decreases due to polymer wrapping. This is shown in Figure 4.5.3.

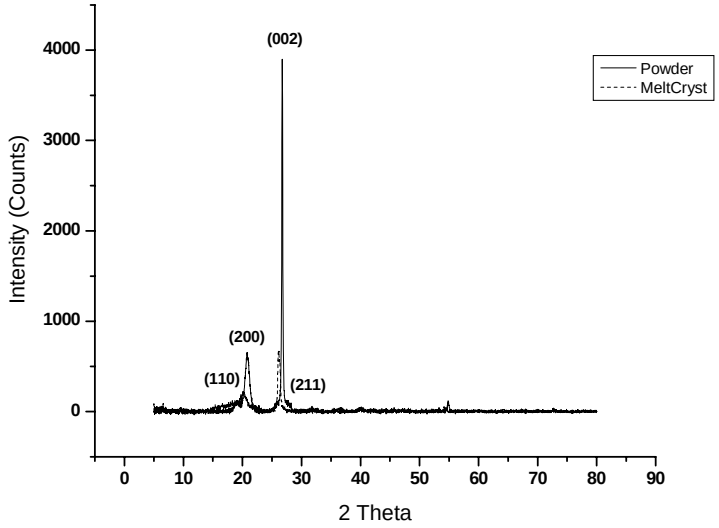

Figure 4.5.3. XRD of PPS-7 wt% graphite melt crystallized sample

4.5.3. SEM Analysis of PPS-ExGr Melt Crystallized Sample

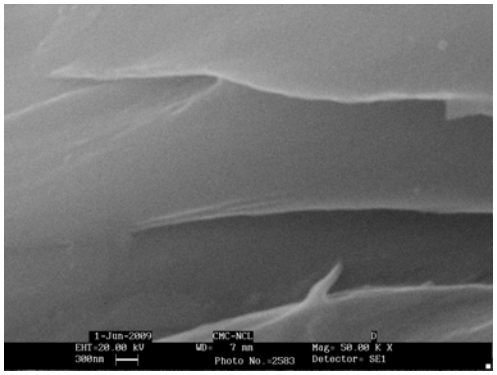

Figure 4.5.3. SEM picture of cross section of PPS-3 wt% ExGr melt crystallized sample

The SEM picture shown in Figure 4.5.3 clearly shows that the individual nanosheets are separated by polymer penetration due to decrease in the viscosity at high temperature. Due to the increase in interparticle distance, the conductivity becomes less in melt crystallized samples.

4.5.4. Melt Crystallized PPS-CNF Composites

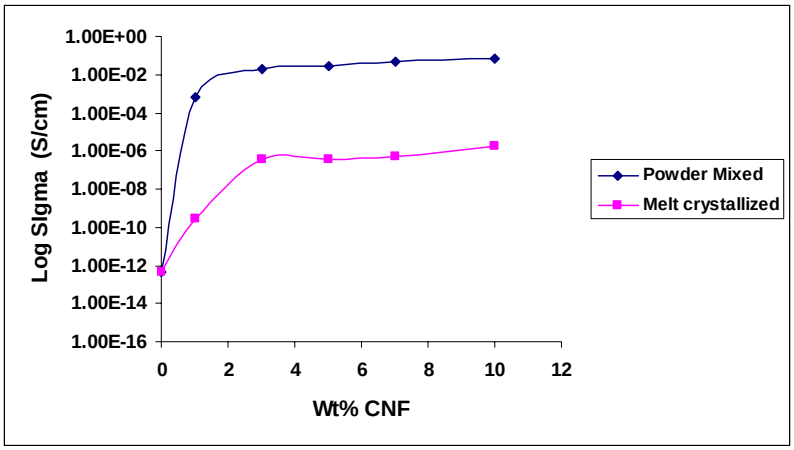

Figure 4.5.4. Effect of preparation route on the through plane conductivity of PPS-CNF composites

The above Figure 4.5.4 shows that the percolation threshold of PPS-CNF composites prepared by melt crystallization route is higher than that of powder mixed samples. In the former case, the percolation threshold is around 2 wt% CNF and in the later case, it is at 0.2 wt% CNF. The decrease in through plane conductivity of melt crystallized samples is due to increase in the interparticulate distance since the connectivity between the particles is diminished.

4.5.5. SEM Analysis of Melt Crystallized PPS-CNF Composites

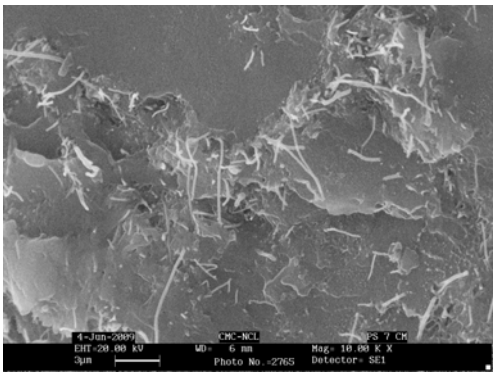

(a)

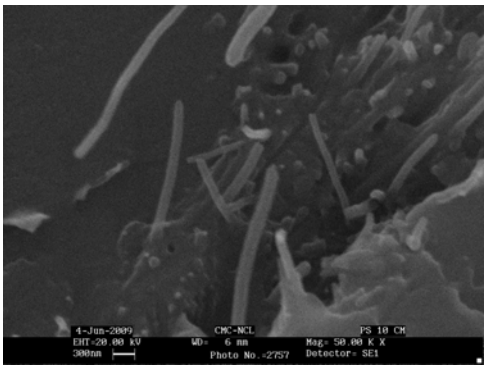

(b)

Figure 4.5.6. SEM pictures of melt crystallized a) PPS-7 wt% CNF b) PPS-10 wt% CNF composites

The above Figures 4.5.5.a and b strongly support that CNFs are buried as well as the interdistance between them is increased. There exists variation in the distribution of

CNFs which is the reason for obtaining higher percolation threshold in melt crystallized samples compared to powder mixed ones.

4.5.6. Thermal Conductivity of PPS-graphite Composites

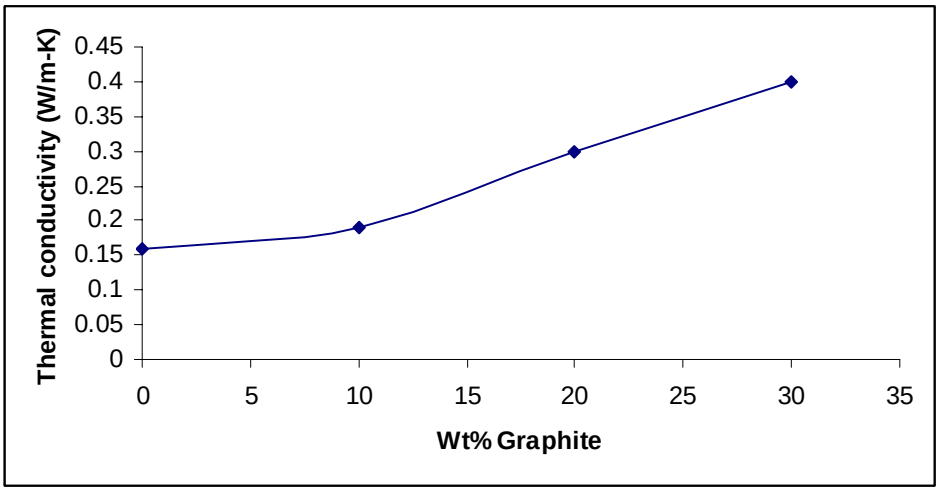

4.5.6. Thermal conductivity of PPS-graphite composites

Normally fiber spinning spool will be made of polymer. Due to the heat generated in the process, the spool gets damaged. In order to make it intact, the spool should be made of thermally conducting material so that it can dissipate heat. As part of application, the thermal conductivity of PPS-graphite system has been measured. PPS has low thermal conductivity of 0.15 W/m-K. Addition of 30 wt% graphite increases the thermal conductivity to 0.4 W/m-K. This has been shown in Figure 4.5.6. Therefore such a system can be used to replace the polymer based spool.

4.5.7. PPS Synthesis

The synthesis of PPS has been described in Chapter-2. The synthesized PPS has been compared with commercial grade Ryton PPS.

4.5.7.1. XRD Analysis

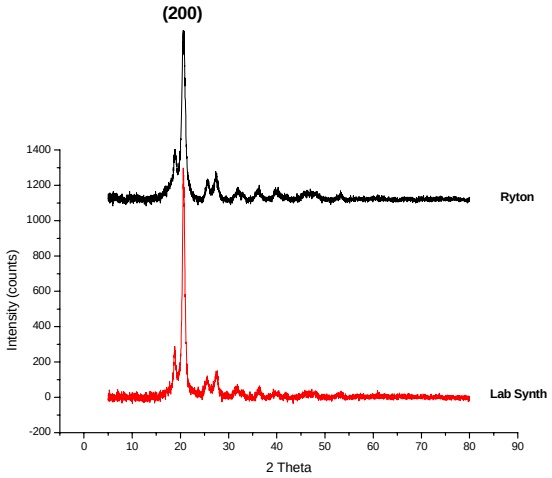

Figure 4.5.7. XRD pattern comparison between synthesized and commercial PPS

The XRD pattern of lab synthesized PPS has been compared with Ryton PPS as shown in Figure 4.5.7 and they match well.

4.5.7.2. DSC Analysis

The DSC of synthesized PPS is shown in Figure 4.5.8. The melting and crystallization temperature matches well with that of commercial one.

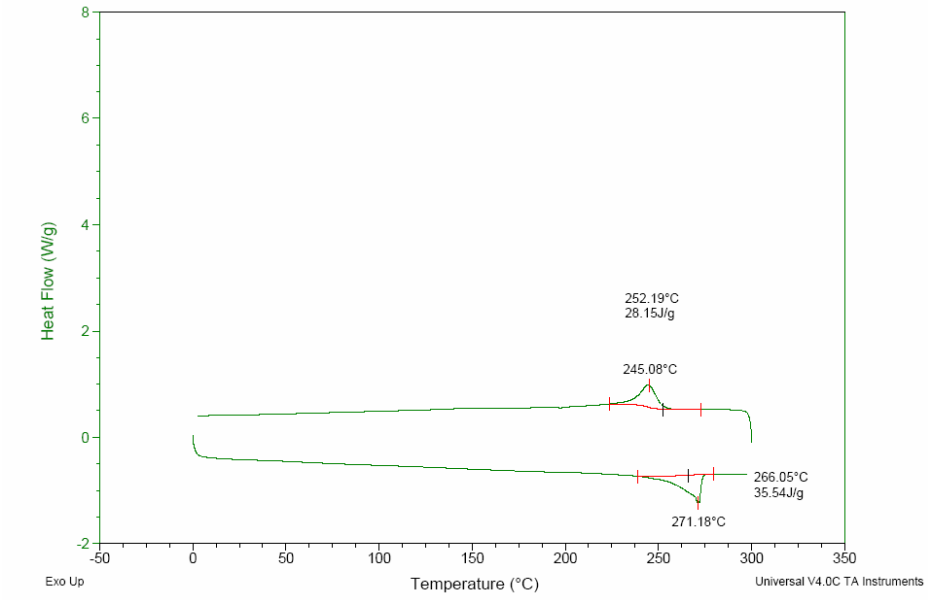

Figure 4.5.8. DSC of synthesized PPS

4.5.7.3. IR Analysis

The IR of synthesized PPS and Ryton PPS are compared in order to evaluate the synthesized PPS. The region between 400 cm^{-1} and 1600 cm^{-1} of synthesized PPS shows various peaks which exactly match with that of standard Ryton PPS. As IR is used here to characterize synthesized PPS, the wave numbers are not assigned. IR of synthesized and commercial PPS is compared in Figure 4.5.9.

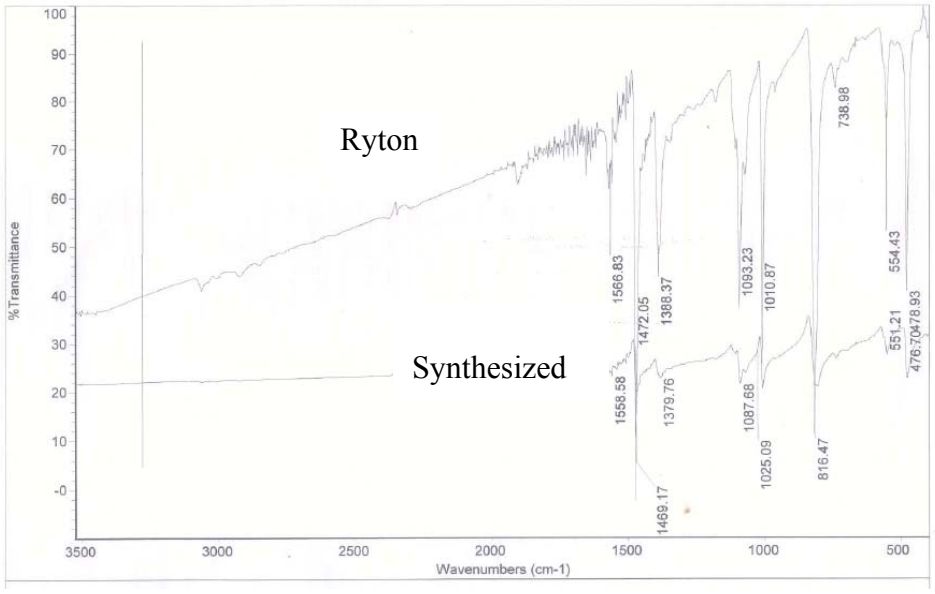

Figure 4.5.9. IR of Ryton and synthesized PPS

4.5.8. In-situ Polymerization Route for Preparing PPS-ExGr Composites

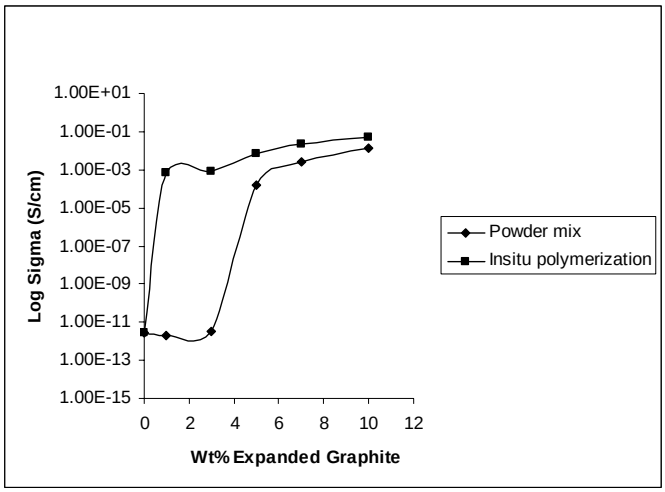

Figure 4.5.10. Through plane conductivity of synthesized PPS-ExGr composites

It is clear from the above Figure 4.5.10 that in-situ polymerization route yields percolation threshold less than 1 wt% where as for the powder mixed composites it is at 3 wt%. In-situ polymerization route results in better dispersion as well as separation of expanded graphite nanosheets. As the aspect ratios of nanosheets are very high, low percolation threshold results.

4.6. Conclusions

In this chapter PPS-graphite based hybrid composites with varying aspect ratio of second conducting fillers such as CB, ExGr and CNF were prepared and studied the effect of aspect ratio on the electrical percolation. In order to understand hybrid composites effect on electrical conductivity, a systematic study was carried out on the electrical properties of binary composites. Furthermore, the study of electrical conductivity variation in binary composites became indispensable to determine the percolation threshold.

The percolation threshold in PPS-graphite composites was found to be at 7 wt%. Below this value, the composites behaved as insulators. Through plane conductivities of PPS-graphite composites were found to be lesser than that of in-plane conductivity due to the alignment of graphite particles along the surface of the pellet. Sintering of PPS-graphite composites above the glass transition temperature of the polymer led to re-orientation of graphite 002 planes along through thickness direction. This resulted in an increase in the through plane conductivity when compared to that of unsintered composites. XRD analysis proved crystallite size reduction and re-orientation of graphite planes after sintering. DSC analysis showed that for PPS-7 wt% graphite the crystallization temperature was increased by 5^{o}C. This result demonstrated the nucleating ability of graphite particles. The percolation exponent signified three dimensional network formations. For PPS-7 wt% graphite-CB hybrid composites percolation threshold was found to be at 1.5 wt% CB. From the dc conductivity study on PPS-CB binary composites, the percolation threshold was identified at 3-5 wt% CB. For less than 3 wt% CB in PPS-7 wt% graphite-x wt% CB, CB particles predominantly occupied intergraphite space as without CB, the composite PPS-7 wt% graphite behaved as an insulator similar was the case without graphite in those composites. AC measurements also proved this result. The increase in the effective

dielectric constant at 0.01 Hz reflected the occupancy of CB in the interspace of graphite particles. The interjunction capacitance with the addition of CB was found to increase from 44 pF for 0 wt% CB in PPS-7 wt% graphite to 75 pF for 3 wt% CB addition in the same. The charge transport for 3.2 wt% CB in PPS-7 wt% graphite was found to be by hopping mechanism below which it was coupled with capacitance effects. Melt crystallization of PPS-graphite binary composites showed higher percolation threshold than the powder mixed samples due to decrease in the polymer viscosity at 300^{o}C resulting in an increase in interparticulate distance of filler particles. Thermal conductivity increased with the addition of graphite and no sharp variation was observed.

PPS-ExGr binary composites were prepared by powder mixing, melt crystallization and in-situ polymerization routes. In powder mixing route, the percolation threshold was identified at 3 wt% ExGr. In-plane conductivity was found to be higher than that of through plane conductivity due to the alignment of nanosheets along the surface of the pellet. In powder mixed samples, sintering at 240^{o}C for one hour led to crystallite size as well as intensity reduction of 002 planes of graphite. Sonication led to the formation of graphite nanosheets as otherwise expanded graphite had more pores. SEM and TEM analysis also proved this result. The dc conductivity study on PPS-7 wt% graphite-x wt% ExGr hybrid composites exhibited a percolation threshold of 0.25 wt% ExGr. The increase in the conductivity was due to the occupation of high aspect ratio nanosheets in the interspace of graphite particles. Effective dielectric constant increased to more than four orders at 0.01 Hz for 0.75 wt% ExGr in PPS-7 wt% graphite when compared to 0 wt% ExGr addition in the same. The interjunction capacitance was evaluated from impedance measurements and found to increase with the addition of ExGr in PPS-7 wt% graphite. DSC analysis on PPS-3 wt% ExGr composite showed an increase of 3^{o}C in the crystallization temperature supporting the nucleating ability of ExGr particles. Percolation exponent of PPS-ExGr composites demonstrated the formation of three dimensional network among the filler particles. Melt crystallized PPS-ExGr composites at 300^{o}C showed increase in the percolation threshold. This finding was attributed to increase in the interparticulate distance due to decrease in the polymer viscosity at that temperature. In-situ polymerized PPS-

ExGr composites exhibited very low percolation threshold i.e., less than 1 wt% due to better separation and dispersion of nanosheets of graphite when compared to powder mixed samples of the same.

PPS-CNF composites were prepared by powder mixing and melt crystallization routes. Powder mixed PPS-CNF composites exhibited a percolation threshold at 0.2 wt% CNF. Sintering at 240^{o}C led to increase in the through plane conductivity of the composites and the in-plane conductivity was found to decrease due to polymer presence at the surface. DSC analysis showed increase in the crystallization temperature for PPS-CNF composites signifying the nucleating ability of CNFs. For PPS-7 wt% graphite-CNF composites, percolation threshold was found at 0.05 wt% CNF. With the addition of CNF in PPS-7 wt% graphite, the interjunction capacitance increased proving the parallel model and also the occupation of CNFs in the interspace of graphite particles. Increase in the effective dielectric constant at low frequency (0.01 Hz) with increase in the loading of CNF also proved the occupation of CNFs in the graphite interspace. Decrease in the aggregate resistance was understood qualitatively from the work function of individual components. Melt crystallized samples exhibited higher percolation threshold when compared to powder mixed one ie., 7 wt% CNF for binary composites due to decrease in the viscosity of the polymer at 300^{o}C which would have resulted in more separation of CNFs. Finally the percolation thresholds in the hybrid composites were found to have inverse relation with aspect ratio of second conducting fillers.

4.7. References

1. Edmonds JT Jr., Hill HW Jr. (Phillips Petroleum Co.). U.S. Patent No. 3,354,129;1967.
2. Rajan CR, Nadkarni VM, Ponrathnam S. J Polym Sci: Part A: Polym Chem 1988;26:2581.
3. Tabor BJ, Magre EP, Boon. Eur Polym J 1971;*7*:1127.
4. Gopakumar TG, Ponrathnam S, Rajan CR, Fradet A. Polymer 1997;38: 2209.
5. Hisamatsu T, Nakano S, Adachi T, Ishikawa M, Iwakura M. Polymer 2000;41:4803.
6. Zou H, Xu W, Zhang Q, Fu Q. J Appl Polym Sci 2006;99:1724.
7. Chen ZB, Liu XJ, Lu RG, Li TS. J. Appl. Polym. Sci., 102, 523 (2006).
8. Zhao YF, Xiao M, Wang SJ, Ge XC, Meng YZ, Compos Sci Technol 2007;67: 2528.
9. Brady DG. J Appl Polym Sci 1976;*20*:2541.
10. Jog JP, Nadkarni VM. J Appl Polym Sci 1985;*30*:997.
11. Radhakrishnan S, Nadkarni VM. Polym Eng Sci 1984; 24:1383.
12. Gabellini G, Bretas RES. J Appl Polym Sci 1996;61:1803.
13. Deporter J, Baird DG. Polymer Composites 1993;14: 201.
14. Zhao YF, Xiao M, Wang SJ, Ge XC, Meng YZ. Compos Sci Technol 2007;67:2528.
15. Huang J, Baird DG, Mcgrath JE. J Power Sources 2005;150:110.
16. Mighri F, Huneault MA, Champagne MF. Polym Engg Sci 2004;44(9):1755.
17. Shimada S, Hiroi T, Ida T, Mizuno M, Endo K, Kurmaev EZ, Moewes A. J Polym Sci:Part B: Polym Phys 2007;45:162.
18. Radhakrishnan S. Die Angewandte Makromol Chem 1986;141:49.

Chapter-5

Polypropylene (PP) Based Composites

5.1. Introduction

Isotactic polypropylene (iPP) is an important stereo regular polymer which is semi crystalline in nature. It exhibits three polymorphs under different conditions. The most common phase, α form has monoclinic structure. Less common phases are β and γ forms and they exist in hexagonal and triclinic structures respectively. The XRD profiles are shown in Figure 5.1.1.

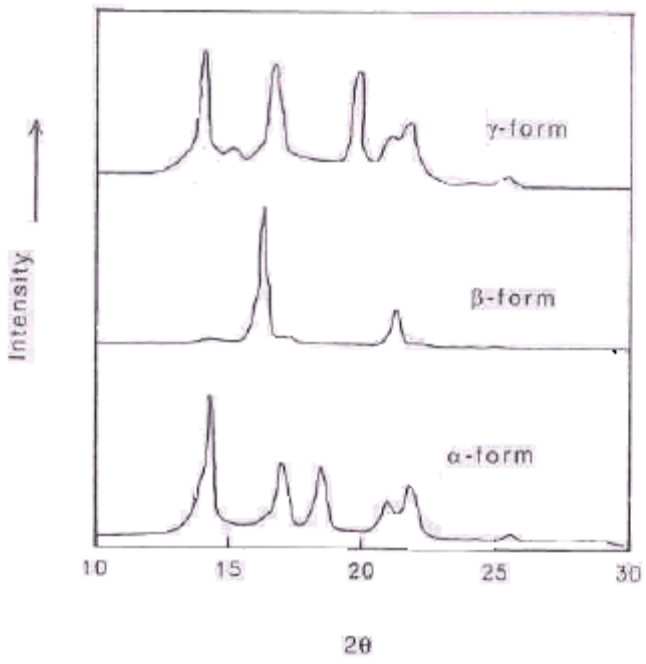

Figure 5.1.1. XRD patterns of polymorphs of iPP

The lattice parameters of different polymorphs of iPP are given in Table 1. β phase can be induced by adding nucleating agents and also tuning the processing conditions as this phase is more uncommon. It is identified from the XRD pattern shown in Figure 5.1.1 in which a peak at 2θ corresponding to16^{o} signifies the presence of β phase. High content of β phase crystals can be produced by shear induced crystallization[1].

Table 1

Lattice parameters of iPP polymorphs

Polymorphs of iPP	Lattice parameters					
	a (A^o)	b (A^o)	c (A^o)	α	β	γ
α form - Monoclinic	6.65	20.96	6.50	90	99.3	90
β form - Hexagonal	19.08	19.08	6.49	90	90.0	120
γ form - Orthorhombic	8.94	9.93	42.41	90	90.0	90

Li *et al*.[2] have reported that more than 90% β phase can be induced by adding pimelic acid based nucleating agents under compression molding. Garbarczyk[3-4] has reported series of crystalline substances like 2-mercapton-benzimidazole, triphenodithiazine, phenothiazin, anthracene and phenanthrene as nucleating agents. Various mechanisms of formation of β phase have been outlined by Li *et al*.[5].

The γ form[6-7] of iPP was first noticed in 1960 and could be generated by different methods. It is mainly produced by crystallization at elevated pressure[8] or with the addition of ethylene and butene[9] with iPP. The crystallization characteristic of α-iPP has been studied in detail under isothermal and non-isothermal conditions. The morphology and crystallization of iPP have been reviewed by Varga[10] and Clark[11].

Electrically conducting composites with graphite in grafted PP has been reported by Shen *et al*.[12] where the composites were prepared by solution mixing and the percolation threshold reported was 0.67 vol%. Kalaitzidou *et al*.[13] have studied the flexural and electrical properties of exfoliated graphite-polypropylene nanocomposites prepared by melt mixing technique and the electrical percolation threshold of these nanocomposites obtained was 0.3 vol %. Zois *et al*.[14] studied ac conductivity and dielectric constant of polypropylene/carbon black (PP/CB) composite systems, whose percolation threshold was calculated to be 6.2 wt %. Gopakumar *et al*.[15] have studied PP-natural graphite, PP-g-MA-graphite composites by melt blending method. They reported the formation of β phase. Katbab *et al*.[16] have studied the electrical properties of PP-EPDM dynamically cross linked thermoplastic vulcazinate-expanded graphite composites prepared by melt mixing route. They have also discussed the effect of microstructure of graphite on the

electrical conductivity and melt rheology. Electromagnetic shielding efficiency of graphite filled polypropylene was reported by Sawai *et al*.[17]. Towards the development of bipolar plates for fuel cell applications, highly loaded PP-graphite conducting binary and hybrid composites with CNF and CB have been reported[18]. In such hybrid composites, the loading of second conducting filler was very high. The percolation threshold of PP-synthetic graphite was reported to be 25 wt%[19] after injection molding. In many injection molded PP-graphite based hybrid composites, electrical conductivity was studied with high loading of the second conducting component grater than 15 wt%[20]. Naficy *et al*.[21] have reported electrical and mechanical properties of PP/PA6 blends with super conductive carbon black. They also investigated the effect of extensional flow on microstructure, mechanical and electrical properties of the blend. Cerezo *et al*.[22] have investigated morphology, thermal stability and mechanical behavior of PP-g-MA layered expanded graphite oxide composites. They had shown that the degradation temperature of the polymer was increased when expanded graphite oxide was mixed with the polymer. Further incorporation of expanded graphite oxide in PP-g-MA increased the storage modulus of the composite. Kalaitzidou *et al*.[23] have investigated thermal, viscoelastic and barrier properties of PP-exfoliated graphite nanoplatelets as a function of aspect ratio of the platelets. The composites were prepared by melt mixing and followed by injection molding. They showed by properly orienting exfoliated graphite nanoplatelets, coefficient of thermal expansion of the matrix can be reduced in two directions. Further the thermal conductivity of the composites was found to increase with the filler addition.

Though wealth of informations is available on the electrical conductivity variation in PP based binary composites, there seems to be void as far as hybrid composites are concerned. Few reports on hybrid composites show that very high loading of both fillers is employed for product development. There are no reports found in the literature on the dc and ac behavior of hybrid composites nearer to percolation threshold. With the aim to address ac as well as dc behavior nearer to the percolation threshold, studies on PP based binary and hybrid composites have been carried out as explained further in the present chapter.

A. Powder Mixed Samples

5.2. PP-graphite and PP-graphite-CB Composites

5.2.1. DC Conductivity Study of Powder Mixed PP-graphite Composites

In order to understand the effect of addition of second conducting filler on the electrical conductivity, PP-graphite binary composites have been prepared and studied first.

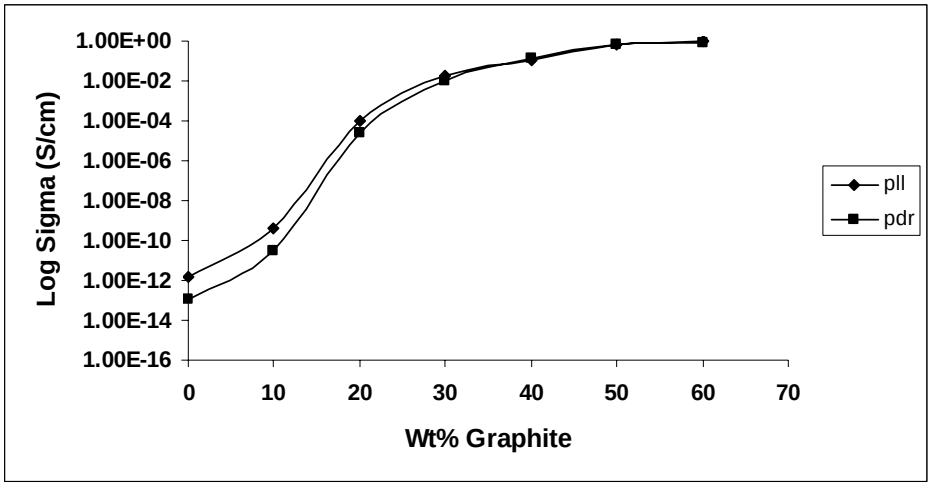

Figure 5.2.1. DC conductivity of PP-graphite composites

The above Figure 5.2.1 shows the variation of dc conductivity of PP-graphite composites. The percolation threshold can be identified at 10 wt% graphite as insulator to semiconductor transition starts there. The variation in in-plane (pll) and through plane (pdr) conductivity is appreciable below the percolation threshold. At higher loading not significant difference between the two conductivities is observed implying anisotropy is nearly equal to one. This value of anisotropy reflects the case of well dispersed state of filler particles in the polymer matrix. After 30 wt% graphite, the conductivities become saturated due to completion in the network formation between fillers. Below percolation threshold, the network would not have resulted and hence the composites behave as insulators.

5.2.2. Effect of Heat Treatment on the Electrical Conductivity

Effect of heat treatment on the electrical conductivity of powder mixed PP-graphite composites has been studied. The composites were sintered at 140^{o}C above the T_g of PP for one hour. Through plane conductivity increases to about one order than in-

plane conductivity which is noticeable after 20 wt% graphite loading in PP as shown in Figure 5.2.2.

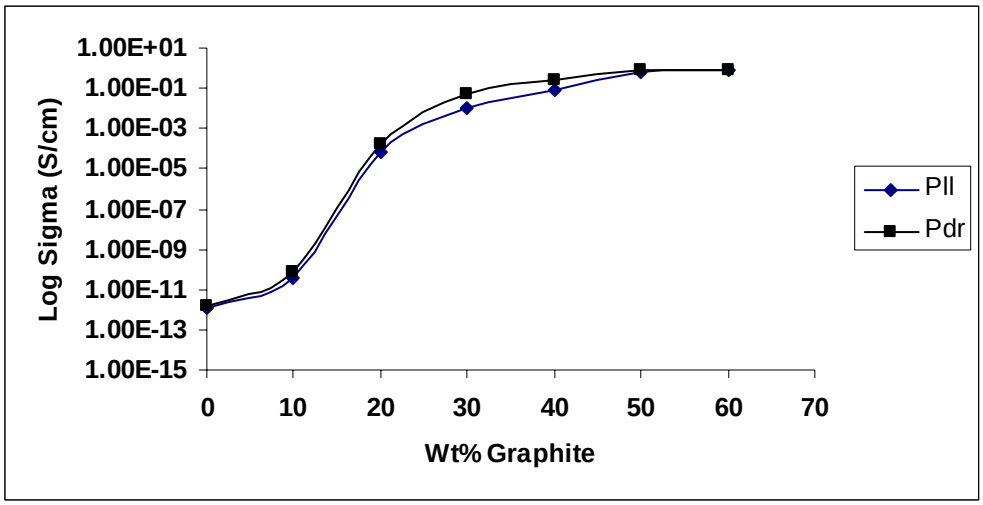

Figure 5.2.2. DC conductivity of PP-graphite composites after sintering

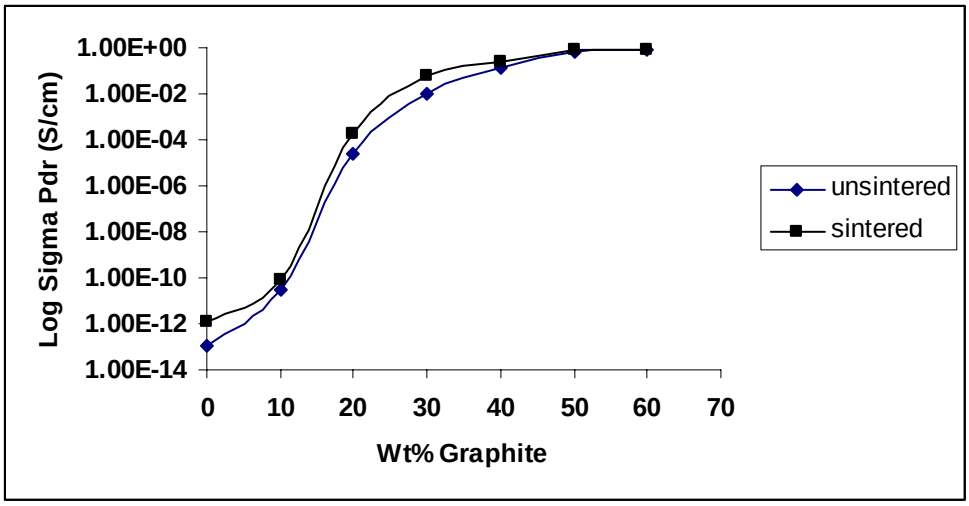

Figure 5.2.3. Through plane conductivity of PP-graphite composites before and after sintering

The through plane conductivity after sintering increases by more than an order at low loading of graphite. Similar difference in the conductivity exists at 30 wt% graphite loading. After that, both values coincide due to complete network formation. XRD analysis is used to explain the observed effect and discussed below.

5.2.3. XRD Analysis of PP-graphite Binary Composites

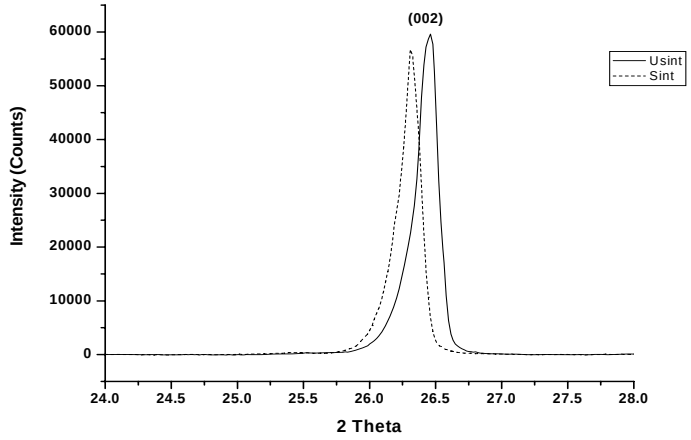

(a)

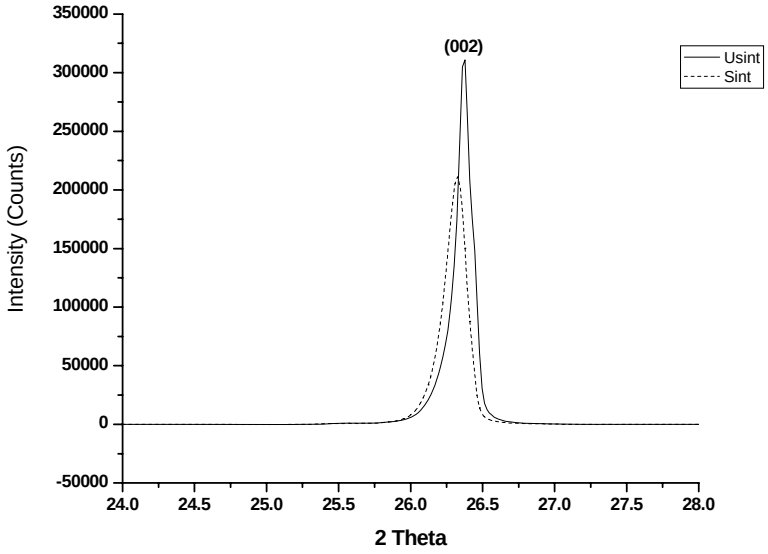

(b)

Figure 5.2.4. XRD patterns of graphite part of a) PP-10 wt% graphite b) PP-40 wt% graphite

It is clear from Figure 5.2.4.a and b that after sintering, reduction in the intensity of 002 reflection of graphite occurs. The increase in FWHM after sintering can be observed. The shift in 2 Theta value towards lower value is very less. Since sintering is done well above the T_g of the polymer, chain movement causes the graphite planes

to re-orient along through thickness direction. This results in decrease in the intensity of 002 reflections. It should be noted that the crystallite size reduction is not much when compared PES based systems after sintering. As PP does not have any polar group, the polymer penetration in to the graphite plane is not significant. Table 2 describes various parameters extracted from the XRD analysis of PP-graphite composites.

Table 2

XRD analysis of PP-graphite composites

Sample	2 Theta		Intensity		Crystallite Size t' (nm)	
	BS	AS	BS	AS	BS	AS
PP-10wt% Graphite	26.462	26.309	59162	56734	67.6	64.2
PP-20wt% Graphite	26.462	26.360	111039	85987	67.6	64.2
PP-30wt% Graphite	26.377	26.360	168405	147195	67.6	64.2
PP-40wt% Graphite	26.377	26.326	310864	211194	67.59	64.2

BS- before sintering, AS- after sintering

The above Table 2 shows that the crystallite size of graphite is reduced by ~ 3 nm for all samples. The intensity reduction exists after sintering supporting re-orientation of graphite 002 planes. Since sintering causes the graphite planes on the surface to re-orient towards through thickness direction resulting in more polymer penetration on the surface under investigation. This is reflected in the XRD of PP part as shown below in Figure 5.2.5. More polymer on the surface of the composites results in decrease in the in-plane conductivity after sintering.

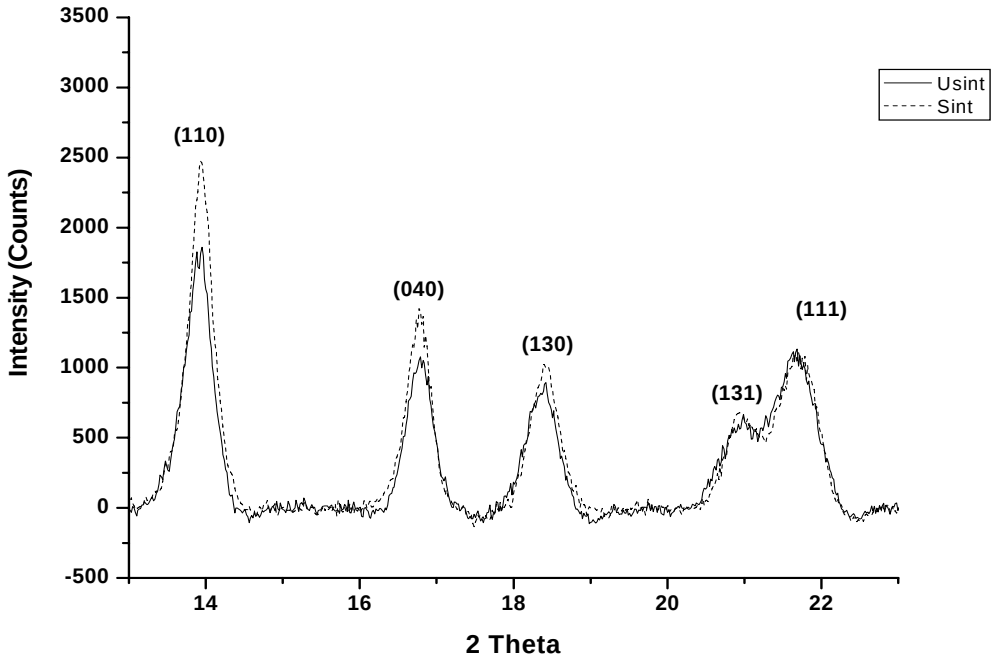

Figure 5.2.5. XRD pattern of PP part of PP-40 wt% graphite

The intensity of major peaks of PP i.e., (110) and (040) increases after sintering indicating the presence of more polymer on the surface of the pellet due to polymer chain movement.

5.2.4. Electrical Conductivity Variation in PP-graphite-CB Hybrid Composites

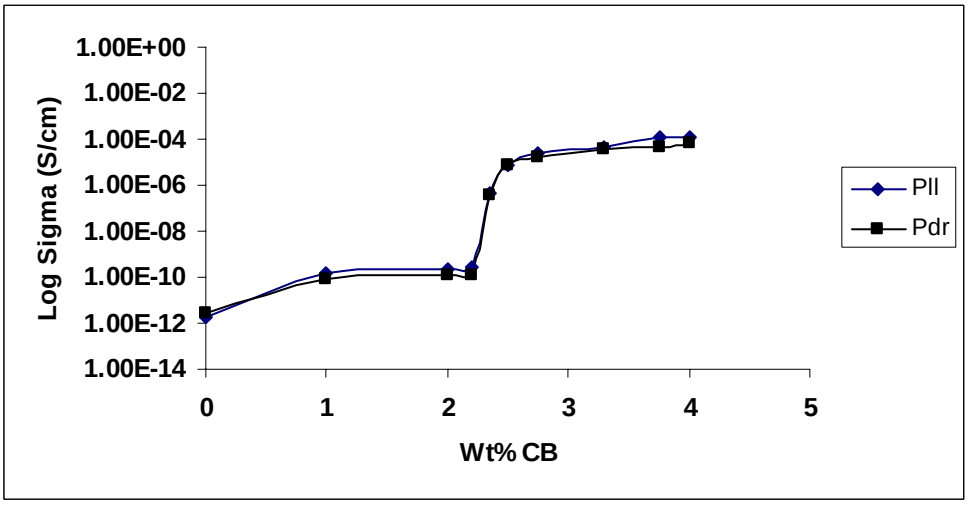

Figure 5.2.6. DC conductivity of PP-7 wt% graphite-CB hybrid composites

In order to understand the effect of addition of CB nearer to the percolation threshold of PP-graphite composites, a particular composition namely PP-7 wt% graphite has been chosen. Up to 2.2 wt% CB addition in PP, the hybrid composites behave as insulators as there may not be network formation between fillers. Above 2.2 wt% CB in PP-7 wt% graphite, the through plane (Pdr) and in-plane (Pll) conductivities increase by more than five orders reflecting the formation of network between filler particles. Both conductivities remain more or less the same within the experimental error suggesting less anisotropy. To achieve the conductivity of what is obtained from PP-7 wt% graphite-2.35 wt% CB, 15-20 wt% of graphite without CB will be required. Thus the overall filler amount can be reduced in hybrid composites. Further the density of graphite is much higher than CB so that reducing graphite amount will reduce the product weight made out of these hybrid composites. Thus hybrid composites are very effective in reducing the percolation threshold as well as the total amount of filler to achieve a particular value of electrical conductivity. In order to understand the effect of carbon black on the through plane conductivity of hybrid composites, dc electrical conductivity variation of PP-CB binary composites with respect to CB loading has been studied and shown in Figure 5.2.7.

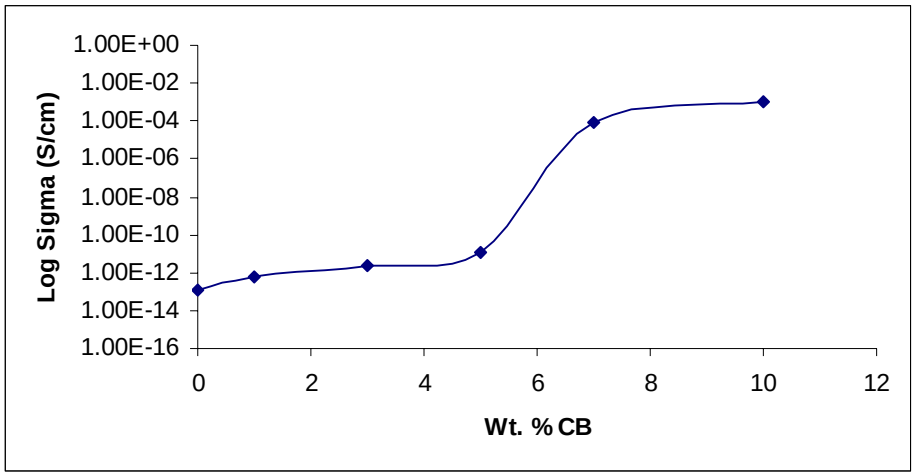

Figure 5.2.7. DC conductivity variation of PP-CB powder mixed composites

The dc conductivity variation of PP-CB composites shows that the percolation threshold lies at 5 wt%. Thus up to 4 wt% CB addition in PP-7 wt% graphite, the conductivity enhancement can be due to the occupation of CB in intergraphite space reducing the barrier for the charge transport. Without graphite, PP-4 wt% CB behaves

as an insulator. This point will be proved in the effective dielectric constant measurement section of PP based hybrid composites.

5.2.5. Frequency Dependent Conductance of PP-7 wt% graphite-CB Hybrid Composites

Figure 5.2.8.a shows the variation of conductance of PP-7 wt% graphite-CB hybrid composites with varying concentration of CB. It is clear that PP-7 wt% graphite-2.2 wt% CB remains as insulator as this composition shows the variation of conductance typical to that of an insulator. For insulators, the conductance increases with the entire frequency range.

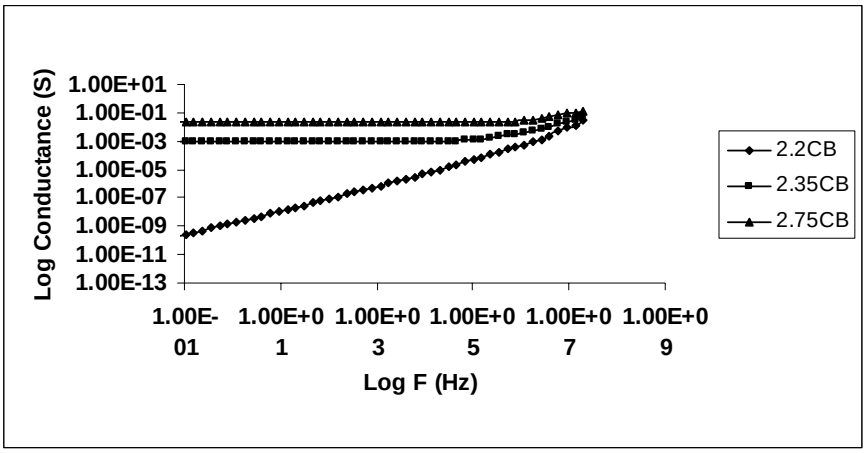

(a)

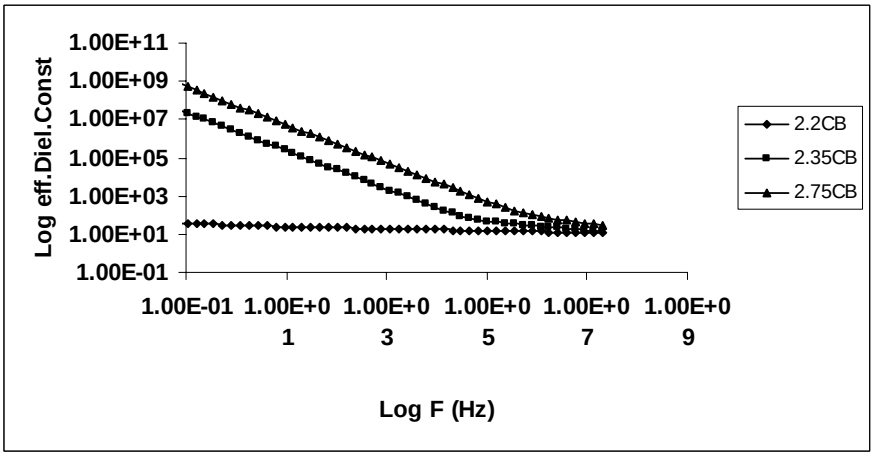

(b)

Figure 5.2.8. a) AC conductance b) Effective dielectric constant vs frequency of PP-7 wt% graphite-CB hybrid composites

With further addition of CB, plateau region appears representing dc conductance of the composite as the barrier for the charge transport is decreased. The frequency at which the conductance starts increasing is shifted to higher value with higher loading of CB implying the enhanced conductance of samples. The increase in the conductance with the addition of 2.35 wt% CB in PP-7 wt% graphite is attributed to the occupation of CB in the intergraphite space. Without graphite, the range of CB loadings employed will result in insulating composites. To verify this particular aspect, effective dielectric constant of hybrid composites with respect to frequency and CB content has been measured and shown in Figure 5.2.8.b. Considering conducting particle-polymer-conducting particle assembly as a parallel plate capacitor, occupation of CB in between graphite particles will be equivalent to decreasing the distance between parallel plates. Hence the effective dielectric constant and interjunction capacitance should increase with CB addition. Increase of effective dielectric constant by six orders for 2.35 wt% CB in PP-7 wt% graphite when compared to 2.2 wt% CB in the same at 0.01 Hz proves the point. Thus CB predominantly occupies intergraphite space.

5.2.6. Charge Transport in PP-7 wt% graphite-CB Hybrid Composites

Table 3

Exponent 'n' from ac conduction plot

Sample	Exponent 'n'
1. PP-7 wt% graphite-2.2. wt% CB	1.34
2. PP-7 wt% graphite-2.35 wt% CB	0.87
3. PP-7 wt% graphite-2.75 wt% CB	0.56

It is clear from Table 3 that the exponent 'n' obtained from the slope of ac conductance vs frequency is less than one for loading of CB greater than or equal to 2.35 wt% in PP-7 wt% graphite signifying hopping conduction. From the following equation 1, the exponent 'n' is obtained.

$$\Sigma_{tot} = \sigma_0 + A\,\omega^n \qquad (1)$$

Σ_{tot} - total conductivity, σ_0 - DC conductivity and n – exponent (<1 for hopping conduction). Below 2.35 wt% CB in PP-7 wt% graphite, the charge transport is coupled with capacitive effects as the exponent becomes greater than one.

5.2.7. Impedance Analysis of PP-7 wt% graphite-CB Hybrid Composites

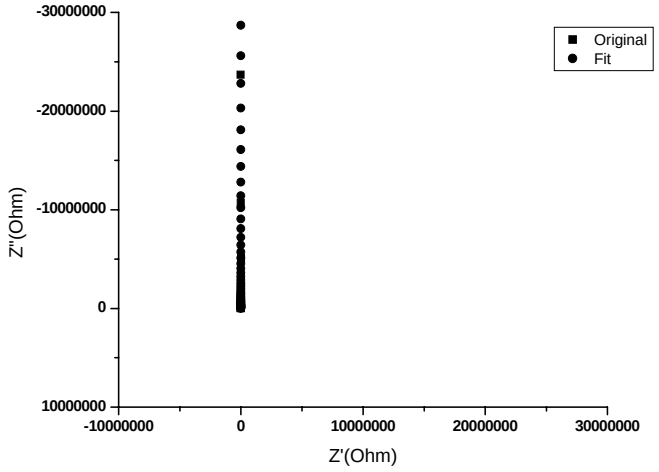

(a)

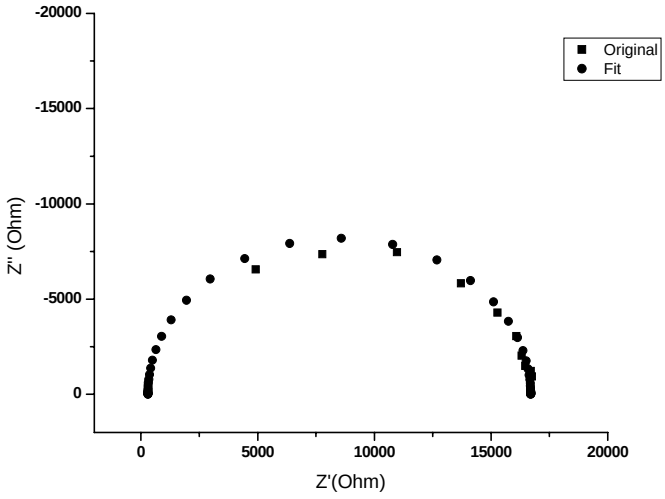

(b)

Figure 5.2.9. Impedance plots of a) PP-7 wt% graphite b) PP-7 wt% graphite-2.75 wt% CB

The insulating PP-7 wt% graphite and conducting PP-7 wt% graphite-2.75 wt% CB impedance plots are shown in Figure 5.2.9.a and b respectively. With the addition of more CB, semicircular response in Argand plane can be clearly seen, suggesting that the material can be replaced by parallel resistor-capacitor with a series resistor equivalent circuit as described in Chapter-3. Furthermore, the diameter of the semicircle represents dc resistance of the sample which decreases with more CB loading in the hybrid composites. This will be the case for conducting samples. The interjunction capacitance can be calculated when real and imaginary parts of impedance become equal at a particular frequency ω_{max}. The interjunction capacitance C is calculated by the following equation

$$C = 1/ (\omega_{max} R_p) \quad (2)$$

Where R_p is the bulk resistance.

Table 4 describes various model parameters. It can be seen that the interjunction capacitance indeed increases with the addition of CB in PP-7 wt% graphite. It increases to 52.2 pF for 2.75 wt% CB addition in PP-7 wt% graphite from 31 pF for 0 wt% CB in the same. Thus the model assumed earlier i.e., CB particles predominantly occupy intergraphite space is true. With the addition of 2.75 wt% CB, the bulk resistance drops down signifying that the composite has become more conducting.

Table 4

Impedance parameters extracted from the model for PP-graphite-CB system

Sample	R_a(Ohm)	R_p(Ohm)	C (pF)
1. PP-7 wt% graphite	600	$6.8x10^{12}$	31.0
2. PP-7 wt% graphite-2.75 wt% CB	300	16400	52.2

It is worth to note that the aggregate resistance also decreases with increase in the CB loading. This phenomenon can be explained in terms of work function of individual components. The work function of PP is 5.7 ev[24] and that of graphite is 4.6 eV. The work function of CB is 4.8 eV as mentioned in Chapter-3 for PES-graphite-CB system. Without CB, for the charge transport from polymer to graphite, a barrier of 1.1 eV needs to be crossed by the charges as the barrier is essentially the difference in

work function of materials in contact. When CB particles lie in between polymer and graphite, a barrier of 0.9 eV need to be crossed by the charges. Thus if more CB particles are found in between polymer and graphite, more charges will be transported to graphite via CB and hence the aggregate resistance decreases. This configuration can be considered as being connected in series through out the sample volume and hence charge transport occurs from one end of the electrode to the other. It should be remembered that a potential is applied for measuring resistance which drives the charges in one direction. The work function diagram is schematically represented in Figure 5.2.10.

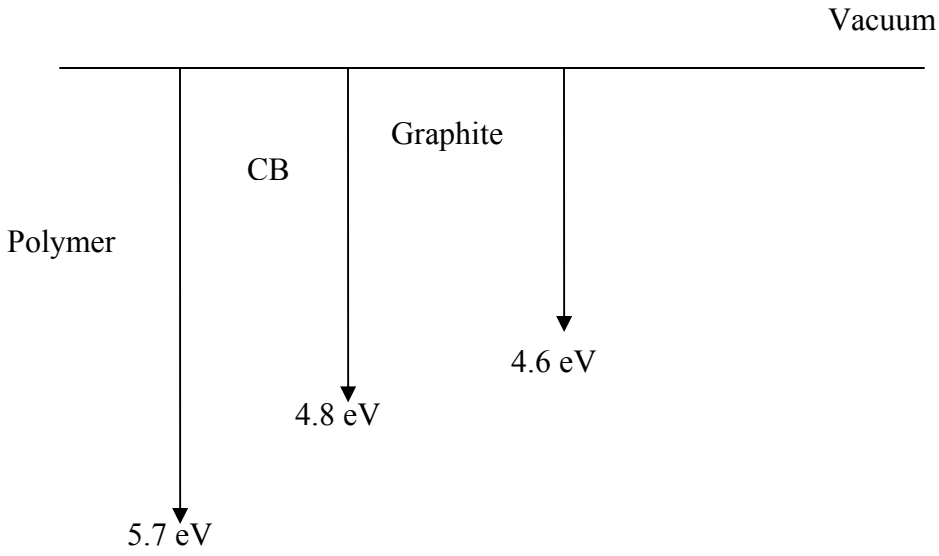

Figure 5.2.10. Work function diagram of components in hybrid composites

5.2.8. DSC Analysis of PP-graphite Composites

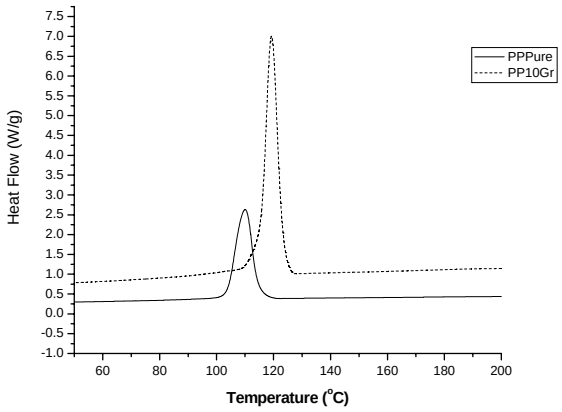

Figure 5.2.11. DSC cooling curve of PP and PP-10 wt% graphite

The first cycle cooling curve of pure PP and PP-10 wt% graphite is shown in Figure 5.2.11. The crystallization temperature and change in enthalpy of crystallization are mentioned in Table 5 as given below.

Table 5

DSC analysis of PP, PP-graphite composite

Sample	T_c (^oC)	ΔH_c (J/g)
PP Pure	110.03	114.53
PP-10wt% graphite	119.25	81.78

The increase in the crystallization temperature to 9^{o}C with the addition of graphite in PP reflects the nucleating ability of graphite particles. However, the crystallinity of the polymer decreases because of agglomeration of graphite particles reducing the effective crystallized portion in the composite. It has been reported for PP-synthetic graphite composites prepared by melt mixing that the crystallization temperature increases by 20^{o}C for 60 wt% graphite in PP[17]. However the grade of PP and the one used in our research are different along with graphite and the processing routes. From XRD analysis, the crystallinity in this grade of PP has been reported to be ~60% by Khare *et al*.[25].

5.3. PP-ExGr, PP-graphite-ExGr Composites

5.3.1. DC Conductivity Study of PP-ExGr Composites

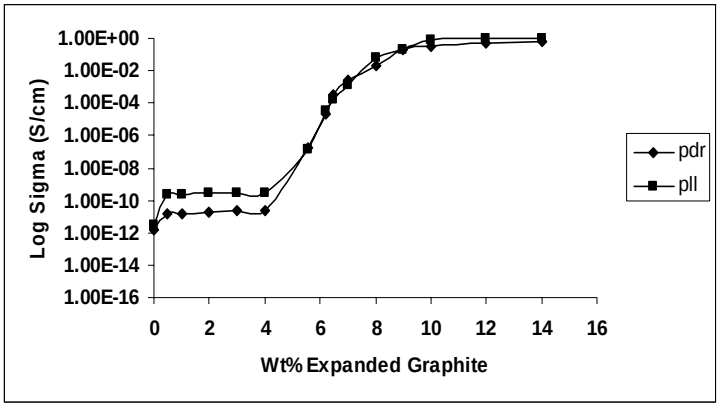

Figure 5.3.1. DC conductivity of powder mixed PP-ExGr composites

Percolation type variation of dc conductivity of PP-ExGr composites can be seen from Figure 5.3.1. The percolation threshold can be identified at 4 wt%. Expanded

graphite particles were sonicated before mixing with PP leading to the formation of nanosheets. Before the percolation threshold, significant variation in in-plane (pll) and through plane conductivities (pdr) can be seen. At least one order difference in the two conductivities can be noted. In-plane conductivity is higher than the through plane due to the alignment of nanosheets along the surface of the pellet as high pressure compaction was employed for making pellets. Above the percolation threshold, both conductivities more or less match signifying unit anisotropy. The saturation in conductivities occurs above 10 wt% ExGr due to complete network formation between the filler nanosheets. Below the percolation threshold insufficient formation of network causes the composites to remain as insulators.

5.3.2. Percolation Exponent of PP-ExGr Composites

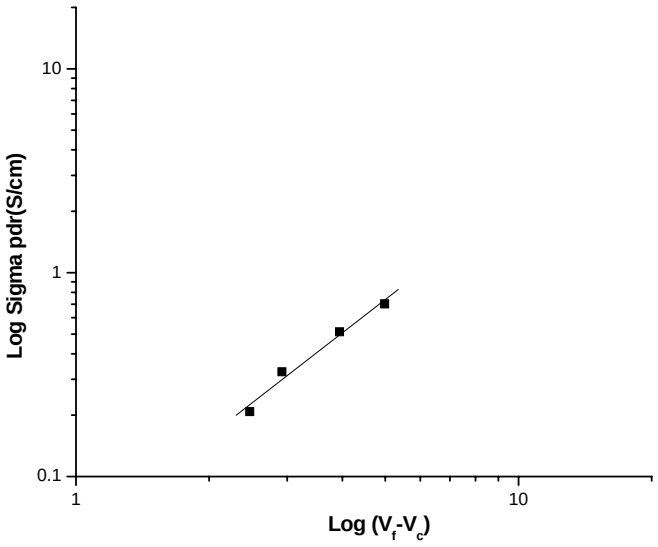

Figure 5.3.2. Log σ_{pdr} vs Log (V_f-V_c) plot of PP-ExGr composites

As explained in chapter-3 for PES-graphite composites, plot of Log σ_{pdr} vs. Log (V_f - V_c) yields percolation exponent where the symbols have their usual meaning. For this system the exponent obtained is 1.63 which is close to that of 3D network.

5.3.3. Effect of Heat Treatment on the Electrical Conductivity of PP-ExGr composites

In order to understand the effect of heat treatment on the electrical conductivity of PP-ExGr composites, the composites were sintered at 140^{o}C below the melting temperature of PP (~165^{o}C) for one hour as no significant variation in electrical conductivity above this time was observed. There is a significant increase in the through plane conductivity (Sigma pdr) after sintering below saturation compositions which has been shown in Figure 5.3.3. The increase in the conductivity can be explained on the basis of XRD results.

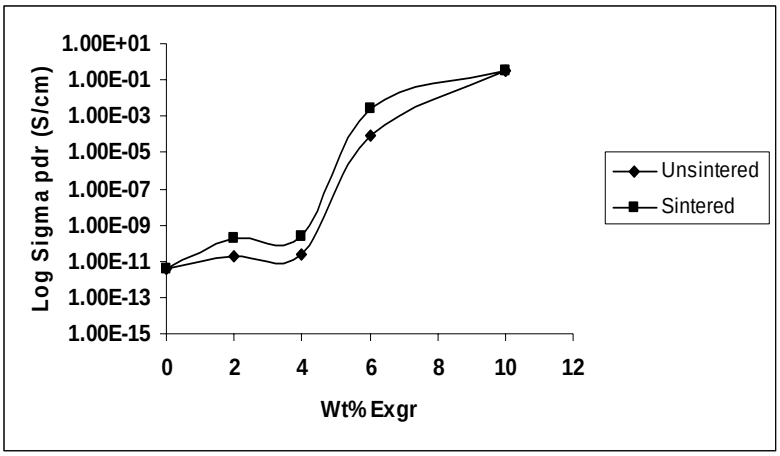

Figure 5.3.3. Through plane conductivity variation before and after sintering of PP-ExGr composites

5.3.4. XRD Analysis of PP-ExGr Composites

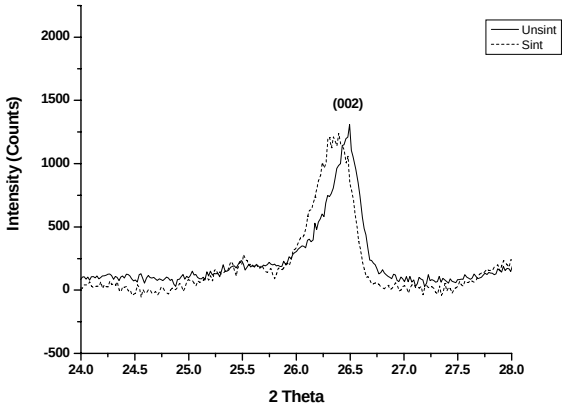

(a)

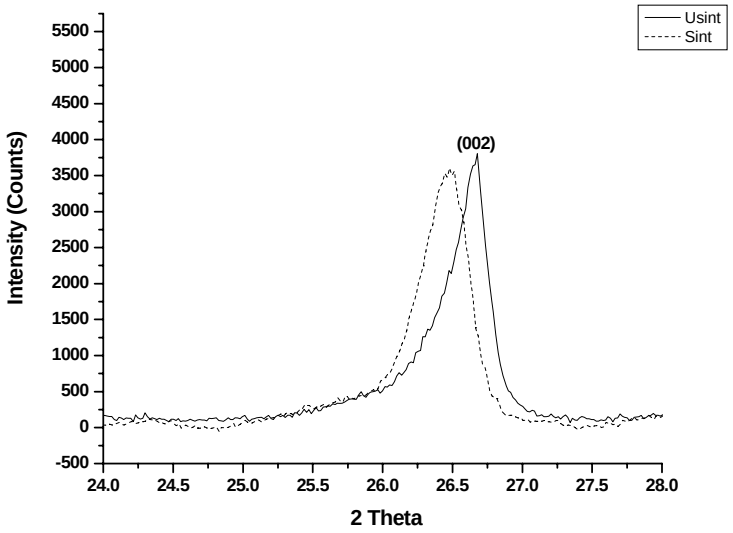

(b)

Figure 5.3.4. XRD patterns of a) PP-1 wt% ExGr b) PP-3 wt% ExGr powder mixed composites

The above XRD patterns show the graphite part of PP-1 wt% ExGr and PP-3 wt% ExGr before and after sintering. It is clear from the diffractograms that after sintering, the crystallite size decreases as FWHM corresponding to 002 reflections of graphite increases. The crystallite size reduction leads to better dispersion and increased surface area resulting in better contact between filler particles along the through thickness direction and hence the corresponding conductivity increases. The intensity of 002 reflection of graphite is reduced after sintering but not to that extent observed in the case of PES based composites. Reduction in 2 Theta after sintering signifies polymer penetration in to the graphite planes. High pressure compaction followed by heat treatment would have pushed polymer chains in to the layers of graphite. As there are no functional groups present in PP, one has to arrive at the above conclusion. Table 6 summarizes various parameters extracted from the XRD analysis of PP-ExGr composites.

Table 6

XRD analysis of PP-ExGr composites

Sample	2 Theta		Intensity		Crystallite Size (t') (nm)	
	BS	AS	BS	AS	BS	AS
PP-1wt% Expanded Graphite	26.695	26.544	1308	1212	28.5	25.2
PP-3wt% Expanded Graphite	26.679	26.477	3805	3603	28.5	24.8
PP-4wt% Expanded Graphite	26.562	26.377	3961	3745	28.5	24.5

Crystallite size reduction and re-orientation of graphite 002 planes after sintering can be understood from the above Table 5.

5.3.5. Effect of ExGr on the DC Conductivity of PP-7 wt% graphite Composite

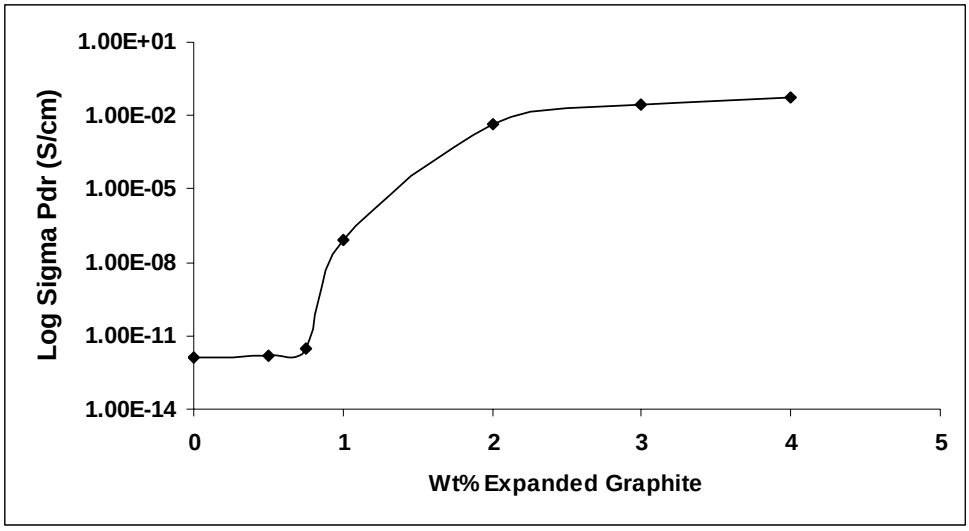

Figure 5.3.5. DC conductivity of PP-7 wt% graphite-ExGr composites

The dc through plane conductivity (Sigma pdr) of PP-7 wt% graphite with the addition of ExGr after sonication in acetone for five hours is shown in Figure 5.3.5.

Up to 0.75 wt% ExGr addition, the composites behave as insulators due to insufficient network formation between fillers. Above 0.75 wt% ExGr, the conductivity starts increasing and saturates at 3 wt% because of completion of network formation between the filler particles. The increase in the conductivity could be due to the occupation of ExGr nanosheets in the interspace of graphite particles as without ExGr sheets, PP-7 w% graphite behaves as an insulator and without graphite, PP-ExGr composites up to 4 wt% are insulators. Thus it can be concluded that the occupation of ExGr particles in the interspace of graphite reduces the barrier for the charge transport and hence the conductivity increases. This point can be proved by studying ac behavior of the hybrid composites.

5.3.6. Frequency Dependent Conductance of PP-7 wt% graphite-ExGr Composites

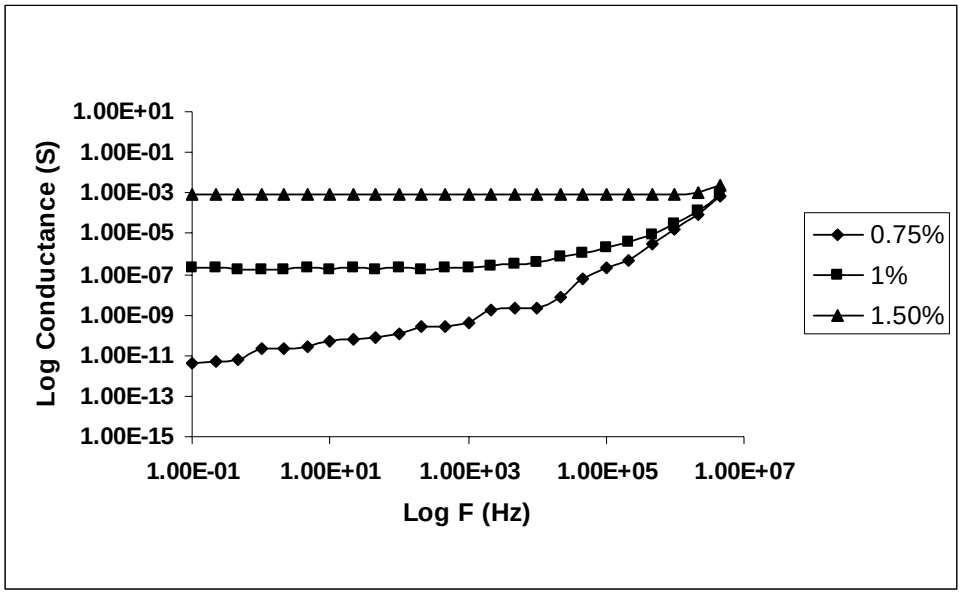

(a)

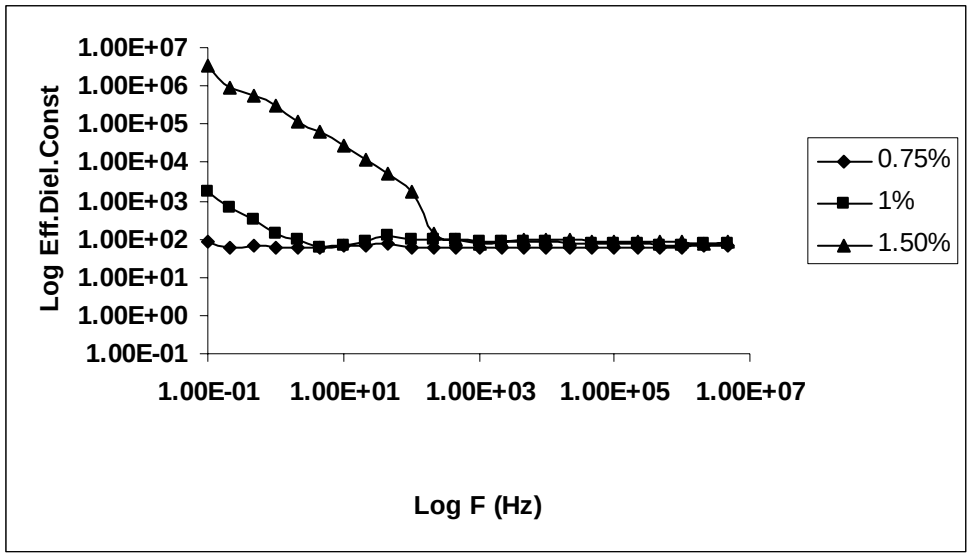

(b)

Figure 5.3.6. a) AC conductance b) Effective dielectric constant vs frequency of PP-7 wt% graphite- x wt% ExGr composites (x = 0.75, 1, 1.5)

With the addition of 0.75 wt% ExGr in PP-7 wt% graphite, the composite exhibits typical variation of conductance corresponding to that of insulators in the entire frequency range. With 1 wt% ExGr addition, plateau region originates indicating higher dc conductivity and the frequency dependent conductance starts at higher frequency. There exists at least eight orders increase in dc conductance for 1.5 wt% ExGr in PP-7 wt% graphite when compared to 0.75 wt% ExGr in the same. This has been shown in Figure 5.3.6.a. Conducting particle-polymer-conducting particle configuration can be thought of as a parallel plate capacitor with dielectric in between. When the second conducting particles occupy the interspace between the first particles, the interparticulate distance is decreased eventually leading to increase in effective dielectric constant and interjunction capacitance. To prove this point the effective dielectric constant variation with frequency has been measured and shown in Figure 5.3.6.b. It can be seen that the effective dielectric constant decreases with increase in the frequency and after some frequency practically remains constant. The effective dielectric constant of 1.5 wt% ExGr in PP-7 wt% graphite at 0.01 HZ is more than four orders higher than that of 0.75 wt% ExGr in the same. As already mentioned without ExGr, PP-7 wt% graphite will be an insulator and whose dielectric constant remains very low. Similarly without graphite PP-1.5 wt% ExGr will behave

as an insulator which will also exhibit a low dielectric constant. Therefore it can be concluded that the ExGr nanosheets will occupy predominantly intergraphite space with the range of loading employed in the hybrid composites.

5.3.7. Charge Transport in PP-7 wt% graphite-ExGr Hybrid Composites

Table 7

Exponent 'n' from equation 1 for PP-7 wt% graphite-ExGr hybrid composites

Sample	n
1. PP-7 wt% Graphite-0.75 wt% ExGr	2.245
2. PP-7 wt% Graphite-1 wt% ExGr	2.133
3. PP-7 wt% Graphite-1.5 wt% ExGr	0.642

Table 7 shows the exponent 'n' variation, evaluated from the slope of conductance vs frequency plot (after conductance starts increasing with frequency), which decreases with ExGr addition. For 1.5 wt% ExGr in PP-7 wt% graphite, it is less than one signifying hopping conduction. For other compositions below 1.5 wt% ExGr in the same, the charge transport is coupled with capacitance effects.

5.3.8. Impedance Analysis of PP-7 wt% graphite-ExGr Composites

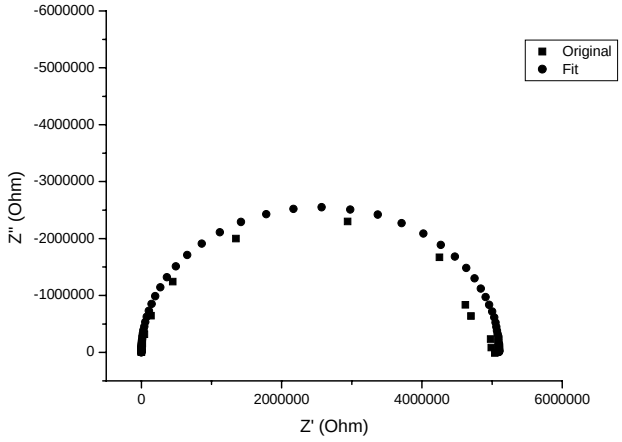

(a)

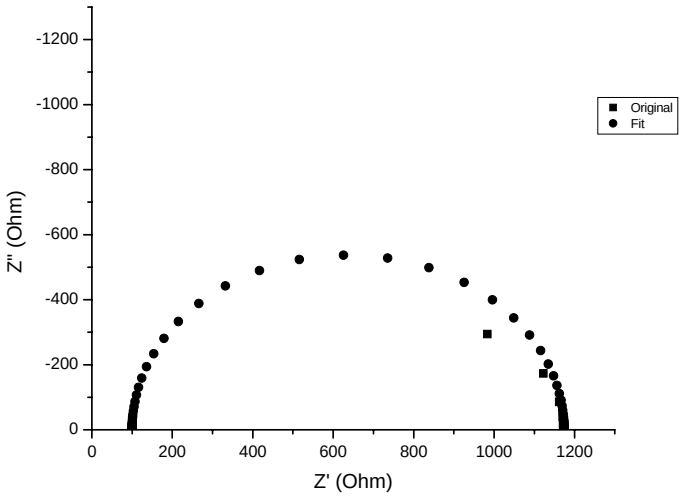

(b)

Figure 5.3.7. Impedance plots of a) PP-7 wt% graphite-1 wt% ExGr b) PP-7 wt% graphite-1.5 wt% ExGr powder mixed composites

In order to evaluate interjunction capacitance of hybrid composites, impedance measurement has been carried out. As already mentioned in previous Chapters that a conducting polymer composite can be replaced by an equivalent circuit which comprises of parallel resistor-capacitor connected to a series resistor. It can be seen from the impedance plots of PP-7 wt% graphite-1 wt% ExGr and PP-7 wt% graphite-1.5 wt% ExGr shown in Figure 5.3.7.a and b respectively that they trace semicircle in Argand plane and hence parallel model can be invoked. With the addition of more ExGr, the diameter of the semicircle decreases indicating enhanced conductivity of samples. Various model parameters after fitting the experimental points to parallel model are given in Table 8.

Table 8

Model parameters for PP-7 wt% graphite-ExGr hybrid composites from impedance measurement

Sample	R_a (Ohm)	R_p (Ohm)	C (pF)
1. PP-7wt%graphite- 0.75 wt% ExGr	400	$3.2x10^{12}$	37.0
2. PP-7wt%graphite- 1 wt% ExGr	300	$5.1x10^{6}$	49.0
3. PP-7wt%graphite- 1.5 wt% ExGr	100	1074	61.7

R_a refers to the aggregate resistance, R_p represents bulk resistance of the sample and C is the interjunction capacitance.

It is vivid from the above Table 8 that addition of 1.5 wt% ExGr in PP-7 wt% graphite decreases the bulk resistance by eight orders when compared to 0.75 wt% ExGr addition in the same. Also it can be noted that the interjunction capacitance increases to 61.7 pF for PP-7 wt% graphite-1.5 wt% ExGr from 37 pF for PP-7 wt% graphite-0.75 wt% ExGr. Thus the assumption of occupation of ExGr nanosheets predominantly in between graphite particles is true. It can also be gauged from Table 8 that the aggregate resistance decreases with the addition of ExGr. When two materials of different conductivities contact each other, work function of them comes in to picture for the charge transfer. Since the ExGr work function is not reported in the literature, it is presumed that it will be higher than that of graphite as it has less conductivity than graphite. When ExGr nanosheets lie in between polymer and graphite, the barrier is reduced for the charge transport and hence the aggregate resistance decreases with increase in ExGr loading.

5.3.9. SEM Analysis of PP-ExGr Composites

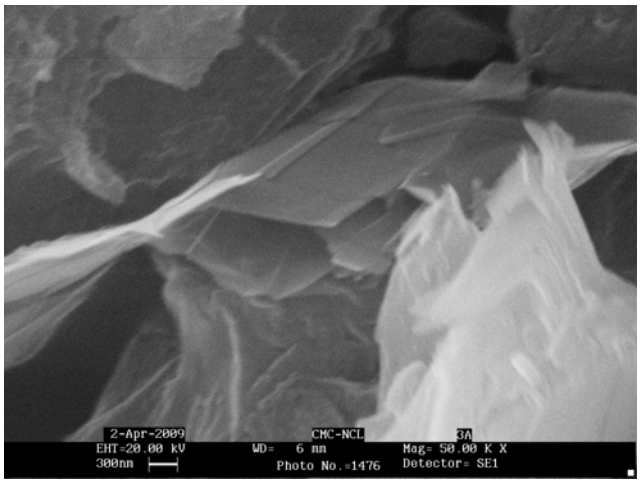

Figure 5.3.8. SEM image of cross section of PP-6 wt% ExGr composite

The nanosheets formed after sonication of porous expanded graphite can be clearly seen in the above Figure 5.3.8. Since the aspect ratio of them is high facilitating better contact between them at low loading resulting in low percolation threshold. The sheets connecting the adjacent ones can be seen.

5.3.10. DSC Analysis of PP-ExGr Composites

As crystallization effects are focused, only the cooling cycle of the DSC thermogram is shown in Figure 5.3.9. The crystallization temperature of the polymer matrix increases when ExGr is added to PP. It is clear from the Figure 5.3.9 that an increment of 14^{o}C in the crystallization temperature for 4 wt% ExGr in PP prepared by powder mixing route results indicating the nucleating ability of the filler.

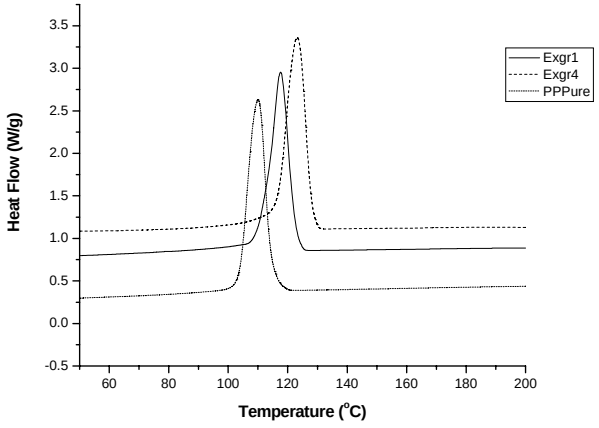

Figure 5.3.9. DSC of PP pure, PP-1 wt% ExGr and PP-4 wt% ExGr

Table 9 summarizes various parameters extracted from the DSC analysis of PP-ExGr composites. The crystallinity decreases with the loading of ExGr as obtained for PP-graphite composites reflecting the agglomerated state of filler particles. An enhancement of 14^{o} in the crystallization temperature reflects the nucleating ability of filler particles. Since the increase in T_c for 4 wt% ExGr in PP is higher than 1 wt% Exgr in the same, the value of that composite is reported in Table 9.

Table 9

DSC analysis of PP-ExGr and PP-7 wt% graphite-ExGr composites

Sample	T_c (^{o}C)	ΔH_c (J/g)
1. PP Pure	110.03	114.53
2. PP-4 wt% ExGr	123.70	107.20

5.4. PP-CNF and PP-graphite-CNF Composites

5.4.1. DC Conductivity of PP-CNF Binary Composites

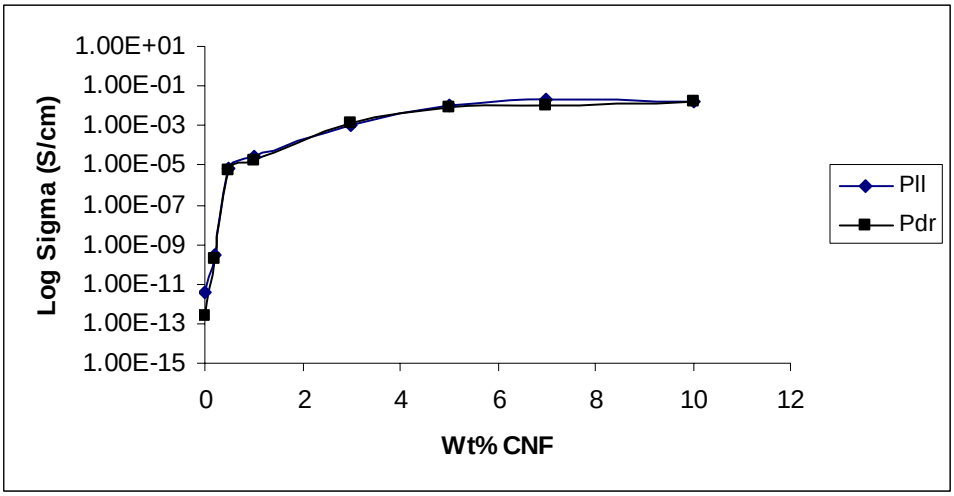

Figure 5.4.1. DC conductivity variation of PP-CNF powder mixed composites

The above Figure 5.4.1 shows that the percolation threshold for PP-CNF binary composites lies at 0.2 wt% due to high aspect ratio of CNF. Below percolation threshold, the composites behave as insulators and above that they become more conducting due to the formation of network between fillers. After 3 wt% CNF, the

conductivities saturate due to completion in the formation of network. It can be seen that both in-plane (Pll) and through plane (Pdr) conductivities remain more or less the same signifying unit anisotropy reflecting better dispersion of fillers in the polymer matrix. At lower loading in-plane conductivity is slightly higher than the through plane one.

5.4.2. Dimension of Network Formation in PP-CNF Composites

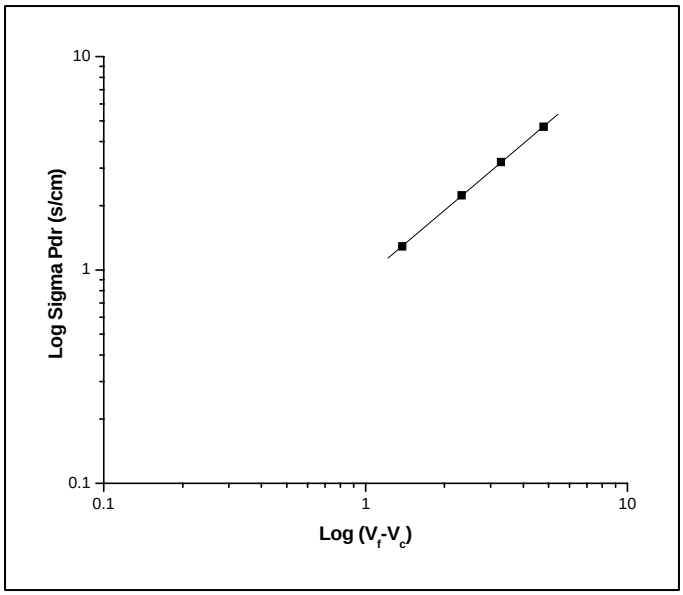

Figure 5.4.2. Log conductivity vs Log (V_f-Vc) plot

In order to find out the dimension of network formation between fillers, percolation equation mentioned in Chapter 3 has been used to evaluate the same. A plot of log conductivity vs log (V_f -Vc) leads to the exponent 't''' where the symbols have the usual meaning as mentioned in equation 1 in Chapter-3. For these composites, a value of 1.1 is obtained which is close to that of two dimensional network formation values as reported for other systems also[26]. Through plane conductivity is considered for the evaluation of the exponent.

5.4.3. SEM Analysis of PP-CNF Composites

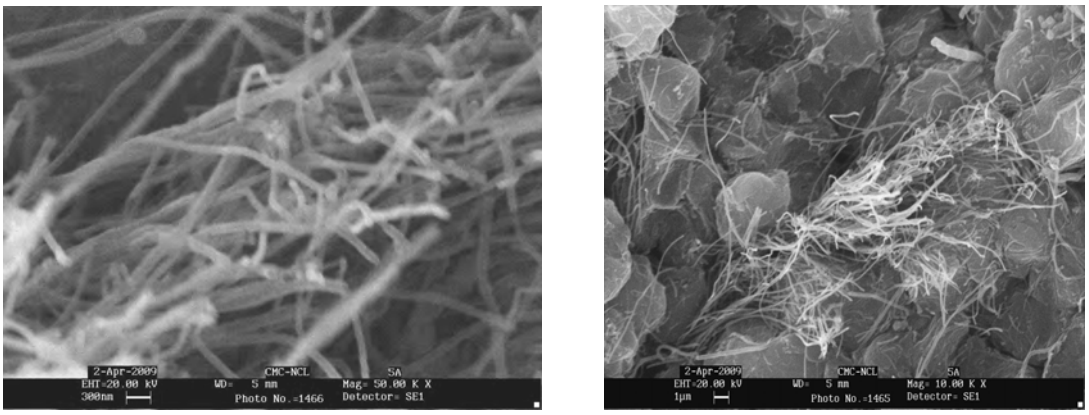

Figure 5.4.3. SEM pictures of cross section of PP-7 wt% CNF composite

Figure 5.4.3 shows SEM pictures of cross section of PP-7 wt% CNF composites in different magnifications. The interpenetrating and high aspect ratio carbon nanofibers burried in the polymer matrix can be clearly seen. The high aspect ratio CNFs lead to better contact between them at low loading itself resulting in low percolation threshold.

5.4.4. Electrical Conductivity of PP-graphite-CNF Hybrid Composites

In order to understand the effect of high aspect ratio filler namely CNF as second conducting filler in PP-graphite composites, hybrid composites with different CNF loading in PP-7 wt% graphite composite have been prepared by powder mixing route. The variation of through plane conductivity (Sigma pdr) with varying loading of second conducting component namely the CNFs is shown in Figure 5.4.4. The percolation threshold lies well below 0.2 wt%. Taking the average, it lies at 0.1 wt% CNF. Such a low percolation threshold is obtained due to nanofiber surface area and the occupation of them in between graphite particles reducing the barrier for the charge transport.

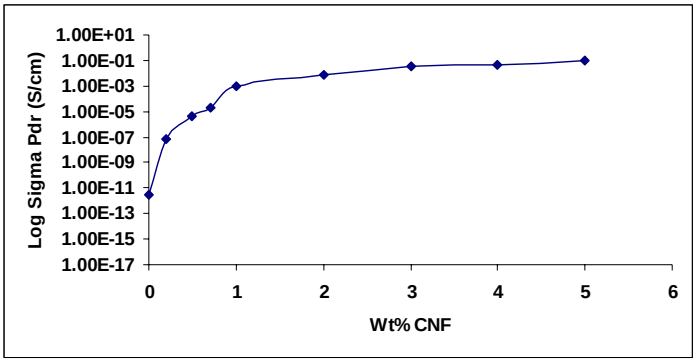

Figure 5.4.4. Through plane conductivity of PP-7 wt% graphite-CNF composites

After 1 wt% CNF in PP-7 wt% graphite, saturation in the conductivity is obtained due to completion in the network formation.

5.4.5. AC Behavior of PP-graphite-CNF Composites

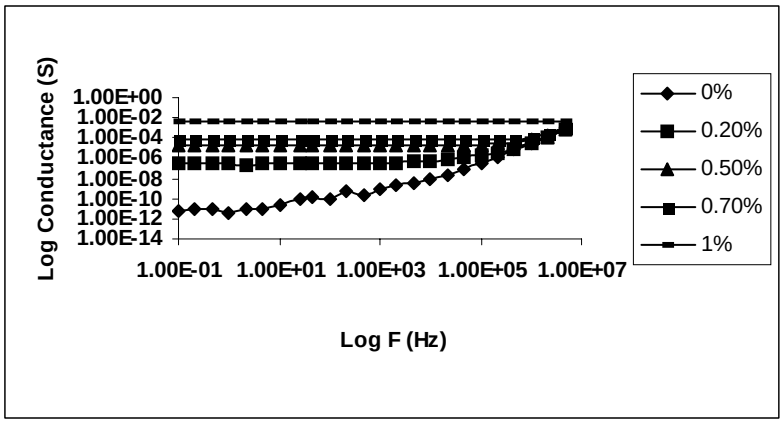

(a)

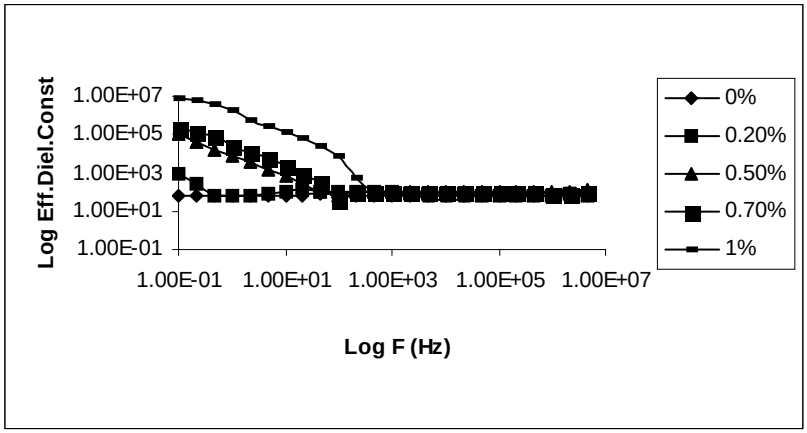

(b)

Figure 5.4.5. a) AC conductance b) Effective dielectric constant vs frequency of PP-7 wt% graphite-CNF composites

In order to find out charge transport in PP-7 wt% graphite-ExGr hybrid composites, room temperature ac conductance with respect to loading of second conducting filler namely CNFs has been studied. Without CNF addition in PP-7 wt% graphite, the composite exhibits insulating behavior as plateau region is absent and the conductance starts increasing with the frequency. With the addition of CNF, plateau region appears and the frequency dependent conduction starts at high frequency. With higher loading of CNF, the plateau region extends further and the frequency at which the conductance starts increasing is shifted to higher value. To find out charge transport in these hybrid composites a plot of log Sigma vs. log F is made which yields a slope as mentioned in equation 1.

Table 10

Exponent 'n' extracted from equation 1

Sample	'n'
1. PP-7wt% Graphite	2.409
2. PP-7wt%Graphite-0.2wt% CNF	2.343
3. PP-7wt%Graphite-0.5wt% CNF	2.280
4. PP-7wt%Graphite-0.7wt% CNF	1.887
5. PP-7wt%Graphite-1wt%CNF	0.110

Table 10 summarizes exponent 'n' values for different loadings of CNF in PP-7 wt% graphite. It is clear that for 1 wt% CNF in PP-7 wt% graphite, the charge transport is by hopping mechanism as the exponent is less than one. For other compositions it is coupled with capacitive effect. Since the investigated ranges of compositions are above the percolation threshold, the occupancy of CNF in the interspaces of graphite can be proved by studying the ac behavior of binary composites. In Figure 5.4.5.b, the increase in the effective dielectric constant can be attributed to both CNF-polymer-CNF and graphite-polymer-CNF-polymer-graphite junctions. In order to delineate the effect due to the occupancy of CNFs in the intergraphite space, ac behavior of PP-CNF binary composites are discussed below.

5.4.6. AC Behavior of PP-CNF Binary Composites

The effective dielectric constant variation with frequency of PP-CNF binary composites is shown in Figure 5.4.6.

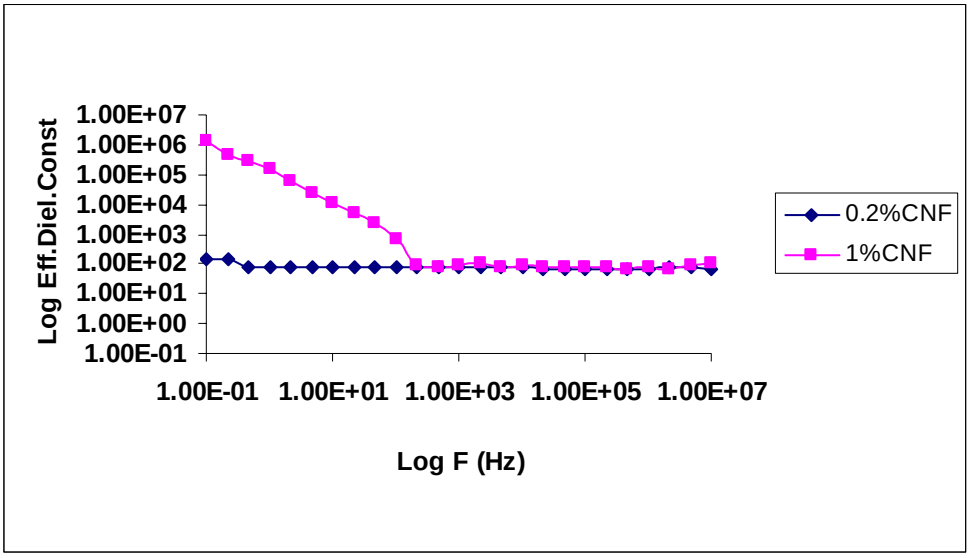

Figure 5.4.6. Effective dielectric constant vs. frequency of PP-CNF composites

On comparing the effective dielectric constant of PP-0.2 wt% CNF with PP-7 wt% graphite-0.2 wt% CNF composites, one order enhancement in the same at 0.01 Hz is due to the occupancy of CNF in the intergraphite space. The same is true for 1 wt% CNF in PP-7 wt% graphite. In this conducting sample especially in the binary composite, two CNFs with polymer in between constitutes parallel plate capacitor and the increase in the effective dielectric constant can be attributed to only CNF distribution. The effective dielectric constant at 0.01 Hz is ~10^6. The same is increased to 10^7 when mixed with PP-7 wt% graphite. Since PP-7 wt% graphite is an insulator, one order increase in the effective dielectric constant is due to graphite-CNF-graphite configuration with polymer in between. Similarly the increase in the interjunction capacitance between binary and hybrid composites for the same loading of CNF can be used to find out the effect of CNF occupation in between graphite particles on the electrical conductivity. Impedance analysis of both binary and hybrid composites are shown in Figure 5.4.7.

5.4.7. Impedance Behavior of PP-CNF Binary Composites

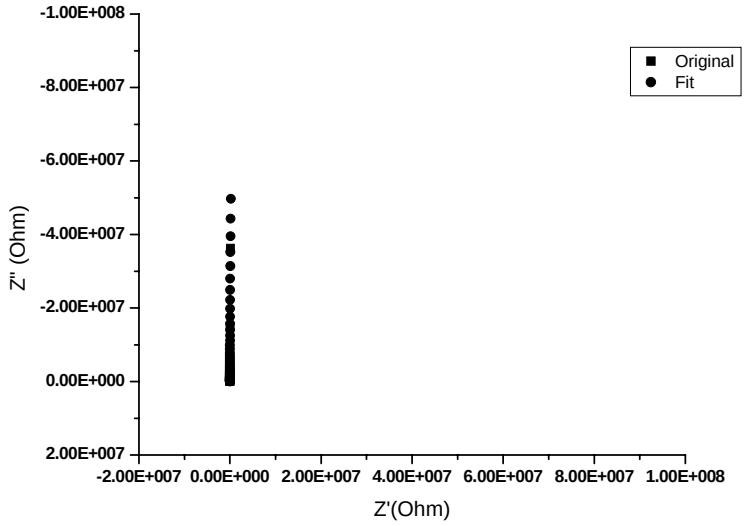

(a)

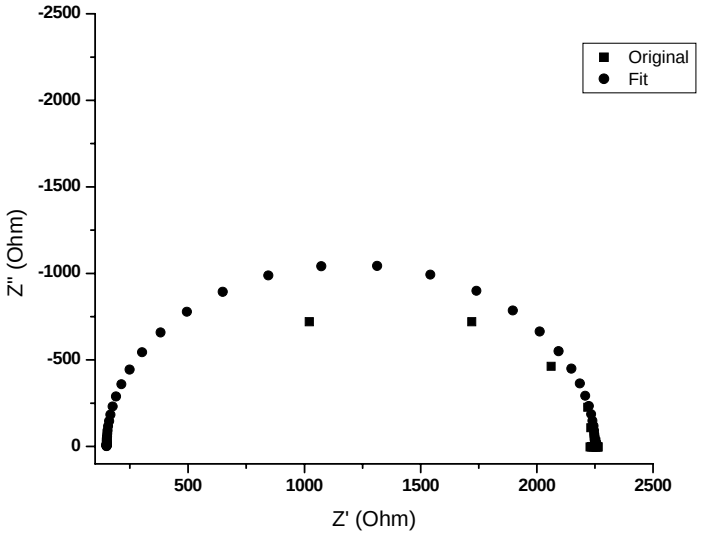

(b)

Figure 5.4.7. Impedance plots of a) PP-0.2 wt% CNF b) PP-1 wt% CNF

Figures 5.4.7.a and b show impedance plots of 0.2 and 1 wt% loadings in PP respectively. The plots clearly show that with the addition of CNF, the diameter of the semicircle decreases signifying enhanced conductance of samples. The semicircular

response of the composite with higher loading of CNF in Argand plane suggests that parallel model can be used to fit the experimental data. Table 11 summarizes various parameters extracted from the impedance plots of PP-CNF binary composites.

Table 11

Model parameters for PP-CNF composites extracted from impedance measurement

Sample	R_a (Ohm)	R_p (Ohm)	C (pF)
1. PP-0.2wt% CNF	300	1.26×10^{10}	32
2. PP-1wt% CNF	150	2100	68

Symbols have the usual meaning as explained in chapter-3. It is clear that with 0.2 wt% CNF addition in PP, the interjunction capacitance due to CNF-polymer-CNF junctions is 32 pF. This result is useful to extract the interjunction capacitance due to graphite-CNF-graphite junctions which is done after measuring the impedance response of hybrid composites. The aggregate resistance decreases with the addition of CNF due to better contact between the filler particles.

5.4.8. Impedance Analysis of PP-graphite-CNF Hybrid Composites

To calculate interjunction capacitance in hybrid composites, impedance behaviors of PP-7 wt%-0.2 wt% CNF and PP-7 wt% graphite-0.7 wt% CNF samples have been shown in Figure 5.4.8.a and b respectively. The samples exhibit semicircular response which proves that they can be replaced by parallel model i.e., resistor-capacitor in parallel configuration with a series resistor.

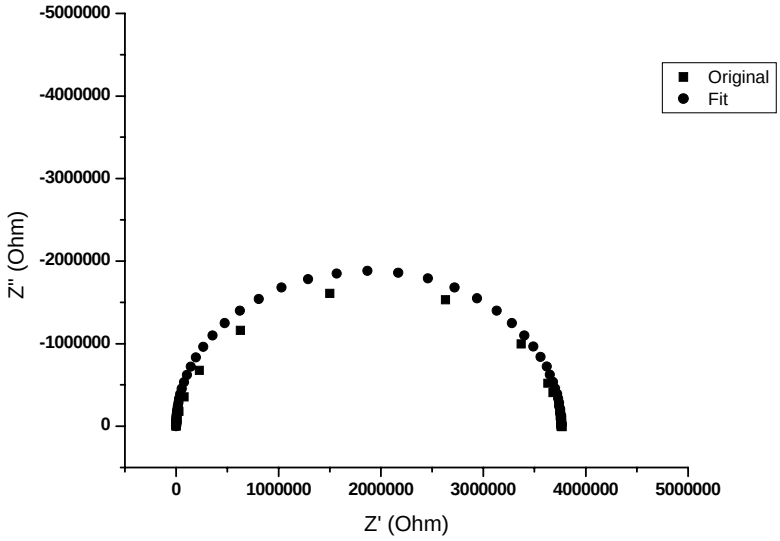

(a)

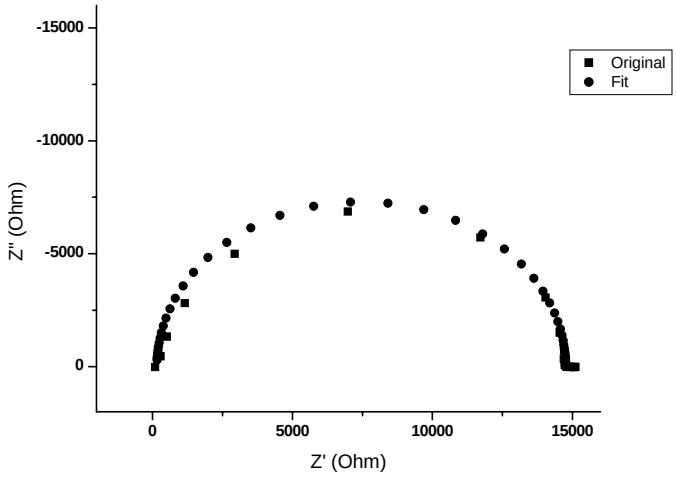

(b)

Figure 5.4.8. Impedance plots of a) PP-7 wt% graphite-0.2 wt% CNF b) PP-7 wt% graphite-0.7 wt% CNF

The bulk resistance decreases as signified by the reduction in the diameter of the semicircle with higher loading of CNF. Table 12 summarizes various model parameters extracted from the impedance behavior of samples fitted to parallel model.

Table 12

Model parameters of PP-7 wt% graphite-CNF hybrid composites

Sample	R_a(Ohm)	R_p(Ohm)	C(pF)
1. PP-7wt%Graphite	600	$6.8x10^{12}$	31.0
2. PP-7wt%Graphite-0.2wt%CNF	500	$3.76x10^{6}$	41.5
3. PP-7wt%Graphite-0.5wt% CNF	250	52700	48.0
4. PP-7wt%Graphite-0.7wt% CNF	200	14500	56.0

From the above Table 12 it can be seen that the addition of CNF decreases the bulk resistance of the sample due to the reduction in the barrier for the charge transport. The interjunction capacitance increases with CNF addition in PP-7 wt% graphite. For 0.2 wt% CNF in PP-7 wt% graphite, the interjunction capacitance obtained is 41.5 pF. Without graphite, PP-0.2 wt% CNF exhibited 31 pF. Thus the increment in the interjunction capacitance of 10 pF in hybrid composites is due to the occupation of CNFs in the interspace of graphite particles. Similar argument shall be invoked for other conducting samples as well. Further it can be noted that the aggregate resistance decreases with the addition of CNF in PP-7 wt% graphite. This can be understood in terms of work function of individual components. The work function of the polymer is 5.7 eV and that of CNF is 5.0 eV. Graphite work function is 4.6 eV. In the absence of graphite, for the charge transfer from the polymer to graphite a barrier of 1.1 eV need to be crossed. When CNF is present in between the polymer and graphite, a barrier of 0.7 eV needs to be crossed by the charges and hence more charges will be transferred to graphite via CNF. Thus when CNF concentration is increased, more CNFs will be found in between the polymer and graphite resulting in the enhanced charge transport to graphite via CNF. Thus the aggregate resistance decrease can be understood. The configuration of polymer-CNF-graphite can be connected in series through out the volume of the sample and hence graphite-CNF-graphite junction can

be realized. For the measurement of electrical resistance, field is applied which causes the charges to flow along one direction.

5.4.9. DSC Analysis of PP-CNF, PP-graphite-CNF Composites

In order to prove the nucleating ability of CNF in PP, only cooling DSC thermogram is shown in Figure 5.4.9. There exists 17°C enhancement in the crystallization temperature of PP when 3 wt% CNF is added to PP. Similarly for PP-7 wt% graphite-1 wt% CNF hybrid composites, the crystallization temperature increases by 15°C as shown in Figure 5.4.10.

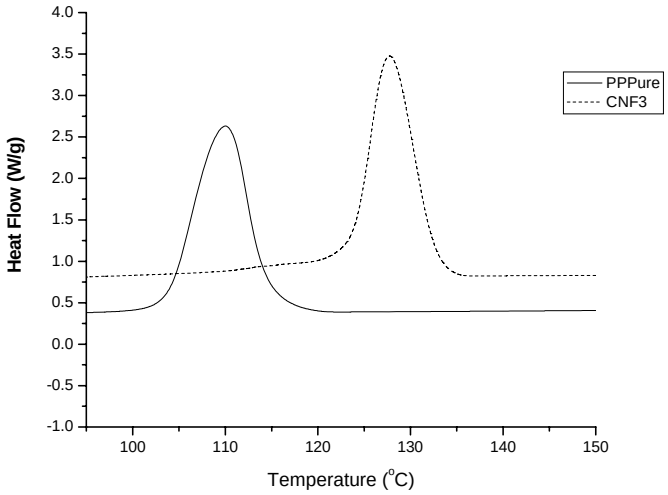

Figure 5.4.9. DSC cooling curve of pure PP and PP-3 wt% CNF composite

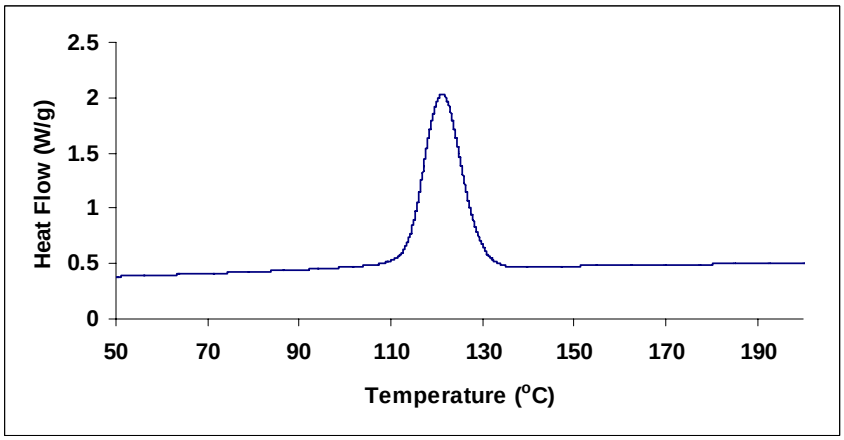

Figure 5.4.10. DSC cooling curve of PP-7 wt% graphite-1 wt% CNF

Since in hybrid composites both fillers are graphitic, there is no cumulative effect of them in increasing the crystallization temperature of PP. However crystallinity

becomes less which is signified by the decrease in the area of the crystallization curve of filled PP when compared to that of pure PP. This could be due to agglomeration of filler particles which reduces the effective area of crystallized portion in binary and hybrid composites than pure PP. Table 13 summarizes different parameters extracted from the DSC cooling curve.

Table 13

Parameters extracted from DSC cooling curve of PP-CNF and PP-7 wt% graphite-1 wt% CNF

Sample	T_c(^{o}C)	ΔH_c (J/g)
1.PP Pure	110.30	114.53
2.PP-3wt% CNF	127.75	107.60
3.PP-7wt% Graphite-1wt% CNF	125.16	98.26

The increase in the crystallization temperature is higher in the case of binary composite than that of hybrid composite. The better dispersion in the former case implying more polymer area will be in contact with the filler and hence T_c and crystallinity is higher than hybrid composite. In the later case, since the total loading of fillers is high and can lead to agglomeration resulting in incomplete wetting of the polymer.

5.5. Effect of Aspect Ratio of Second Conducting Filler on the Electrical Percolation of Powder Mixed PP-graphite-filler (Filler-CB, ExGr and CNF)

The second conducting fillers are sonicated for five hours before mixing with the polymer. The mixed polymer-filler system is sonicated further for half an hour before being poured in a Petri dish for drying the solvent. The aspect ratio of them after sonicating for five hours is taken for finding the diameter of CNF, thickness of expanded graphite and the diameter of CB as mentioned in Chapter-4. The same values have been taken as the conditions remain the same. It is obtained that the electrical percolation thresholds of hybrid composites have inverse relation with the aspect ratio of second conducting components as shown in Figure 5.5.

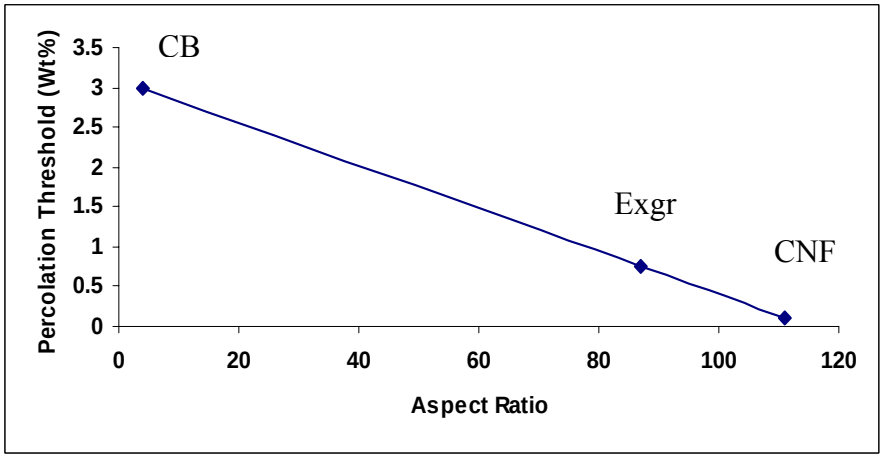

Figure 5.5. Aspect ratio of second filler vs percolation threshold

B. Melt Crystallization

5.6. DC Conductivity of Melt Crystallized PP-graphite Composites

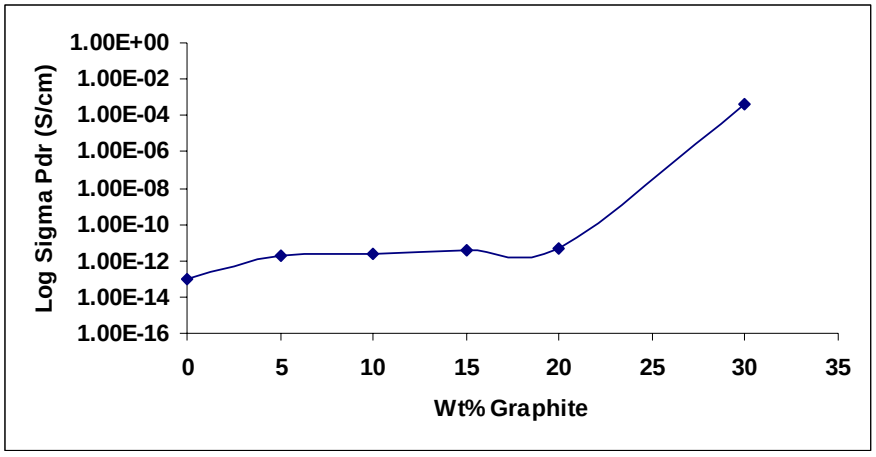

Figure 5.6. Through plane conductivity of melt crystallized PP-graphite composites

PP-graphite composites are melted at 180^{o}C and then immediately transferred to water. The polymer layer engulfing the composites on the surface is removed by scratching with polish paper. The electrical resistance is measured along through thickness direction.

Figure 5.6 clearly shows that the percolation threshold in melt crystallized PP-graphite composites lies at 20 wt%. This is higher when compared to that obtained in powder mixed samples (10 wt%). The increase in the percolation threshold can be attributed to the increase in interparticulate distance due to the formation of

transcrystals which will be proved in XRD analysis section. When the interparticulate distance is increased, the barrier for the charge transport will become high eventually resulting in poor conductivity.

5.6.1. XRD Analysis of Melt Crystallized PP-graphite Composites

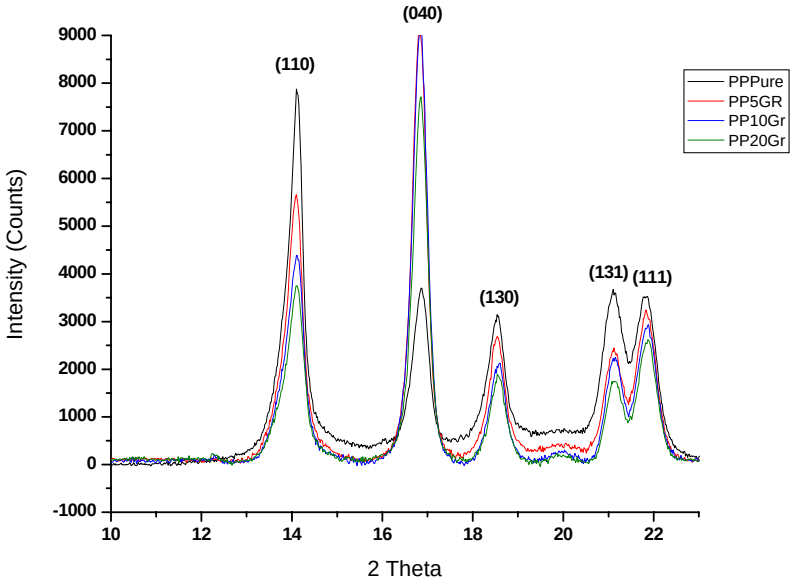

Figure 5.6.1. XRD patterns of melt crystallized PP-graphite composites

Five major reflections of monoclinic α-phase of PP are given in the following Table 14.

Table 14

Standard reflections of alpha phase of PP

2 Theta	Plane (hkl)
14.0	(110)
16.8	(040)
18.6	(130)
21.2	(131)
21.8	(111)

Melt crystallized PP-graphite composites exhibit a strong b-plane orientation which is revealed through increase in the intensity of 040 reflection of PP in XRD as shown in Figure 5.6.1. The observed effect can be explained in terms of transcrystalline morphology discussed as follows.

Semicrystalline polymers when reinforced with various types of organic/inorganic reinforcements like fibers not only improve mechanical properties but also morphology and crystallinity. Fibers may act as heterogeneous nucleating agents and nucleate crystallization along the interface with sufficiently high density of nuclei. These nuclei will hinder the lateral extension and growth in one direction namely perpendicular to the fiber surfaces and result in columnar crystalline layers with limited thickness. The mechanism by which transcrystalline layers occur is not fully understood and there are no rules to predict the appearance of transcrystallinity in a particular polymer matrix/fiber system. Fiber topography, surface coating of the fiber and processing conditions of the composites have been reported to influence transcrystallinity. The phenomenon is highly specific to filler-matrix combination. The following factors have been reported for transcrystal formation.

1. Epitaxy between fiber and the matrix
2. Topography of the fiber
3. Mismatch of thermal coefficients between fiber and the matrix
4. Thermal conductivity of the fiber
5. Chemical composition of the fiber surface
6. Surface energy of the fiber
7. Processing conditions such as cooling rate, temperature etc.

Saujanya *et al*.[27] have explained transcrystals formation in PET fiber filled PP composites through lattice mismatch theory. From the lattice parameters of α-phase of PP and with that of PET, the lattice mismatch between b-axis of PP and twice c-axis of PET is less than 3% while that between c-axis of PP and b-axis of PET is less than 8.5%. They further reported that the bc planes of PP crystals get aligned initially along the fiber axis of PET fibers and subsequently these crystals grow with preferential b-plane orientation. Thus the alignment of b-axis of PP cystallites gives rise to change in intensity of 040 reflection . It is further reported when the lattice

mismatch factor is less than 10%, epitaxial growth of one phase over the other can be expected. According to lattice mismatch theory, the mismatch factor δ is defined as

$$\delta = |pl_s - ql_g| / |l_s| \times 100 \quad (3)$$

Where l is the lattice parameter along any axis; p and q are integers. The subscripts s and g represent substrate and growing media. The lattice parameters of graphite and monoclinic α phase are given below.

Graphite : a=b=2.46 A^o, c=6.7 A^o

PP : a=6.5 A^o, b=20.9 A^o, c=6.5 A^o

The lattice mismatch factor is less than 3% when lattice parameter c of graphite and a and c of PP are considered. Thus ac planes of PP get aligned along the filler edges and grow along the b-axis. The transcrystalline morphology increases the interparticulate distance of fillers and hence in melt crystallized samples, the percolation threshold is higher than that of powder mixed samples. For one dimensional structure like CNT in PP prepared by solid state mechano chemical pulverization process results in b-plane orientation[28]. Table 15 summarizes the XRD analysis on the melt crystallized PP-graphite composites. Yukata *et al*.[28] have reported for PP-CNT composites prepared by melt mixing route that when the intensity ratio of of α-PP (110) reflection to (040) reflection is greater than 1.5, a-axis of PP will be found along the surface. When the same is less than 1.3, a strong b-plane orientation will be observed. In our case we observed b-plane orientation as the ratio I_{110}/I_{040} after melt crystallization becomes less than 1.3. The b-plane orientation of PP crystals is because of the formation of transcrystals at filler edges due to less lattice mismatch.

Table 15

XRD analysis of PP part of melt crystallized PP-graphite composites

Sample	2 Theta	Intensity-I(Counts)	I_{hkl}/I_{040}
PP pure	14.101 (110)	7874	2.12
	16.872 (040)	3698	1.00
	18.538 (130)	3143	0.85
	21.008 (131)	3611	0.98
	21.802 (111)	3523	0.95
PP-5 wt% graphite	14.100 (110)	5661	0.62
	16.853 (040)	9122	1.00
	18.537 (130)	2689	0.30
	21.121 (131)	2445	0.27
	21.835 (111)	3243	0.36

5.7. PP-ExGr, PP-graphite-ExGr Melt Crystallized Composites

5.7.1. DC Conductivity of Melt Crystallized PP-ExGr Composites

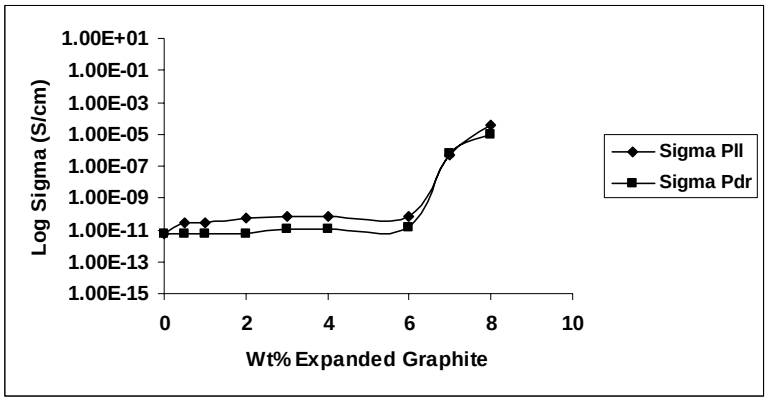

(a)

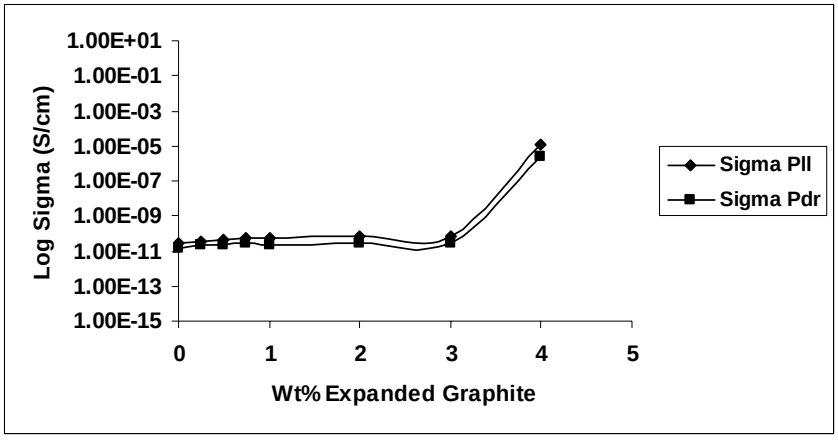

(b)

Figure 5.7. Melt crystallized a) PP-ExGr b) PP-7 wt% graphite-ExGr composites

Figures 5.7.a and b show electrical conductivity variation in melt crystallized PP-ExGr binary and PP-7 wt% graphite-ExGr hybrid composites respectively. After melting at 180^{o}C, polymer coated filler forms sheet which up on scraping with polish paper yields a fresh surface for electrical measurements. The percolation threshold in binary PP-ExGr composites is at 6 wt% where as for powder mixed samples it is at 4 wt%. Sigma Pll refers to in-plane conductivity and Sigma Pdr refers to through plane conductivity. In-plane conductivity is slightly higher than the through plane conductivity. The transcrystals formation perpendicular to the filler surface results in decrease in through plane conductivity. In PP-7 wt% graphite-ExGr hybrid composites, the percolation threshold is identified at 3 wt% where as for powder mixed hybrid composites it is at 0.7 wt%. The higher percolation threshold can be attributed to the transcrystalline morphology of PP crystals which further increases interparticulate distance in melt crystallized samples. The transcrystallinity is proved by the strong b-plane orientation as evidenced by the XRD results.

5.7.2. XRD Analysis of Melt Crystallized PP-ExGr Composites

In order to find out any structural change of polymer due to melt crystallization process, XRDs of few representative samples of PP-ExGr composites are shown in Figure 5.7.1. They are compared with that of melt crystallized pure PP at the same temperature. The intensity of (110) melt crystallized pure PP is higher than that of other peaks. After sonication, ExGr nanosheets are added to PP and melt crystallized.

The b-plane orientation of PP is due to transcrystals formed at the edges of the filler. Expanded graphite essentially has graphite structure.

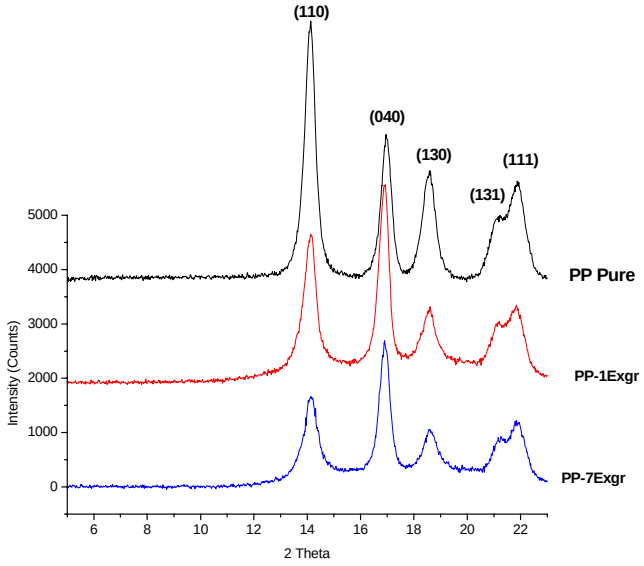

Figure 5.7.1. XRD of melt crystallized pure PP, PP-1 wt% ExGr and PP-7 wt% ExGr

As explained in the section of PP-graphite melt crystallized samples, the lattice mismatch factor of a and c axes of PP and c-axis of graphite is less than 3% which can induce transcrystals of PP with b-plane orientation. Similar result has been reported for PP-CNT composites where CNT aids b-plane orienatation[27] when composites are prepared by mechano chemical synthesis. The formation of transcrystals is due to the heterogeneous nucleation as many nucleating sites will be existing on the surface as well as edges of the filler. The transcrystals increase the interparticulate distance and hence melt crystallized samples exhibit higher percolation threshold. XRD analysis of melt crystallized PP-ExGr is shown in Table 16. Since the intensity ratio of (110) to (040) is less than 1.3 for melt crystallized PP-ExGr composites, a strong b-plane orientation exists. Anisotropy in dc electrical conductivity of melt crystallized samples results due to higher through plane resistance because of transcrystals growth perpendicular to the filler surface.

Table 16

XRD analysis of PP part of melt crystallized PP-ExGr samples

Sample	2 Theta	Intensity-I(Counts)	I_{hkl}/I_{040}
PP pure	14.137 (110)	4723	1.79
	16.959 (040)	2637	1.00
	18.591 (130)	1973	0.75
	21.158 (131)	1125	0.42
	21.872 (111)	1780	0.68
PP-1 wt% ExGr	14.130 (110)	2733	0.74
	16.935 (040)	3635	1.00
	18.601 (130)	1395	0.38
	21.168 (131)	1107	0.30
	21.831 (111)	1406	0.39

5.8. Melt Crystallized PP-CNF and PP-graphite-CNF Composites

5.8.1. DC Conductivity of Melt Crystallized PP-CNF Composites

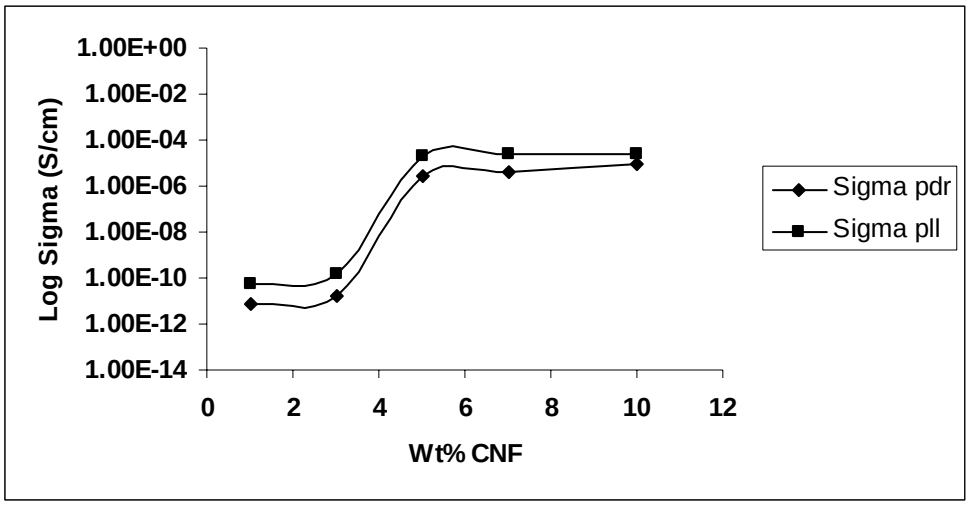

(a)

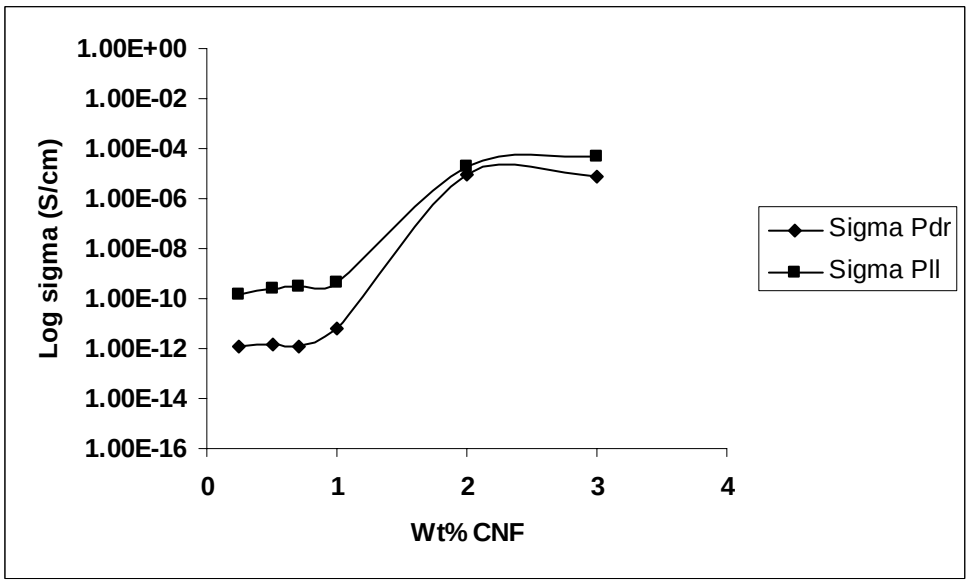

(b)

Figure 5.8.1 Melt crystallized a) PP-CNF b) PP-7 wt% graphite-CNF composites

The melt crystallized PP-CNF binary composites exhibit a percolation threshold of 3 wt% as shown in Figure 5.8.1.a which is much higher than that of powder mixed samples. For the later case the percolation threshold lies at 0.2 wt% CNF. The increase in the percolation threshold is due to increase in the inter fiber distance because of transcrystals formation which is reflected in the XRD as strong b-plane

orientation is observed for melt crystallized samples. Sigma Pll refers to in-plane conductivity which is higher than the through plane conductivity denoted as sigma Pdr. The transcrystals formed at the edges of the filler particles, would have arranged in the perpendicular direction resisting the charge flow along that direction and hence the through plane conductivity is found to be lesser than that of in-plane conductivity. Similar trend is observed for PP-7 wt% graphite-CNF hybrid composites as shown in Figure 5.8.1.b. The percolation threshold in hybrid composites is also increased. Figure 5.8.2 clearly depicts the effect of processing routes on the through plane electrical conductivity of PP-CNF binary composites.

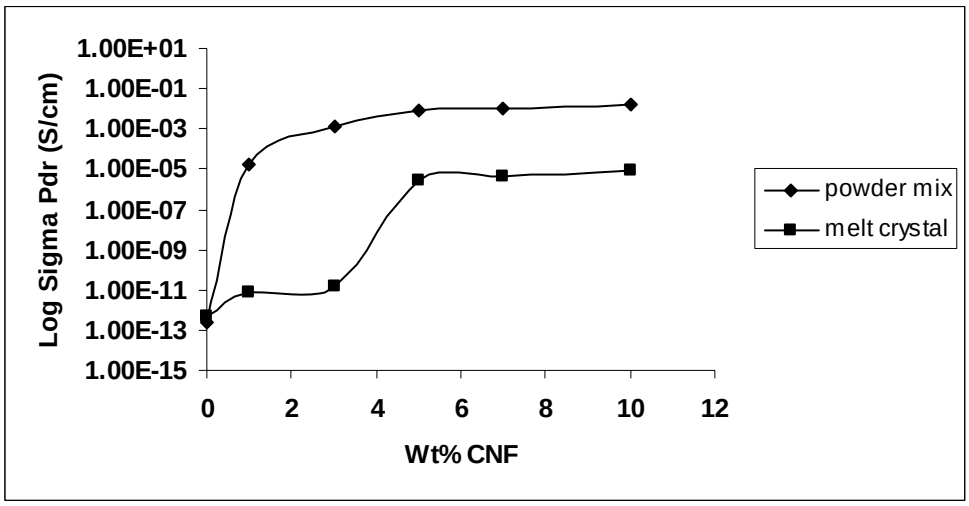

Figure 5.8.2. Effect of processing route on the through plane conductivity of PP-CNF binary composites

It can also be seen from the above Figure 5.8.2 that the through plane conductivity in the saturation region of melt crystallized PP-CNF binary composites are lower than that of the same prepared by powder mixing route. This is due to the fact that transcrystals of PP in the melt crystallized samples increase interparticle distance as it cannot be reduced below a certain value because of the hindrance of those crystals. Essentially the lattice parameters of CNF are same as that of graphite. The lattice mismatch factor suggests that the transcrystals will grow at the edges of CNF increasing the interparticulate distance. The XRD results prove this point.

5.8.2. XRD Analysis of Melt Crystallized PP-CNF Composites

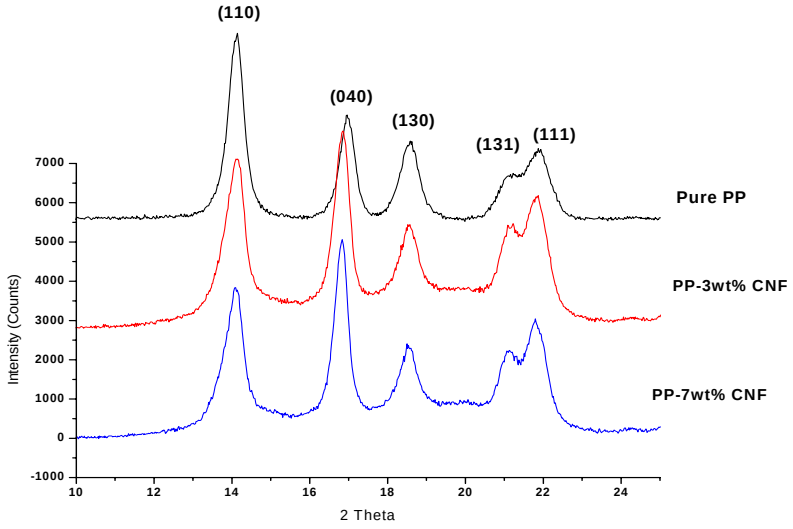

Figure 5.8.3. XRD patterns of melt crystallized PP, PP-3 wt% CNF and PP-7wt% CNF

Similar to the case of melt crystallized PP-graphite, PP-ExGr, PP-CNF composites also exhibit b-plane orientation of PP crystals as shown in Figure 5.8.3 where the intensity of 040 reflection of PP in melt crystallized composites is higher than that of 110 reflection. CNF aids in the formation transcrystals of PP at the edges as well as surface with b-plane orientation. This is due to the lattice mismatch as explained in PP-graphite melt crystallized sample section. CNF is graphitic in nature possessing same lattice parameters as that of graphite.

C. Thermal Conductivity Studies

5.9. Thermal Conductivity Studies on PP-graphite, PP-CNF Composites

Fiber spinning spools which are conventionally made of plastics get damaged due to the heat generated in that process. Hence they can be replaced by thermally conducting materials. The thermal conductivities of PP-graphite and PP-CNF binary composites have been measured and shown in Figure 5.9.a and b respectively. For PP-graphite composites, the thermal conductivity increases from 0.14 W/m-K to 0.9 W/m-K for 50 wt% graphite loading. Similarly for PP-CNF composites, it increases

from 0.14 W/m-K to 0.23 W/m-K for 10 wt% CNF. Thus these electrically and thermally conducting composites can be used to replace the plastic fiber spinning spool.

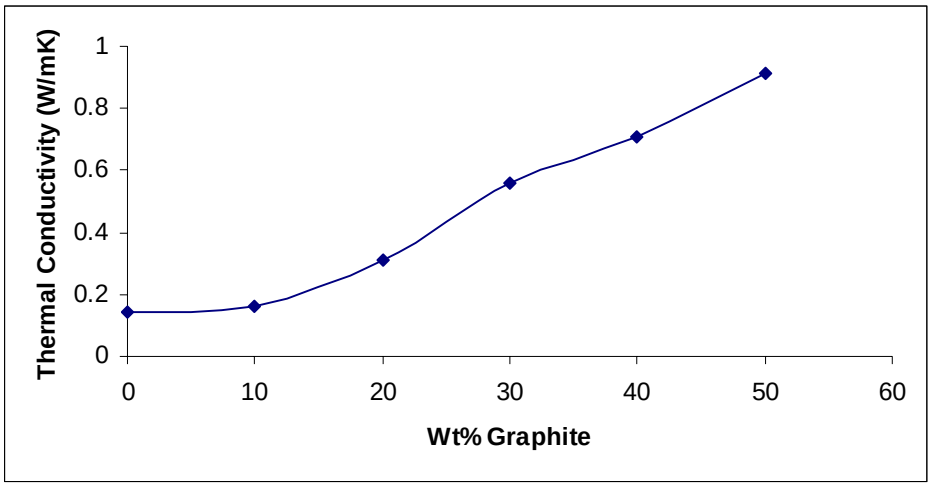

(a)

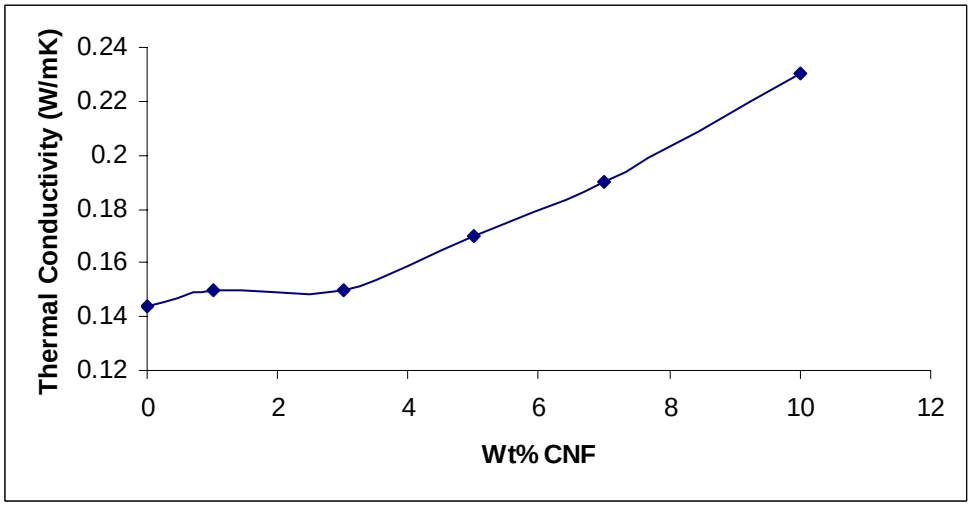

(b)

Figure 5.9. Thermal conductivities of a) PP-graphite b) PP-CNF powder mixed composites

5.10. Conclusions

PP-graphite binary composites were prepared by powder mixing route and from dc conductivity studies, percolation threshold was identified at 10 wt%. Effect of heat treatment above the T_g of the polymer for binary composites was studied. Sintering at 140^oC for one hour led to crystallite size and intensity reduction of graphite 002 planes. Crystallite size reduction was specifically observed from the increase in FWHM of graphite 002 reflection after sintering. Intensity reduction was understood in terms of re-orientation of graphite 002 planes. After sintering, enhancement in the through plane conductivity was observed due to re-orientation of graphite 002 planes along the through thickness direction. At least one order enhancement in the through plane conductivity was obtained at various loadings. One particular composition namely PP-7 wt% graphite was chosen to study the effect of addition of different aspect ratio fillers such as CB, ExGr and CNF.

The effect of addition of CB in PP-7 wt% graphite on the dc electrical conductivity was studied. Percolation threshold of 2.2 wt% CB was obtained for hybrid composites. Further in-plane and through plane conductivities change marginally suggesting that the anisotropy was close to one. The frequency dependent conductance of PP-7 wt% graphite-CB showed insulator to semiconductor transition with increasing loading of CB. PP-7 wt% graphite and PP-7 wt% graphite-2.2 wt% CB behaved as insulators. With 2.35 and 2.75 wt% CB addition in PP-7 wt% graphite, plateau region appeared and extended further with higher loading. The plateau region signified dc conductance. The frequency dependent conductance started at higher frequency with increasing loading of CB. This showed that the samples became more conducting. The charge transport in PP-7 wt% graphite-2.75 wt% CB was by hopping mechanism. For less than 2.75 wt% CB in hybrid composites, it was coupled with capacitance effects. The enhancement in the conductivity because of the addition of CB in PP-7 wt% graphite was due to the occupation of CB in the graphite interspace. This could be so because without CB, PP-7 wt% graphite behaved as an insulator. Without graphite, up to 4 wt% CB addition in PP, the composites behaved as insulators suggesting the lower effective dielectric constant of that composite. Graphite-polymer-graphite configuration was considered as a parallel plate capacitor with

dielectric in between. When CB particles lie in between graphite particles, the distance between parallel plate capacitor got reduced and eventually resulted in the increase in effective dielectric constant and interjunction capacitance. When the effective dielectric constant at 0.01 Hz of PP-7 wt% graphite-2.75 wt% CB was compared with 2.2 wt% CB in the same, more than seven orders enhancement was obtained for the former case proving the occupation of CB particles in intergraphite space. Through impedance measurement, the interjunction capacitance was found out and it indeed increased from 31 pF for 2.2 wt% CB in PP-7 wt% graphite to 52 pF for 2.75 wt% CB in PP-7 wt% graphite which supported the model. Parallel model was used to fit the experimental impedance data. The aggregate resistance was decreasing with increase in the loading of CB which was explained on the basis of individual filler's work function. The result proved that the charge transfer from the polymer to CB occurred first and then to graphite via CB. So addition of more CB would have resulted in more charges being transferred to graphite via them and thus the aggregate resistance decrease was understood. DSC analysis on PP-graphite binary composites proved the nucleating ability of graphite as the crystallization temperature was increased by 9^{o} for 10 wt% graphite in PP when compared to that of pure PP.

The powder mixed PP-expanded graphite (ExGr) composites exhibited an electrical percolation threshold of 4 wt%. Below the percolation threshold, in-plane conductivity was found at least one order higher than the through plane conductivity. After 10 wt% ExGr addition in PP, the conductivity was saturated due to completion in the network formations. Percolation exponent suggested 3D network formation in these binary composites. Sintering at 140^{o}C for one hour of PP-ExGr composites showed re-orientation and crystallite size reduction as explained for PP-graphite composites. Since expanded graphite was sonicated well before adding to PP, it resulted in nanosheets formation which was proved by SEM and TEM studies. After sintering, the through plane conductivity got increased by at least one order when compared to that of unsintered samples due to re-orientation of graphite nanosheets along the through thickness direction. The effect of addition of ExGr in PP-7 wt% graphite on electrical conductivity was investigated and a percolation threshold of 0.75 wt% was obtained. Frequency dependent conductivity study showed insulator-

semiconductor transition with increasing loading of ExGr. The origin of plateau region signified that the samples were more conducting. The charge transport in PP-7 wt% graphite-1.5 wt% ExGr was by hopping mechanism and below 1.5 wt% ExGr in the same resulted in the transport coupled with capacitance effects. The increase in the conductance could be attributed to the occupation of ExGr sheets in the intergraphite space as without ExGr, the composite behaved as an insulator. Similar was the case for the composites without graphite till the maximum loading of ExGr employed in this study of hybrid composites. The interjunction capacitance obtained from impedance measurements, increased to 61.7 pF for 1.5 wt% ExGr in PP-7 wt% graphite from 37 pF for 0.75 wt% ExGr in the same. The aggregate resistance extracted from the parallel model was found to decrease with ExGr loading. DSC analysis on PP-4 wt% ExGr suggested the nucleating ability of ExGr nanosheets as the crystallization temperature was increased by 14^{o}C. However, the crystallinity of the binary composite was decreased.

PP-CNF binary composites prepared by powder mixing route showed a percolation threshold of 0.2 wt%. The in-plane and through plane conductivities more or less remain the same suggesting good dispersion of CNF in the polymer matrix. For hybrid composites, the percolation threshold was found to lie at 0.1 wt%. The binary composites were characterized by SEM which showed the interpenetrating structure of CNF. AC behavior showed insulator-semiconductor variation with the addition of more CNF. The charge transport was found to be by hopping mechanism at higher CNF loading and at lower loadings it was coupled with capacitive effects. The increase in the effective dielectric constant at low frequency i.e., 0.01 Hz to five orders for 1 wt% CNF in PP-7 wt% graphite when compared to 0.2 wt% CNF in the same was obtained. Through impedance measurement, interjunction capacitance due to the occupation of CNF in the interspace of graphite was evaluated. The aggregate resistance decrease with increasing loading of CNF was explained on the basis of individual filler's work function. The DSC result proved the nucleation ability of CNF when powder mixed with PP as the crystallization temperature of PP crystals was increased by 15^{o}. The aspect ratio of second conducting fillers was found to have inverse relation with the percolation threshold.

Melt crystallized PP-graphite, PP-ExGr, PP-CNF, PP-7 wt% graphite-ExGr and PP-7 wt% graphite-CNF showed higher percolation threshold when compared to powder mixed samples of same compositions due to transcrystals formation by epitaxial growth on the filler edges resulting in increased interparticulate spacing. The XRDs of melt crystallized binary composites showed a strong b-plane orientation of PP crystal which was explained on the basis of transcrystallinity. Finally as part of application, the thermal conductivity of PP-CNF and PP-graphite composites were measured. The conducting composites can replace plastic fiber spinning spool.

5.11. References

1. Dragaum H, Muschik H. J Polym Sci 1997;B15:1779
2. Li JX, Cheung WL. J Mater Process Technol 1997;63:472.
3. Garbarczyk, J.; Paukszta, D. Polymer 1981;22:562.
4. Garbarczyk, J.; Paukszta, D. Colloid Polym Sci 1985;263:985.
5. Li X, Hu K, Ji M, Huang Y, Zhou G. J Appl Polym Sci 2002;86:633.
6. Keith HD, Padden Jr FJ, Walker NM, Wyckoff HW. J Appl Phys 1959;30:1485.
7. Turner-Jones A, Cobbold AJ. J Polym Sci Part B: Polym. Lett. 1968, 6, 539.
8. Sauer JA, Pae KD. J Appl Phys. 1968;30:4950.
9. Turner-Jones A. Polymer 1971;12:487.
10. Varga J. In Polypropylene-Structure, Blends and Composites; Karger-Kocsis J, Ed. Chapman & Hall: London; 1995; Vol. 1. 10.
11. Clark EJ, Hoffman JD. Macromolecules 1984;17: 878.
12. Shen JW, Chen XM, Huang WY. J Appl Polym Sci 2003;88:1864.
13. Kalaitzidou K, Fukushima H, Drzal LT. Compos Sci Technol 2007;67:2045.
14. Haralampos Z, Lazaros A, Maria O. Macromol Symp 2001;170:249.
15. Gopakumar TG, Page DJYS. Polym Engg Sci 2004;44(6):1162.
16. Katbab AA, Hrymak AN, Kasmadjian K. J Appl Polym Sci 2008;107:3425.
17. Sawai P, Banerjee S. J Appl Polym Sci 2008;109:2054.
18. RungsimaY, Fowler M, Tzoganakis C, Yuhua W, Taylor M. Macromol Symp 2008;264:34.
19. Julia A. King etal. J Appl Polym Sci 2009;112:425.
20. Dweiri R, Sahari J. J Power Sources 2007;171:424
21. Naficy S, Garmabi H. Compos Sci Technol 2007;67:3233.
22. Cerezo FT, Preston CML, Shanks RA. Macromol Mater Eng 2007;292:155.
23. Kalaitzidou K, Fukushima H, Drzal LT. Carbon 2007;45:1446.
24. Rajopadhye NR, Bhoraskar SV. J Mater Sci Lett 1986;5:503.
25. Khare A, Mitra A, Radhakrishnan S. J Mater Sci 1996;31:5691.
26. Hidden G, Boudou L, Remaury S, Nebarra P. Martinez Vega J. J Opto Electro Adv Mater 2004;6(3):1065.

27. Saujanya C, Radhakrishnan S. Polymer 2001;42:4537.
28. Yutaka O, Takashi S, Toshikazu I, Masatoshi M, Takao N. Polym Engg Sci 2001;41(3):408.

Chapter-6

Summary and Conclusions

Conducting polymer composites (CPCs) find extensive applications in EMI shielding devices, bipolar plates for fuel cells etc. Depending on the end applications, the conductivity of the composites can be tailor made by varying the loading of fillers. The electrical conductivity of CPCs is mainly governed by filler particle size, dispersion, aspect ratio and orientation along with the processing routes. The parameter such as percolation threshold, at which the conductivity of CPCs increases considerably, should be minimized. In order to obtain very high conductivity in binary composites, enhancement in the loading of filler particles need to be employed. However, the filler loading can be minimized by using nanofillers such as graphene, CNT, CNF etc in binary composites which are expensive and thus limit their widespread applications. Nevertheless, strategies of using these expensive fillers in small quantities can be followed so that enhancement in the conductivity can be achieved by the reduction of both percolation threshold and filler loading. Thus the present dissertation deals with the study of electrical conductivity variation in hybrid and binary composites. Three polymer matrices such as amorphous Polyether sulfone (PES), semicrystalline Polyphenylene sulfide (PPS) and Polypropylene (PP) were chosen to study the effect of crystallinity on the electrical conductivity of the resultant hybrid composites. Furthermore, to study the effect of aspect ratio of fillers on the electrical conductivity of binary and hybrid composites, fillers such as graphite, carbon black (CB), expanded graphite (ExGr) and carbon nanofiber (CNF) were chosen. The summary and conclusions obtained from the above mentioned study are described below.

The dc electrical conductivity variation of PES-graphite binary composites was studied to determine the percolation threshold. The composites were prepared by both solution blending and powder mixing routes. Percolation threshold in solution blended binary composites was found to lie between 5-10 wt%. One particular composition namely, PES-7 wt% graphite has been chosen to study the effect of different aspect ratio fillers like CB, ExGr and CNF. Solution blended PES-7 wt% graphite-CB composites exhibited low percolation threshold than powder mixed samples, due to enhanced graphite particle size reduction obtained by the former route. The effect of sintering above T_g of the polymer facilitated the re-orientation of

graphite 002 planes along through thickness direction as well as reduction in crystallite size resulting in higher through plane conductivity. The re-orientation of graphite 002 planes and crystallite size reduction after sintering was more pronounced in solution blended PES-graphite composites than powder mixed samples. Polymer penetration in between graphite planes as evidenced by the shift in the 2 Theta towards lower value in XRD was found to be more pronounced in solution blended PES-graphite samples.

The enhancement in the through plane conductivity after sintering was also observed in PES-ExGr and PES-CNF binary composites. Further sintering resulted in enhancement in the hardness of PES-graphite composites when compared to unsintered samples. DSC analysis on PES based binary composites supported the nucleating ability of filler particles as evidenced by increase in T_g of the polymer after filler addition. More concentration of graphite was needed to enhance the T_g of the polymer by 11^oC. The same level of enhancement was obtained by adding 5 wt% CNF and 3 wt% ExGr respectively in PES. The result showed that low concentration of high aspect ratio fillers was sufficient to increase the T_g by the value which would have been obtained by higher loading of low aspect ratio fillers. This was attributed to the increase in the surface area of the high aspect ratio fillers at low loading, wetting the polymer thoroughly. The increase in the T_g of the polymer by the addition of graphite, ExGr and CNF demonstrated better interaction between the polymer and fillers.

The ac behavior of hybrid composites with CB, CNF and Exgr as second conducting fillers in PES-7 wt% graphite showed insulator-semiconductor transition with increase in the loading of second conducting fillers. The percolation threshold obtained from the dc conductivity study in these hybrid composites exhibited inverse relation with the aspect ratio of the second filler particles. The preparation process was also found to affect the percolation threshold. Solution blended PES-7 wt% graphite-CB hybrid composites showed lower percolation threshold (0.7 wt% CB) than the powder mixed samples (1.3 wt% CB). The aspect ratio of fillers in the polymer was increasing in the order CB < CNF < ExGr. The predominant occupation of second conducting fillers in between graphite particles was proved by impedance

and effective dielectric constant measurements. The interjunction capacitance was found to increase with increase in the loading of second filler in PES-7 wt% graphite. The decrease in aggregate resistance with the addition of second conducting filler was better understood from the work function of individual components in the hybrid composites. With the addition of CB, thermal conductivity of solution blended PES-graphite-CB composites was increased.

The dc electrical conductivity variation of powder mixed PPS-graphite composites showed that the percolation threshold lie at 7 wt%. Similarly PPS-ExGr and PPS-CNF powder mixed binary composites were prepared after dispersing fillers in acetone thoroughly and the percolation threshold was found to be inversely related to the aspect ratio of filler particles. The aspect ratio increased in the order graphite < ExGr < CNF. Sintering process above the T_g of the polymer on graphite, ExGr loaded composites resulted in the reduced crystallite sizes of the filler particles along with re-orientation of graphite 002 planes. This phenomenon resulted in enhanced through plane conductivity. DSC analysis on these binary composites proved the nucleating ability of the fillers as the crystallization temperature was increased after filler loading.

The percolation threshold of PPS-7 wt% graphite-filler (filler = CB, ExGr and CNF) powder mixed bybrid composites had inverse relation with the aspect ratio of the second conducting fillers. AC measurements showed insulator-semi-conductor transition with increase in the loading of second fillers. The loading at which hopping conduction started was found be inversely related to the aspect ratio of second conducting particles in hybrid composites. The predominant occupation of second filler particles in the graphite interspace in hybrid composites was proved by impedance and effective dielectric constant measurements. The interjunction capacitance and effective dielectric constant at 0.01 Hz increased at higher loading of second conducting fillers. Consequently, the aggregate resistance in these hybrid composites decreased with the loading of second conducting filler particles. This result was better understood in terms of reduction in the barrier for the charge transport because of the occupation of second conducting fillers in the interspace of graphite particles.

Melt crystallization of binary and hybrid composites showed higher percolation threshold compared to that of powder mixed samples due to increase in the interparticulate distance at that temperature. Thermal conductivity of PPS-graphite composites was found to increase with the addition of graphite. The PPS-ExGr composites prepared by in-situ polymerization route resulted in very low percolation threshold (<1 wt%) due to better delamination of ExGr sheets which resulted in enhanced dispersion and contact between them.

Similar to PPS based composites, powder mixed PP-graphite, PP-ExGr and PP-CNF composites were made and the percolation threshold of such composites showed inverse relation with the aspect ratio of the filler particles. The percolation threshold obtained in PP-graphite, PP-ExGr and PP-CNF was 10, 4 and 0.2 wt%, respectively. Sintering process especially above the T_g of the polymer was to increase the through plane conductivity due to re-orientation of graphite 002 planes. In addition, the crystallite size of filler particles was reduced after sintering. This particular aspect resulted in increased contact, surface area and better distribution of filler particles in the polymer matrix. DSC analysis on the binary composites showed enhanced crystallization temperature supporting the nucleating ability of such type of filler particles. The increase in the crystallization temperature was found to be higher for CNF filled composites due to its high aspect ratio, which would have had many nucleating sites.

The dc conductivity studies on powder mixed PP-7 wt% graphite-filler (filler = CB, Exgr and CNF) showed that the percolation threshold was found to be inversely related to the aspect ratio of second conducting fillers. The aspect ratios varied in the order CB < ExGr < CNF. AC measurements on those hybrid composites showed insulator-semiconductor transition with increase in loading of the second conducting filler particles. The barrier for the charge transport was decreased due to the presence of second conducting fillers in the interspace of graphite particles. The increase in the effective dielectric constant at 0.01 Hz and interjunction capacitance with the addition of second fillers in hybrid composites proved the occupation of second conducting filler in the interspace of graphite particles.

Melt crystallized PP based binary composites exhibited higher percolation threshold due to the formation of transcrystalline morphology predominantly on the fillers edges. This was concluded from the strong b-plane orientation of PP crystals as witnessed by XRD patterns where the intensity of 040 reflection of PP was increased after melt crystallization. The b-plane orientation was due to epitaxial growth of PP crystals on graphitic filler edges with b-axis parallel to the surface under investigation. Due to transcrystals growth on the filler edges, through plane conductivity was decreased.

From the results obtained, the effect of polymer matrix on the dc electrical conductivity can be understood. The electrical percolation threshold of hybrid composites such as PES-graphite-CB, PPS-graphite-CB and PP-graphite-CB prepared by powder mixing route can be compared to understand the role of polymer matrix. The following Table 1 summarizes the percolation threshold in different polymer based hybrid composites.

Table 1

Percolation threshold variation with different polymer matrices in graphite-CB based hybrid composites

Sample	Percolation Threshold (Wt%)
1. PES-7 wt% graphite-CB	1.3
2. PPS-7 wt% graphite-CB	1.5
3. PP-7 wt% graphite-CB	2.2

Before making hybrid composites, all polymers were sieved (100 mesh) and then used. Thus the powder mixing route for the preparation of hybrid composites fixed the average particle size of polymers. PES is totally an amorphous polymer. PPS and PP are semi crystalline polymers. The percolation threshold is less for amorphous polymer based hybrid composites. The crystallinity increases from PPS to PP. More the crystallinity, the charge transport became difficult in insulating polymers leading to higher percolation threshold. Similar conclusion can be drawn from the impedance analysis of different polymer based hybrid composites.

Table 2

Impedance parameters for PES-7 wt% graphite-CB powder mixed samples

Sample	R_a (Ohm)	R_p (Ohm)	C (pF)
1. PES-7 wt% graphite	250	$5.0x10^{11}$	33
2. PES-7 wt% graphite-2 wt% CB	150	$2.45x10^{5}$	58

Table 3

Model parameters for PPS-7 wt% graphite-CB powder mixed hybrid composites

Sample	R_a (Ohm)	R_p (Ohm)	C (pF)
1. PPS-7 wt% graphite	350	$6.8x\ 10^{11}$	32
2. PPS-7 wt% graphite-2 wt% CB	220	$3.1x10^{6}$	51
3. PPS-7 wt% graphite-3 wt% CB	120	6600	75

Table 4

Model parameters for PP-7 wt% graphite-CB powder mixed composites

Sample	R_a (Ohm)	R_p (Ohm)	C (pF)
1. PP-7 wt% graphite	600	$6.8x10^{12}$	31.0
2. PP-7 wt% graphite-2.75 wt% CB	300	16400	52.2

Table 2-4 show the model parameters extracted from the impedance analysis of powder mixed PES-7 wt% graphite-CB, PPS-7 wt% graphite-CB and PP-7 wt% graphite-CB respectively. Comparing the data on the impedance spectroscopy for the three systems, it is evident that R_s and R_p increase in the order PP > PPS > PES for the same concentration of graphite. These result suggest that the charge transport in PES-graphite is better than both PPS-graphite and PP-graphite composites. It may be pointed out that the crystallinity in the PES is nil (amorphous) while PPS and PP have 40% and 60% respectively. Thus, it is favorable to choose an amorphous polymer matrix with high temperature stability such as PES for making graphite composite plates. Moreover, hybrid composites are very effective in reducing the percolation

threshold as well as total filler content. In order to achieve low electrical percolation threshold, high aspet ratio fillers and amorphous polymer matrices can be chosen.

List of publications

- S. Radhakrishnan, **B.T.S. Ramanujam**, A. Adhikari, and S. Sivaram. "High Temperature Polymer – Graphite Hybrid Composites for Bipolar Plates: Effect of Processing Conditions on Electrical Properties" *J. Power Sources* 163, 702– 707, (2007).

- **B.T.S. Ramanujam**, R.Y. Mahale, S. Radhakrishnan. "Polyether sulfone-expanded graphite conducting composites: Charge transport and impedance characteristics" Under review in Composites Science and Technology.

- **B.T.S. Ramanujam**, S. Radhakrishnan. "Direct route for preparation of expanded/ nanographite-polyether sulfone conducting composites" *to be communicated*.

- **B.T.S. Ramanujam**, S. Radhakrishnan. "Influence of carbon black on the electrical properties of Polyether sulfone-Graphite hybrid composite: Evaluation of a model based on impedance analysis" *to be communicated*.

- **B.T.S. Ramanujam**, S. Radhakrishnan. "Charge transport and impedance analysis of Polyphenylene sulfide-expanded graphite conducting composites" to *be communicated*.

- **B.T.S. Ramanujam**, S. Radhakrishnan. "Influence of carbon black on the electrical properties of Polyether sulfone-graphite hybrid composite: Evaluation of a model based on impedance analysis" *to be communicated*.

Presentations in conferences

- **B.T.S. Ramanujam**, S. Radhakrishnan. "Electrical properties of Polyphenylene sulfide-Carbon nanofiber conducting composites: Bipolar material for fuel cells" in WHEC-2010 (18^{th} **W**orld **H**ydrogen **E**nergy **C**onference), **May 2010**, to be held in **Essen, Germany.**

- **B.T.S. Ramanujam**, S. Radhakrishnan. "Polyphenylene sulfide-graphite hybrid composites: charge transport and impedance characteristics" in APM-2010 trends & technology (International conference on **A**dvancements in **P**olymeric **M**aterials), **February 2010, CIPET Bhubaneswar, India.**

- **B.T.S. Ramanujam**, S. Radhakrishnan. "Electrical properties of conducting polyphenylene sulfide- graphite hybrid composites" ICEP-2008 (**I**nternational **C**onference on **E**lectroactive **P**olymers), **October 2008**, **Jaipur, Rajastan, India.**

- **B.T.S. Ramanujam**, S. Radhakrishnan. "Structure development and "electrical properties of PP-Graphite hybrid composites for fuel cell applications" in ICAM-2008 (**I**nternational **C**onference on **A**dvance **M**aterials), **February 2008**, **Kottayam, Kerala, India**.

- **B.T.S. Ramanujam**, S. Radhakrishnan. "Charge Transport Processes in Conducting Polyether sulfone-nanographite hybrid composites" ICAMA-2007 (**I**nternational **C**onference on **A**dvanced **M**aterials and **A**pplications), **August 2007**, **Shivaji University, Kolhapur**.

- **B.T.S. Ramanujam**, S. Radhakrishnan. "Electrical Properties of PES-Graphite, PP-Graphite composites" ICEP-2007 (**I**nternational **C**onference on **E**lectroactive **P**olymers), **February 2007**, **Goa University, Goa, India**.

- **B.T.S. Ramanujam**, S. Radhakrishnan. "Electrical Properties of Solution Blended Polyether sulfone-graphite Composites" **MACRO-2006**, **December 2006**, **NCL, Pune, India.**